AD-A162 352 FRACTURE BEHAVIOR OF BORON ALUMINUM COMPOSITES AT ROOM 1/3
AND ELEVATED TEMPE (U) DREXEL UNIV PHILADELPHIA PA
DEPT OF MECHANICAL ENGINEERING AN J AWERBUCH APR 85
UNCLASSIFIED AFOSR-TR-85-1099 AFOSR-79-0079 F/G 11/4 NL

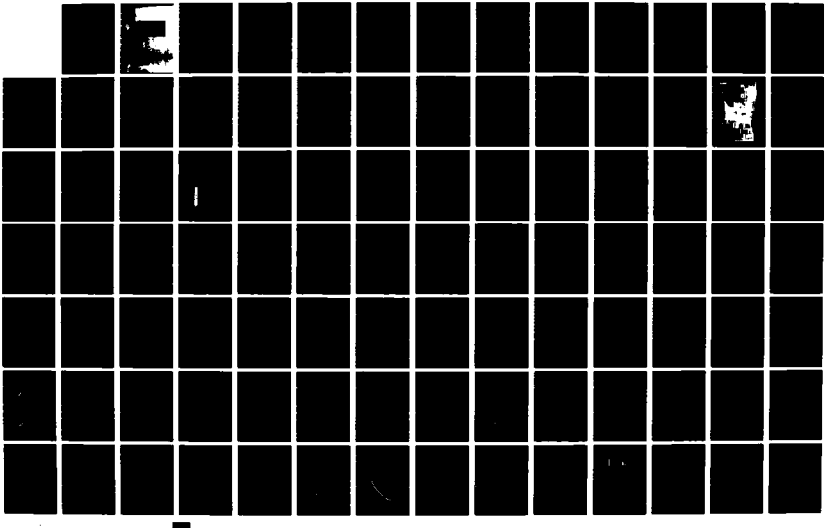

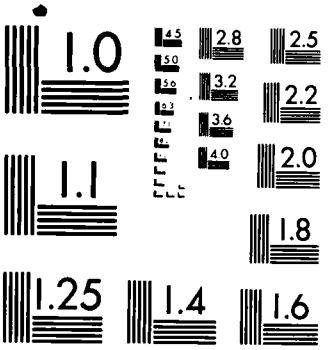

MICROCOPY RESOLUTION TEST CHART
NATIONAL BUREAU OF STANDARDS-1963-A

FRACTURE BEHAVIOR OF BORON ALUMINUM COMPOSITES AT ROOM AND ELEVATED TEMPERATURES

(2)

FRACTURE BEHAVIOR OF BORON ALUMINUM COMPOSITES AT ROOM AND ELEVATED TEMPERATURES

Jonathan Awerbuch

Department of Mechanical Engineering and Mechanics

Drexel University

Philadelphia, Pennsylvania 19104

FINAL REPORT

AFOSR GRANT NO. 79-0079

PERIOD: April 1, 1979 - April 14, 1984

Approved for Public Release: Distribution Unlimited

for

Director of Aerospace Sciences

Air Force Office of Scientific Research

Bolling AFB, Washington, D.C. 20332

REPORT DOCUMENTATION PAGE	READ INSTRUCTIONS BEFORE COMPLETING FORM
1. REPORT NUMBER: AFOSR-TR- 9	2. GOVT ACCESSION NO.: AD-A162 352	3. RECIPIENT'S CATALOG NUMBER:
4. TITLE (and Subtitle): FRACTURE BEHAVIOR OF BORON ALUMINUM COMPOSITES AT ROOM AND ELEVATED TEMPERATURES	5. TYPE OF REPORT & PERIOD COVERED: Final Grant Report April 1, 1979 - April 14,1984
	6. PERFORMING ORG. REPORT NUMBER:
7. AUTHOR(s): Jonathan Awerbuch	8. CONTRACT OR GRANT NUMBER(s): AFOSR 79-0079
9. PERFORMING ORGANIZATION NAME AND ADDRESS: DREXEL UNIVERSITY, Department of Mechanical Engineering & Mechanics	10. PROGRAM ELEMENT, PROJECT, TASK AREA & WORK UNIT NUMBERS: 61102F 2302/B2
11. CONTROLLING OFFICE NAME AND ADDRESS: Director of Aerospace Sciences, Air Force Office of Scientific Research, Bolling AFB, Washington, D.C. 20332	12. REPORT DATE: April 1985
	13. NUMBER OF PAGES: 264
14. MONITORING AGENCY NAME & ADDRESS(if different from Controlling Office)	15. SECURITY CLASS. (of this report): Unclassified
	15a. DECLASSIFICATION DOWNGRADING SCHEDULE
16. DISTRIBUTION STATEMENT (of this Report): Approved for Public Release; Distribution Unlimited	
17. DISTRIBUTION STATEMENT (of the abstract entered in Block 20, if different from Report)	
18. SUPPLEMENTARY NOTES	
19. KEY WORDS (Continue on reverse side if necessary and identify by block number): Composite laminates; boron/aluminum; fracture behavior; crack tip damage; crack opening displacement; K-calibration; compliance curves; deformation characteristics; notch sensitivity; toughness; failure modes; non-destructive testing; acoustic emission.	

20. ABSTRACT (Continue on reverse side if necessary and identify by block number)

This ~~Final~~ Report describes the results of research work on the deformation characteristics and failure mechanisms and processes of center-notched boron/aluminum laminates at room and elevated temperatures. The research program has been divided into two major directions, namely experimental and analytical studies, each of which has been divided into separate Tasks to address the variety of subjects involved in the study of fracture behavior of composite laminates.

Employing a wide range of experimental techniques and procedures, this

DD FORM 1 JAN 73 1473 EDITION OF 1 NOV 65 IS OBSOLETE

program has focused on the deformation characteristics in both the elastic and inelastic ranges, crack tip damage growth, notch sensitivity, toughness, failure mechanisms and processes and failure modes. The primary experimental technique has been to utilize the interferometric displacement gage (IDG) through which the actual crack opening displacement (COD) could be measured at room and elevated temperatures, resulting in precise load-COD and local compliance curves. Special attention has also been given to nondestructive examination techniques, in particular the acoustic emission technique, for monitoring internal damage initiation and progression during quasi-static and low cycle fatigue loading. Microstructural studies of the fracture surface morphologies have been conducted as well. The experimental studies contributed to the understanding of the effect of laminate configuration and test temperature on the fracture behavior of the subject material. The appropriate experimental methodology (e.g. the IDG and AE techniques) for characterizing a new composite material system has been established.

The analytical study has focused in three major directions, namely: 1. predicting the elastic behavior; 2. application of semi-empirical fracture models for predicting the notch sensitivity; and 3. application, extension and modifications of approximate mechanistic models for predicting the deformation characteristics of unidirectional composites. In the elastic region excellent agreement between predicted (for orthotropic materials) and experimental global and local compliance calibration curves has been established. An extensive critical review of the most commonly used semi-empirical fracture models proposed to predict the notched strength of composite laminates has been conducted, and all models were compared with an extensive data bank. Consequently, the appropriateness of the various models has been determined. Significant efforts have been directed toward predicting the deformation characteristics and damage progression of unidirectional metal-matrix composites. The effect of a variety of intrinsic and extrinsic variables has been analyzed and modification of the existing model is proposed, incorporating the actual shear stress-strain curve of the matrix material. Excellent agreement between experimental load-COD curves and prediction has been established for unidirectional boron/aluminum.

This Final Report furnishes a summary of the research results on the various Tasks addressed in this program. Each Section, reporting the results of a particular Task, is self-contained and includes its own independent Summary, Introduction, Research Results and Discussion, and Conclusions. An extensive list of references is also included.

FOREWARD

This research program has been conducted in the Composite Materials Laboratory, Department of Mechanical Engineering and Mechanics, Drexel University. The micro-structural studies were conducted in the Department of Materials Engineering with Dr. M.J. Koczak as research investigator.

Several graduate and undergraduate students participated in this program. Mr. H.E. Perkinson, who received his M.Sc. degree, participated in the initial phases of the program. Mr. M.S. Madhukar, a Ph.D. student (graduating Summer 1985) has actively participated in all phases of the research since January 1981 and has conducted the bulk of the experimental and analytical work. Sixteen undergraduate students (co-op, part-time and Senior Design) took part in specimen preparation, experimental work, data reduction and analyses.

The program monitors were Colonel Joseph D. Morgan, III, Dr. Anthony K. Amos and Major David A. Glasgow. The Principal Investigator wishes to thank them for their support and encouragement. All three spent considerable time and effort discussing with us the technical aspects of the research program.

TABLE OF CONTENTS

I. ABSTRACT

This Final Report describes the results of research work on the deformation characteristics and failure mechanisms and processes of center-notched boron/aluminum laminates at room and elevated temperatures. The research program has been divided into two major directions, namely experimental and analytical studies, each of which has been divided into separate Tasks to address the variety of subjects involved in the study of fracture behavior of composite laminates.

Employing a wide range of experimental techniques and procedures, this research program has focused on the deformation characteristics in both the elastic and inelastic ranges, crack tip damage growth, notch sensitivity, toughness, failure mechanisms and processes and failure modes. The primary experimental technique has been to utilize the interferometric displacement gage (IDG) through which the actual crack opening displacement (COD) could be measured at room and elevated temperatures, resulting in precise load-COD and local compliance curves. Special attention has also been given to nondestructive examination techniques, in particular the acoustic emission technqiue, for monitoring internal damage initiation and progression during quasi-static and low cycle fatigue loading. Microstructural studies of the fracture surface morphologies have been conducted as well. The experimental studies contributed to the understanding of the effect of laminate configuration and test temperature on the fracture behavior of the subject material. The appropriate experimental methodology (e.g. the IDG and AE techniques) for characterizing a new composite material system has been established.

The analytical study has focused in three major directions, namely: 1. predicting the elastic behavior; 2. application of semi-empirical fracture models for predicting the notch sensitivity; and 3. application, extension and modifications of approximate mechanistic models for predicting the deformation characteristics of unidirectional composites. In the elastic region excellent agreement

between predicted (for orthotropic materials) and experimental global and local compliance calibration curves has been established. An extensive critical review of the most commonly used semi-empirical fracture models proposed to predict the notched strength of composite laminates has been conducted, and all models were compared with an extensive data bank. Consequently, the appropriateness of the various models has been determined. Significant efforts have been directed toward predicting the deformation characteristics and damage progression of unidirectional metal-matrix composites. The effect of a variety of intrinsic and extrinsic variables has been analyzed and modification of the existing model is proposed, incorporating the actual shear stress-strain curve of the matrix material. Excellent agreement between the experimental load-COD curves and prediction has been established for unidirectional boron/aluminum.

This Final Report furnishes a summary of the research results on the various Tasks addressed in this program. Each Section, reporting the results of a particular Task, is self-contained and includes its own independent Summary, Introduction, Research Results and Discussion, and Conclusions. An extensive list of references is also included.

II. INTRODUCTION

2.1 General

Metal-matrix composites are currently being considered for the so-called "primary" structural applications in a variety of aircraft and aerospace structures. From several aspects they are superior to most resin-matrix composites, e.g. in elevated temperature performance, transverse and shear strengths, impact resistance, and susceptibility to the potential problem of moisture absorption, etc.

In recent years several new metal-matrix composites systems have been developed, e.g. SiC/aluminum (filamentary and whiskers), graphite/aluminum, SiC/titanium-aluminides, graphite/magnesium, etc. Among the variety of the metal-matrix composites available, the boron/aluminum system has received most of the attention in the research and application studies. It is of interest to note, however, that most efforts were directed toward unidirectional boron/aluminum, and emphasis has been placed on the metallurgical aspects of the interaction among the constituents, optimizing the fabrication procedures and the trade-off between strength and toughness. Relatively, little work has been recorded on the notch sensitivity of boron/aluminum laminates. Also, in spite of the recognized advantages of this material system under larger operating temperature ranges, very little information is available regarding the effect of temperature on the notch sensitivity of the subject material.

The importance of understanding the fracture behavior of metal-matrix composites can be demonstrated from the results of recent studies on hard object impact damage of metal-matrix composites. The results of these studies indicate that induced impact damage can be presented as through-the-thickness cracks for post-impact residual strength predictions.

2.2 Research Objectives

The primary objective of this study has been to characterize the fracture behavior of boron/aluminum composites at room and elevated temperatures experimentally and analytically. Although the program focused on a specific material system, many of the epxerimental procedures developed and employed, test methodology established, and analyses used, etc. can be extended to any metal-matrix composite system. Thus, this research program should also be viewed in the more general context of advancing the understanding of the fracture behavior of any new composite system.

This study concentrated on six different laminates: $[0]_8$, $[90]_8$, $[\pm 45]_{2s}$, $[0/90]_{2s}$, $[0/\pm 45/90]_s$, and $[0/\pm 45/0]_s$, all constituted of 140 μm (5.6 mil) diameter boron filaments in a 6061-F aluminum alloy. Center notched specimens with six notch length-to-width ratios, ranging from 0.05 to 0.5, were tested at temperatures ranging from 21°C (70°F) to 371°C (700°F).

Among the different issues addressed are:

- Load-crack opening displacement (COD) curves using the laser interferometric displacement gage technique.
- Far-field load-displacement curves using the standard compliance gage.
- Local and global compliance curves.
- K-calibration curves.
- Fracture strength and notch sensitivity.
- Crack tip damage growth, deformation characteristics and failure modes.
- Microstructural analysis of failure modes, e.g., examination of fiber, matrix, and interface by optical and electron microscopy techniques.

- Detection of damage mechanisms and internal damage through X-ray radiography, ultrasonic C-scan, and acoustic emission.
- Monitoring damage growth through acoustic emission, e.g. location and amplitude distribution histograms of events, counts and count rate, and cumulative event amplitude distribution.
- Acoustic emission studies on constituents and "simple" structures.
- Correlating acoustic emission information with actual deformation characteristics and failure modes.
- Fracture behavior of unidirectional versus laminated boron/aluminum.
- Effect(s) of elevated temperatures on fracture behavior.
- Mechanical properties (elastic constants) at room and elevated temperatures.
- Effect(s) of constituents (e.g., fiber, matrix) on fracture behavior.
- Determining the proper test methodology to be employed in characterizing a new composite material system.
- Comparison of experiments with the associated analyses predicting the elastic behavior, deformation characteristics, notched strength, etc.

2.3 Research Program

Emphasis in this research program has been placed on the deformation characteristics, crack tip damage growth, notch sensitivity, toughness and failure mechanisms and processes. Special attention has also been given to nondestructive evaluation of damage initiation and progression. Effects of elevated temperatures on damage progression, notch sensitivity, failure processes, etc. have been investigated through a variety of experimental techniques and the results were compared

with the relevant available analyses. In short, this study concentrated on the details of the load-deformation flaw growth shown schematically in Figure 1.

The research program has been divided into two major phases, namely experimental and analytical studies, each of which has been divided into sub-Tasks as shown in the block diagram of Figure 2. Brief statements on these various Tasks are given below.

I. Experimental Program:

The experimental program has addressed a variety of subjects such as mechanical properties, elastic and inelastic deformation characteristics, nondestructive evaluation of damage initiation and progression, notch sensitivity, failure modes, etc. The specific methodologies used and types of information obtained were:

1. Load-Displacement: determine the basic mechanical properties and global (far-field) load-displacement curves using the conventional procedures of employing room and elevated temperature strain gages and compliance gages.

2. Load-COD: characterize the deformation characteristics and crack tip damage growth using an interferometric displacement gage (IDG) technique for accurate measurement of crack opening displacement (COD) in real-time at room and elevated temperatures.

3. Damage Initiation and Progression: identify the appropriate nondestructive testing technique for monitoring damage growth. Emphasis has been placed on the acoustic emission technique and visual observation through the closed-circuit television (CCTV) to monitor the failure processes and damage initiation and progression during quasi-static and fatigue loading at room temperature.

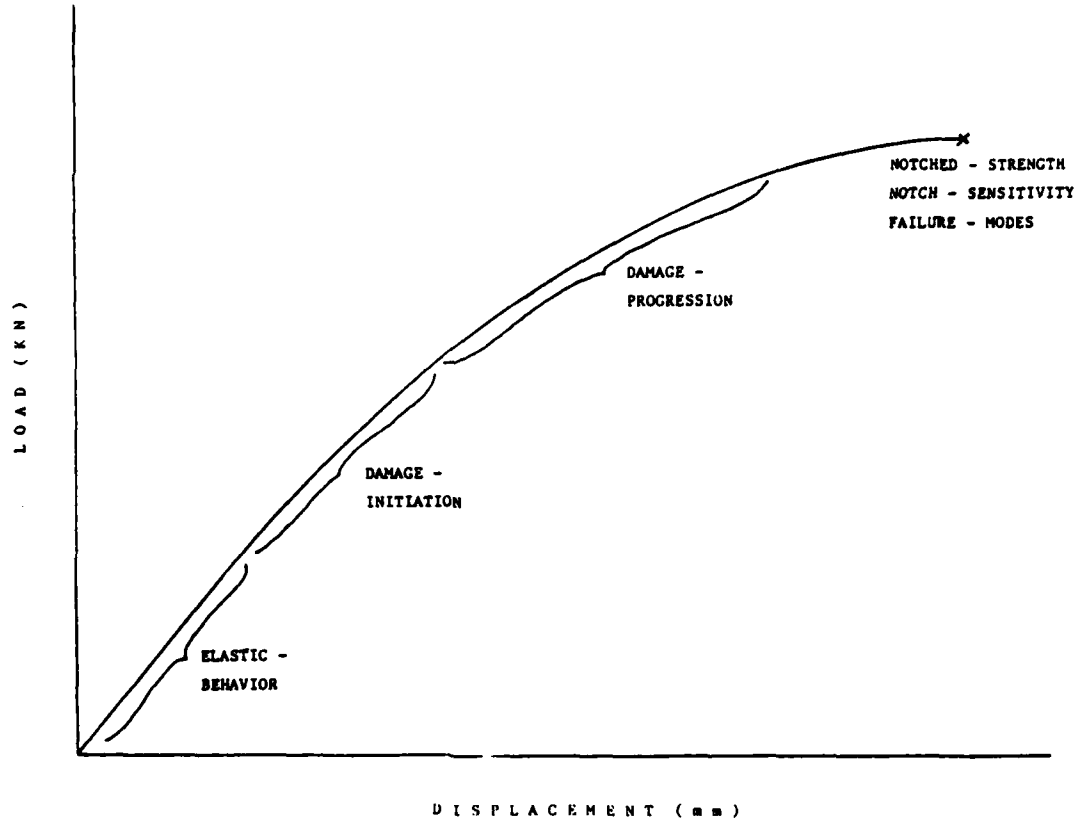

Figure 1. Schematic of load-displacement curve for notched composite laminates. Subjects of research are indicated.

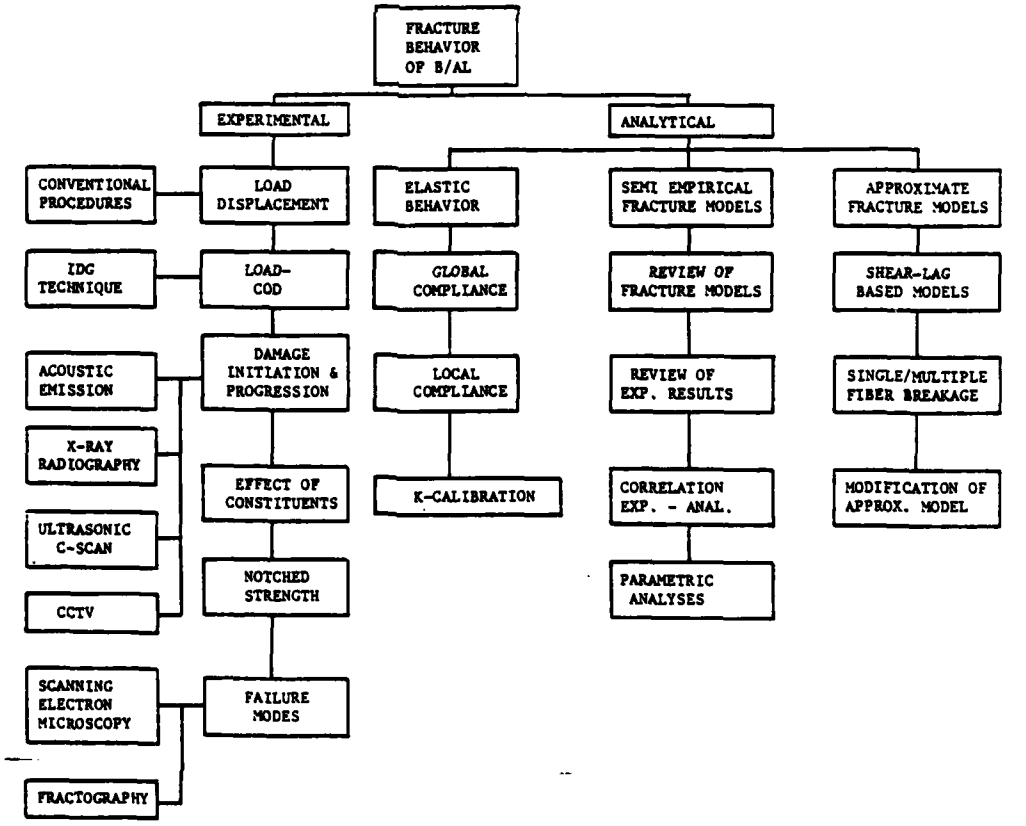

Figure 2. Block diagrams indicating experimental and analytical subjects of research.

4. Effect of Constituents: determine the mechanical properties of the aluminum matrix and strength of the boron fibers as part of the quality control study of the subject material.

5. Notched strength: determine the effects of laminate configuration and elevated temperatures on the notch sensitivity and toughness.

6. Failure Modes: determine the micro-failures and quality of fabrication using the scanning electron microscope and fractography.

The purpose of the experimental study was not merely to generate and furnish quantitative data but also to establish the appropriate methodology to be employed (e.g. the IDG and AE techniques) in characterizing a new composite material system. The experimental study also contributes to the understanding of the failure mechanisms and processes of boron/aluminum laminates, e.g. the IDG and AE studies furnished the necessary information to determine the applicability of the various analytical models for predicting various aspects of the fracture behavior of metal-matrix composites.

II. Analytical Program

The analytical study has focused in three major directions, namely: predicting the elastic behavior application of semi-empirical models for predicting the notched strength, and application of approximate mechanistic models for predicting the deformation characteristics of unidirectional composites. More specifically, the following issues were addressed:

1. Elastic Behavior: characterize the elastic response of center notched boron/aluminum laminates at room and elevated temperatures.

2. Global Compliance: apply the energy release rate approach to predict the global compliance and compare with the experimental results obtained at room temperature with the conventional compliance gage.

3. Local Compliance: apply the elastic stress analysis for orthotropic materials to predict the local crack opening displacement of metal-matrix composites, and compare these predictions with the experimental results obtained at room and elevated temperatures with the IDG technique.

4. K-Calibration: determine the applicability of the isotropic width correction factor for boron/aluminum laminates by comparing it with the experimental results obtained using the IDG technique.

5. Semi-Empirical Fracture Models: apply the most commonly used fracture models to predict the notch sensitivity of composite laminates.

6. Review of Fracture Models: conduct a critical review of all the most commonly used semi-empirical fracture models and assess their appropriateness and their usefulness for predicting the notched strength of composite laminates containing a straight crack, a circular hole and impact damage.

7. Review of Experimental Results: collect and review the available notched strength data of boron/aluminum laminates reported in the open literature and those generated in this research program. Determine the effect of intrinsic and extrinsic parameters (e.g. laminate configuration, stacking sequence, constituents, temperature, notch shape, etc.) on the notch sensitivity and toughness of composite laminates.

8. Correlation Between Experiments and Analyses: compare all the experimental data reviewed with all the fracture models reviewed and establish the applicability of each model.

9. Parametric Analyses: determine the applicability of the various parameters associated with the different fracture models as measures of notch sensitivity.

10. Approximate Fracture Models: review and apply existing approximate analytical models predicting the deformation characteristics of unidirectional metal-matrix composites and compare these predictions with the experimental results (load-COD curves and notched strength) obtained at room and elevated temperatures. Also, conduct parameteric analyses to determine the effect of constituents on the stress concentration factor, load-COD curves, extent of plastic zone, etc.

11. Shear-Lag Based Models: review all the existing shear-lag based models predicting the deformation characteristics of unidirectional composites and compare the predictions with experimental load-COD curves to determine their applicability to metal-matrix composites.

12. Single/Multiple Fiber Breakage: determine whether the basic assumptions made in the various fracture models are appropriate for boron/aluminum, namely: 1. catastrophic fracture of the composite follows the breakage of the first (single) intact fiber at the notch tip; 2. matrix material assumed to be linear, bi-linear or elastic-perfectly plastic.

13. Modification of Fracture Models: modify and develop a new fracture model which incorporates the actual shear stress-strain behavior of the metal matrix.

2.4 Research Accomplishments

With a few exceptions all the Tasks of this research program have been fully accomplished. Furthermore, the research program has been expanded much beyond the

original objectives with the ultimate goal of achieving as comprehensive and complete a characterization of the fracture behavior of metal-matrix composites as possible. Thus, tasks such as monitoring acoustic emission during low cycle fatigue, the comprehensive review of the semi-empirical fracture models, the application and modification of the shear-lag based models, etc. were all added to the original program. Consequently, certain issues have only been partially addressed, primarily regarding the effect of constituents on the fracture behavior of unidirectional boron/aluminum. This issue will be pursued independently during the coming year.

The following issues are yet to be completed: 1. elevated temperature load-COD curves to failure of $[\pm 45]_{2s}$ laminate; 2. elastic properties of the multidirectional laminates at elevated temperatures; 3. completion of the comparison between the shear-lag based models and the experimental load-COD curves; and 4. completion of the modified fracture model developed during the course of this program so that it will be fully operational. All these issues are concurrently underway and will be completed by the end of August 1985.

In the characterization of metal-matrix composites it is essential to establish a better understanding of the effect of fabrication procedures on the performance of the composite. Issues such as interface integrity, the relations between thermal/mechanical processing, interface and mechanical properties, etc. have not been addressed in this research program. In order to optimize fabrication procedures in regard to performance and cost, and to better understand the trade-off between strength and toughness, further research in this area will be required.

2.5 The Final Report

This Final Report highlights the research results on the various Tasks addressed in this program. Brief descriptions of all Experimental Procedures are given in Section III. The subsequent Sections furnish a brief summary of the research results. Each Section is self-contained and includes its independent Summary, Introduction, Research Results, Conclusions, List of References and Figures.

It is emphasized that the subjects and results contained in this Final Report are described in an abbreviated format. Details of the research are contained in over 20,000 Figures. These can be obtained from the Principal Investigator upon request.

2.6 Publications and Presentations

The research results for two of the subjects addressed in this program are being published in two journal articles. At least seven additional publications will be submitted within the coming year and are in the process of being prepared for publication. In addition, numerous presentations of the results have been made in conferences, workshops, short courses and seminars during the program duration.

a. Publications

Awerbuch, J. and Madhukar, M., "Notched Strength of Composite Laminates: Predictions and Experiments - A Review", Journal of Reinforced Plastic and Composites, Vol. 4, No. 1, 1985, pp. 3-160, to be published.

Madhukar, M. and Awerbuch, J., "Monitoring Damage Progression in Center Notched Boron Aluminum Laminates Through Acoustic Emission", Composite Materials: Testing and Design (Seventh Conference), American Society of Testing and Materials, STP _ _ _ , 1985, to be published.

b. Workshops and Short Courses

"Metal Matrix Composites Analysis, Testing and Design", UCLA Workshop in Cooperation with the U.S. Department of Defense Metal Matrix Composites Information Analysis Center (MMCIAC). Principal Lecturer on "Fracture and Impact Behavior" (including lecture notes) Los Angeles, California, June 14-18, 1982. Also, held at the University of Maryland, College Park, Maryland, February 28 - March 4, 1983.

"Failure Mechanisms in Composites", an International workshop held in the Institute for Structural Mechanics, The German Aerospace Research Establishment, Braunschweig, Germany, July 5-9, 1982. Organizer, coordinator and principal lecturer on five different subjects related to Failure Mechanisms in Composites (including lecture notes).

"Acoustic Emission From Composites in Fatigue", Pre-symposium Educational Seminar, First International Symposium on Acoustic Emssion From Reinforced Plastics, Society of Plastic Industry, San Francisco, California, July 18, 1983.

"Composite Materials Workshop", Principal Lecturer, Katholiek Univerteit Leuven, Leuven, Belgium, June 4-8, 1984. Lectures on (Including Lecture Notes): Notch Strength Predictions of Composites - A Review, Impact Damage in Composites - A Review, Failure Mechanisms in Composites- A Review, Acoustic Emission in Composites - A Review.

"Advanced Materials - Recent Advances in the Nondestructive Evaluation of Materials", Principal Lecturer on "Acoustic Emission in Composite Laminates, A Review" (including lecture notes), sponsored by Michigan State University, U.S. AMMRC and DARPA, Traverse City, Michigan, September 9-11, 1984.

c. Conference Presentations and Seminars

"Deformation Characteristics and Failure Modes in Composite Materials", a seminar given in the Deutsche Forschungs - und Versuchsanstalt fur Luft - und Raumfahrt E.V. (DFVLR), Institut fur Strukturmechanik, Braunschweig, Federal Republic of Germany, December 11, 1979.

"Impact Damage, Notch Sensitivity and Fracture Behavior of Composites", seminar given in Texas A&M University, November 28, 1979. Also presented in the Deutsche Forschungs - und Versuchsanstalt fur Luft - und Raumfahrt e.V. (DFVLR), Institut fur Strukturmechanik, Braunschweig, Federal Republic of Germany, December 18, 1979.

"Effects of Constituents on Fracture Behavior of Unidirectional Boron/ Aluminum Composites", presented in the symposium on "Fracture Modes in Metal Matrix Composites: in the 1980 annual meeting of the American Institute of Mining, Metallurgical and Petroleum Engineers (AIME), 24-28 February, 1980, Las Vegas, Nevada.

"Notch Sensitivity of Boron Aluminum Laminate", Presented in the 5th Annual Conference on Composites and Advanced Ceramic Materials, The American Ceramic Society, Cocoa Beach, Florida, January 18-22, 1981.

"Potential of Acoustic Emission in Monitoring Damage in Composite Materials", Seminar given at the Air Force Materials Laboratory, Wright Patterson AFB, Dayton, Ohio, November 5, 1981.

"Deformation and Failure Characteristics of Center Notched Boron Aluminum (6061)": (with M. Madhukar and M.J. Koczak), presented in the symposium on Fracture Modes in Metal Matrix Composites", the 1982 Annual Meeting of the American Institute of Mining, Metallurgical and Petroleum Engineers (AIME), Dallas, Texas, February 1982.

"Application of Acoustic Emission as an NDT Tool for Monitoring Damage in Composite Materials", seminar given in Vought Corporation, Dallas, Texas, February 15, 1982.

Ibid, in a seminar given in Texas A & M, College Station, Texas, February 18, 1982.

Ibid, in a seminar given in General Dynamics, Dallas/Fort Worth, Texas, February 19, 1982.

"Fracture Behavior and Deformation Characteristics of Metal Matrix Composites", seminar given in South-West Research Institute, San Antonio, Texas, March 1, 1982.

"Application of Acoustic Emission as an NDT Tool for Monitoring Damage in Composite Materials", presented in the Sixth Meeting of the Committee for Acoustic Emission in Reinforced Plastics (CARP), of the Society of Plastics Industry, San Antonio, Texas, March 3, 1982.

"Acoustic Emission During Damage Progression in Composites", Seminar given in the Air Force Office of Scientific Research (AFOSR), Bolling AFB, Washington, D.C., August 27, 1982.

"Acoustic Emission Techniques for Monitoring Damage During Quasi-Static and Fatigue Loading of Composite Materials", Seminar given in the Naval Air Development Center (NADC), Warminster, PA, September 16, 1982.

"Monitoring Damage Progression in Boron/Aluminum Laminates Through Acoustic Emission", (with M. Madhukar), presented in the 103rd Winter Annual Meeting of the American Society of Mechanical Engineers, November 14-19, 1982, Phoenix, Arizona.

"Potential of Acoustic Emission Technique for Monitoring Damage During Quasi-static and Fatigue Loading of Composite Materials", Symposium on NDE of Criticality of Defect in Composite Laminates, Organized by the Materials Sciences Corporation, Sponsored by the Naval Air Development Center, Valley Forge, PA, May 23-24, 1983.

"Acoustic Emission as an NDT Tool for Composites Under Quasi-Static and Fatigue Loading", presented in the Ninth Annual Mechanics of Composites Review, Department of the Air Force, Dayton, Ohio, October 24-28, 1983.

"Application of Acoustic Emission in Monitoring Damage Accumulation During Fatigue Loading in Boron/Aluminum Laminates", (with M. Madhukar), presented in the Winter Annual Meeting of the American Society of Mechanical Engineers, Boston, MA, November 13-18, 1983.

"Acoustic Emission Monitoring of Boron/Aluminum Laminates (with M. Madhukar), presented in the Eighth Meeting of the Committee for Acoustic Emission in Reinforced Plastics (CARP), of the Society of Plastics Industry, Salt Lake City, Utah, March 6-8, 1984.

"Monitoring Damage Progression in Boron/Aluminum Laminates Through Acoustic Emission" (with M. Madhukar), presented in the Seventh Composite Materials: Testing and Design, American Society for Testing and Materials, April 2-4, 1984, Philadelphia, PA.

"Detection of Failure Modes in Boron/Aluminum Monolayer Through Acoustic Emission" (with M. Madhukar), presented in the 1985 TMS-AIME Annual Meeting, New York, New York, February 24-28, 1985.

d. Anticipated Publications

Deformation and Failure Characteristics of Center-Notched Unidirectional Boron Aluminum at Room and Elevated Temperatures.

Detection of Damage Initiation and Progression in Center-Notched Boron/Aluminum Laminates During Low Cycle Fatigue Loading Through Acoustic Emission.

Effect of Temperature on Notch Sensitivity of Center-Notched Boron/Aluminum Laminates.

Fracture Behavior of Center-Notched Boron/Aluminum Laminates at Room and Elevated Temperatures.

Compliance Curves and K-Calibration of Center-Notched Boron/Aluminum Laminates at Room and Elevated Temperatures.

Effect of Matrix Ductility on the Deformation Characteristics of Center-Notched Unidirectional Boron/Aluminum.

Detection of Failure Modes in Boron/Aluminum Monolayer Through Acoustic Emission.

III. EXPERIMENTAL PROCEDURE

3.1 Introduction

The experimental procedure employed in this program included a variety of techniques from which the material mechanical properties, fracture behavior, deformation characteristics, and failure modes and processes were examined. These techniques include: a laser interferometry displacement gage for obtaining local load-crack opening displacement (COD) curves at room and elevated temperatures from which local compliance curves and the K-calibration factor were obtained; a standard compliance gage for obtaining far-field load-displacement curves together with global compliance curves; and standard strain-gages for characterizing the material elastic properties at room and elevated temperatures. In addition, nondestructive inspection techniques were employed, including acoustic emission and X-ray radiography for characterizing the internal damage prior to, during, and after failure of the composite laminates. Particular attention has been placed on monitoring damage initiation and progression through acoustic emission during quasi-static and low cycle fatigue loading. Post-failure examinations of the fracture surfaces were carried out as well using scanning electron microscopy and optical microscopy techniques.

This wide range of experimental techniques and the comprehensive experimental program supported a detailed characterization of the fracture behavior of boron/aluminum laminates. Implementation of these techniques required the purchasing of various laboratory equipment and instrumentation and extensive preparation of software for data acquisition and analysis, all of which has been executed throughout the research program. A general view of part of the testing facility is shown in Figure 1. The following is a brief description of the different experimental techniques and procedures employed.

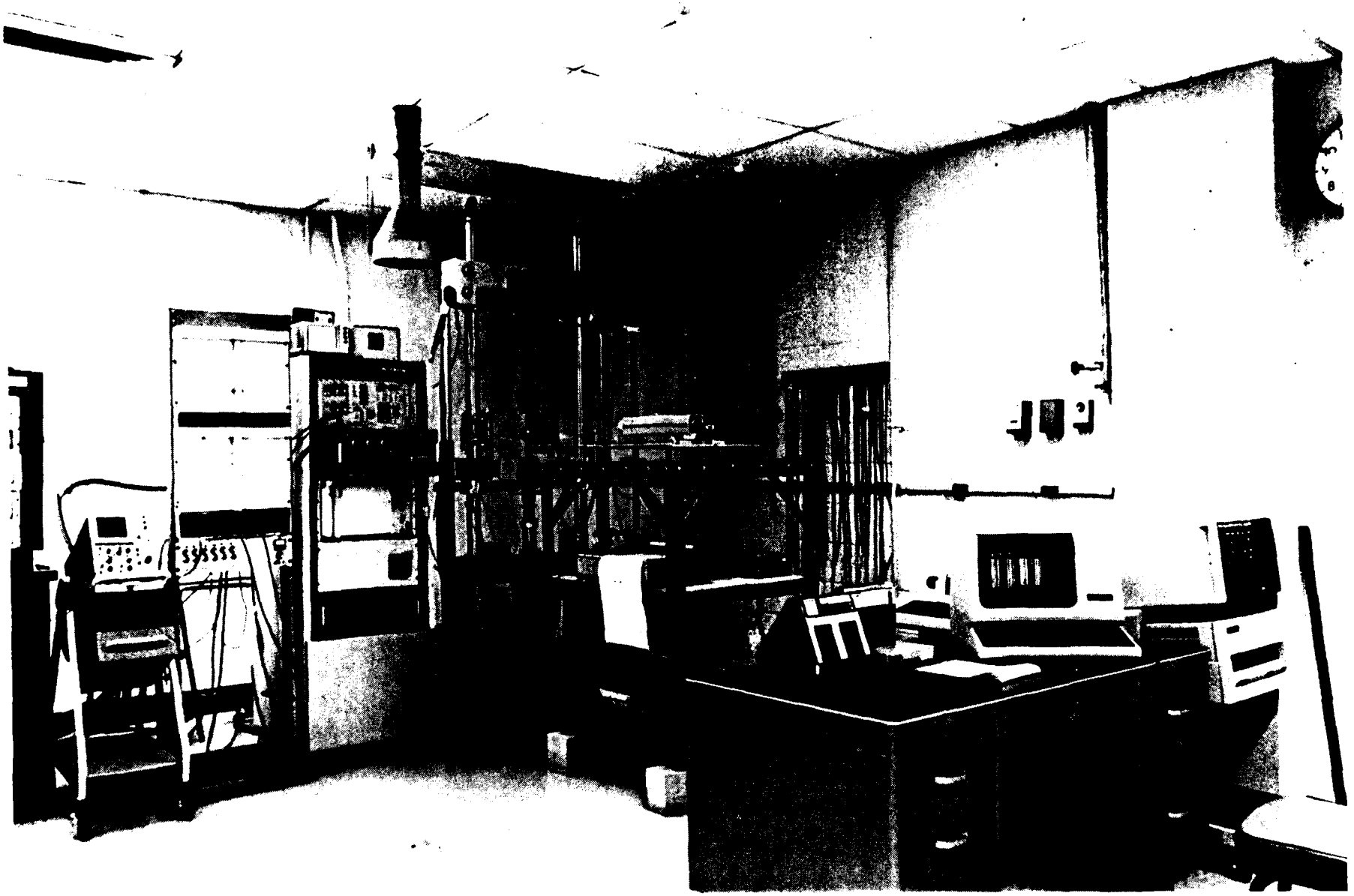

Figure 1. A general view of the testing facilities.

3.2 Material and Specimen Preparation

Six different 5.6 mil boron/aluminum 6061-F laminates were tested in this program, namely; $[0°]_8$, $[90°]_8$, $[\pm45]_{2s}$, $[0/90]_{2s}$, $[0/\pm45/0]_s$ and $[0/\pm45/90]_s$. The laminates were fabricated by D.W.A. Composite Specialties, Inc. with approximately 45-50% fiber volume fraction. The plates, approximately 200 x 200 x 1.3 mm (8.0 x 8.0 x 0.052 inch), were machined by Electro Discharge Machining (E.D.M.) into 200 x 25 mm (8.0 x 1.0 inch) for the notched tensile coupon specimens and 200 x 12.5 mm (8.0 x 0.5 inch) for the unnotched tensile coupon specimens. One half inch was left at both sides of the plates. Center notches of 1.27, 2.54, 5.08, 7.62, 10.16 and 12.7 mm (0.05, 0.1, 0.2, 0.3, 0.4 and 0.5 inch) long and 0.37 mm (0.015 inch) wide were introduced by E.D.M. All notches were perpendicular to the loading direction.

Each specimen was carefully measured at three locations along the length to ensure a minimum acceptable uniformity in specimen dimensions. Maximum variation was measured to be 0.05 mm (0.002 inch) in width and less than 0.025 mm (0.001 inch) in thickness. The location of each specimen on each of the plates was recorded so that designation of specimens according to test procedure, notch length, etc. could be made randomly to ensure reliable test results. Plates were catalogued numerically according to supplier code number and each of the spcimens within each plate was numbered according to its location and lay-up.

From each plate representative specimens were pulled out and tested for ultimate strength and stiffness. All machined notches were inspected under the microscope to examine for edge damage, and photographs were taken and data were recorded. Additional quality control testing was conducted by determining the mechanical properties of the constituents, i.e. fiber and matrices. For this purpose, individual fibers allotted for each composite plate were tested quasi-statically (to determine strength) and results were correlated with the composite strength for each plate fabricated. Matrix material was fabricated along the same procedure as the composite and its stress-strain curve was obtained to determine the effect of fabrication procedure on the metal-matrix mechanical properties.

Aluminum end tabs 25 x 25 x 1.3 mm (1.0 x 1.0 x 0.05 inch) were applied to all specimens and glued with epoxy onto the specimen ends. The surface preparation of the aluminum tabs and specimens and the curing procedures were similar to those applied in bonding strain gages. This procedure of specimen tabbing and the choice of tabbing material was found to be more advantageous in reducing unwanted emission emanating from the gripping area than the glass/epoxy tabbing material often used in testing composite coupons. All failures occurred within the gage length of the specimen.

3.3. Mechanical Test Program

Uniaxial quasi-static and constant amplitude low cycle fatigue tests were performed on a closed loop servo-hydraulic Instron testing machine (Model 1331). The quasi-static tests were carried out under stroke control mode at a rate of 0.05 in/min (0.002 mm/min). Each specimen was instrumented with an extensometer to obtain the "global" stress-strain curve. A selected number of specimens were strain-gaged to obtain "local" stress-strain curves (at room and elevated temperature) and to ensure that the extensometer data (recorded at room temperature only) were reliable. The extensometer was applied for the notched specimens as well in order to obtain "global" load-displacement curves and global compliances. Steps were taken to ensure loading axiality, and for a selected number of specimens the axiality of loading was verified. For all specimens, initial stiffness, stress-strain curves, stress and strength data were recorded.

Damage progression and failure processes were monitored through acoustic emission during low cycle fatigue loading in order to verify the applicability of this technique as a non-destructive examination procedure. All fatigue tests were carried out under load control mode at constant amplitude tension-tension loading. Different dynamic stress levels were applied at frequencies of 0.1 and 1.0 Hz. Specimens were cylced up to 10,000 or 15,000 cycles. Initial loading (first cycle)

was carried out quasi-statically to obtain additional stress-strain curves (or load-displacement curves for the notched specimens).

All run-out specimens were tested for residual strength properties, i.e. post-fatigue compliance and strength. Residual properties were compared with the initial properties obtained for the same specimen and the corresponding effect of the fatigue loading was determined.

All quasi-static test results were recorded on X-Y-Y recorders to monitor the test progression in real-time. The testing system was also interfaced with a data acquisition system (PDP 1103 Model MINC-11 of Digital Equipment Corporation). Post-test analyses provided complete load-displacement curves, stress-strain curves and mechanical properties such as strength and stiffness. Print-outs of stress-strain data in tabular form were also available.

3.4 Laser Interferometric Displacement Gage (IDG)

The laser interferometric technique has been successfully employed to measure the crack -opening-displacement (COD) of the center notched unidirectional metal matrix composite [1-3]. This technique enables measuring the COD very close to the crack surfaces (gage length of 500 μm) and was found to be highly sensitive in detecting crack tip damage, very accurate in the submicron scale, and simple to utilize. Moreover, this technique can be used in a large range of environmental temperatures [4]. Since a major effort in the experimental program of this research was the study of the fracture behavior of boron/aluminum laminates at elevated temperatures, the IDG was found to be highly advantageous for this purpose.

A detailed description of the IDG technique and the data reduction procedure can be found in [1], highlights of which are given below. When a coherent monochromatic light from a laser source impinges upon two closely adjacent, reflecting indentations on the sample, it is reflected (diffracted) back at an angle α_o with respect to the incident beam. The diffracted beams overlap, generating interference

fringe patterns on either side of the incident laser beam. As the distance, d, between the indentations changes, due to the applied load, the two fringe patterns move. As this movement is observed from a fixed position, at an angle α_o, it can be related to the change in distance, δd, between the indentations.

The equation locating the bright interference fringes is [5]: $d \sin \alpha_o = m\lambda$, where m is the fringe order (m = 0, ±1, ±2, ±3 ...), λ is the wave length of the laser beam, d is the spacing between indentations and α_o is the angle between the incident and reflected beams.

The change in distance between indentations, i.e. the displacement δd, is related to the change in fringe order, δm, at the fixed observation point by: $\delta d = \lambda \delta m / \sin \alpha_o$, where δm is the number of fringes (or fraction of fringes) passing the fixed observation position.

Using a laser beam wavelength, λ, of 0.6328 μm (He-Ne laser) and $\alpha_o = 45°$ the calibration constant $\lambda / \sin \alpha_o$ is approximately 0.95 μm. Thus, a fringe motion of $\delta m = 1$ corresponds to a displacement of about one micron. Since a shift of one half fringe movement is easily detectable, a resolution of the measurement easily reduces to a submicron scale. The displacement range in this technique is limited and depends on the spacing between indentations, dimensions of the indentations, and the power of the recording system. However, a displacement range of up to 300 μm was easily obtained in our experiments.

In order to obtain clear fringe patterns, the specimens should have a fairly flat, smooth and reflective surface. A shallow reflective indentation of a pyramidal shape was applied to the specimen surface on either side of the center of the crack with a Lietz microhardness tester. The dimensions of the indentations are approximately 50 x 50 μm. The original distance between the two indentations is about 500 μm, with edges normal and parallel to the crack surfaces, as shown in Figure 2.

The instrumentation system for measuring the crack opening displacement is simple and economical. Essentially, a similar system to the one described in [6]

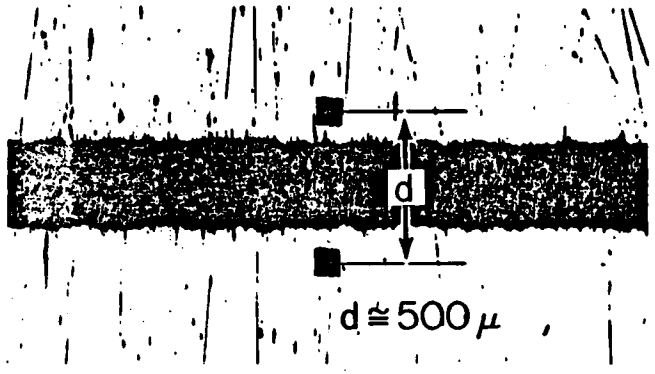

Figure 2. Photographs of indentations located on both surfaces at the center of the notch.

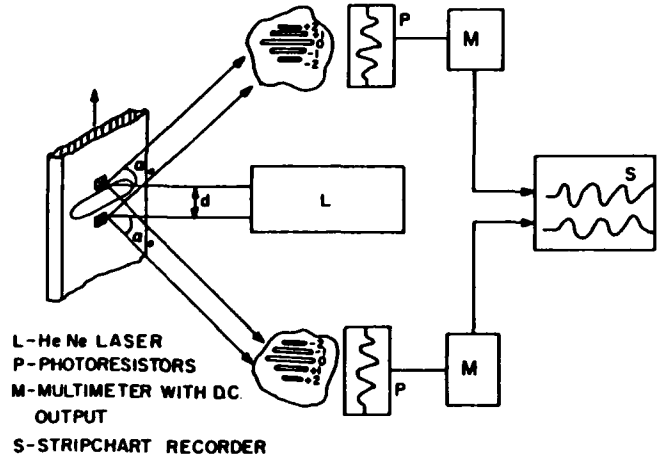

Figure 3. Schematic view of the laser interferometric displacement technique. Nominal value of d is 0.5 mm (0.02 inch) and α_o is typically 45°.

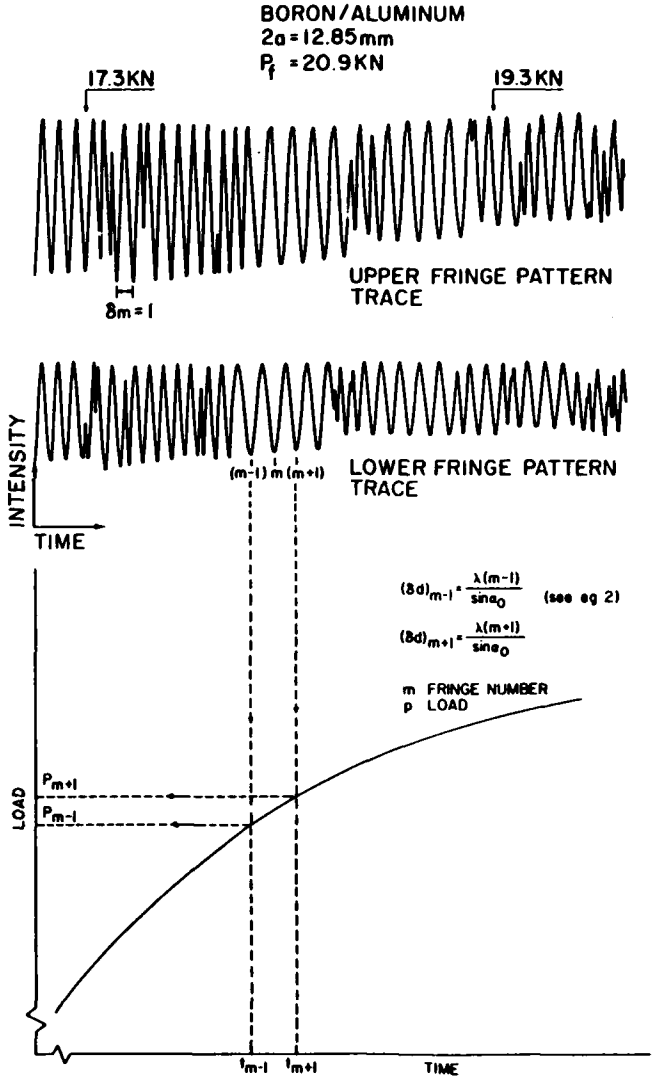

Figure 4. Schematic view of data reduction from the IDG records.

has been employed in this program, Figure 3. A comprehensive description of the laser interferometric technique is given in [7].

Figure 4 shows a typical intensity plot obtained on the stripchart recorder as the fringe patterns pass by the two stationary photoresistors. This particular plot (Figure 4) is for a boron/aluminum specimen having a 12.85 mm (0.5 inch) long crack. The data reduction of these signals is fairly easy, although very time consuming. Correlating the time at which various maxima and minima occur ($\delta m = 0, 1/2, 1, 1\ 1/2 \ldots$) with the load-time plot obtained from the Instron chart recorder output yields the required load-COD curve, Figure 4. Fringe motion occurs with any rigid body motion of the sample. However, rigid body motion can be eliminated by averaging the displacement obtained from the upper and lower (Figure 3) photoresistors [7].

In order to eliminate the time consuming process of data reduction and to increase accuracy, efforts were made to interface the IDG system with a data acquisition system (MINC 11 of Digital Equipment Corporation). For this purpose a special computer program was developed which enabled rapid and accurate calculations of the local compliance (i.e. the inverse of the slope of the load-COD curve) and plots of the final load-COD curves.

3.5 Non-Destructive Testing (NDT)

3.5.1 Introduction

Significant efforts in this research program have been directed toward the monitoring of damage initiation and progression in boron/aluminum laminates during quasi-static and low cycle fatigue loading. The purpose of this part of the research was three-fold: 1. identify and select the most appropriate NDT tool; 2. develop the proper testing methodologies and determine the variables most relevant to damage identification; and 3. investigate the failure mechanisms and processes in boron/aluminum laminates. Three non-destructive testing techniques have been considered namely; X-ray radiography, ultrasonic C-scan and acoustic emission.

The X-ray radiography applied was a Hewlett-Packard Faxitron model 43804 N X-ray cabinet with a 3 mA continuous current and beryllium window (0.63 mm thick), used with a focal distance of 6.45 mm. The specimens were X-rayed at 20 KV and exposed for 10 minutes. All photographs used Polaroid Type 57 film. It has been concluded that the standard X-ray radiography technique, as applied in this program, can detect crack tip damage and that it yields good resolution in boron/aluminum monolayers. However, the resolution is quite poor in thick (e.g. eight layers) boron/aluminum multidirectional laminates, and the procedure of obtaining reliable results is highly time consuming. The radiographs reveal primarily fiber breakage.

The ultrasonic C-scan technique was applied at the ultrasonics laboratory at Drexel University. The results obtained for a few specimens immediately indicated, as expected, that this technique does not detect any of the internal damages typical to boron/aluminum laminates. The ultrasonic C-scan technique is applicable for cases of significant matrix disbording and interfacial failures, however, these failure modes rarely occur in boron/aluminum laminates, therefore the ultrasonic C-scan technique proved to be inadequate.

Based upon the preliminary results obtained with these two NDT techniques, special attention has been given in applying the acoustic emission technique. The results indicated that it can detect and locate damage initiation and progression, and identify failure modes and processes, etc., all in real-time. Although the acoustic emission technique cannot determine size and shape of internal damage, it has the potential to determine damage criticality and material quality. Since significant program emphasis has been placed on this technique (see Sections VII and VIII), details of the instrumentation settings and parameters are given below.

3.5.2 Acoustic Emission

For all specimens tested in this program (quasi-static and low cycle fatigue loadings), acoustic emission (AE) was monitored using Dunegan/Endevco 3000

series AE instrumentation. The most pertinent operating parameters are: Transducer type S9204, system threshhold level of 1 Volt, fixed gain of 40 dB preamplifier, post-amplifier gain control of 40 dB, dead time = 3 msec. Transducers were placed at both ends of the specimen with an interim distance of approximately 127 mm (5.0 in). The length of the specimen between the transducers is divided into 100 segments for the purpose of monitoring line location, and these segments correspond to locations "0" through "100" in the location distribution histograms.

Spatial filtering (window) has been employed to eliminate unwanted noise, e.g. from the grip regions and end tabs. In order to record the emission (i.e. counts, events, and events amplitude) generated from the notch tip regions only, the pre-selected "window" has been set at 40-60, i.e., only the emission generated in locations "40" through "60" was counted and processed. Thus, the experimental results of counts and events versus load curves and the amplitude distribution histograms of events are for the emission generated from within the "window". The location distribution histograms of events, however, display all the events occurring throughout the specimen gage length between the pair of transducers. Note that the length of the pre-selected window corresponds, approximately, to the length of the compliance gage of 25 mm.

A variety of AE parameters have been recorded and studied and their inter-correlations have been analyzed. The most important parameters are:

1. Accumulative events versus load.
2. Accumulative counts versus load.
3. Count rate versus load.
4. Accumulative counts versus accumulative events.
5. Accumulative events versus displacement.
6. Accumulative counts versus displacement.
7. Count rate versus displacement.
8. Location distribution histograms at various load levels.
9. Amplitude distribution histograms at various load levels.

10. Cumulative Events Amplitude Distribution (CEAD) at various load levels.
11. "b" slope as a function of load and number of events.
12. Accumulative events versus number of cycles.
13. Event rate versus number of cycles.
14. Parameters 8-10 at various numbers of cycles.

These results were also correlated with the laminate mechanical properties, e.g. load-displacement curves, notched strength and notch sensitivity, post-fatigue global compliance and residual strength, etc. A block diagram of the experimental set-up is shown in Figure 5.

For a few specimens preliminary tests were conducted with a new AE instrumentation system installed recently. This AE system, of Physical Acoustics Corporation (PAC-3000/3004) is a microprocessor-controlled instrumentation. It allows for detailed and elaborate post-test analysis of the AE events such as event amplitude, rise-time, duration, energy and frequency spectrum accumulated during loading, including data filtering according to different criteria. The instrumentation settings, transducers selected, etc. are all similar to those used with the Dunegan/ Endevco AE system.

3.6 Failure Modes and Damage Progression

For a selected number of specimens of each laminate configuration, subjected to various elevated temperatures, fracture surfaces were examined through scanning electron microscope (SEM). The examinations were conducted in order to verify the AE results. In order to obtain a better view of the fracture surface morphology and better understand the different micro-failure mechanisms, stereo or three-dimensional views of the fracture surfaces were also obtained. The purpose of these examinations was four-fold: 1) to evaluate the fabrication quality of the specimen material tested; 2) to study the effect of elevated temperatures on the fracture surface morphology; 3) to examine the dominant micro-failure mechanisms; and

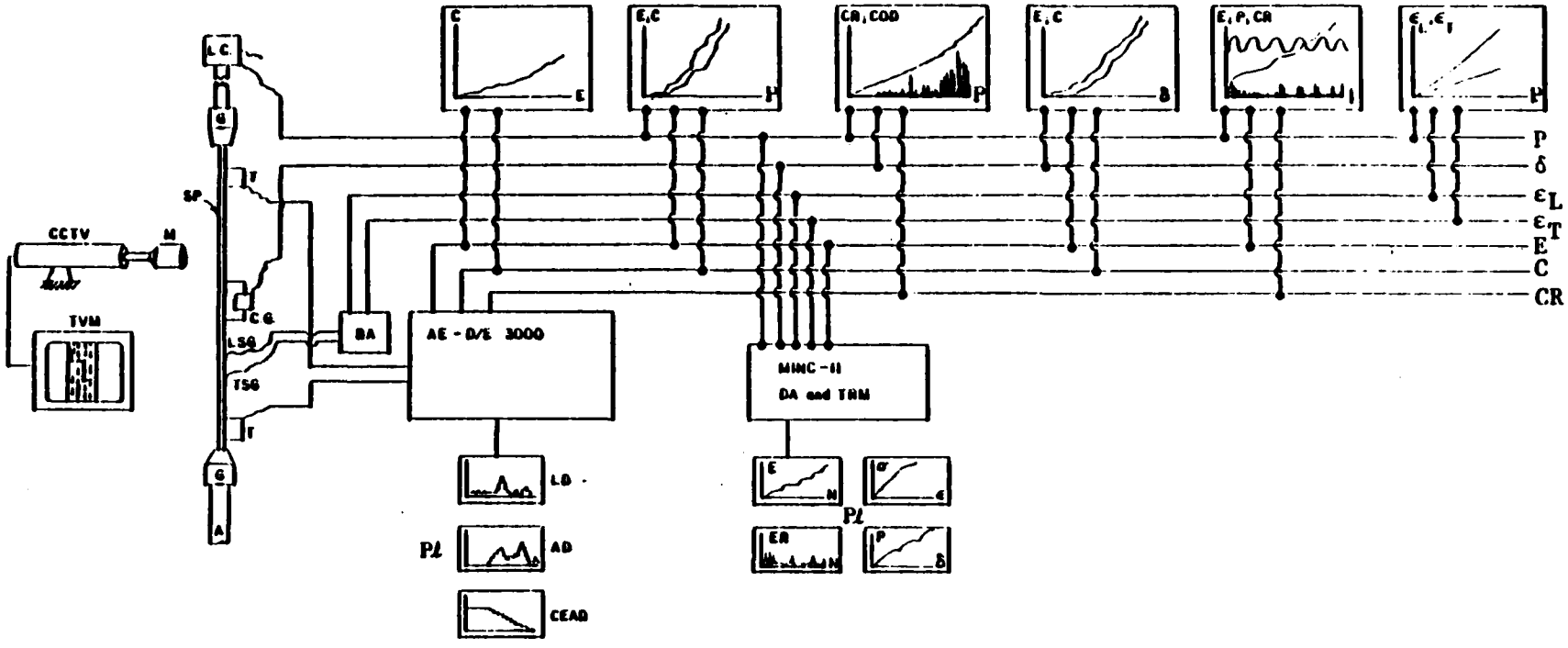

A - Actuator
AD - Amplitude Distribution (Plotter)
AE - Acoustic Emission System
BA - Bridge Amplifier
C - Counts
CG - Compliance Gage
CCTV - Closed Circuit TV System
CR - Count Rate
DA - Data Acquisition System (MINC-11)
E - Events
ER - Event Rate
G - Grips
LC - Load-Cell
LD - Location Distribution (Plotter)
LSG - Longitudinal Strain Gage
M - Microscope
N - Number of Cycles
P - Load
Pl - Plotter
SP - Specimen
T - Transducer (AE)
TSG - Transverse Strain Gage
TRM - Terminal (MINC-11)
TVM - Television Monitor
t - time
ϵ_L - Longitudinal Strain
ϵ_T - Transverse Strain
δ - Displacement
σ - Stress

Figure 5. Scematic of acoustic emission experimental set-up.

4) to distinguish between static and fatigue fracture surface morphologies. Several specimens were loaded to a predetermined load level, unloaded, and the matrix was dissolved. Crack tip damage extension and the number of broken fibers were inspected through the SEM. Photomicrographs were prepared as well to monitor internal damage and to determine actual fiber volume fraction and fiber uniformity.

Damage progression during quasi-static and fatigue loading was also monitored in real-time via a closed-circuit television (CCTV) system which provided a clear view of the crack tip region at the specimen surface at magnifications up to 250X. The observed damage progression was also correlated with the acoustic emission results and fracture surface morphologies. Results were recorded on video cassette recorder tapes which can be replayed during demonstration or presentations of the program results and for measuring crack tip damage extension.

3.7 Test Matrix

The results presented in this Final Report are based on the extensive experimental program described previously, Figure 2. It consists of the following test matrix:

Base-line mechanical properties: 45 tests

Global compliance at room temperature: 155 tests

Local compliance at room and elevated temperatures: 85 tests

Monitoring acoustic emission during quasi-static loading: 57 tests

Monitoring acoustic emission during low cycle fatigue loading: 37 tests

Notched strength at room and elevated temperatures: 255 tests

Examination of fracture surface morphologies at room and elevated temperatures: 45 tests.

3.8 References

1. J. Awerbuch and H.T. Hahn, "K Calibration of Unidirectional Metal Matrix Composites", J. of Composite Materials, Vol. 12, July 1978, pp. 222-237.

2. J. Awerbuch and H.T. Hahn, "Crack Tip Damage and Fracture Toughness of Unidirectional Boron/Aluminum Composite", J. of Composite Materials, Vol. 13, April 1979, pp. 82-107.

3. J. Awerbuch and H.T. Hahn, "Crack Tip Damage and Fracture Toughness of Unidirectional Borsic/Titanium Composite", Experimental Mechanics, 1980, pp. 105-125.

4. W.N. Sharpe, Jr., "Preliminary Development of an Interferometric Strain Gage for Use on Nosetip Materials Subjected to Thermal Shock," AFML-TR-76-63 Air Force Materials Laboratory, 1976.

5. F.A. Jenkins and H.E. White, Fundamentals of Optics, McGraw-Hill, New York, 1957.

6. D.E. Macha, W.N. Sharpe, Jr. and A.F. Grant, Jr., "A Laser Interferometry Method for Experimental Stress Intensity Factor Calibration", ASTM STP 601, American Society for Testing and Materials, 1976, p. 490.

7. W.N. Sharpe, Jr., "Interferometric Surface Strain Measurement," International Journal of Nondestructive Testing, Vol. 3, 1971, p. 56.

IV. COMPLIANCE CURVES AND K-CALIBRATION

4.1 Summary

The compliance calibration as a function of the initial crack length has been calculated for all six boron/aluminum laminates. Two different compliance calibration curves were established: the global compliance based on the far-field displacement measured by means of the conventional compliance gage, and the local compliance based on the crack opening displacement (COD) measured across the crack surfaces by means of the laser Interferometric Displacement Gage (IDG) technique, described in Section III. The compliance curves obtained with the IDG technique were found to be the more sensitive. Consequently, the IDG technique has been applied to establish the local compliance calibration curves at elevated temperatures ranging from 21°C (70°F) to 316°C (600°F). The experimental compliance curves obtained with both techniques were compared with predictions and good agreement has been established. It has been demonstrated that the K-calibration curves of the boron/aluminum laminates studied are similar to those established for isotropic materials.

4.2 Introduction

A great deal of interest has been directed in recent years toward the characterization of crack tip damage growth in composites. Most studies have dealt with the case of composite laminates subjected to quasi-static loading, however, recent efforts have increasingly been directed toward the understanding of crack tip damage progression during fatigue loading.

Studies on crack tip damage growth in composites have focused primarily on the graphite/epoxy laminates. The X-ray radiography technique is usually used to determine matrix cracking and delamination while other techniques, e.g.

thermography, attempt to determine the overall damaged zone. Through the classical visual observations, employed in structural metals, only the surface damage can be identified. In composites, however, internal non-visual damage (e.g. broken fibers) might be critical. In other words, the strandard examination techniques for damage in composites do reveal the failure process but not necessarily the critical, or "effective", crack extension.

The "effective" crack growth can be obtained, for example, through the compliance matching procedure. When a base line compliance calibration curve is available for a given material system the effective crack tip damage can be determined by comparing the instantaneous compliance with the compliance calibration curve. Thus, damage progression with load, or number of cycles, can be established. The accuracy of this procedure will depend upon the experimental procedure employed. In this study, the IDG technique has been applied in order to obtain accurate measurements of crack opening displacements.

The major objectives of this study are summarized below:

1. Develop a test methodology to measure crack opening displacement of composites at elevated temperatures.

2. Develop software for interfacing the IDG with a data acquisition system to obtain load-COD curves in real time.

3. Determine experimentally the compliance calibration curves at room and elevated temperatures

4. Determine experimentally the K-calibration for the subject laminates.

5. Correlate the experimental results with predictions.

4.3 Compliance Curves

4.3.1 Global Compliance at Room Temperature

From both test procedures (IDG and Compliance gage), the compliance

calibration as a function of the initial crack length has been calculated. Since two different displacements were measured, the appropriate compliances were defined accordingly: the local compliance, C_ℓ, is based on COD obtained from the IDG, and the global compliance, C_g, is based on the far-field displacement.

The global compliances were measured directly from the load-displacement curves obtained with the compliance gage, when the recording system was set on higher resolution. The results shown for two of the laminates in Figure 1 indicate significant scatter in the values of the global compliance. Moreover, the global compliance is not sensitive to initial crack length. The compliange gage (gage length of 25.4 mm (1.0 inch)) records both the crack opening due to the actual crack tip damage and the elastic deformation of the bulk of the material within the gage length. Thus, the effect of the crack tip damage on the total deformation recorded by this technique is relatively small. The scatter in the results could be due either to small differences in mounting the compliance gage on the specimens or to the inherent scatter in the subject material, or to a combination thereof.

The prediction of the global compliance is based on the application of the energy release rate approach. The formulation is well established in the literature, e.g. [1], and will not be repeated here. The expression used for C_g prediction for a center notched specimen is:

$$C_g = \frac{\alpha}{E_x B}\left[1.566(2a/W)^2 + 0.268(2a/W)^3 - 0.438(2a/W)^4 + 1.865(2a/W)^5 + 0.247(2a/W)^6 - 0.393(2a/W)^7 + 0.911(2a/W)^8\right] + \frac{L}{BWE_x} \qquad (1)$$

where W and B are the specimen width and thickness, respectively, 2a is the initial crack length, L is the gage length of the compliance gage, and E_x is the axial stiffness of the laminate.

The orthotropic correction factor, α, (being 1 for quasi-isotropic laminates) is given by:

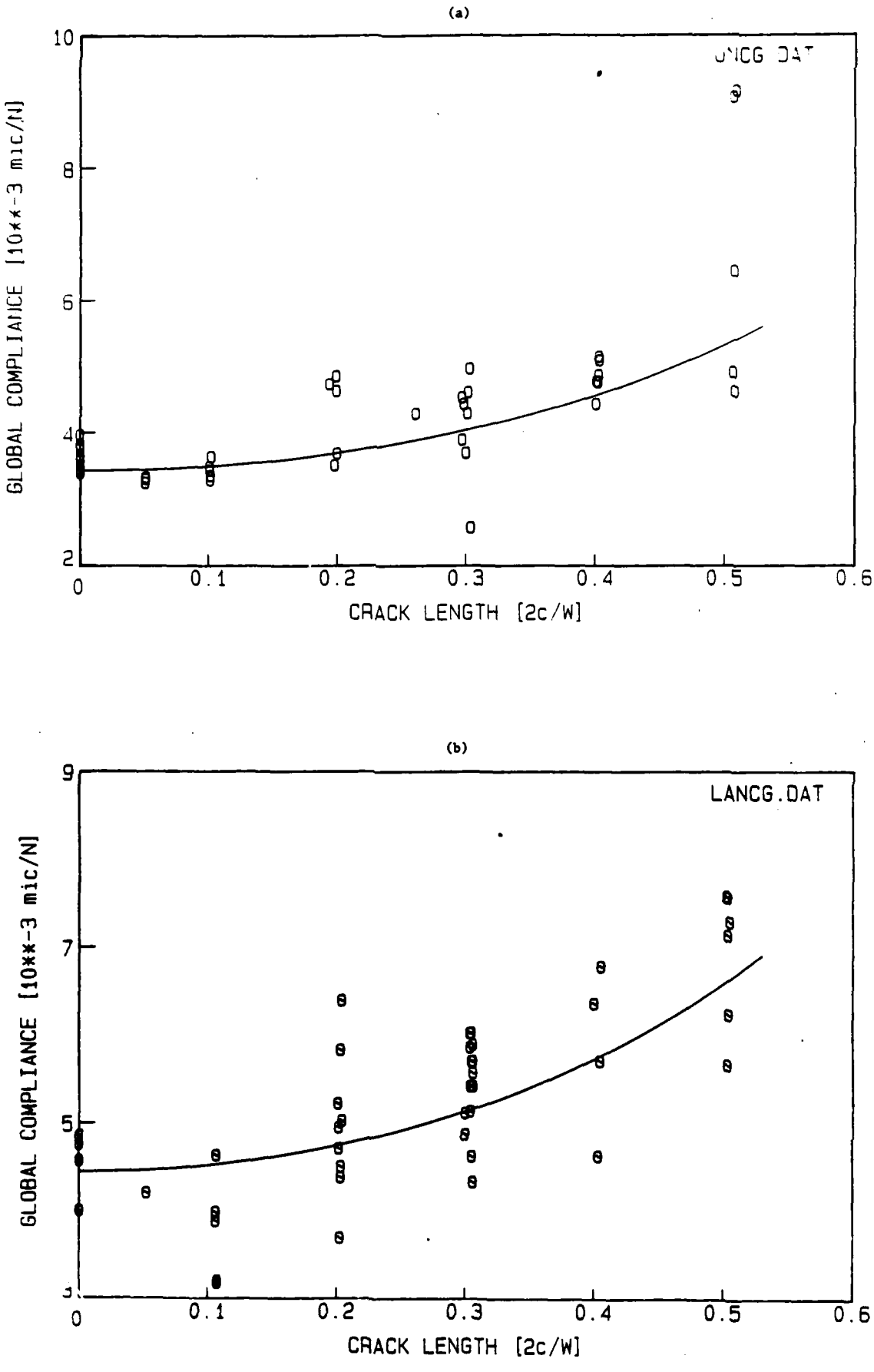

Figure 1. Global compliance versus crack length: a. $[0]_8$, $\alpha = 1.2$; b. $[0/\pm45/0]_s$, $\alpha = 1.05$ laminates.

$$\alpha = \frac{1}{S_{22}} \left[\frac{S_{11}S_{22}}{2}\right]^{1/2} \left[\frac{S_{22}}{S_{11}} + \frac{2S_{12} + S_{66}}{2S_{11}}\right]^{1/2} \quad (2)$$

where S_{ij} are the orthotropic plate compliances and the width correction factor Y used in Equation (1) is [2]:

$$Y = 1 + 0.1282(2a/W) - 0.2881(2a/W)^2 + 1.5254(2a/W)^3 \quad (3)$$

Note that Equation (3) uses the isotropic width correction factor. It has been shown previously, e.g. [1], that this expression of Y is applicable for composites. Further discussion on the applicability of the isotropic width correction factor for boron/aluminum laminates will be discussed later in this Section.

The comparison between the experimental results for the global compliance and prediction according to Equation (1) is shown in Figure 1. Due to the large scatter in the experimental results no conclusive comparison can be made. However, the experiments follow the trend of the predicted global compliance values. For different laminates different values of global compliance were recorded, as predicted when the appropriate material elastic constants are used.

4.3.2 Local Compliance at Room Temperature

In order to obtain accurate data on the local compliance, each specimen was loaded to a predetermined load level (about 10% of the expected failure load) and then unloaded. This procedure was repeated three to six times. An examination of the load-COD curve reveals that the unloading curves as well as the subsequent loading curves are linear. In some instances, the first unloading revealed a very small amount of permanent crack opening, approximately 1-2μm, which indicates a small amount of crack tip damage. However, this damage is subcritical and practically does not affect the compliance measurements. A representative set of three initial loading curves, obtained at room and elevated temperatures for a

unidirectional specimen, are shown in Figure 2 together with the local compliance values, C_ℓ. The experimental data in the Figure were obtained from the readings of the upper and lower photocells, as described in Section 3.4. The dashed lines are the best fit obtained through linear regression and the solid line is the average value of the crack opening displacement. The results indicate that the values of C_ℓ (the inverse of the slope of the solid lines in Figure 2) are very close to each other, having a very small standard deviation (S.D.). Similar results were obtained for all other laminates studied, e.g. Figure 3. At elevated temperatures the IDG measurements also result in highly reproducible values of the local compliance as shown in Figures 2-3.

The local compliance as a function of initial crack length for four different laminates is shown in Figure 4. The local compliance values shown in the Figure are the average values of the three to six loadings conducted for each specimen mentioned previously. The results shown in Figure 4 indicate that the local compliance is highly sensitive to crack length, much more so that the global compliance values shown in Figure 1, and exhibits relatively small scatter. The higher sensitivity of the local compliance curves enables a more accurate determination of the crack tip damage zone size.

The actual crack opening displacement (COD) can be predicted from elastic stress analysis, and the local compliance curve can be calculated and compared with the experimental COD (and compliance) obtained with the IDG. Since the COD was practically measured at the crack surfaces (gage length of 0.02 inch) and at the center of the crack, the predicted displacement v in the loading direction of the top crack surface is given by [3-5]:

$$v = \frac{2\sigma a \alpha}{E_x} Y \qquad (4)$$

Since the COD is the relative displacement at the center of the crack, which is equal to 2v, the local compliance becomes:

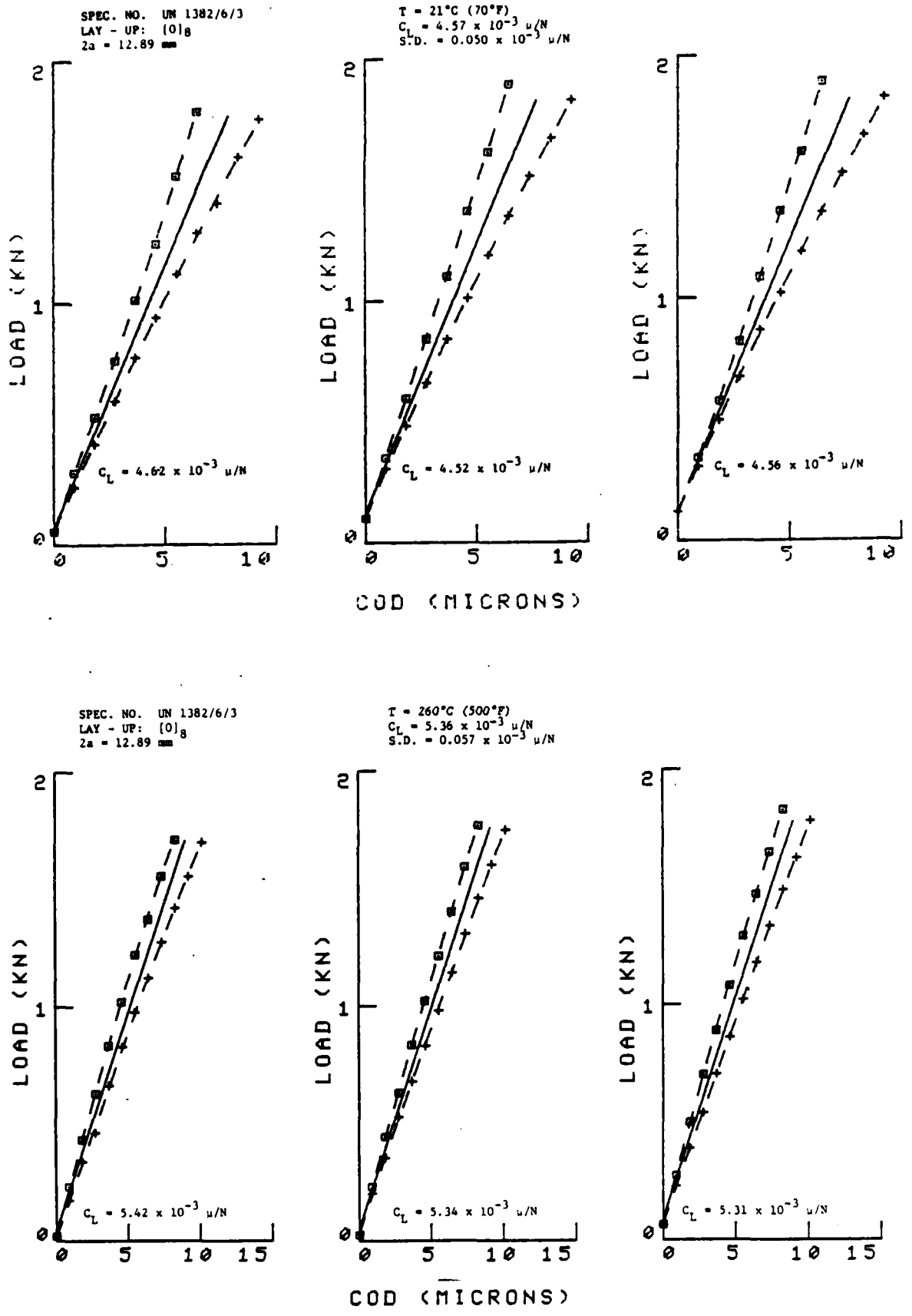

Figure 2. Example of three load-COD curves at initial loading for unidirectional boron/aluminum specimen obtained with the IDG at room and elevated temperatures.

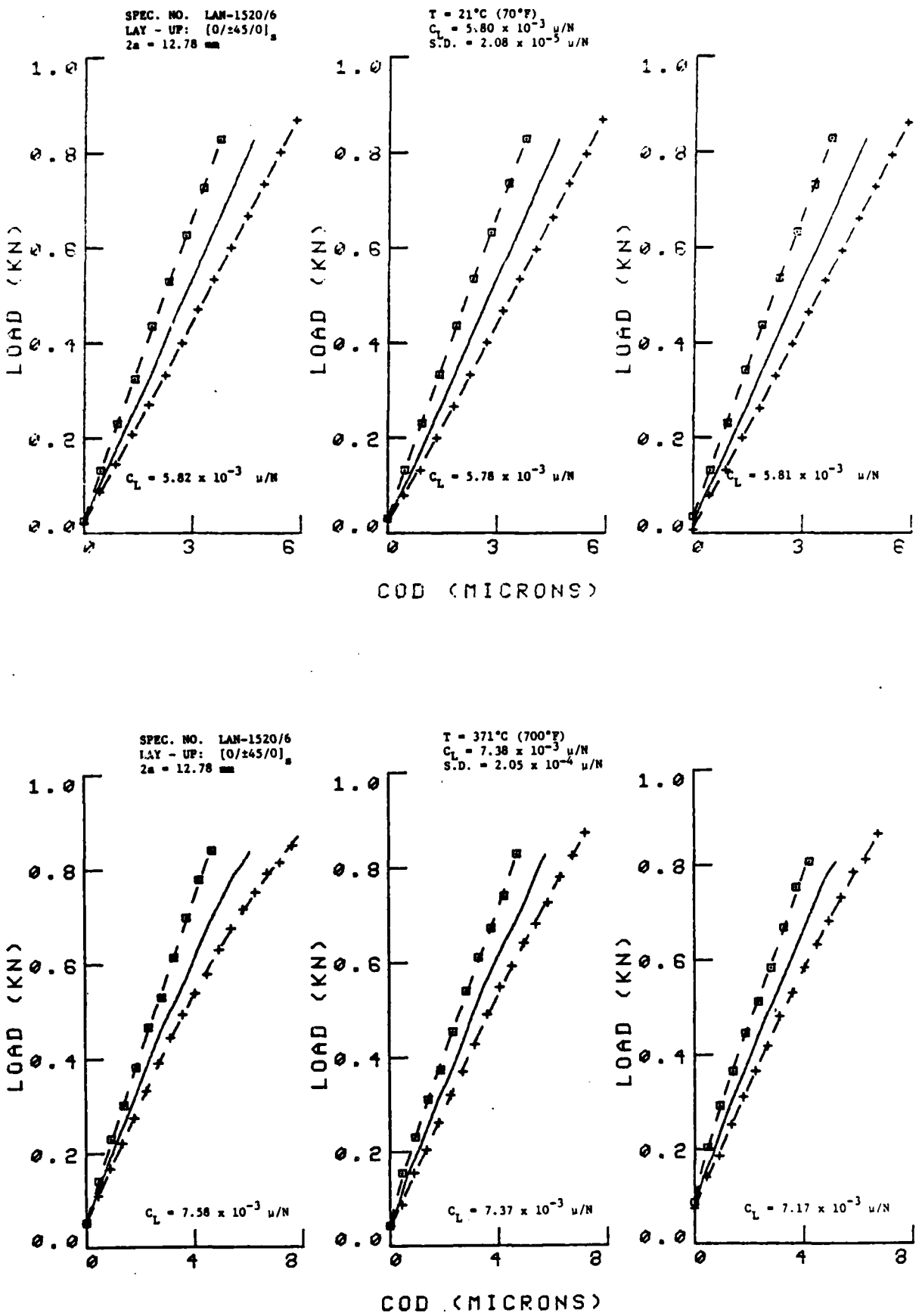

Figure 3. Example of three load-COD curves at initial loading for $[0/\pm45/0]_s$ boron/aluminum laminate obtained with the IDG at room and elevated temperatures.

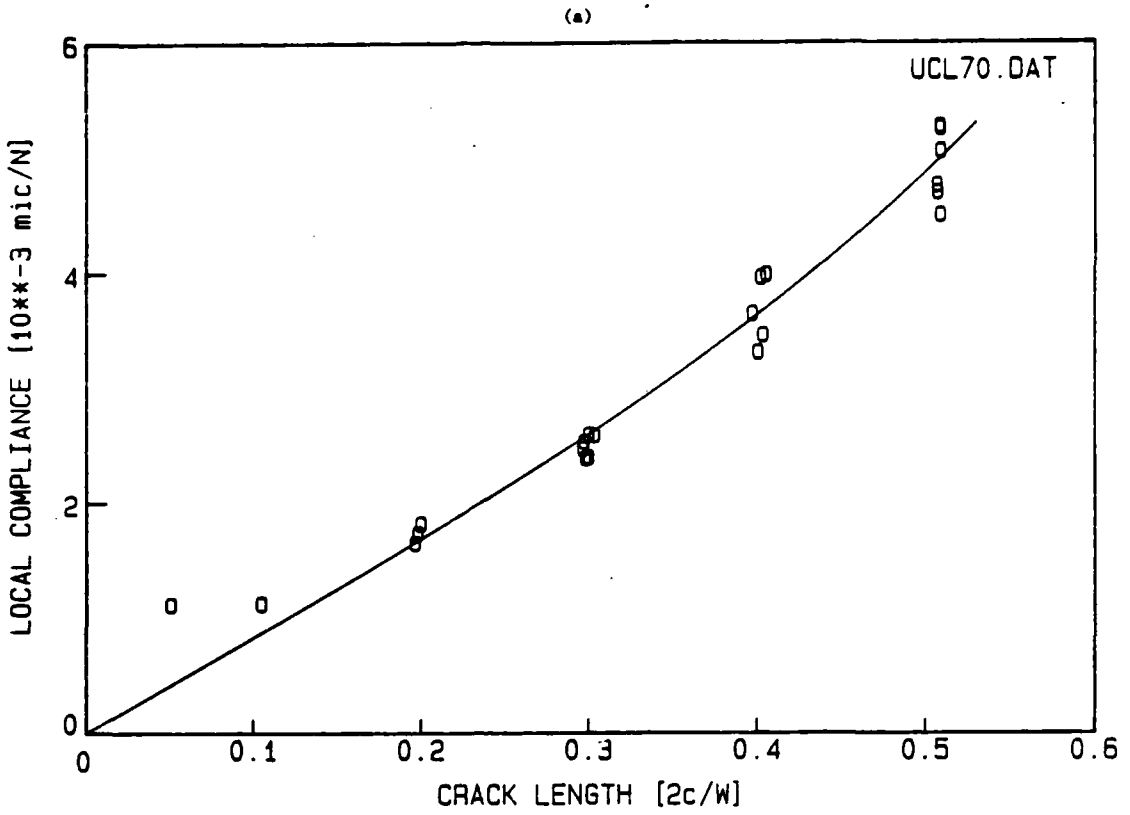

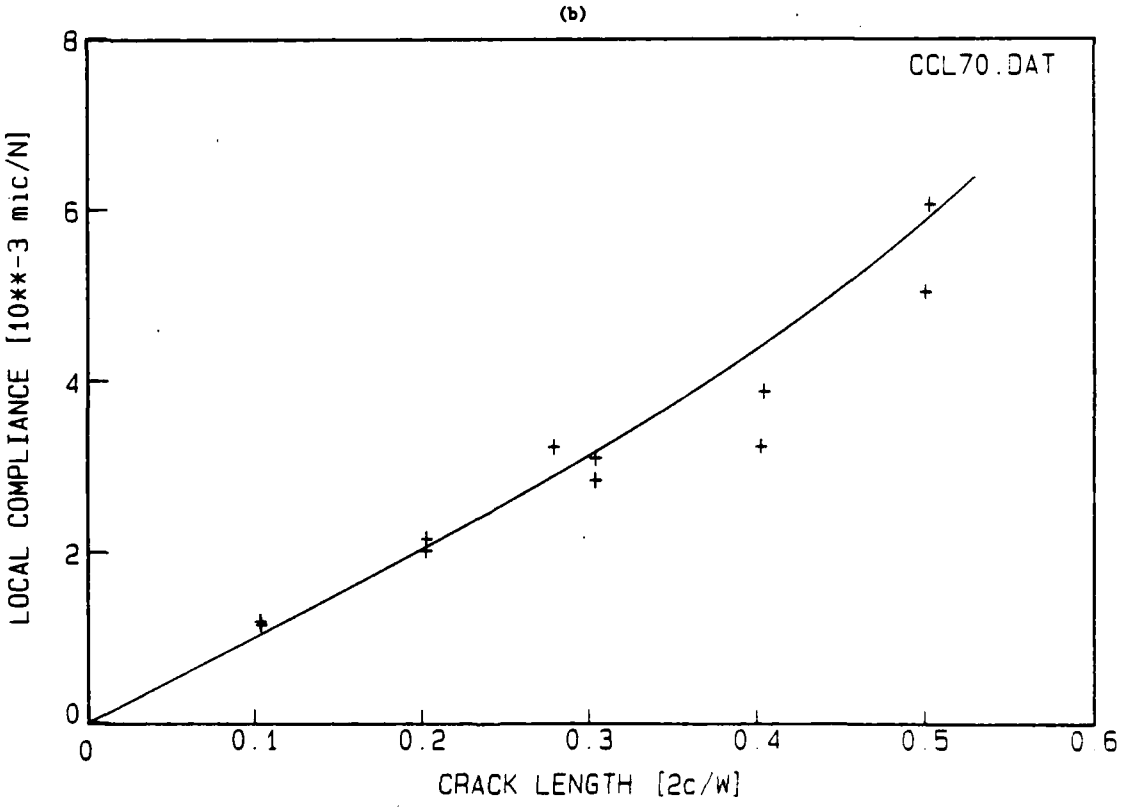

Figure 4. Local compliance versus crack length: a. $[0]_8$, $\alpha = 1.2$; b. $[0/90]_{2s}$, $\alpha = 1.05$; c. $[0/\pm45/90]_s$, $\alpha = 1.0$; d. $[0/\pm45/0]_s$, $\alpha = 1.05$ laminates.

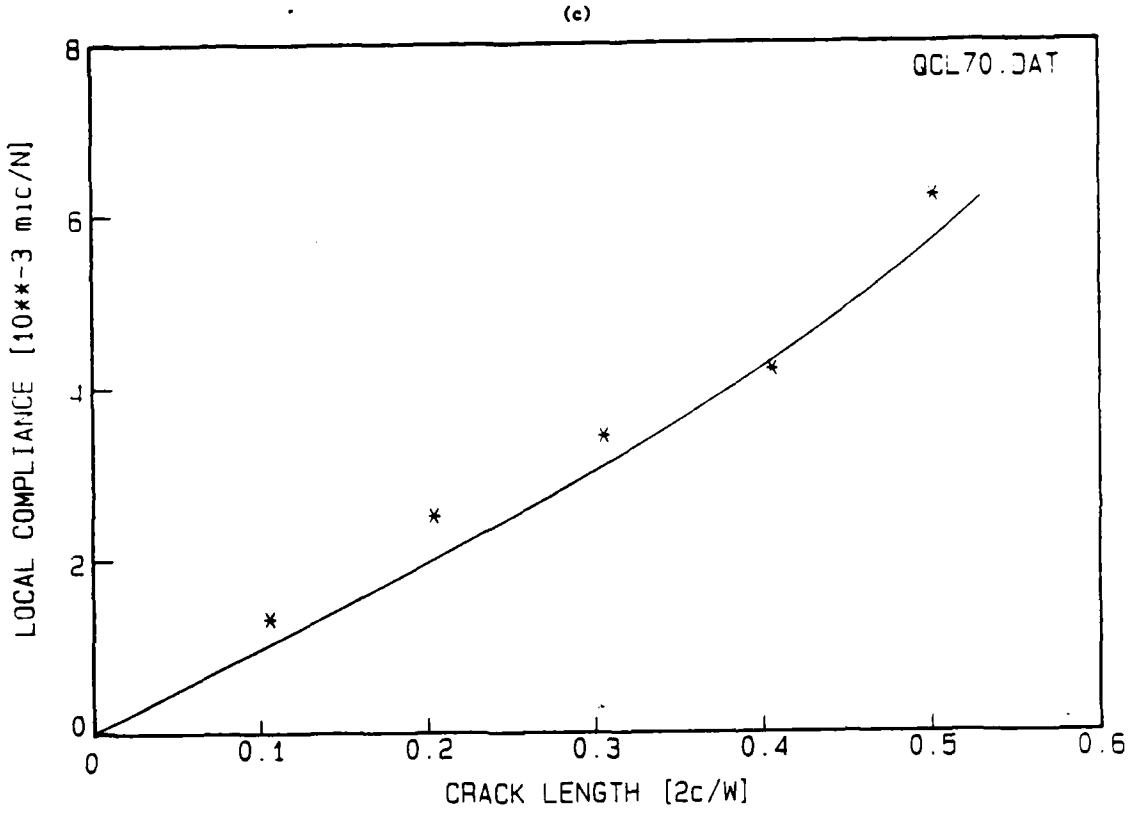

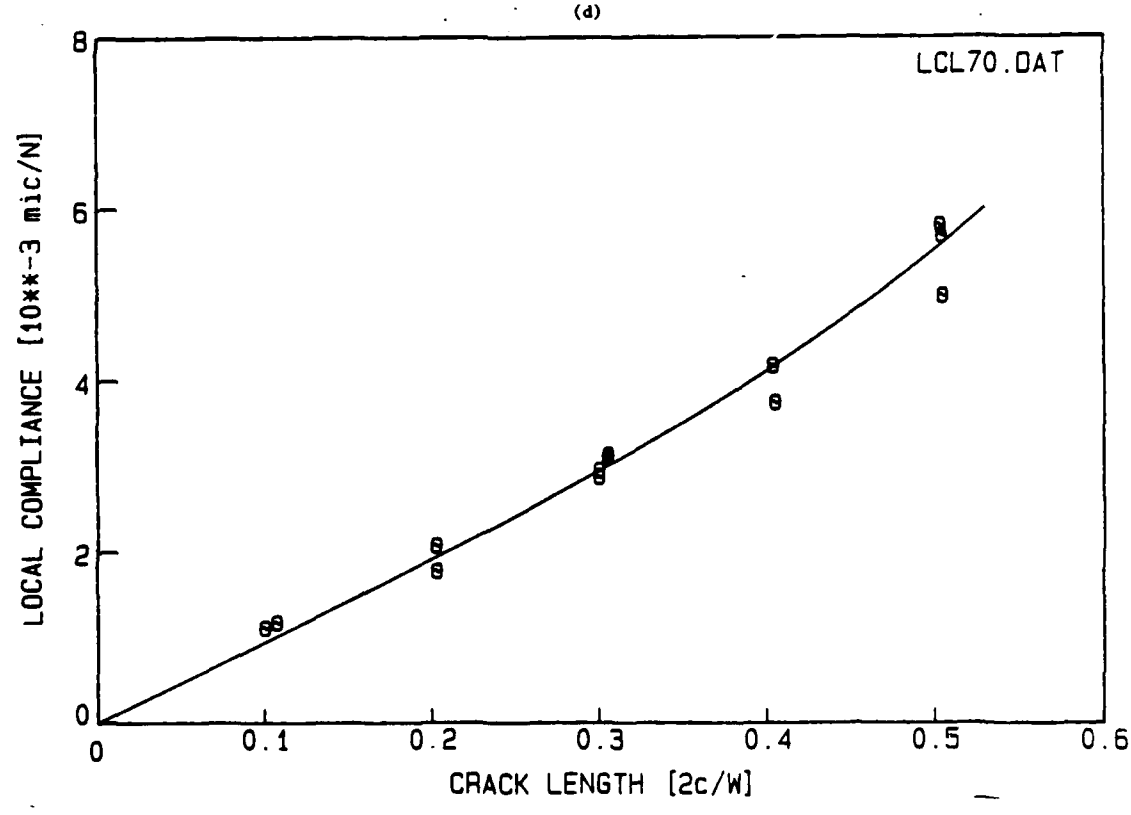

Figure 4. Continued.

$$C_\ell = \frac{COD}{BW} = \frac{2\alpha}{E_x B} \frac{2a}{W} Y \quad (5)$$

The predicted local compliance curve (Equation (5)), based on the isotropic Y, was compared with the experimental results and an excellent agreement has been established for all laminates studied, Figure 4.

The experimental compliance can also serve for calculating the width correction factor Y by rewriting Equation (5) as follows:

$$Y = \frac{E_x B}{2\alpha} \frac{C_\ell}{2a/W} \quad (6)$$

The term C_ℓ (2a/W) is the secant slope to each experimental value of the compliance in Figure 4. Thus Y is proportional to this slope. A comparison between the experimental results for Y and Equation (6) is shown in Figure 5, evincing quite a good correlation for the larger crack lengths. For the smaller crack lengths the scatter is quite high, but it must be remembered that any experimental scatter in compliance measurements causes a larger error in the slope, $C_\ell/(2a/W)$, for small crack lengths. Also, the analytical equations formulated for sharp cracks will no longer apply to real cracks of a smaller length, since the crack width-to-length ratio becomes larger. In addition, any crack tip damage will have a more significant effect on the elastic compliance so that the initial slope of the subsequent loading-unloading curve may not accurately represent the compliance. However, analytically, the deviation of Y from the isotropic values is negligible as the crack length gets smaller [6], and no K-calibration is needed for small cracks. Y is smaller than 1.001 for cracks having 2a/W less than 0.1, thus poor correlation for small cracks is of little significance.

4.3.3 Local Compliance at Elevated Temperatures

Elevated temperatures load-COD and local compliances were obtained for all laminates studied. Comparison between the compliance values obtained at room and elevated temperatures, Figures 2-3, shows that local compliance increases

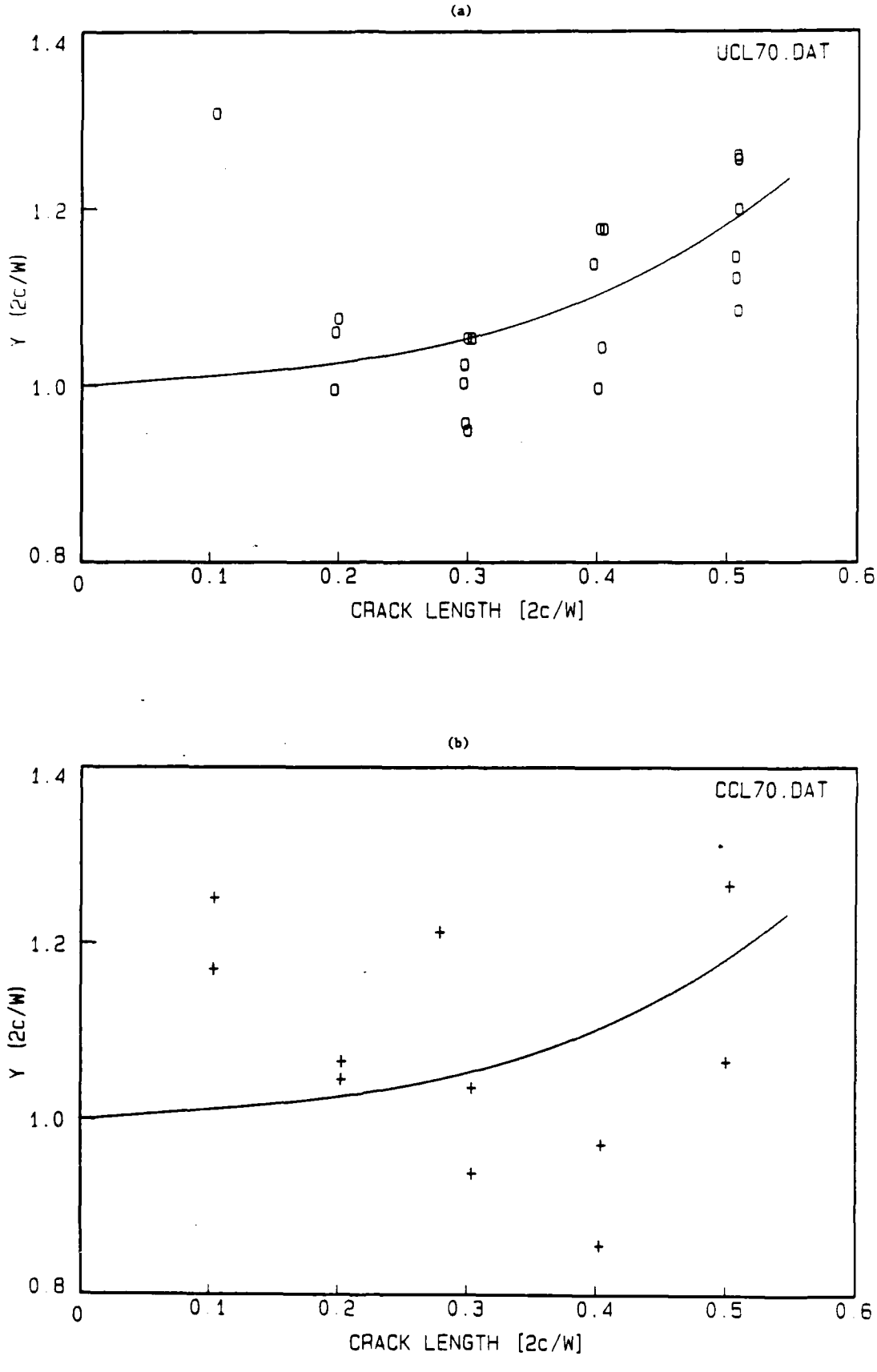

Figure 5. Comparison of experimental K-calibration factors with theoretical isotropic curve (Equation (3)) for: a. $[0]_8$; b. $[0/90]_{2s}$; c. $[0/\pm45/90]_s$; d. $[0/\pm45/0]_s$ laminates.

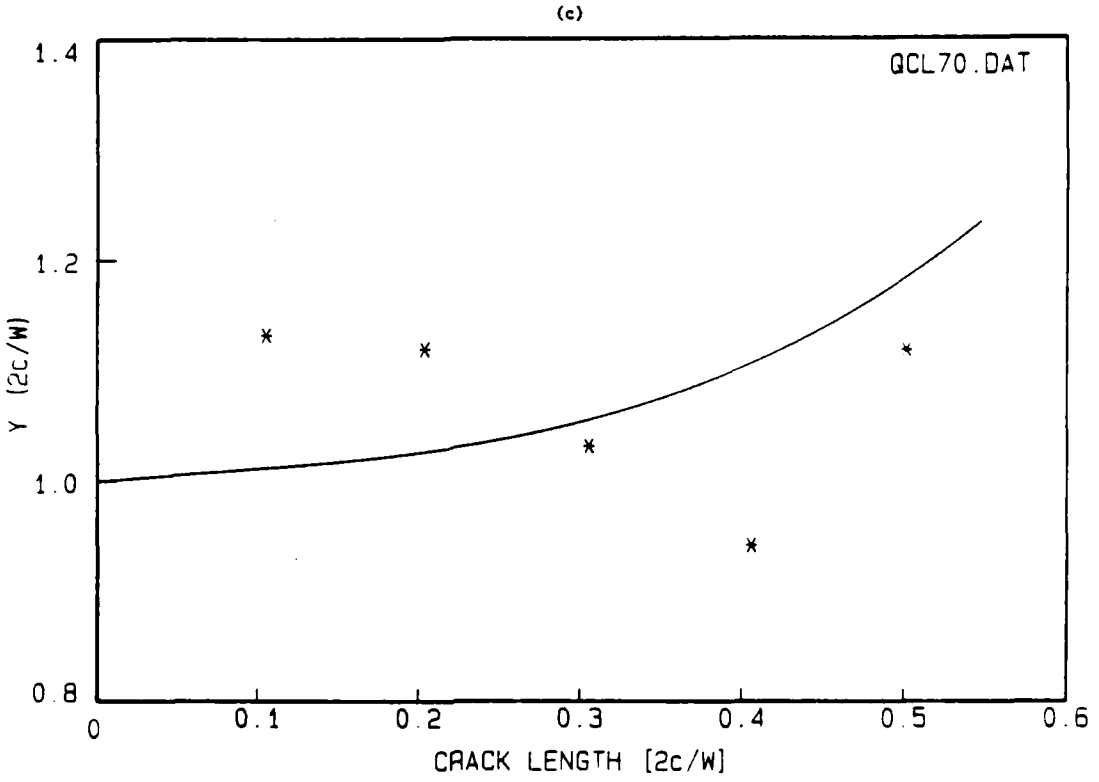

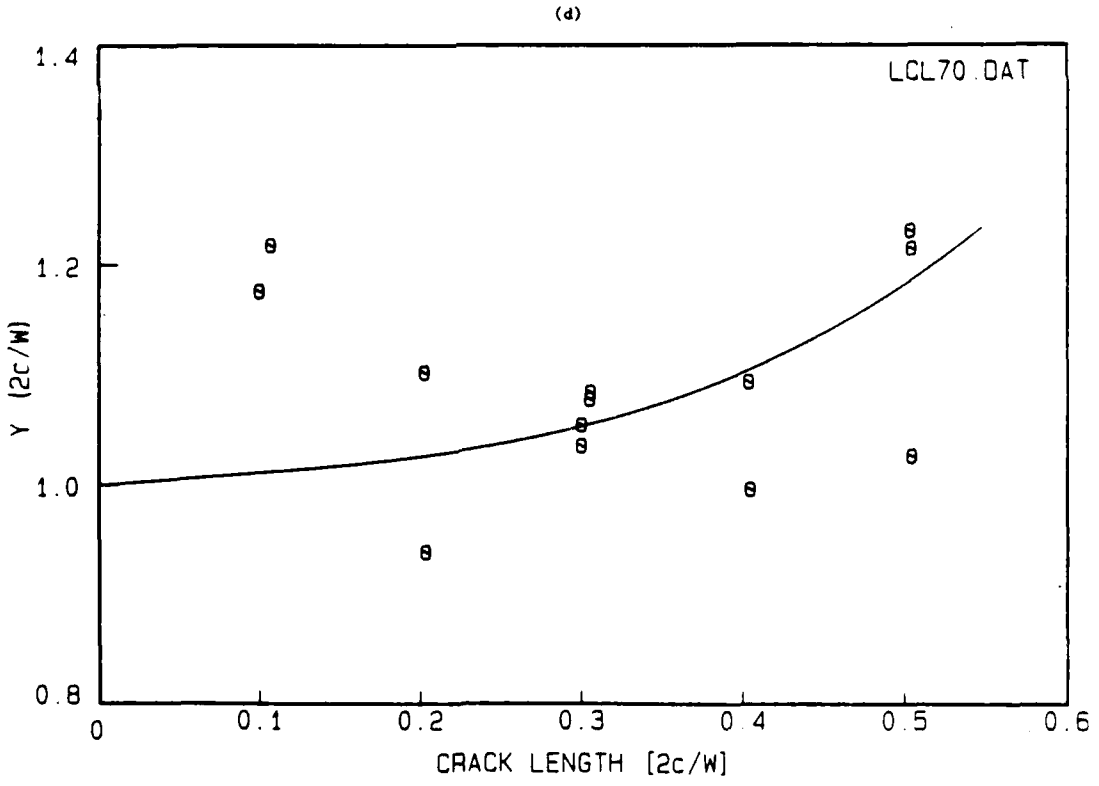

Figure 5. Continued.

with temperature, as expected. Representative results of the local compliance curves at elevated temperatures are shown in Figure 6. The solid lines are the predictions according to Equation 5. In applying Equation 5 the laminate properties at elevated temperatures should be used. It has been determined that the values of E_x remain independent of temperature up to 315°C (600°F). The test program for determining the other laminate elastic constant has not been completed as yet, thus, the values of α (Equation (2)) have been estimated as indicated in Figure 6. It should be noted that α varies approximately between 1.0-1.6, thus the error in predicting the local compliance calibration curve by selecting a median value for α is relatively small.

Special efforts have been placed on precisely determining the effect of temperature on local compliance. In the course of the program it has been established that in order to obtain a reliable relationship between local compliance and temperature, and eliminate the effect of scatter and notch length among the different specimens, all elevated temperature tests should be conducted on the same specimen. Consequently, following the room temperature test, temperature was raised incrementally, in 100°F increments up to 371°C (700°F). At each temperature the specimen was subjected to three to six loading-unloading cycles and local compliance has been determined. The average value of these compliances has been plotted as a function of temperature, Figure 7. Results indicate that at least up to 93°C (200°F), temperature has practically no effect on the local compliance. A further increase in temperature reveals a significant increase in local compliance, primarily beyond 204°C (400°F). The effect of temperature is mostly attributable to differences in the elevated temperature properties of the matrix material. Handbook data on aluminum alloy 6061 indicate significant degradation in mechanical properties and increased ductility as temperature increases beyond 204°C (400°F).

Similar results were obtained, to varying degrees, for all laminate configurations and crack lengths. A summary plot of representative results obtained for

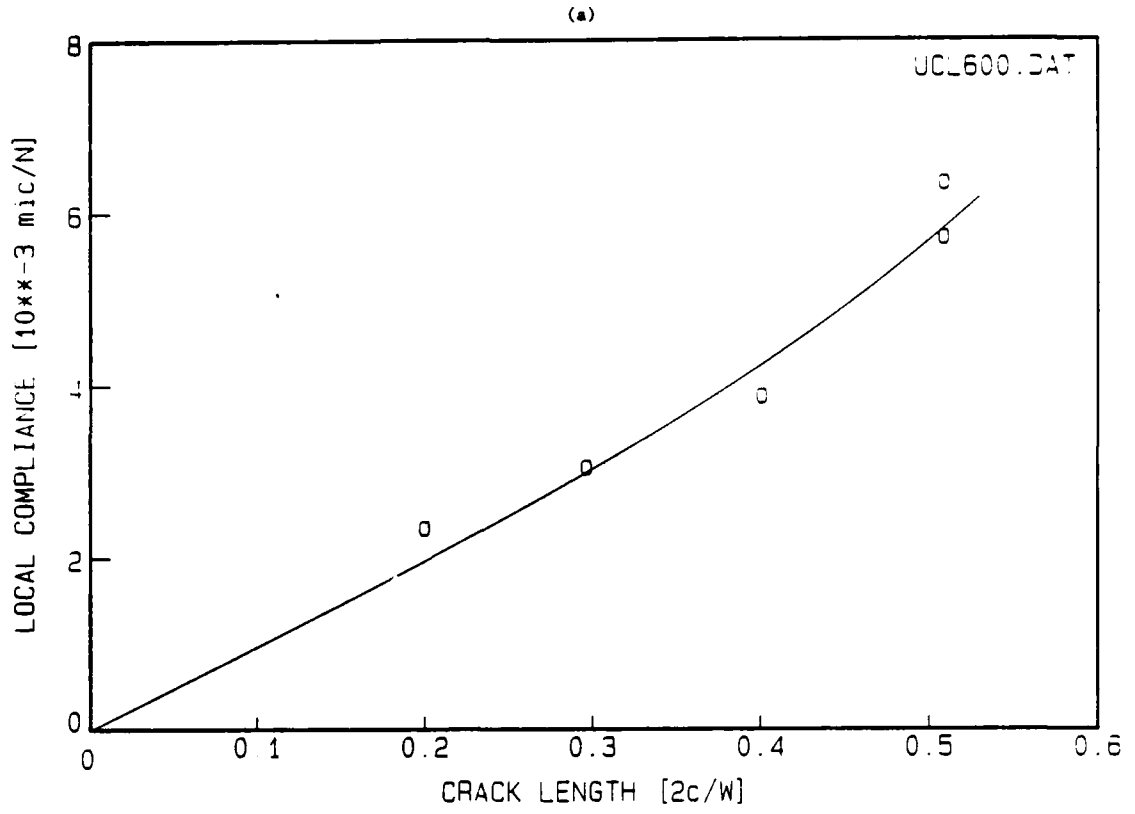

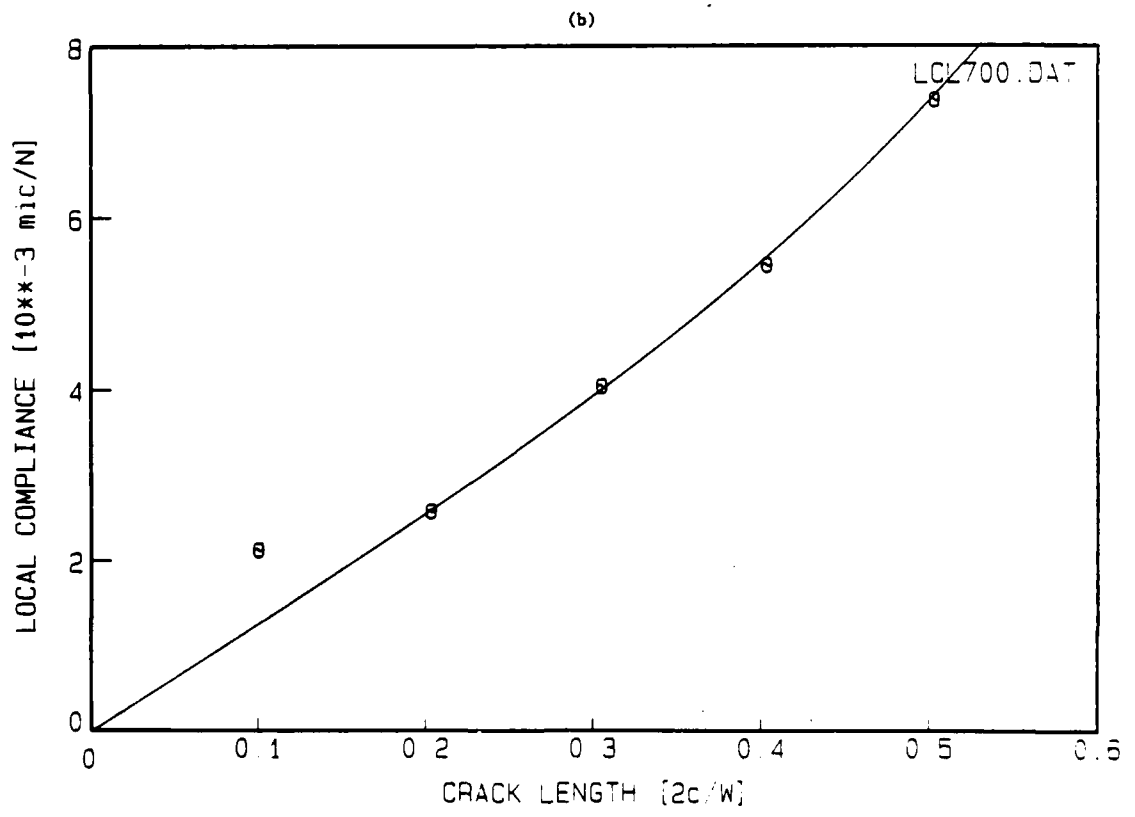

Figure 6. Local compliance versus crack length. a. $[0]_8$ at 315°C (600°F), α = 1.4; b. $[0/\pm45/0]_s$ at 371°C (700°F), α = 1.4.

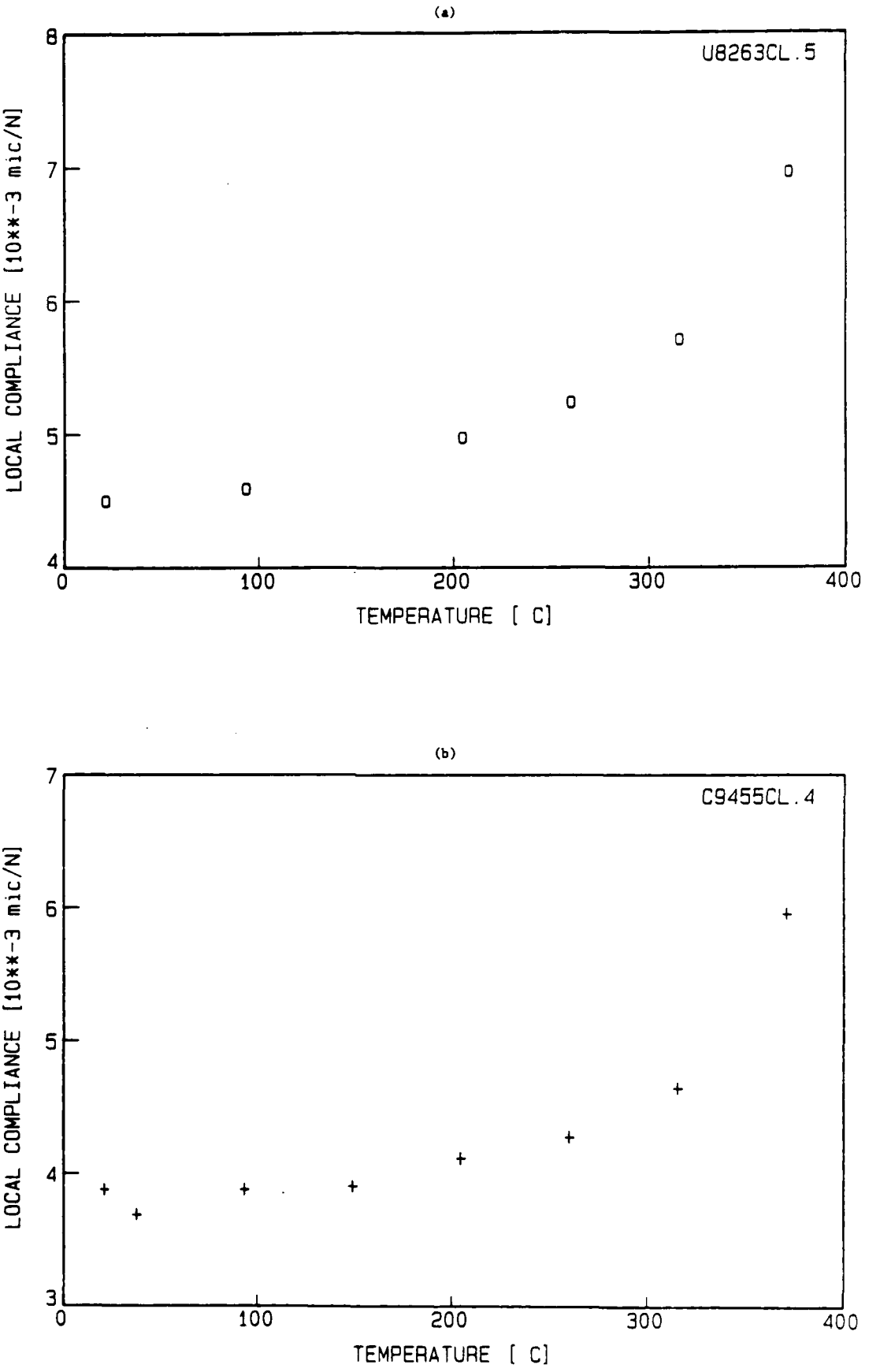

Figure 7. Local compliance versus test temperature for: a. $[0]_8$, 2a/W = 0.509; b. $[0/90]_{2s}$, 2a/W = 0.404; c. $[0/\pm45/0]_s$, 2a/W = 0.305; d. $[0/\pm45/0]_s$, 2a/W = 0.404.

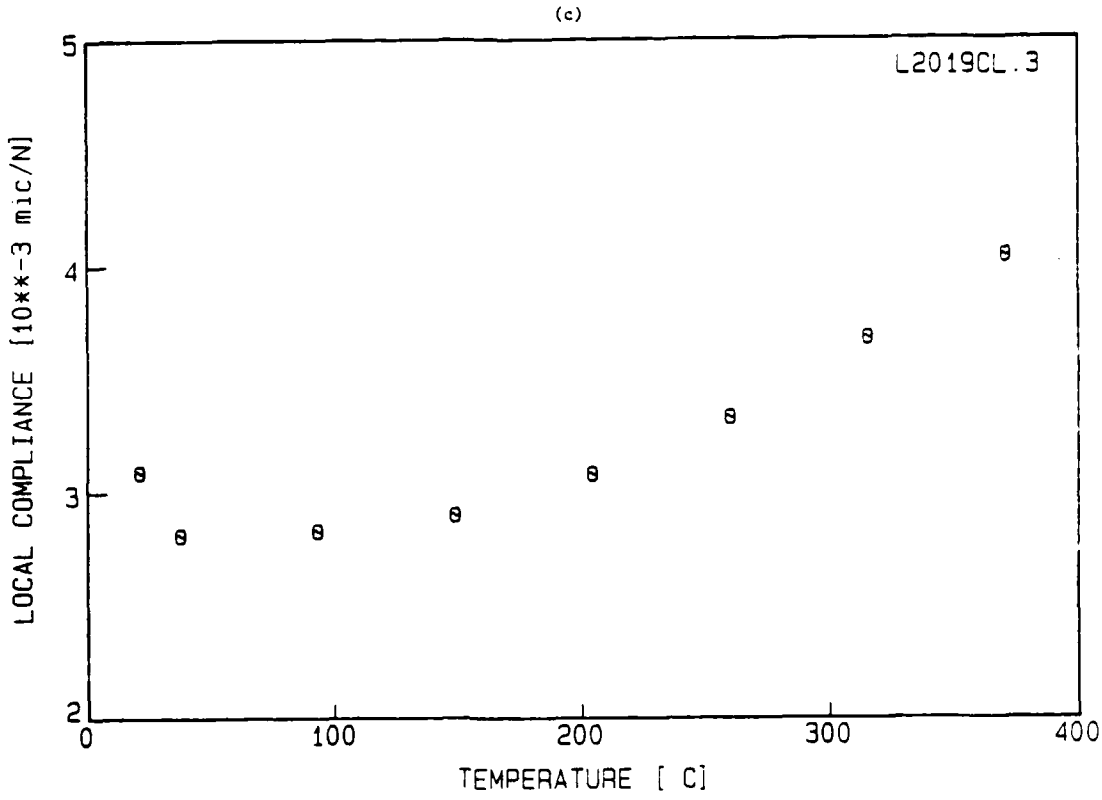

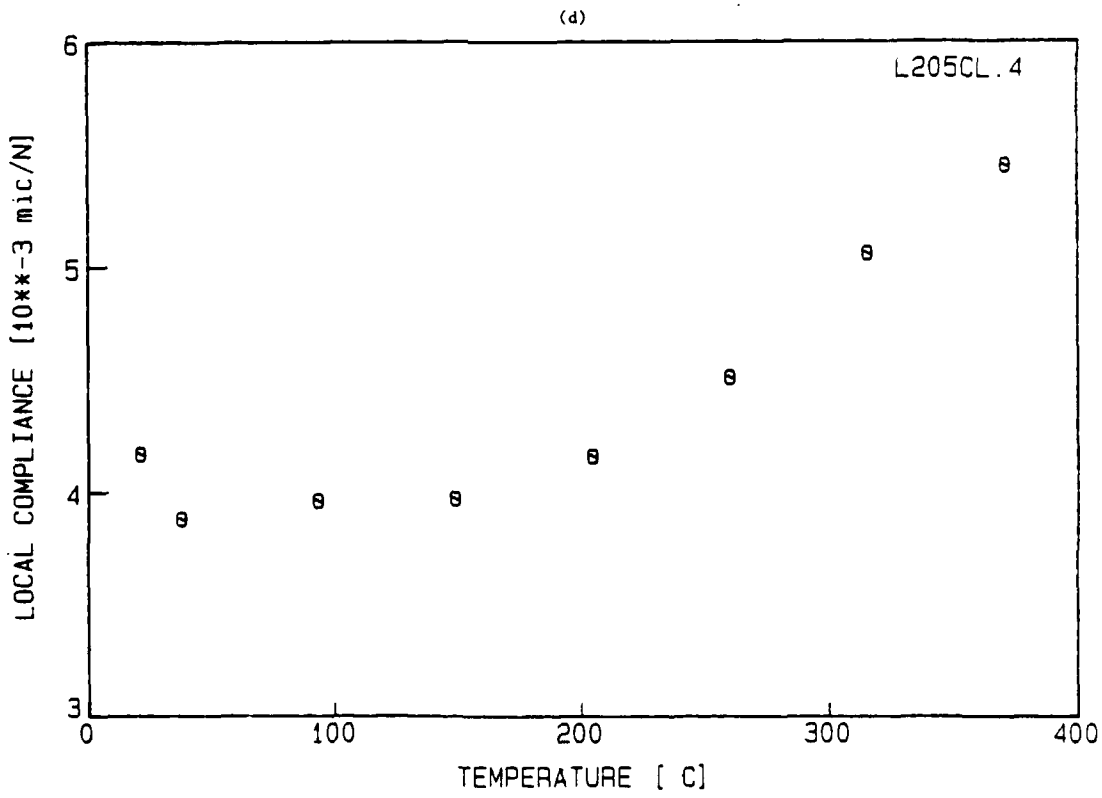

Figure 7. Continued.

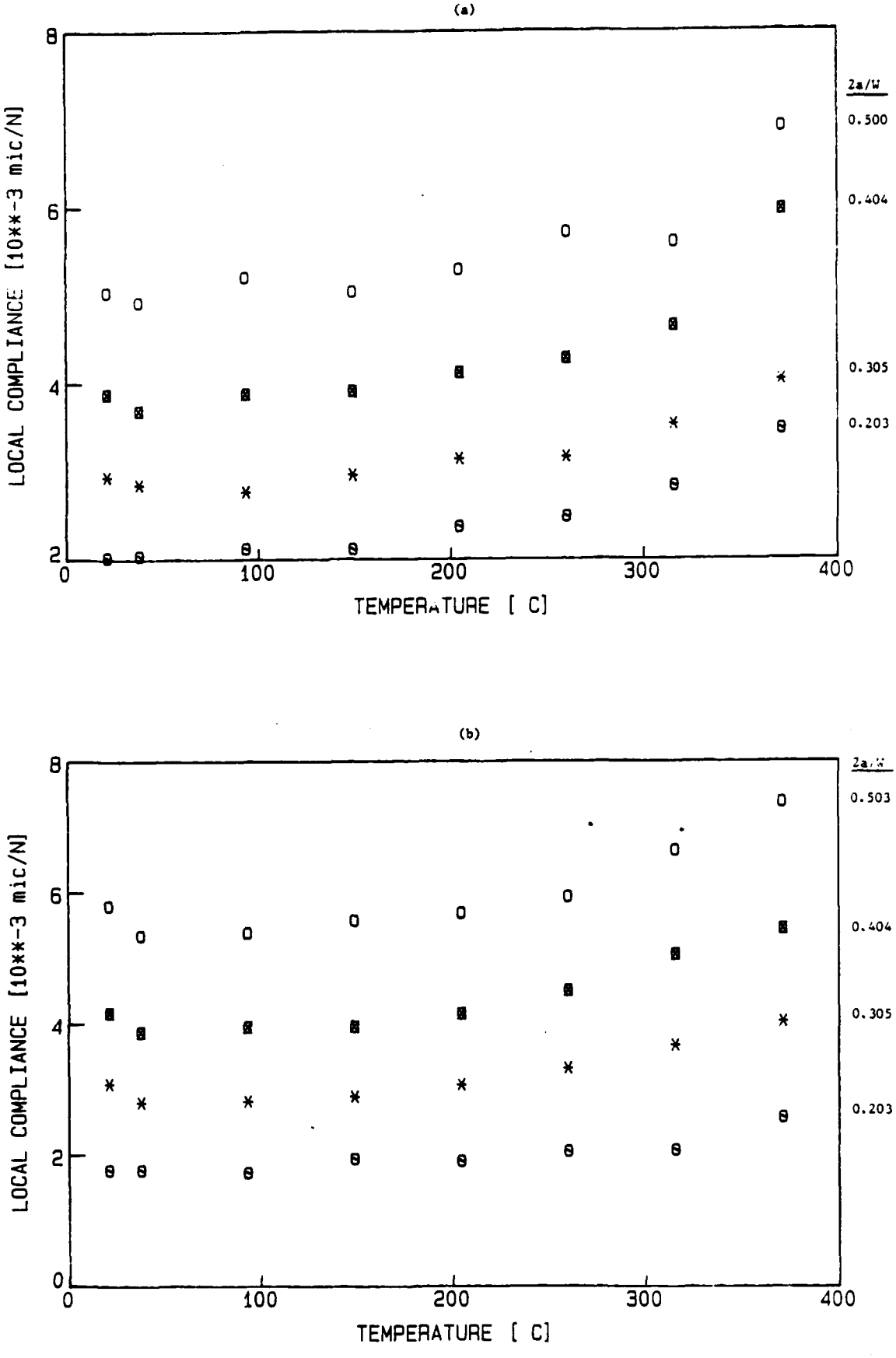

Figure 8. Local compliance versus test temperature for: a. $[0/90]_{2s}$; b. $[0/\pm45/0]_s$ laminates.

different crack lengths is shown in Figure 8, all leading to the conclusions discussed previously.

4.4 Conclusions

The following is a list of the major conclusions of this part of the research:

1. The laser interferometric displacement gage technique has been developed to measure the crack opening displacement of composites at elevated temperatures.

2. The IDG is highly accurate, very sensitive to crack tip damage, and has high resolution (1/4 micron displacement), independent of instrumentation or human errors.

3. Software for interfacing the IDG with the data acquisition system has been successfully developed and employed for data reduction and analyses.

4. Curves at elevated temperatures (371°C) have been successfully obtained.

5. Local compliance curves were obtained for all laminates studied at temperatures up to 371°C (700°F).

6. Local compliance curves were found to be highly sensitive to crack length. Thus, they may serve as a reliable measurement for crack tip damage progression during quasi-static and fatigue loadings.

7. Local compliance curves were found to be highly sensitive to test temperature above the annealing temperature of the aluminum matrix.

8. Significant scatter in experimental results has been observed for short notch lengths. This is due to the high stiffness of the subject material and the large notch length-to-thickness ratio, and possibly due to differences in crack tip radius as well.

9. Good correlation between experiments and prediction of local compliance has been established.

10. It has been demonstrated that the isotropic width correction factor can be applied to center notched boron/aluminum laminates.

11. Global compliance curves were obtained for all center notched laminates studied.

12. Global compliance curves were found to be highly insensitive to notch length for all laminates studied.

13. Significant scatter in experimental results has been observed for all laminates and all notch lengths.

14. Good correlation has been established between experiments and predictions of global compliance curves.

4.5 References

1. J. Awerbuch and H.T. Hahn, "K Calibration of Unidirectional Metal Matrix Composites," J. Composite Materials, Vol. 12, 1978, pp. 222-237.

2. W.F. Brown and J.E. Srawley, in "Plane Strain Crack Toughness of High Strength Metallic Materials," ASTM STP 410, American Society of Testing and Materials, 1966, p. 11.

3. G.C. Sih and H. Liebowitz, "Mathematical Theories of Brittle Fracture," in Fracture, Vol. 2, 3d. H. Liebowitz, Academic Press, N.Y., 1968.

4. S.G. Lekhnitskii, Theory of Elasticity of an Anisotropic Elastic Body, Translated by P. Fern, Holden-Day Inc., 1963.

5. S.G. Lekhnitsikk, Anisotropic Plates, Translated by S.W. Tsai and T. Cheron, Gordon and Breach Science Publishers, N.Y., 1968.

6. I.M. Daniel, R.E. Rowlands and J.B. Whiteside, "Deformation and Failure of Boron/Epoxy Plates with Circular Holes," The Test Methods for High Modulus Fibers and Composites, ASTM STP 521, American Society for Testing and Materials, 1973, p. 143.

V. DEFORMATION CHARACTERISTICS AND DAMAGE PROGRESSION

5.1 Summary

Far-field load displacement curves at room temperature and local load-crack opening displacement (COD) curves at room and elevated temperatures have been obtained for all laminates studied. Special emphasis has been placed on the local load-COD curves obtained with the IDG technique. The study focused on the deformation characteristics and crack tip damage growth as detected from the load-COD curves, and results were qualitatively correlated with the acoustic emission results, failure modes and visually detected damage progression.

Several of the recently developed analytical models predicting the deformation of center notched unidirectional metal-matrix composites have been reviewed. The experimental load-COD curves at room and elevated temperatures were compared with selected models and their applicability has been analyzed.

A simplified preliminary mechanistic model has been developed which proposes some modifications to existing models by incorporating a realistic strain hardening shear stress-strain curve of the matrix material. Comparison of the proposed model with the experimental load-COD curves indicates the validity of the modification. Additional work, primarily in the numerical calculation procedure is still required before the proposed model is fully operational.

5.2 Introduction

In characterizing the fracture behavior of composite laminates numerous studies focus primarily on the notched strength and fracture toughness of the subject material. These ultimate values (at failure) are important in the design criteria of composite structures. However, in order to establish a better understanding of the deformation characteristics, crack tip damage growth, etc., detailed load-COD curves are required. Such information will aid in understanding the effect of laminate configuration,

constituents, material system or environment (e.g. temperature) on the fracture behavior of composite laminates containing stress raisers. Detailed experimental load-COD curves will also aid in establishing the validity of any proposed analytical model for predicting the fracture behavior of composites.

There exist several semi-empirical fracture models which provide a simple procedure for predicting the notch sensitivity of composite laminates [1] (see discussion in Section IX). However, details of the deformation characteristics and crack tip damage zone are not addressed, and in fact they are by-passed by these semi-empirical models. In designing composite structures, however, such an approach is not sufficient for fully understanding the effect of constituents (e.g. fiber stiffness and matrix ductility), fiber diameter, volume fraction, etc. on the performance of metal-matrix composites. If such an understanding were available (through proper modeling), these parameters could be tailored to meet specific design requirements.

Several attempts have been made during the past two decades to develop fundamental analytical procedures for determining the performance of unidirectional filamentary composites containing a straight crack, e.g. [2-22]. Most of these models are the shear-lag approach [2-13] initially proposed in [2] and further modified and extended in [3-13]. Other approaches include approximate mechanistic models, e.g. [14-18], which are operationally simple to apply, or comprehensive finite element codes, e.g. [19-22]. In this study a comparison between the experimental local load-COD curves and predictions according to the models proposed in [14,17] has been made. The approximate model proposed in [17] was further extended for the purpose of this comparison. Efforts are currently being made to incorporate the models proposed in [9]. The comparison also enables the determination of the in-situ properties of the aluminum matrix. Finally, an analytical model which accounts for the actual (nonlinear) shear stress-strain curve of the aluminum matrix has been developed in this program.

It has been shown that the nonlinear behavior of the matrix material can have a profound effect on the performance of the subject material. This proposed model still requires certain modifications, primarily in the numerical calculation procedures, however, preliminary comparisons with experimental load-COD curves indicate the importance of incorporating the nonlinear behavior of the matrix material.

5.3 Experimental Results

As mentioned in Section III, two methods were used to obtain load-displacement curves for the center-notched boron/aluminum laminates. The far-field load-displacement curves were obtained using the 25.4 mm (1.0 inch) conventional compliance gage, while the IDG technique provided the local load-COD curves.

5.3.1 Far-Field Load-Displacement Curves at Room Temperature

Far-field load displacement curves were obtained for all six laminates and for all six crack lengths. Representative results for a notch length-to-width ratio of $2a/W = 0.30$ are shown in Figure 1. For unidirectional specimens, Figure 1a, a certain degree of nonlinearity has been detected, and it increases with crack length. The deviation from linearity occurs at approximately 20% - 30% of ultimate load. For $2a/W$ smaller than 0.2 the load-displacement curves are essentially linear. However, this could be due to the experimental procedure employed, i.e. the knives of the conventional compliance gage are wider than the crack length and thus the displacement recording system may not detect the effect of crack tip damage initiation and progression. As the applied load approaches ultimate value the load-displacement curves for certain specimens may rapidly approach a plateau which results from the sudden formation of fiber/matrix interfacial failure (i.e. splitting) at the crack tips. These sudden increases in displacements occurred randomly and usually at approximately 95-99% of ultimate load.

The load displacement curves obtained for the $[90]_8$ specimens are qualitatively similar to those obtained for the neat aluminum matrix, i.e. following the initial linear portion the load-displacement curve becomes significantly nonlinear, Figure 1b,

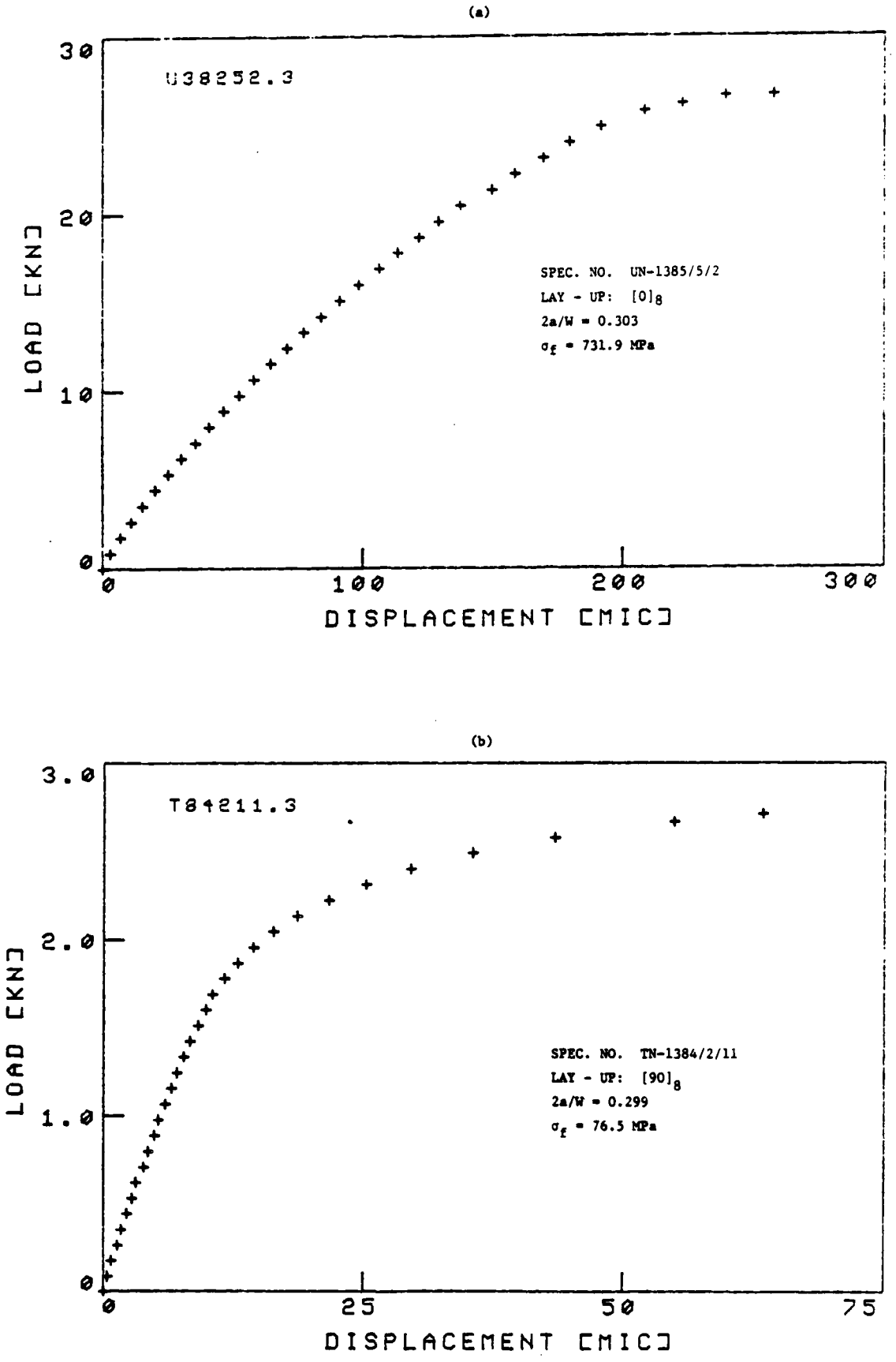

Figure 1. Far-Field load-displacement curves of six boron/aluminum laminates.

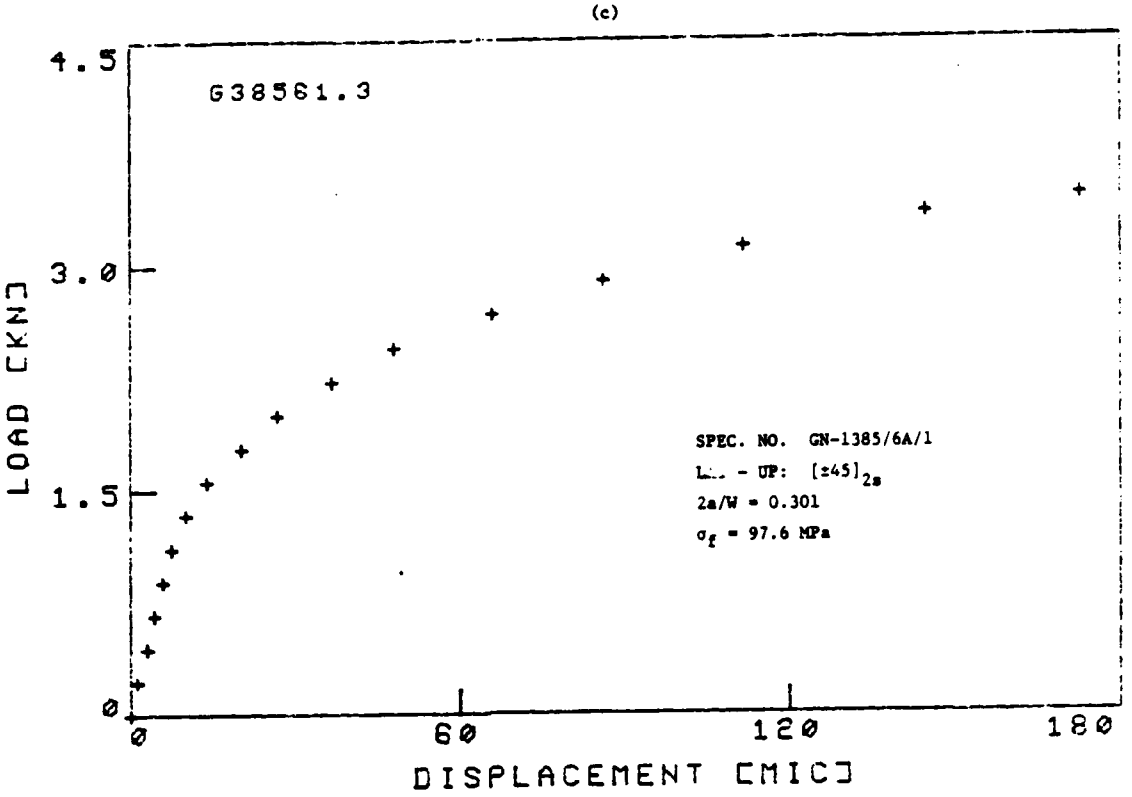

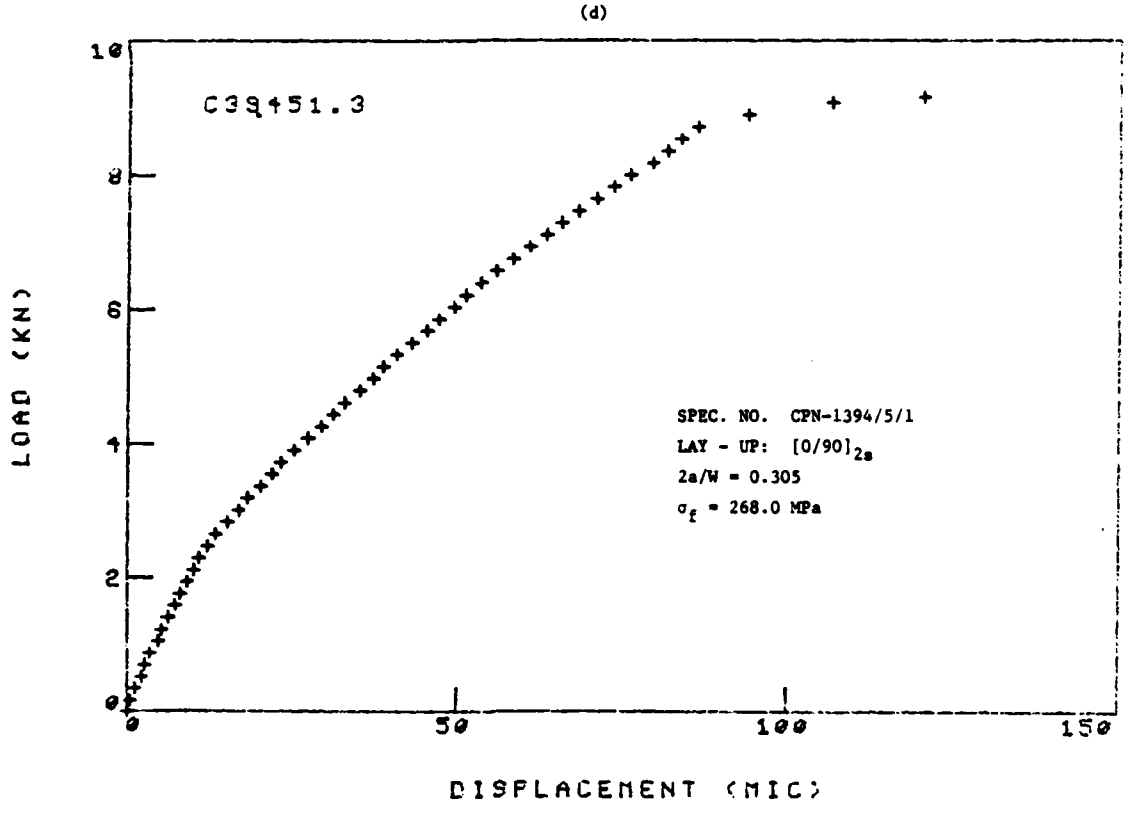

Figure 1. Continued.

(e)

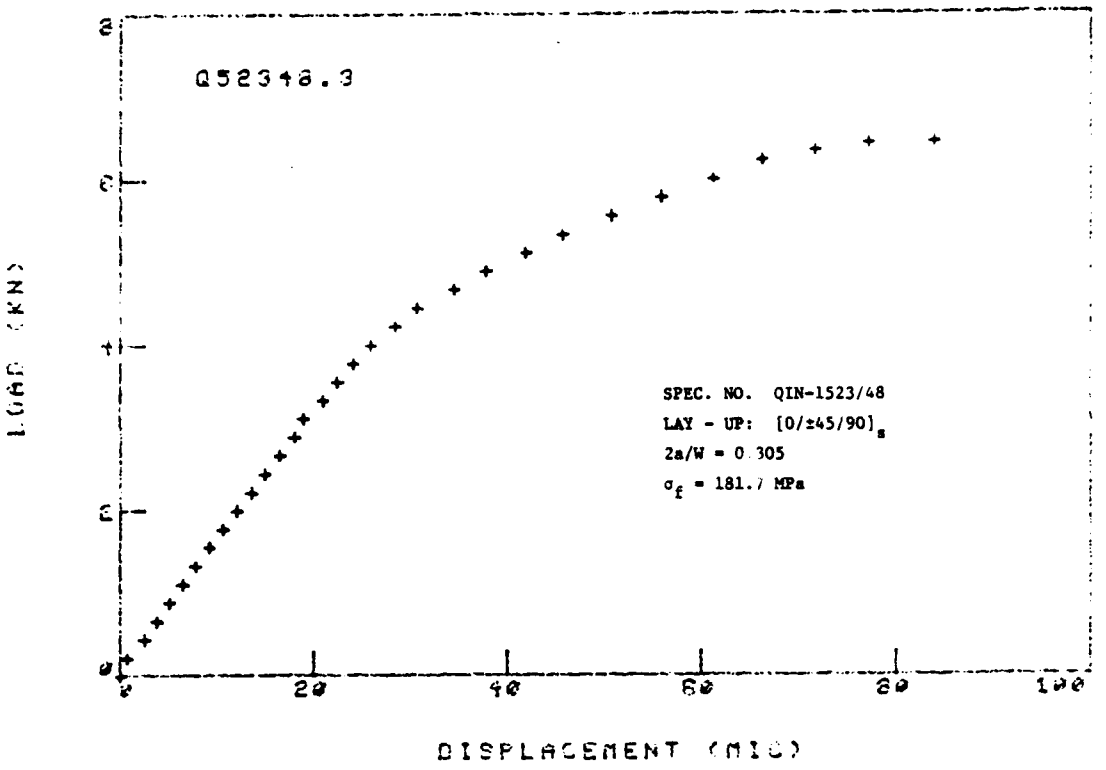

(f)

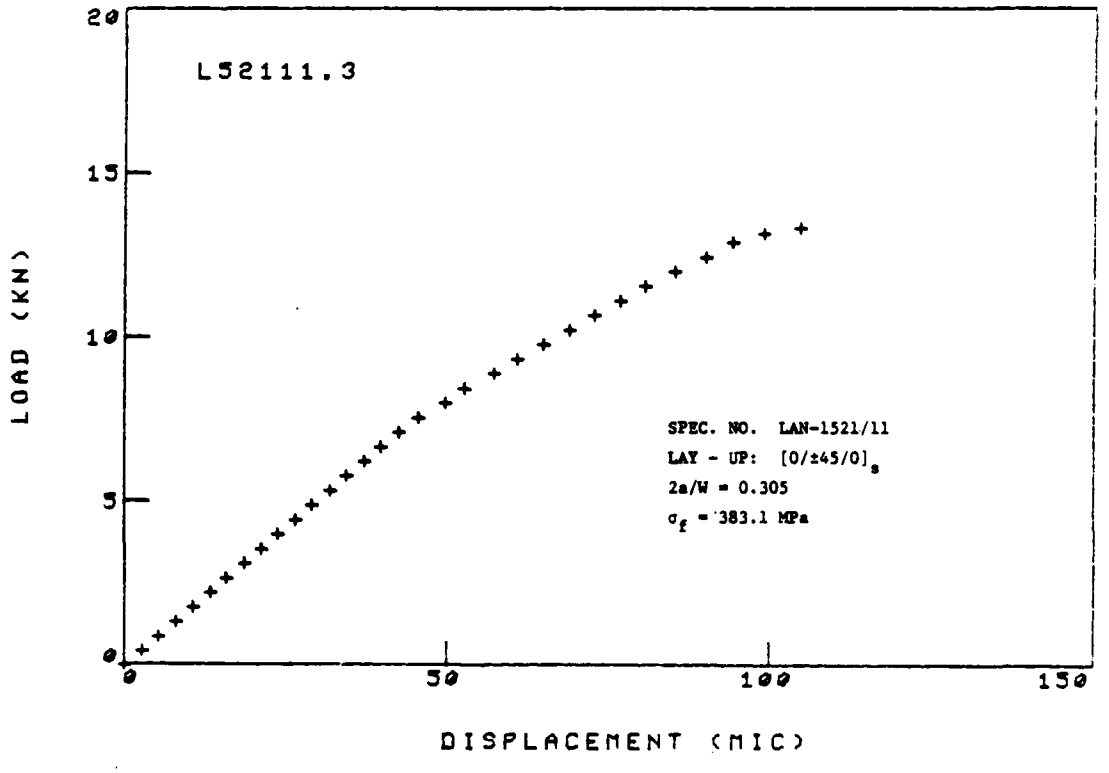

Figure 1. Continued.

having large deformation as the load approaches its ultimate values. It should also be noted that these curves do not follow the expected behavior of having larger compliance and lower ultimate strength with increased crack size. In other words, there is insignificant notch sensitivity and large scatter. The actual deformation prior to failure is, in fact, much higher than that indicated by the load-displacement curves. It should be noted that, as the load approaches its ultimate value, a sudden drop in load occurs, about 20% - 50% of its previous maximum value. Recalling that tests were conducted under stroke control, a sudden increase in crack tip damage, causing a large crack opening, may cause such a drop in load. As loading proceeds, additional slow crack opening is observed until an additional drop in load occurs. This process may repeat itself several times. Thus, under stroke control conditions, a step-wise crack tip damage growth was observed. Similar load-displacement curves were obtained for the $[\pm 45]_{2s}$ laminate, Figure 1c.

The load-displacement curves of the cross-ply laminate exhibit three distinct regions, Figure 1d. The deviation from linearity in the $[0/90]_{2s}$ and $[90]_8$ lay-ups occur at approximately the same load level. Thus, the first knee in the load-displacement curve could be associated with the significant inelastic deformation in the 90° layers. The second knee seems to correspond to the matrix shear deformation along the 0° fibers. Similar knees were obtained also for notched $[0°]_8$ specimens, Figure 1a. In both the $[0/90]_{2s}$ and $[0°]_8$ lay-ups the upper knee occurs at approximately 98% of ultimate. Quasi-isotropic laminates also exhibit three distinct regions, Figure 1e, similar to the cross-ply laminate. The middle region of the load displacement curve, however, exhibits higher nonlinearity due to the presence of the ±45° plies. Finally, the load-displacement curves of the $[0/\pm 45/0]_s$ laminate have two distinct linear regions, where the upper region might be slightly nonlinear for the longer cracks. The presence of the 0° plies (50%) contributes in constraining the ±45° plies from excessive deformation.

Effect of crack length on the load-displacement curves of selected laminates is shown in Figure 2. The results shown in Figure 2 for unidirectional specimens clearly indicate that crack length has little effect on the initial slope of the load-displacement curve, i.e. global compliance is insensitive to crack length, as discussed in Section IV. With increasing load, significantly different curves are obtained for the different crack lengths. Specimens containing longer cracks exhibit higher nonlinearity. This nonlinearity results from the excessive shear plastic deformation along the fibers which develops at the crack tip. Similar results were obtained with the other laminates, e.g. Figure 2b. The linearity in the load-displacement curves for the shorter crack lengths can be attributed to the experimental procedure, i.e. the width of the compliance gage knives is longer than the crack length. Thus, crack tip damage progression might not be detected by the recording system.

Effect of laminate configuration on load-displacement curves is shown in Figure 3 for two different notch length-to-width ratios. Results indicate that the multidirectional laminates (i.e. $[0/90]_{2s}$, $[0/\pm45/90]_{s}$, and $[0/\pm45/0]_{s}$) exhibit significantly less deformation to failure than the laminate's basic building blocks, e.g. $[0]_{8}$, $[90]_{8}$, and $[\pm45]_{2s}$. These differences are attributed to the excessive inelastic deformation occurring within the gage length of the compliance gage. In the $[0]_{8}$ multiple shear plastic zones are formed along the fiber direction emanating from the crack tips. In the $[90]_{8}$ and $[\pm45]_{2s}$ lay ups significant matrix plastic deformation as well as fiber/matrix interfacial failure occur in crack tip regions and throughout the specimen length. In the multidirectional laminates crack tip damage is much more localized. These observations have been confirmed by visual observation through the close-circuit television and by the acoustic emission results as described in Sections VI and VII, respectively. Additional discussion on this issue is given below.

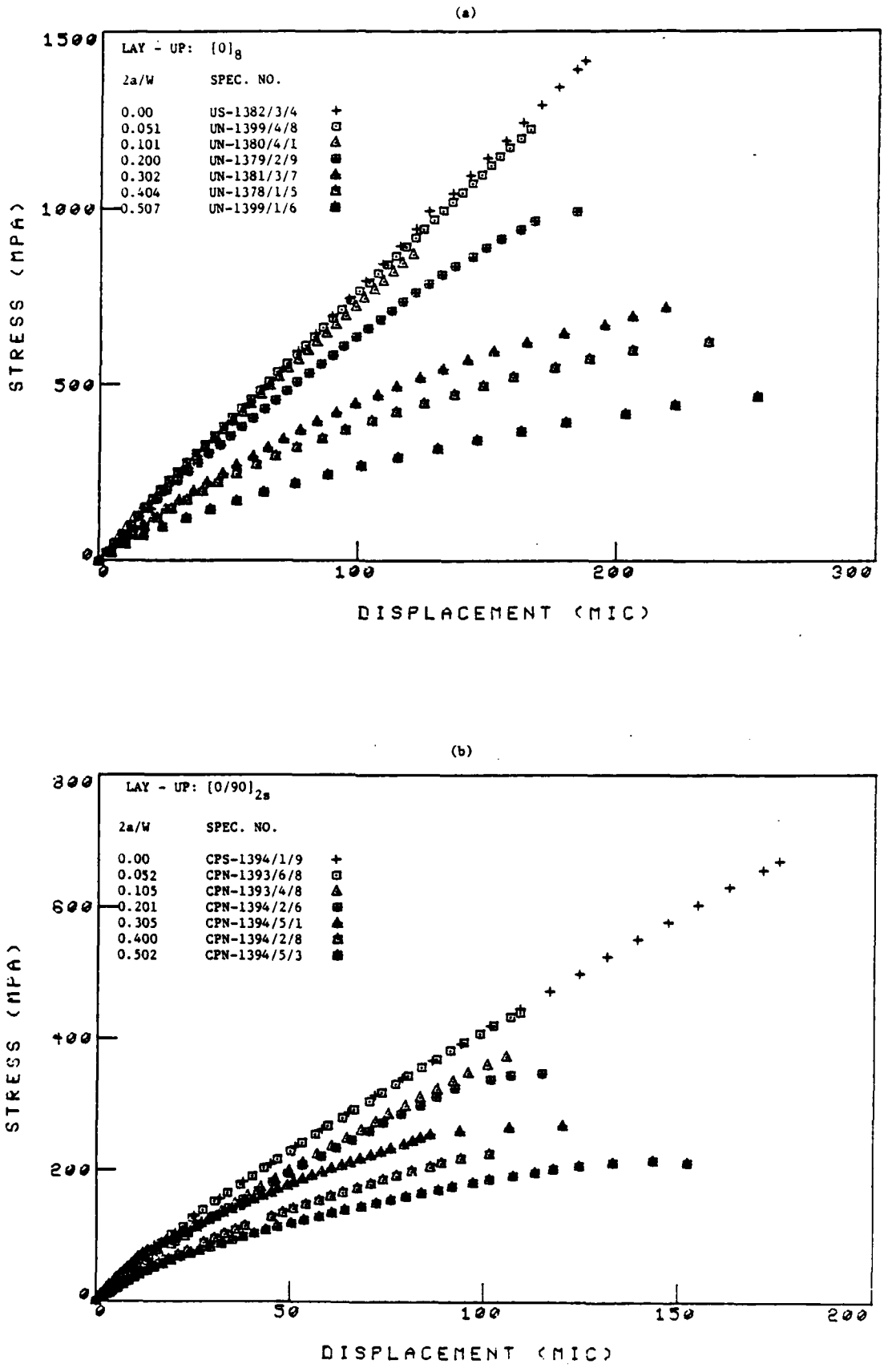

Figure 2. Effect of crack length on far-field load-displacement curves of four boron/aluminum laminates.

(c)

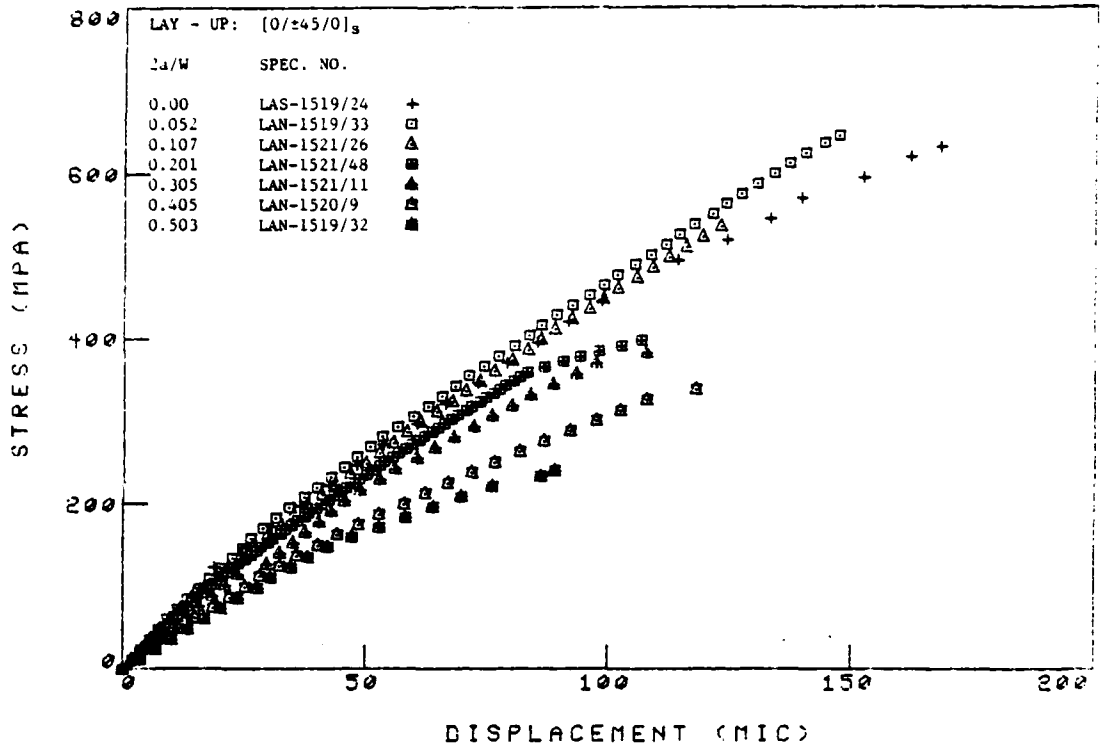

(d)

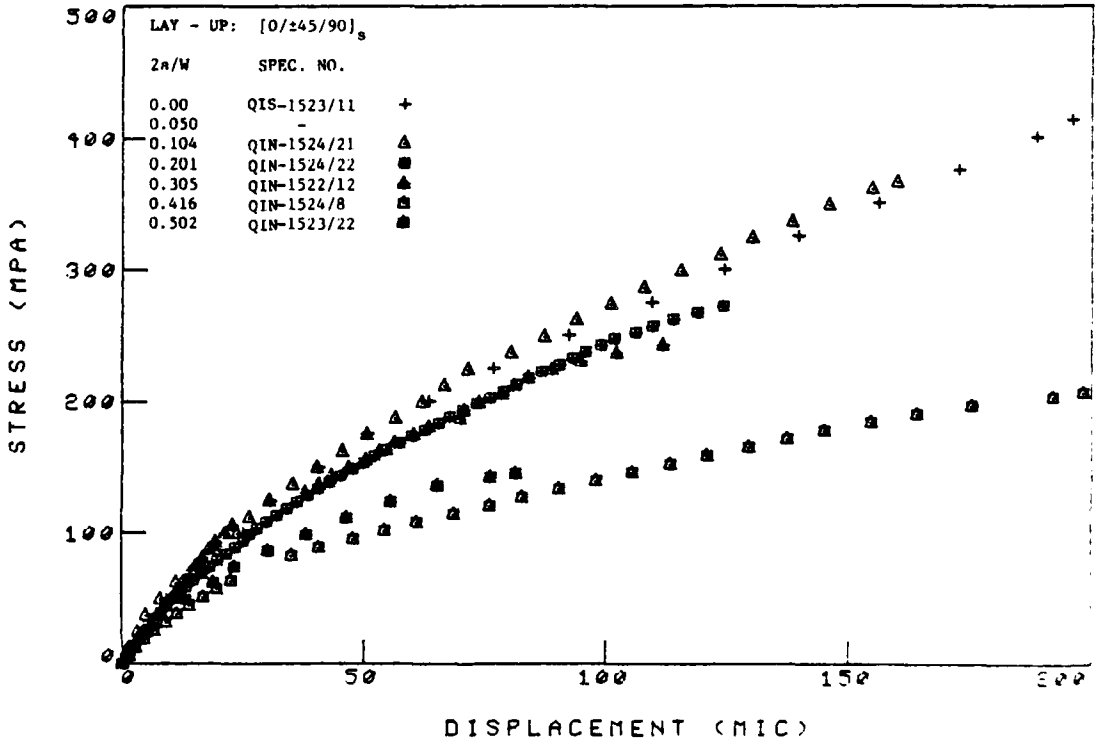

Figure 2. Continued.

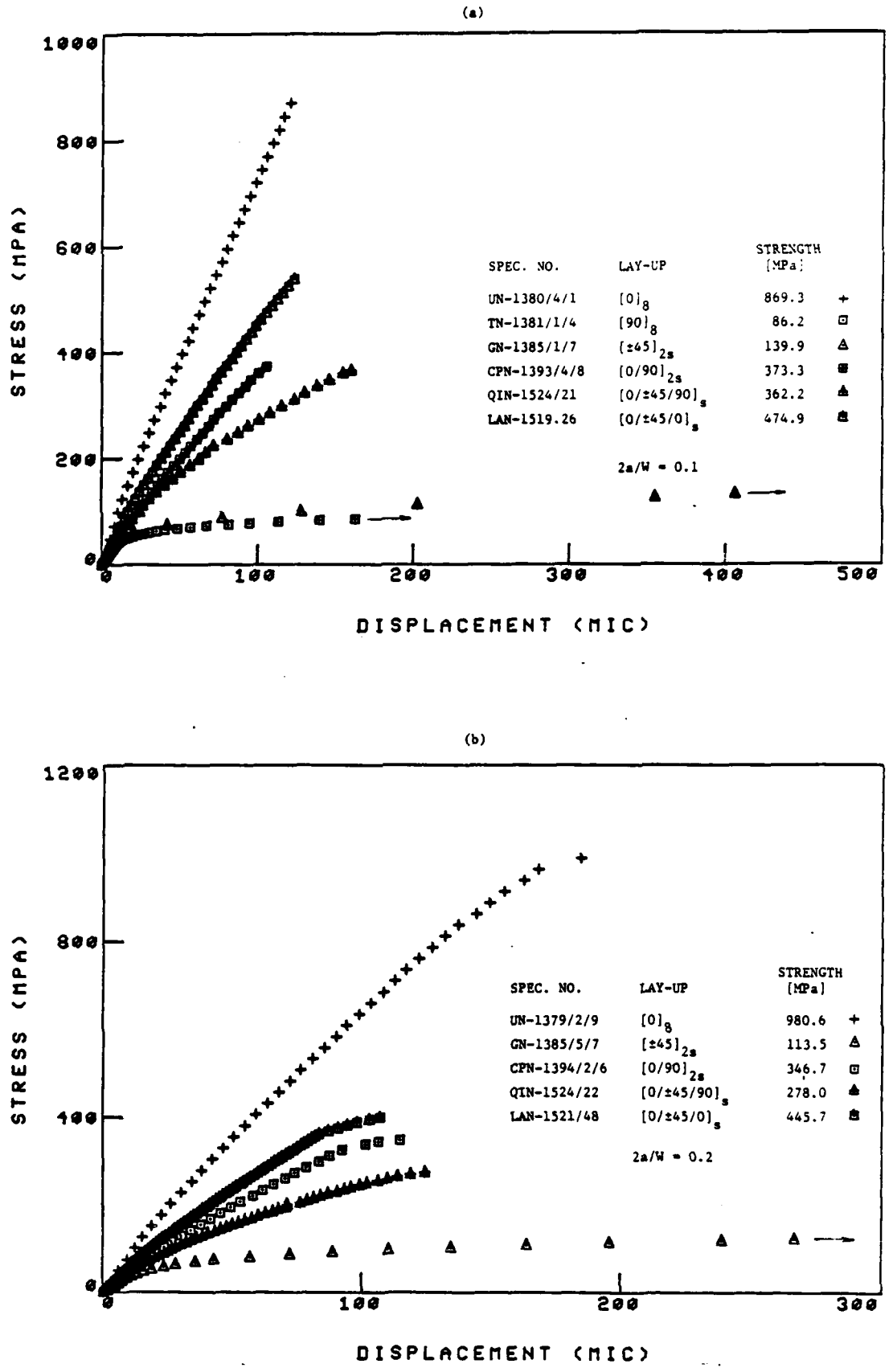

Figure 3. Effect of laminate configuration on far-field load-displacement curves of boron/aluminum laminates: a. 2a/W = 0.1; b. 2a/W = 0.2.

5.3.2 Local Load-Crack Opening Displacement Curves at Room and Elevated Temperatures:

A typical load-crack opening displacement (COD) curve obtained with the laser Interferometric Displacement Gage (IDG) is shown in Figure 4 for a unidirectional specimen having a crack length of 7.6 mm (0.30 inch). The load-COD curve is highly nonlinear, with a rapid increase in COD when the load approached ultimate strength. The rapid changes in COD are due to the crack tip damage growth in the form of fiber breakage and longitudinal shear plastic deformation and splitting (interfacial failure) in the matrix. These damages were also accompanied by audible level of acoustic emission. A detailed examination of the load-COD curves reveals that the load-COD relationship remains highly nonlinear also between loads where there is a rapid increase in COD.

The crack tip damage is manifested by the nonlinearity of the load-COD curves, the large permanent COD remaining upon unloading and by the sudden increases in COD as the load approaches its ultimate value. The permanent COD remaining upon unloading increases with applied load, Figure 5. Upon reloading (or unloading) the load-COD curves are initially linear, however, significant nonlinearity is detected during reloading already at load levels much below the maximum previously applied load. This material response could be attributed to additional damage caused during reloading. Indication of such additional damage is revealed through monitoring of acoustic emission, by what is known as the Felicity Effect. Details of the load-COD seem, indicating an increase in crack tip damage growth. These jumps in COD are more pronounced as the load approaches its ultimate level. It may be noted that the damage growth is accompanied by audible levels of acoustic emission and a qualitative correlation can be found between the acoustic emission and the damage growth detected through COD measurements as discussed in Section VII.

The effect of the crack length on the load-COD curve is shown in Figure 7 for unidirectional specimens. Although the details of each curve cannot be seen in the

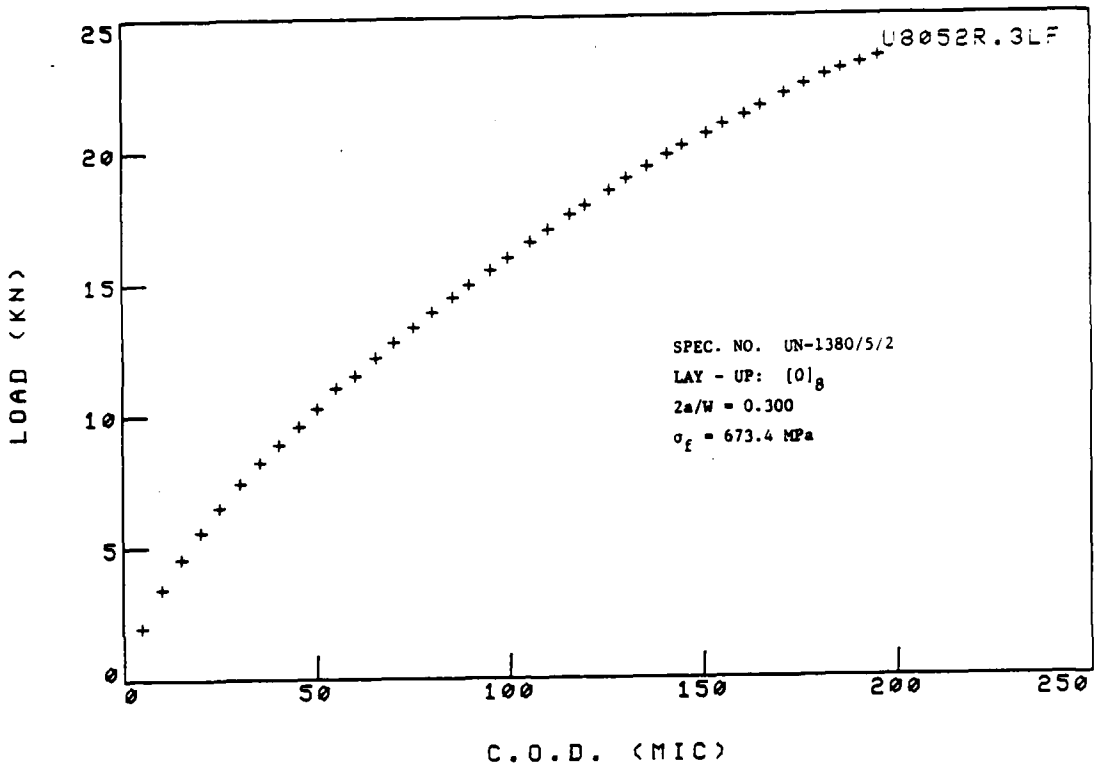

Figure 4. Load-COD curve for unidirectional boron/aluminum specimen.

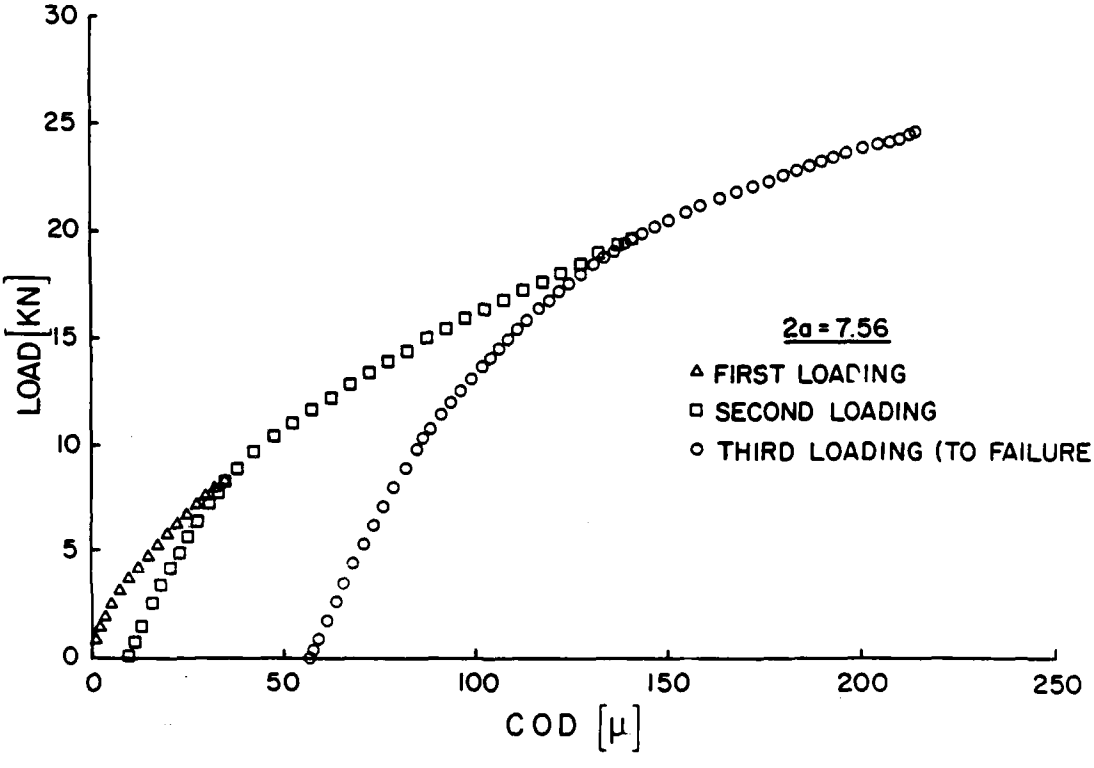

Figure 5. Load-COD (loading-unloading) curves obtained with the IDG for unidirectional boron/aluminum specimen.

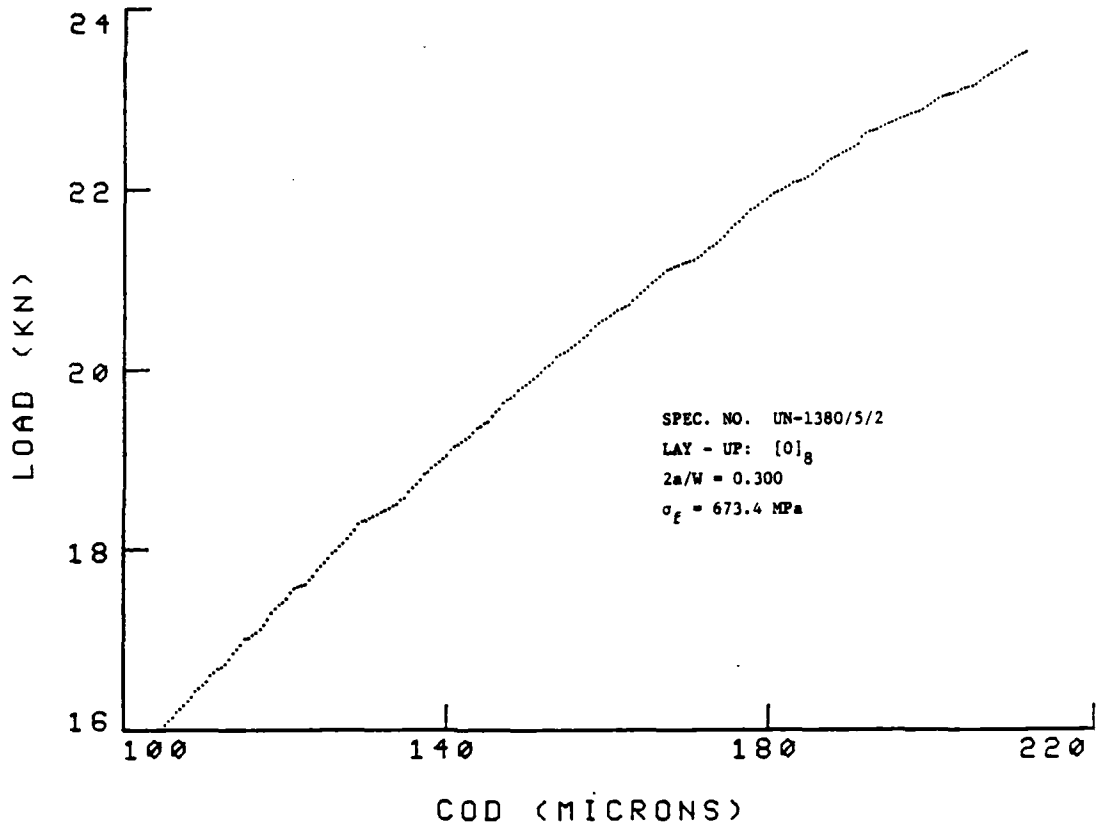

Figure 6. Detail of load-COD curve for unidirectional boron/aluminum specimen (same specimen shown in Figure 4) showing jumps in COD as load approaches its ultimate level.

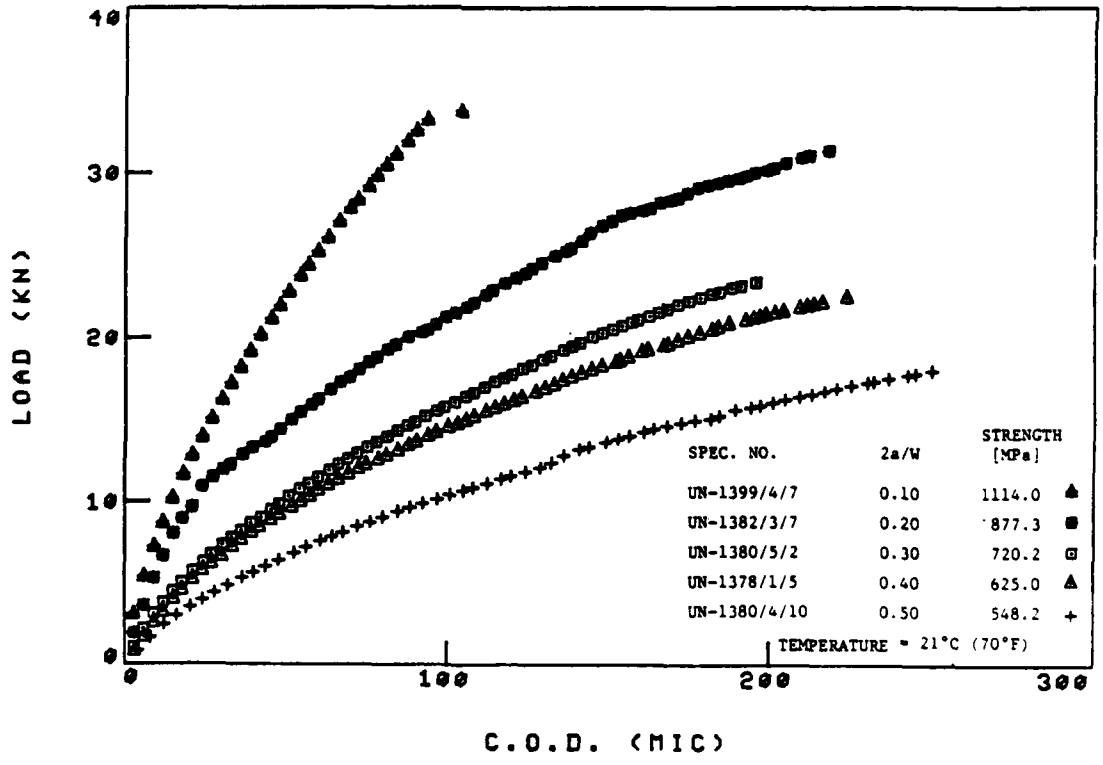

Figure 7. Load-COD curves for various crack lengths for unidirectional boron/aluminum specimens.

Figure, the nonlinearity, rapid increase in COD, and permanent opening upon unloading were obtained for every crack length tested. As expected, these characteristics are more pronounced as crack length increases; that is, the longer the original crack length, the larger the crack tip damage.

For transverse specimens the load-COD curves are more complicated. As the crack tip damage extends, a sudden drop in load occurs, similar to that described previously for the far-field load-displacement curves. This drop in load may in turn cause a potential crack closure. Because the IDG employed in this program cannot distinguish between crack opening and crack closure, the plots of the load-COD curves, shown in Figure 8, have been terminated just prior to the drop in load. Similar results were obtained for $[\pm 45]_{2s}$ laminate, Figure 9. For both lay-ups the load-COD curves rapidly approach a plateau which is indicative of excessive plastic deformation in the crack tip regions.

Load-COD curves for all other laminates were obtained as well, an example of which is shown in Figure 10. The deformation characteristics such as the nonlinear load-COD curves, rapid increase in COD at high load levels and the permanent crack opening upon unloading, are all similar to those discussed previously. However, those features are less pronounced than they are in unidirectional specimens. This indicates that the crack tip damage is more localized for multidirectional laminates, a fact which has been confirmed both from the visual observations (through the closed-circuit television system) and from the fracture surface morphologies discussed in Section VI. For example, the jumps in COD for three different multidirectional laminates are shown in Figures 11-13. The comparison between two of these laminates, Figure 14, illustrates the effect of laminate configuration on the load-COD curves. Finally, comparison among the load-COD curves obtained for all six laminates is shown in Figure 15, which is analagous to the far-field load-displacement curves shown in FIgure 3.

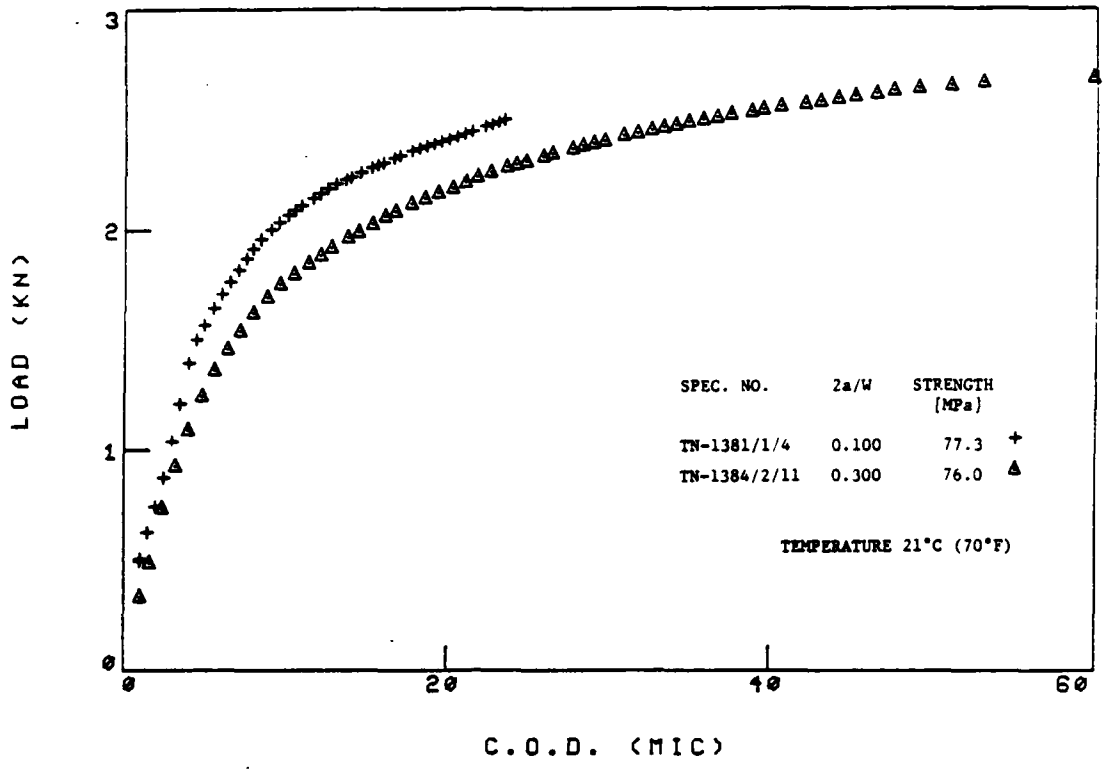

Figure 8. Load-COD curves for two crack lengths for $[90]_8$ boron/aluminum laminates.

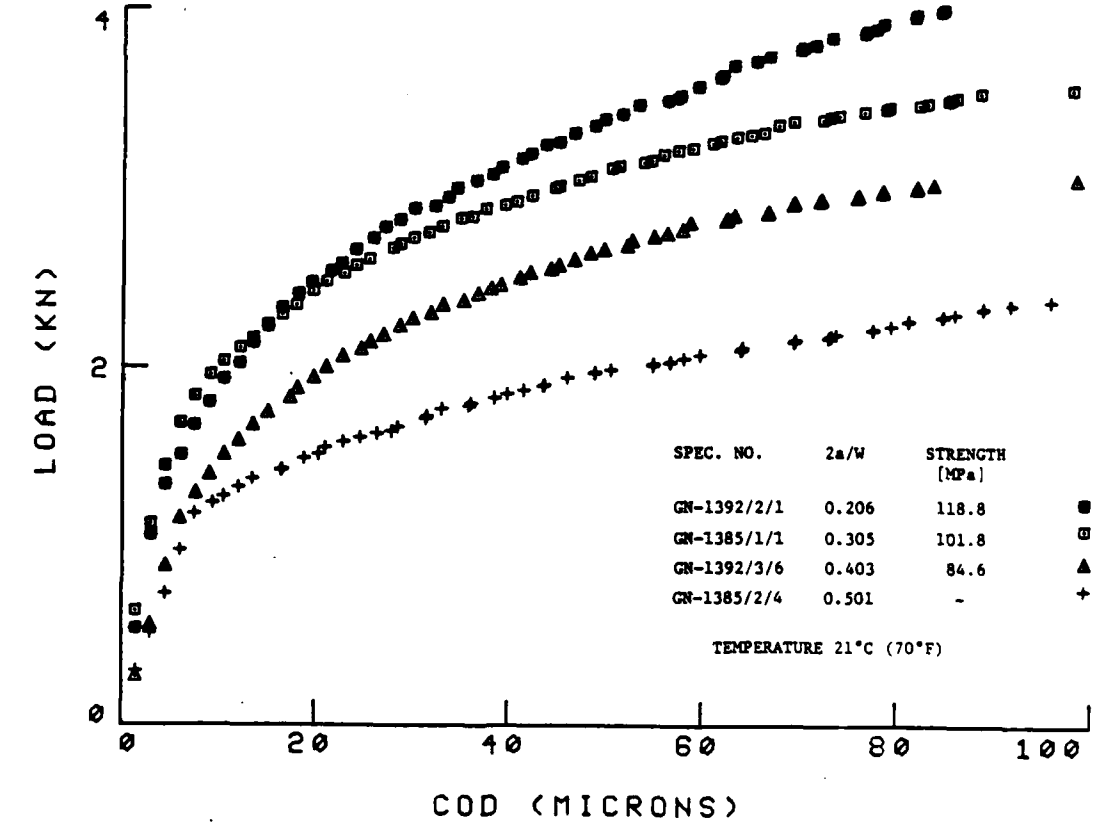

Figure 9. Load-COD curves for various crack lengths for $[\pm 45]_{2s}$ boron/aluminum laminate.

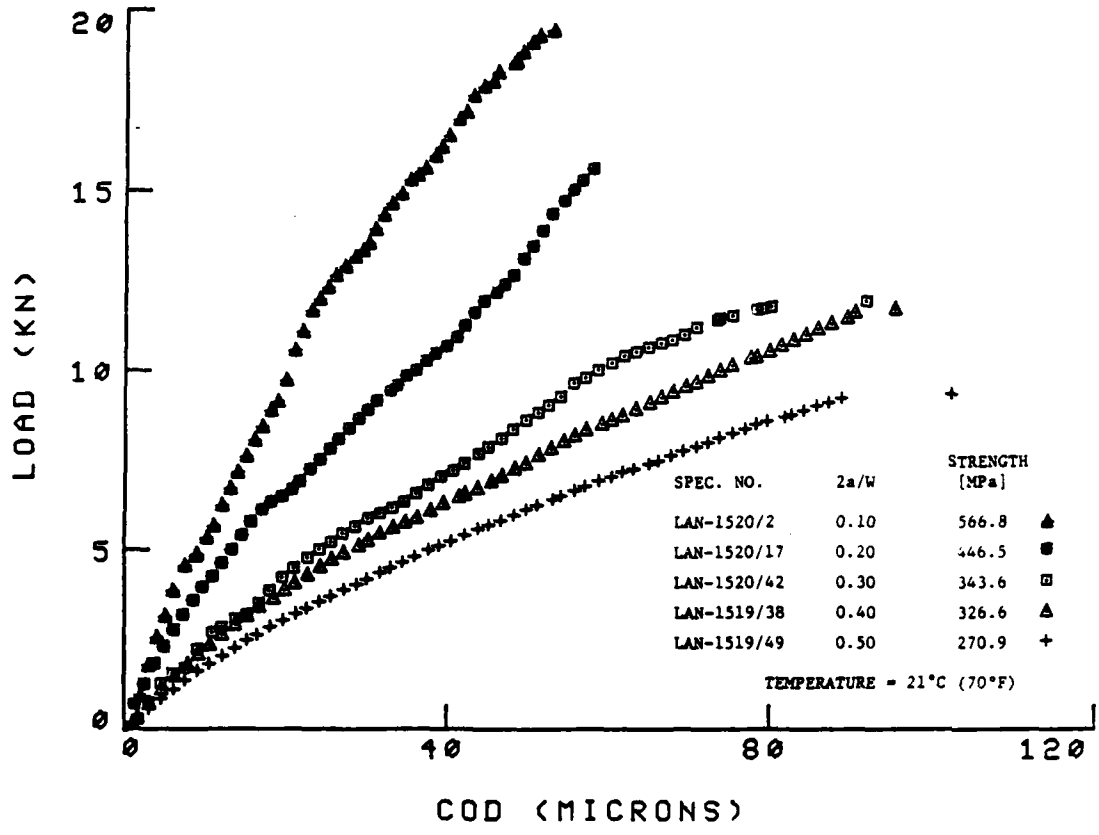

Figure 10. Load-COD curves for various crack lengths for $[0/\pm45/0]_s$ boron/aluminum laminate.

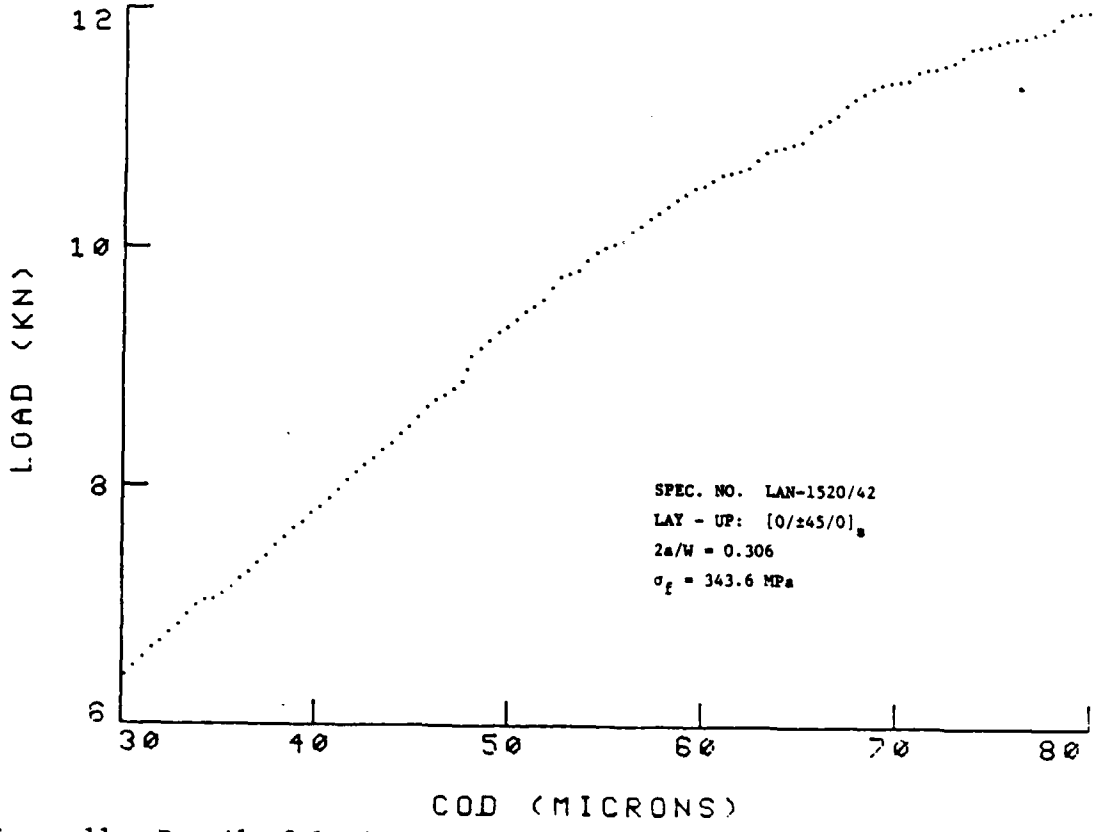

Figure 11. Detail of load-COD curve for $[0/\pm45/0]_s$ boron/aluminum laminate showing jumps in COD as load approaches its ultimate level.

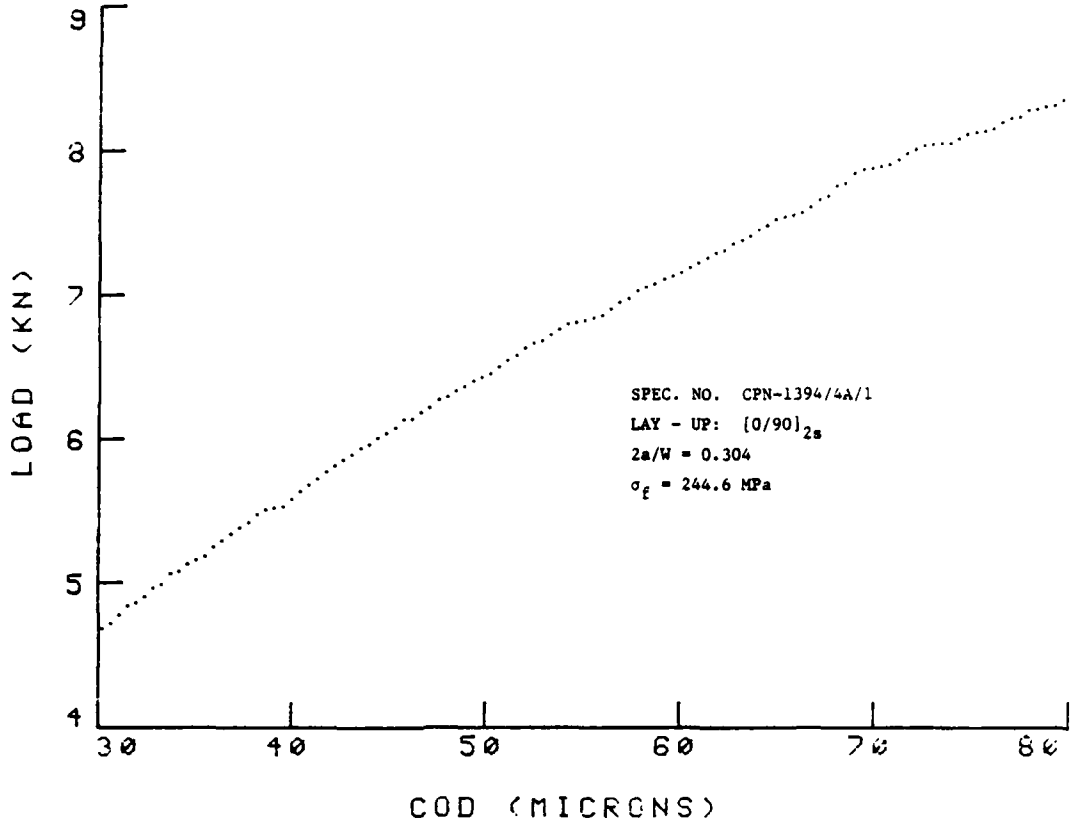

Figure 12. Detail of load-COD curve for $[0/90]_{2s}$ boron/aluminum laminate showing jumps in COD as load approaches its ultimate level.

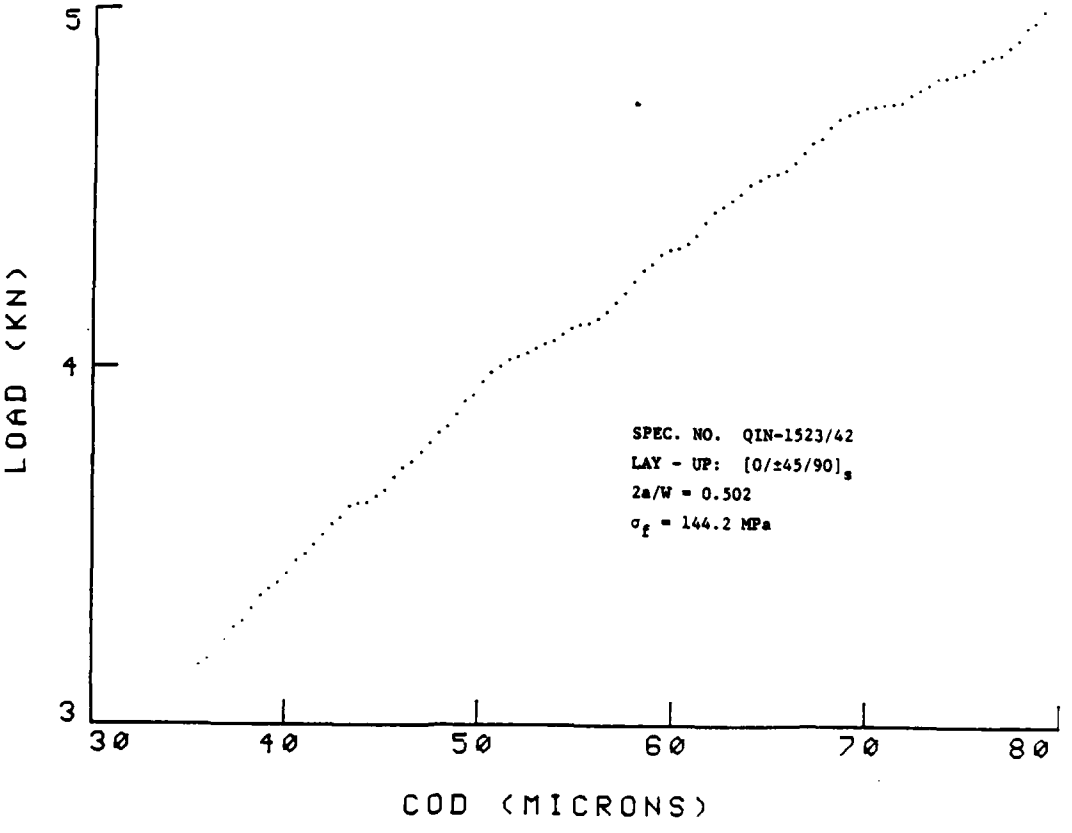

Figure 13. Detail of load-COD curve for $[0/\pm45/90]_s$ boron/aluminum laminate showing jumps in COD as load approaches its ultimate level.

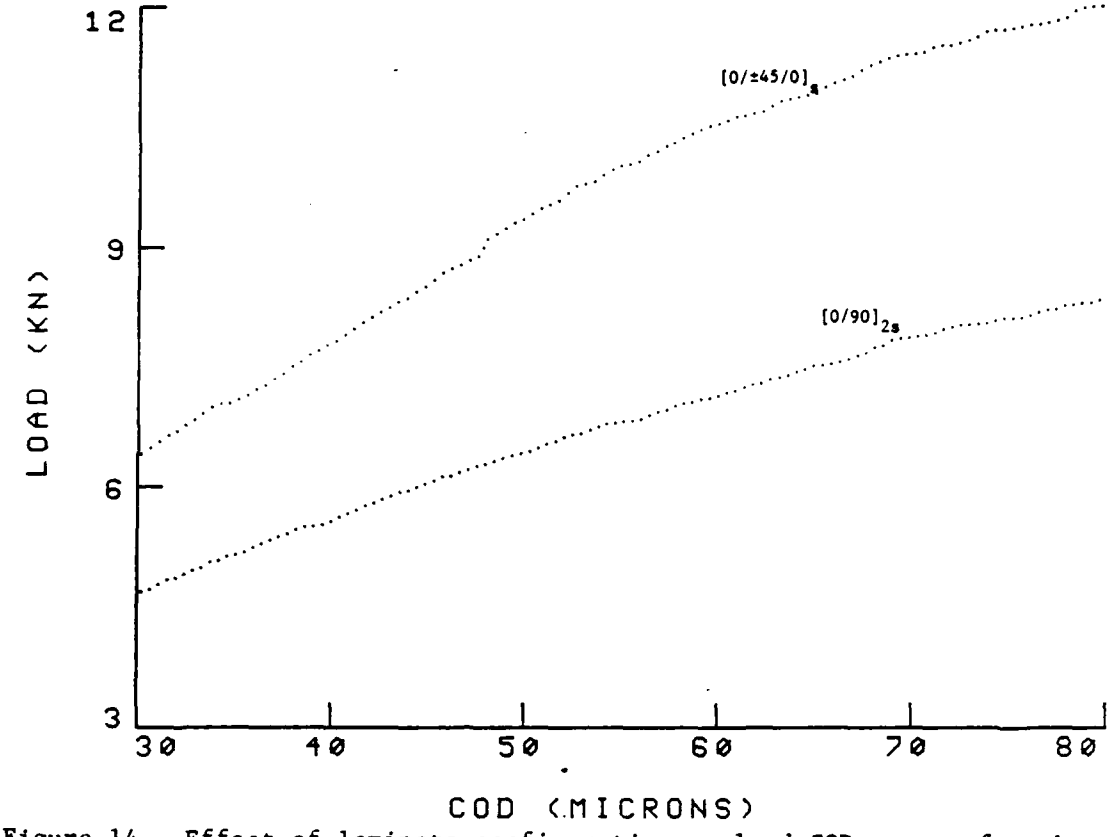

Figure 14. Effect of laminate configuration on load-COD curves for the same specimens shown in Figures 11 and 12. (2a/W = 0.30)

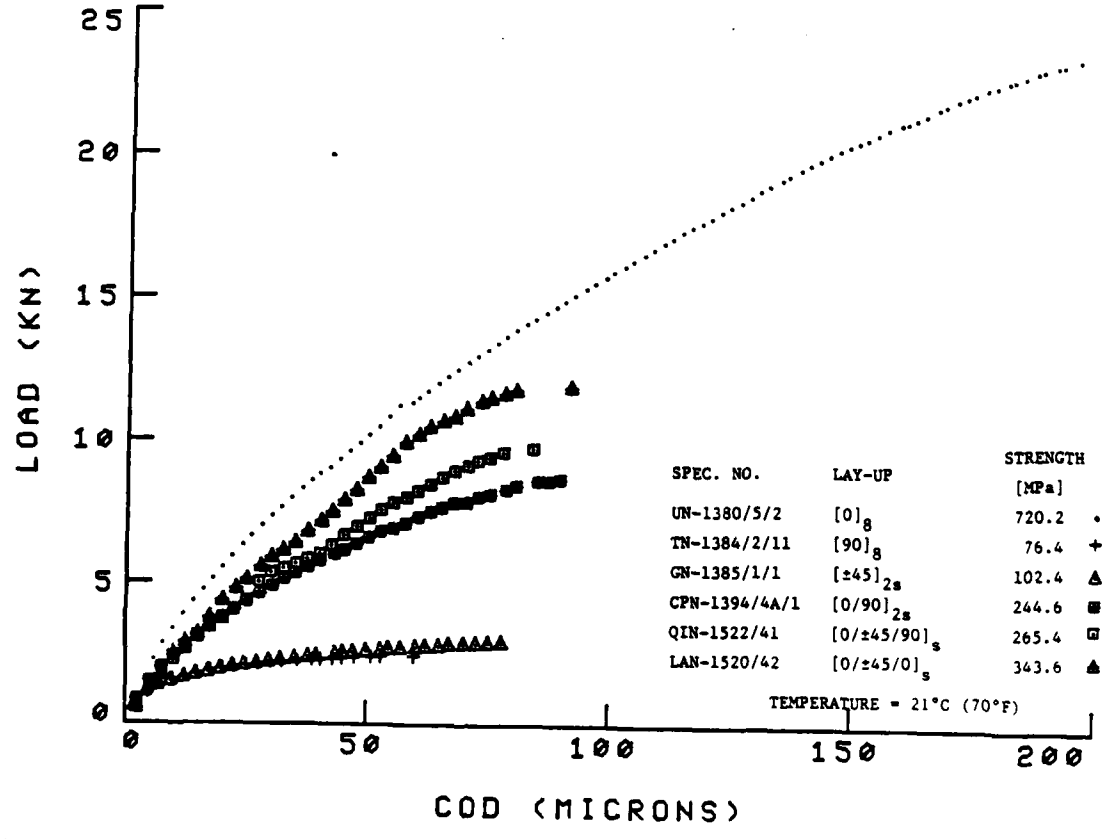

Figure 15. Effect of laminate configuration on load-COD curves.

Elevated temperature load-COD curves were also obtained for all laminates. Figure 16 shows such curves for unidirectional specimens obtained at 315°C (600°F). The results indicate that at this temperature the deformation characteristics are much more pronounced than at room temperature, Figure 7. The increased crack opening is attributed primarily to the increased ductility of the aluminum matrix. Since an increase in notch sensitivity of unidirectional specimens has been observed at 315°C (600°F), as explained in Section X, the increased crack opening can also be attributed to fiber degradation. In order to establish a better understanding of this issue a more detailed study on the effect of temperature on fiber/matrix interface integrity is warranted.

Effect of temperature on the deformation characteristics becomes significant at approximately 204°C (400°F), Figure 17. Results indicate that at least up to 93°C (200°F) temperature has little if any effect and the load-COD curves at 21°C (70°F) and 93°C (200°F) are very similar. A further increase of temperature, up to 204°C (400°F), already reveals a larger nonlinearity in the load-COD curves, resulting in a larger COD at failure as well. When the test temperature is again increased up to 315°C (600°F), a significant effect is observed, Figure 17. Similar results were obtained for all other laminates, e.g. Figures 18 and 19. It should be noted that the increased deformation at a temperature of approximately 204°C (400°F) also corresponds to the significant increase in local compliance, as discussed in Section IV, both of which are attributed primarily to degradation in matrix properties at that temperature.

5.4 Predictions of Load-COD Curves for Unidirectional Boron/Aluminum

5.4.1 Introduction

As previously mentioned, a variety of analytical models have been proposed to predict the deformation characteristics of unidirectional boron/aluminum. These include primarily the shear-lag based models, approximate and mechanistic

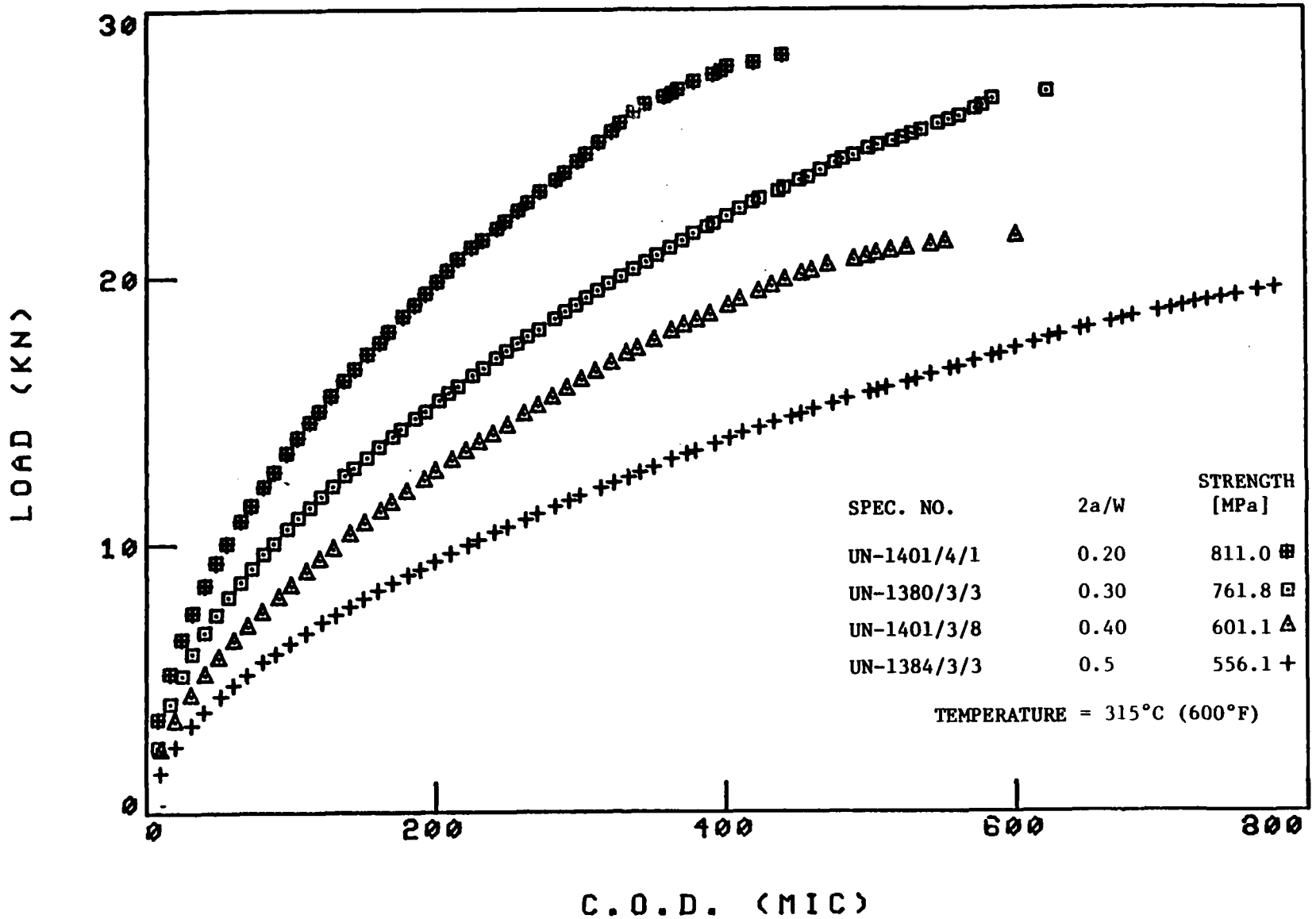

Figure 16. Load-COD curves for various crack lengths for unidirectional boron/aluminum specimens at an elevated temperature.

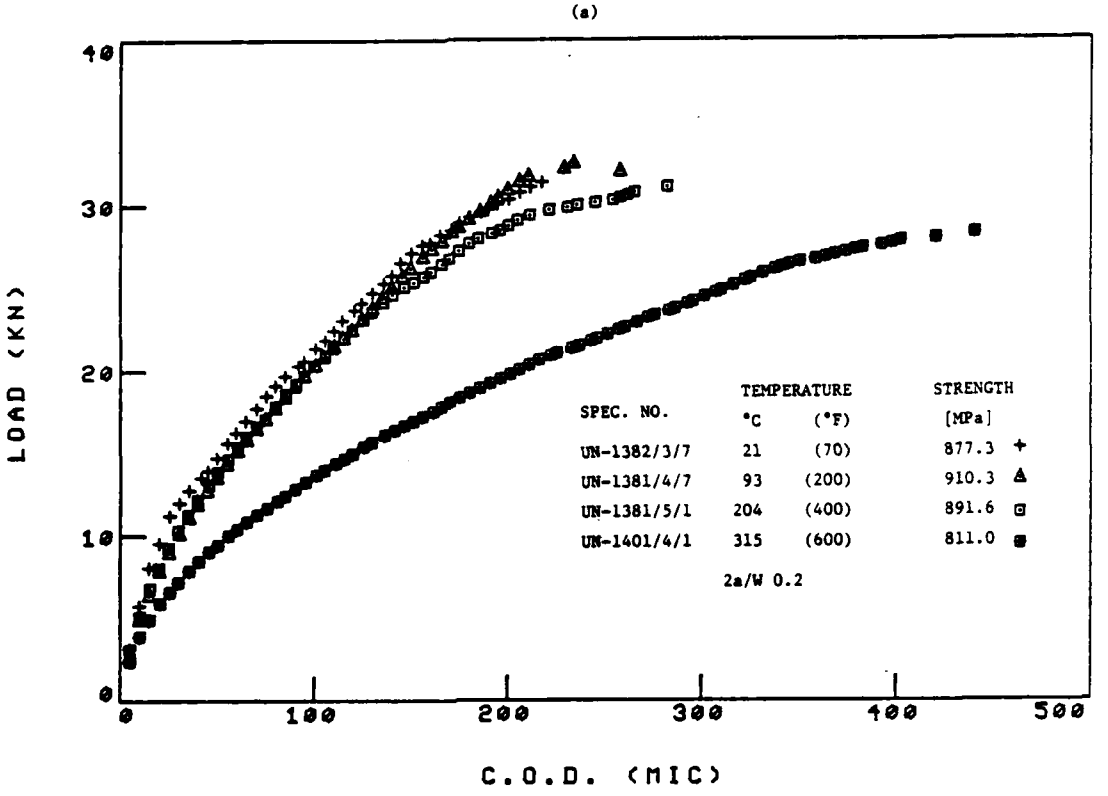

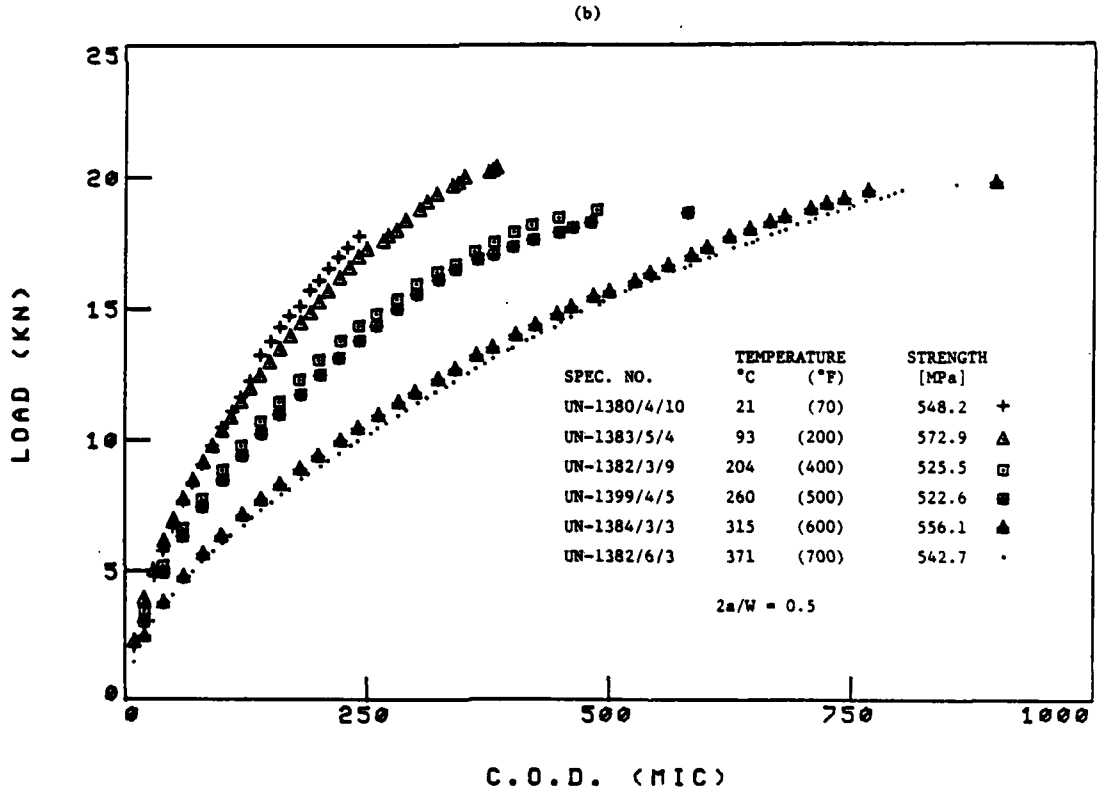

Figure 17. Effect of test temperature on load-COD curves for unidirectional boron/aluminum specimens: a. 2a/W = 0.2; b. 2a/W = 0.5.

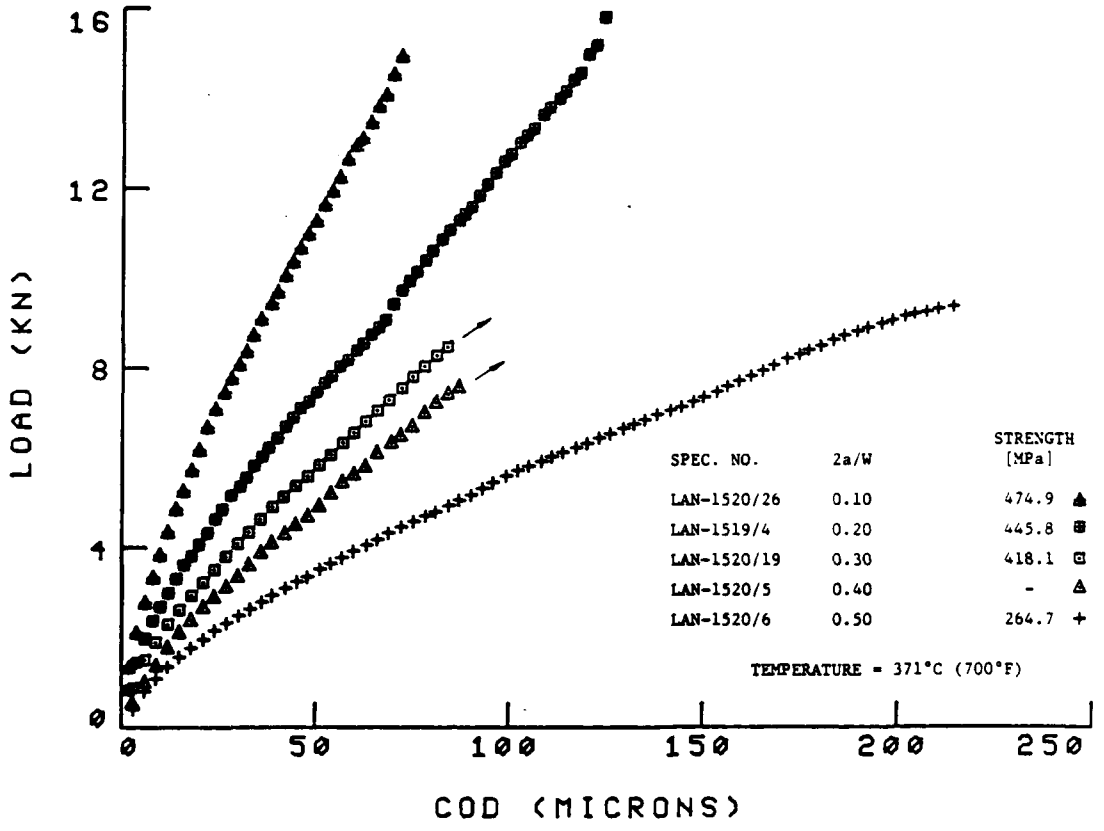

Figure 18. Load-COD curves for various crack lengths for boron/aluminum $[0/\pm45/0]_s$ laminate at elevated temperature.

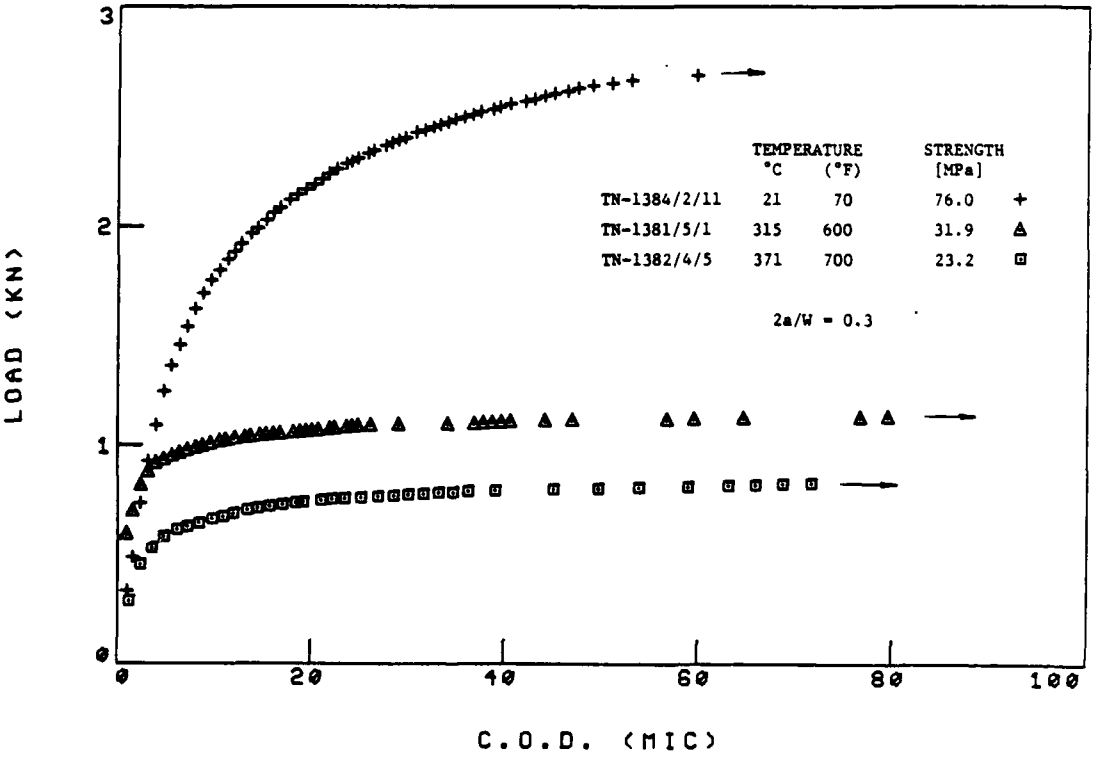

Figure 19. Effect of temperature on the load-COD curves for $[90]_8$ boron/aluminum specimens.

models, and finite element codes. A fundamental approach has been proposed by Hedgepeth [2] in which an idealized two-dimensional array of infinitely long and equally spaced linear-elastic fibers held together by a linear-elastic matrix is analyzed. The array contains a known number of colinear broken fibers (crack) and carries longitudinal tensile stresses at infinity. Fiber stiffness is much larger than the stiffness of the matrix and it is assumed that the fibers carry all the normal stresses while the matrix carries shear stresses only, i.e. the shear-lag assumptions. Poisson's effect is ignored and thus the matrix carries no transverse stresses. The shear stresses in the matrix depend only on the gradients in the longitudinal displacements across the width of the array. Based on these simplifying assumptions, the equilibrium equations yield a second order differential-difference equation which is solved by the influence function technique to obtain the displacements and forces in all fibers. The results show that the elastic fiber stress concentration factor (SCF) is the largest at the first intact fiber (at the crack tip) and it increases with number of broken fibers (crack length).

Eringen and Kim [5] extended the infinite array model and accounted for the transverse normal stresses carried by the matrix as well. All other assumptions are the same as in the Hedgepeth [2] model, however, the shear stress in the matrix depends now on both the longitudinal and transverse displacement gradients. The two resulting governing equations, in the longitudinal and transverse directions, are coupled and they must be solved simultaneously, using the dual integral technique. Two major conclusions could be drawn from this model. First, the inclusion of the transverse stresses resulted in crack tip elastic SCF which is higher by approximately 5% than that obtained by Hedgepeth [2], where the matrix carries shear stress only. Second, the SCF due to broken fibers (crack) is highly localized, i.e. the normal stresses rapidly approach the far-field fiber stress, within 1-2 fibers away from the crack tip.

Goree et al. proposed a series of models [6-13], most of which are summarized in [9]. They extended the Hedgepeth model to include a variety of damages ahead of the crack tip such as longitudinal matrix splitting, yielding, transverse damage ahead of the crack tip, and a combination of these damages, etc. These efforts were made in order to account for the actual damage ahead of the crack tip in predicting the deformation characteristics and notched strength of the composite. These damages were modeled by enforcing the appropriate boundary conditions corresponding to the different types of damage. For example, the longitudinal splitting and yielding were modeled by first assuming that they exist and have a known length. The shear stress was assumed to be zero at the split region and constant (equal to the matrix shear yield stress) across the yield zone. Satisfying continuity of displacements yielded additional equations from which the lengths of the split and yield zone were calculated. In order to model a transverse damage ahead of the crack, it was assumed that the matrix material remains intact and the damaged zone is capable of carrying some reduced load. The transverse damage, therefore, was modelled as a region of reduced stiffness. The notched strength predictions were made by first assuming a transverse damage zone of a size equivalent to one fiber diameter. The far-field stress was computed for this configuration. The transverse damage was then extended and the corresponding increase in the far-field stress was calculated. The process was repeated until successive increases in the transverse damage did not require any additional increase in the far-field stress. It was found that for every initial crack length the transverse damage growth was stable until about seven additional fibers are broken, and catastrophic crack extension followed subsequently.

Goree et al. compared the different types of damage analyzed with experimental results in terms of COD and notched strength. In the case of a ductile matrix, e.g. boron/aluminum, it has been demonstrated that among all the types of damages

considered the inclusions of the transverse damage is the most important. When certain prameters are adjusted, such as the size of the transverse damage, the amount of stiffness reduction in the transverse damage zone, etc., excellent agreement between prediction and experiments has been established. It should be noted here, that when no such damage at the crack tip is taken into account, catastrophic fracture of the composite occurs immediately with the fracture of the first intact fiber.

Reedy [20] employed the principle of a stationary value of the complementary energy and modeled a centrally notched unidirectional monolayer subjected to longitudinal displacements at infinity. The matrix carried only shear stresses and obeyed the elastic-work-hardening Ramberg-Osgood constitutive relationship. The monolayer was divided into finite elements and the governing equations were solved for stresses in the monolayer. The crack tip normal stresses corresponding to increasingly applied longitudinal displacements at infinity were calculated and compared with the prescribed fiber strength. If the crack tip damage fiber exceeded the prescribed fiber strength, crack extension occurred. It was determined from this analysis that at the instant of crack growth the net section 5.6 mil B/Al monolayer containing a 12.7 mm (0.5 inch) long center crack. Stable crack growth under increasing end displacements was predicted, and it was shown that the notch extends its length by 32.8% during stable growth and then unstable fracture follows. For the 5.6 mil boron fibers the 32.8% stable crack growth corresponds to approximately 12 broken fibers. It should be noted that Goree predicted stable crack growth extending until approximately seven fibers are broken and this stable crack extension was independent of the initial crack length. In Goree's model, however, the matrix is elastic-perfectly plastic, and the transverse damage region maintains some reduced stiffness and therefore carries some reduced load.

The aforementioned mechanistic models, based on the equilibrium of a small element in an infinite array of parallel fibers connected by a matrix, do give a great deal of insight into the stress and deformation fields in the monolayer containing a transverse crack. However, in all the formulations explained above the governing equations to be solved are highly complex. Moreover, the number of the equations to be solved can be extremely large. For example, in the formulations of Hedgepeth [2], Eringen and Kim [5], and Goree et al. [9], the number of equations to be solved are at least half the number of broken fibers contained in the notch. The solution techniques are quite involved, and for large cracks the results can be obtained only by solving a large number of highly nonlinear equations. In Reedy's formulation [20] a more realistic matrix behavior is considered and the predictions are in agreement with the experimental observations. The solution procedures, however, can only be implemented thorugh a tedious finite element code.

5.4.2 Shear Analogy Model

The load-COD curves obtained for unidirectional boron/aluminum by the IDG for various crack lengths at room and elevated temperatures, Figures 4, 7, 16, 17, have been compared with the analytical model proposed by McClintock [14-15]. This model accounts for the longitudinal inelastic deformation at the crack tip. As discussed in Sections 5.3 and 6.3, the failure of notched unidirectional boron/aluminum is preceded by crack tip blunting due to the inelastic shear deformation of the matrix in the filament direction. Thus, a comparison between the proposed model and the experimental results seems to be appropriate and will yield an evaluation of the in-situ matrix shear yield strength (or fiber/matrix interface shear strength) at different temperatures. A good agreement between predicted and experimental load-COD curves has been established for center-notched unidirectional boron/aluminum at room temperature [23]. The application of this model to elevated tempeatures load-COD curves is discussed below.

An analytical model predicting the length of the plastic zone, R_p, and the crack opening displacement at the crack tip (ΔV^p) has been suggested in [14,15]. According to [15] the length of the plastic zone, R_p is

$$R_p = \frac{\pi^2}{16} \left(\frac{G_{LT}}{E_L} \right)^{1/2} \frac{aY^2P^2}{\tau_m^2 W^2 B^2} \tag{1}$$

and the corresponding permanent opening of the crack tip is:

$$V^p = \frac{8}{\pi} [\tau_m / (G_{LT} E_L)^{1/2}] R_p \tag{2}$$

where τ_m is the shear yield stress of the matrix and E_L and G_{LT} are the longitudinal and in-plane shear moduli, respectively. Note that ΔV^p predicts crack tip opening displacement (CTOD) but it can be compared to the COD at the center of the crack, measured experimentally, because it was found that the crack surfaces do not deform plastically during crack opening [23]. Thus, combining Equations (1) and (2):

$$\Delta V^p = \frac{\pi}{4} \frac{1}{\tau_m E_L} \left(\frac{2a}{WB^2} \right) Y^2P^2 \tag{3}$$

The elastic COD at the center of the crack, ΔV^e, has been shown to be (see Section IV):

$$\Delta V^e = \frac{2}{E_L B} \frac{Y}{\alpha} \frac{2a}{W} P \tag{4}$$

where α is the orthotropic correction factor:

$$\alpha = \frac{1}{\sqrt{2}} \left[\left(\frac{E_L}{E_T} \right)^{1/2} - \nu_{LT} + \frac{E_L}{2G_{LT}} \right]^{1/2} \tag{5}$$

It has been shown earlier (see Section IV) that the prediction of the elastic COD agrees very well with the experimental results.

The total crack opening displacement will be the sum of the elastic and plastic COD, i.e.:

$$COD = \Delta V^e + \Delta V^p = \frac{Y}{E_L B} \frac{2a}{W} \left(2\alpha + \frac{\pi Y}{4\tau_m WB^2} P \right) P \tag{6}$$

The predicted load-COD curves (Equation 6) have been compared with the experimental results obtained at room temperature as shown in Figure 20. For the purpose of this comparison the matrix shear yield stress, τ_m, was chosen so as to yield good agreement. The results indicate that for all crack lengths similar values could be used for τ_m, which validates the applicability of this model in predicting the deformation of the subject material. The value of τ_m that fits the experimental result best for all six crack lengths in approximately 150 MPa (22 ksi) which agrees with handbook data given for aluminum 6061F of 138 MPa (20 ksi).

The results shown in Figure 20 indicate that in the elastic region the prediction deviates slightly from the experimental COD. This is mainly due to the fact that the analytical model (Equation (1)) predicts the formation of longitudinal plastic deformation, and thus blunting of the crack tip, immediately upon initial loading. however, the first plastic zone appears at a much later stage of loading. The deviation of the prediction from the experimental data becomes more pronounced at higher load levels because the analytical model incorporates only one plastic zone, while for unidirectional 5.6 mil boron/aluminum-6061F at least 5-6 such zones are actually observed prior to failure [23].

At elevated temperatures different (lower) values for τ_m should be used to best fit the prediction with the experimental load-COD, Figures 21-23. This should be expected considering the increased ductility of the aluminum matrix, whose effect on the load-COD characteristics is particularly pronounced in center-notched unidirectional specimens. As in the case of the local compliances (see Section IV), the effect of temperature on the load-COD curves becomes significant at temperatures above 204°C (400°F). This is manifested by the very low values of the matrix yield shear stress, τ_m, required to best fit the data at higher temperatures. It should be noted that in the comparison between prediction and experiments similar values of τ_m were used for all crack lengths at a given temperature.

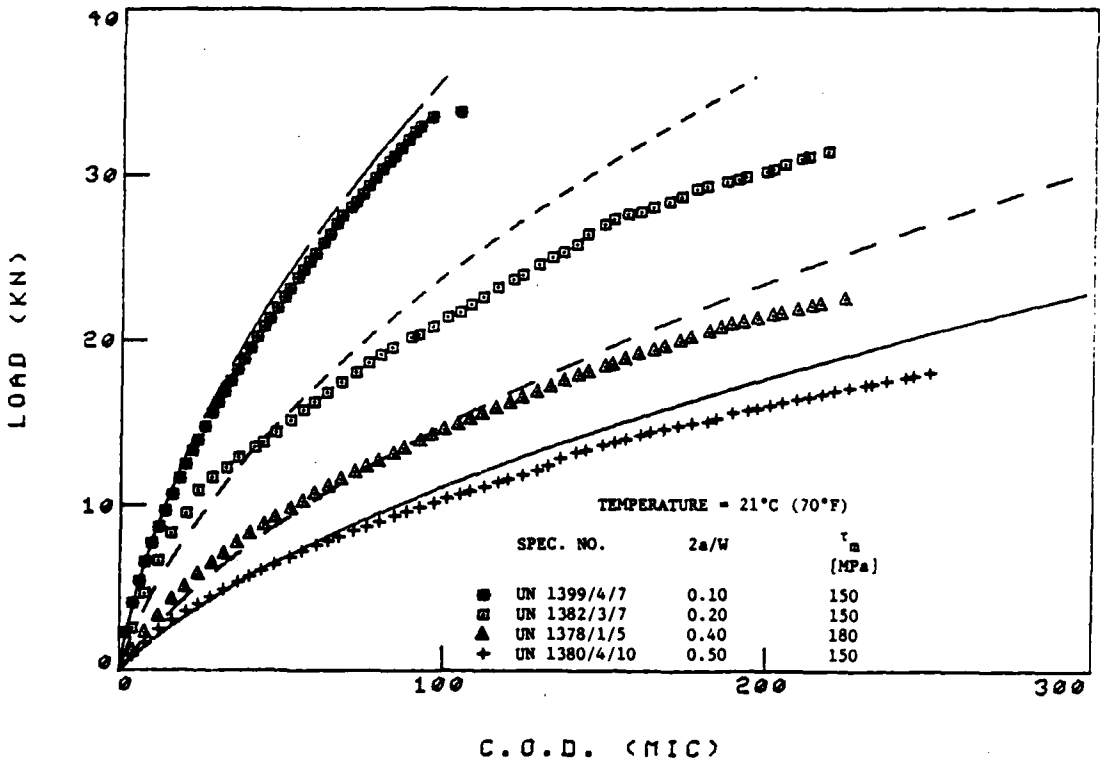

Figure 20. Comparison between predicted (Equation (6)) and experimental load-COD curves for various crack lengths for unidirectional boron/aluminum specimens.

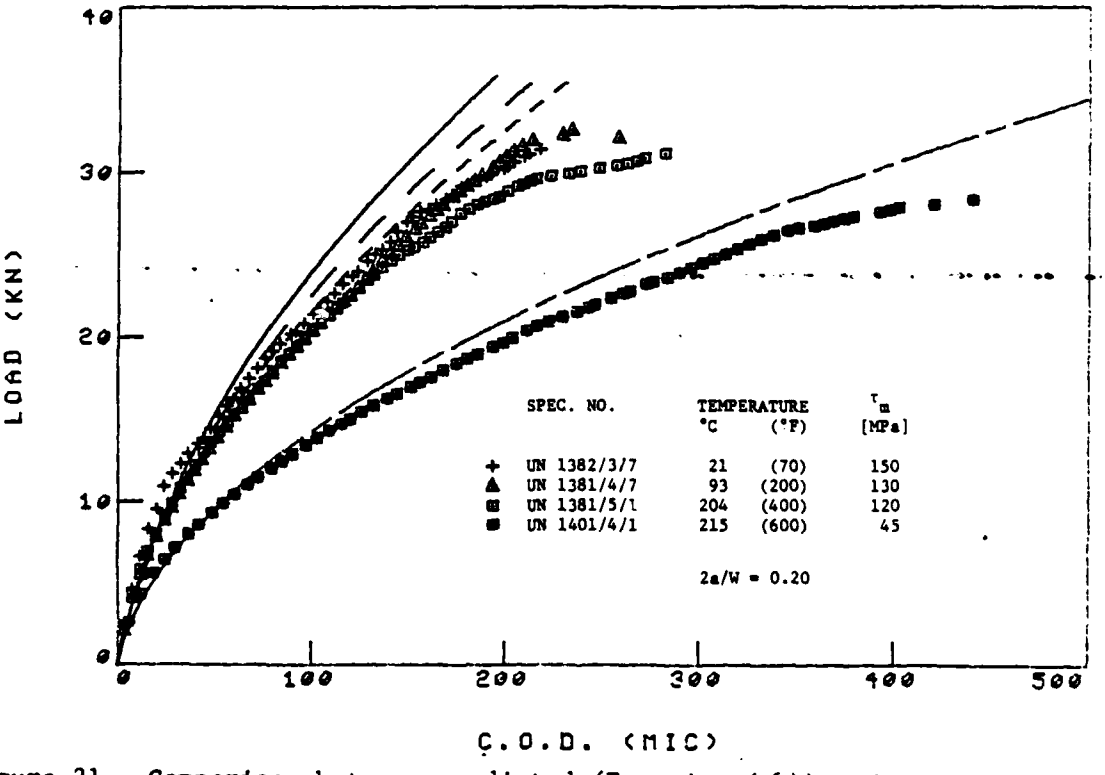

Figure 21. Comparison between predicted (Equation (6)) and experimental load-COD curves at different test temperatures for unidirectional boron/aluminum specimens, 2a/W = 0.2.

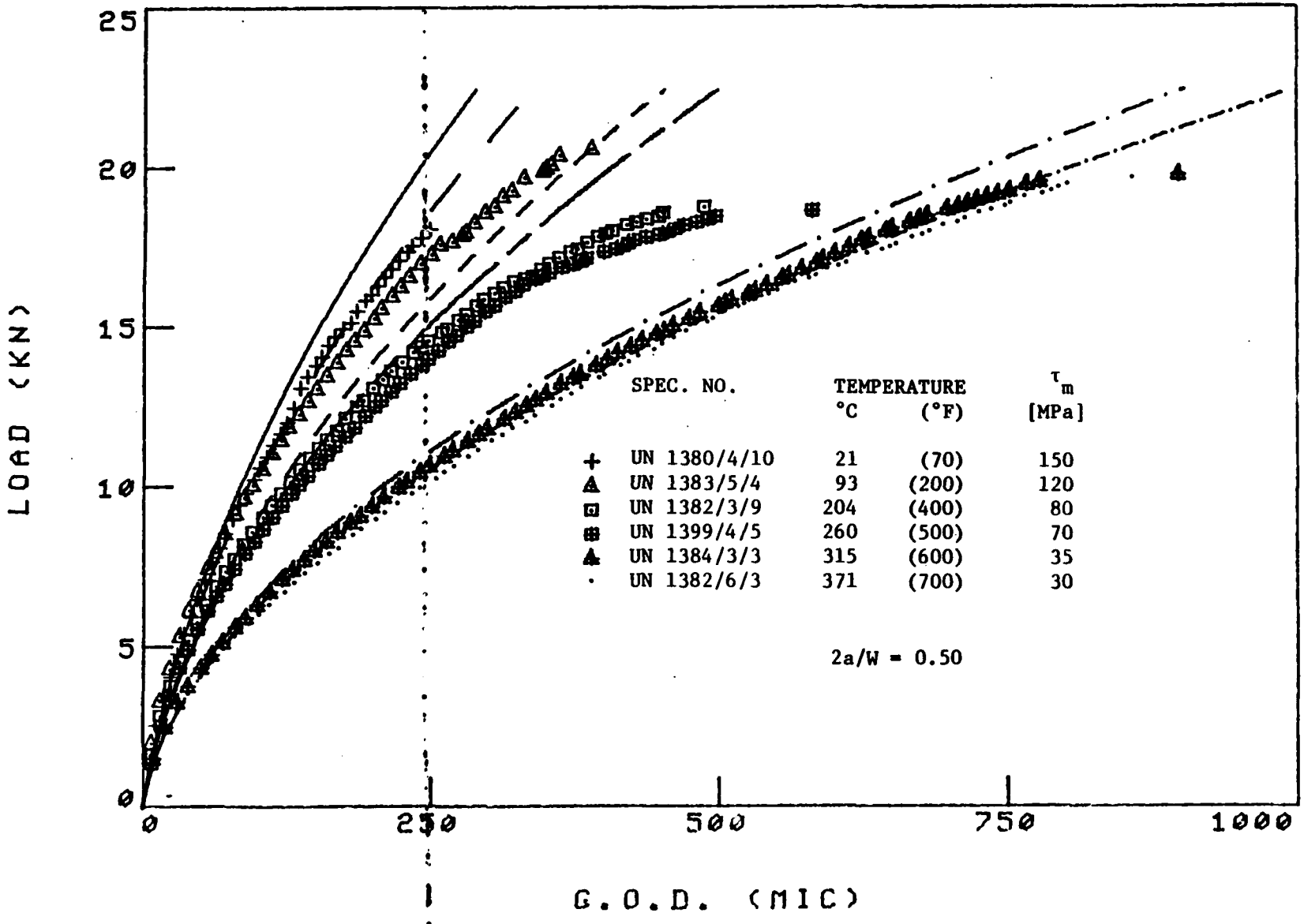

Figure 22. Comparison between predicted (Equation (6)) and experimental load-COD curves at different test temperatures for unidirectional boron/aluminum specimens, 2a/W = 0.5.

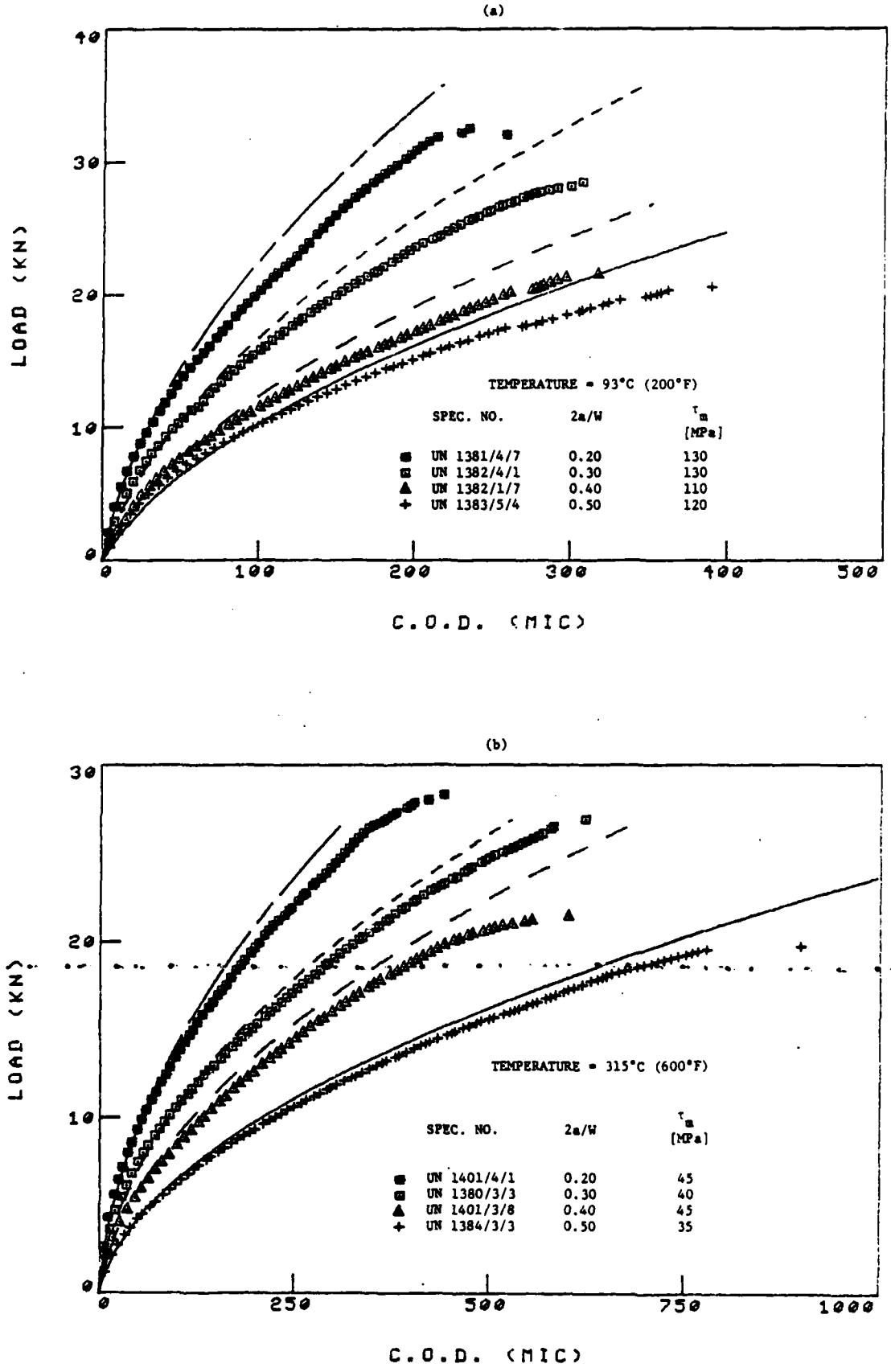

Figure 23. Effect of crack length on load-COD curves for unidirectional boron/aluminum specimens at elevated temperatures.

5.4.3 Lumped-Fiber Model

In most of the models explained above it has been shown that the effect of the notch in terms of fiber SCF is highly localized at the crack tip. Thus, while the fiber stresses are high at the crack tip they rapidly approach the far-field stress within a few fibers away from the crack tip. Consequently, a detailed knowledge of the stress distribution of every fiber is not necessary and the analysis can be restricted, without loss of accuracy, to the stress distribution in the first few fibers ahead of the crack tip only.

Accordingly, Zweben [17] greatly simplified the shear-lag analysis and proposed an approximate model called the "Lumped Fiber Model". Instead of considering every fiber, the displacement fields are lumped into three different regions, Figure 24, namely; core of broken fibers, first intact fiber next to the crack, and the remaining fibers (far-field region). The basic shear-lag assumptions in this formulation are the same as in Hedgepeth's analysis except that the matrix in the bay between the core and the first intact fiber is allowed to yield. However, the matrix is restricted to be either elastic-perfectly plastic or birttle. A longitudinal inelastic zone between the core and the first intact fiber and emanating from the crack tip is assumed to exist. The matrix in the inelastic zone can only be in one of two states, that is, completely yielding (matrix plastic deformation) or completely splitting (fiber/matrix separation).

For a given size of inelastic zone, the governing equations have been formulated for small elements located at the core and the first intact fiber within and outside the inelastic zone, Equations (7-10). The boundary and continuity conditions to be satisfied are given by Equations (11) and (12), respectively. In addition to these conditions the solution must ensure that the matrix stresses are such that

EQUILIBRIUM EQUATIONS:

	Core of n broken fibers	First intact fiber	Region
(7)	$nE_fA_f \frac{d^2u_o}{dx^2} - 2\eta\tau_m h = 0$	(8) $E_fA_f \frac{d^2u_1}{dx^2} - (u_1 - \frac{\sigma}{E_f}x)\frac{G_m h}{d} + \eta\tau_m h = 0$	$0 \leq x \leq a$
(9)	$nE_fA_f \frac{d^2u_o}{dx^2} - 2\frac{G_m h}{d}(u_o - u_1) = 0$	(10) $E_fA_f \frac{d^2u_1}{dx^2} + \frac{G_m h}{d}(\frac{\sigma}{E_f}x - 2u_1 + u_o) = 0$	$x \geq a$

BOUNDARY CONDITIONS:

	Core of n broken fibers	First intact fiber
(11)	(a) $p(\infty) = p \rightarrow E_fA_f \frac{du_o(\infty)}{dx} = 0$	(b) $p(\infty) = p \rightarrow E_fA_f \frac{du_1(\infty)}{dx} = p$
	(c) $p(o) = 0 \rightarrow nE_fA_f \frac{du_o(o)}{dx}$	(d) $u_1(o) = 0$

CONTINUITY CONDITIONS:

(12)	$0 \leq x \leq a$		$x > a$
(a)	$u_o(a)$	=	$u_o(a)$
(b)	$\frac{du_o(a)}{dx}$	=	$\frac{du_o(a)}{dx}$
(c)	$u_1(a)$	=	$u_1(a)$
(d)	$\frac{du_1(a)}{dx}$	=	$\frac{du_1(a)}{dx}$

where:

u_o...Displacement of fiber in the core
u_1...Displacement of first intact fiber
E_f...Fiber stiffness
τ_m...Matrix yield shear stress
G_m...Matrix shear modulus
a...Inelastic zone size
η...Shear transfer factor (=0, or = 1)
h...Plate thickness
A_f..Fiber cross-sectional area
p...$E_fA_f \frac{du}{dx}$

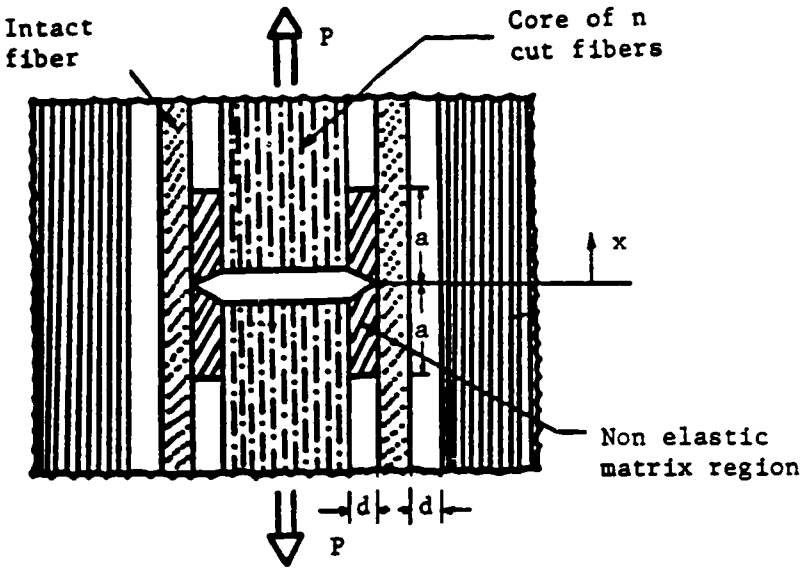

Figure 24. Schematic of Lumped Fiber Model.

$$(13) \qquad (u_o(a) - u_1(a))\, G_m/d = \tau_m$$

The second order governing differential Equations (7-10), are solved, and imposing the conditions of Equations (11-12) results in a set of nonlinear algebraic equations. Due to the lumped analysis the number of these algebraic equations remains the same for all the initial notch sizes. The solution of these equations can be obtained by assuming an inelastic zone length and computing the corresponding far-field stress. Thus having obtained the variation of inelastic zone length with applied far-field stress, the longitudinal displacement and stress fields can be obtained.

It is shown by this simplified anaylsis that the growth of the inelastic zone is significantly different for brittle, Figure 25, and elastic-perfectly plastic matrices, Figure 26. In both the cases, the far-field stress at which the inelastic zone initiates decreases with increasing crack length. In the case of a brittle matrix, however, the inelastic zone (fiber-matrix interfacial splitting), after it initiates, increases very rapidly with increasing applied stres until a stress level

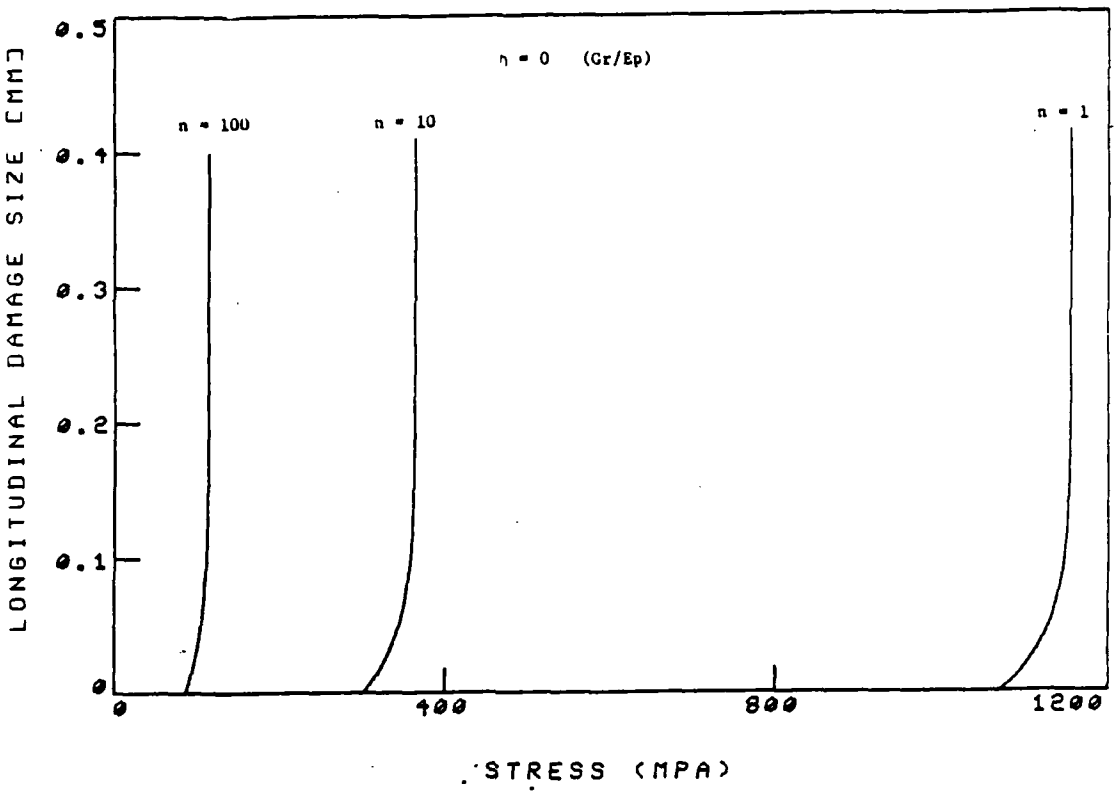

Figure 25. Predicted longitudinal damage zone size in unidirectional graphite/epoxy containing a center crack according to the Lumped Fiber Model.

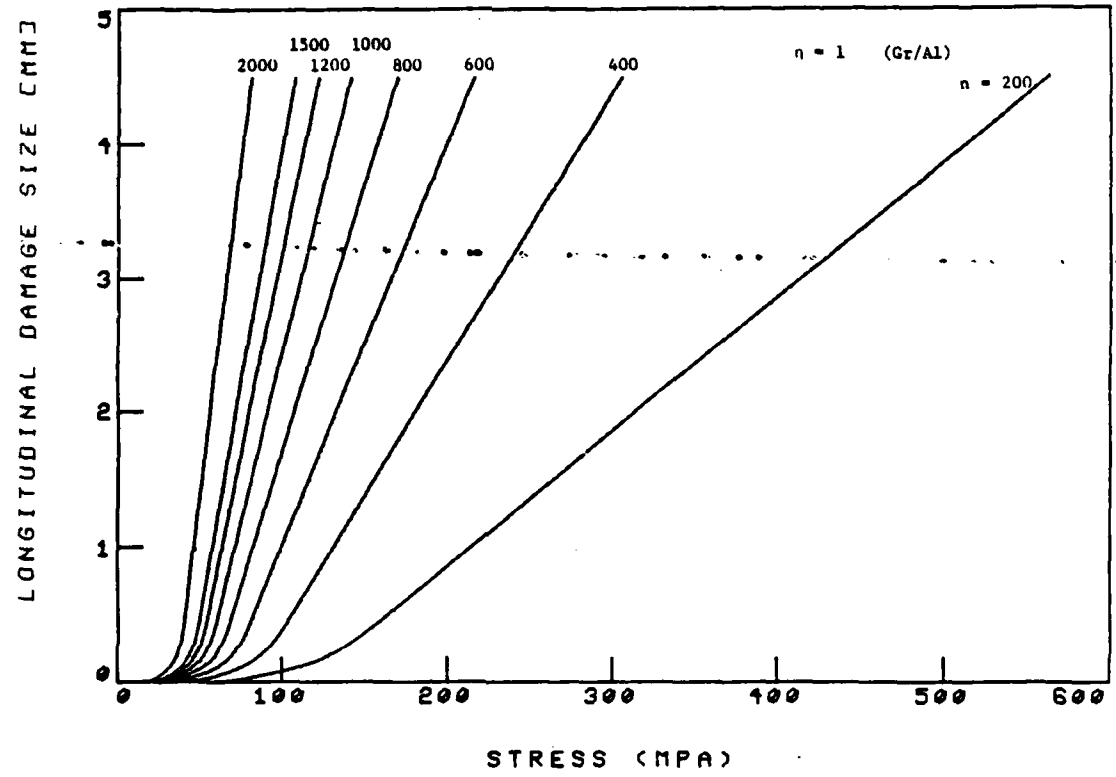

Figure 26. Predicted longitudinal damage zone size in unidirectional graphite/aluminum containing a center crack according to the Lumped Fiber Model.

is reached where splitting increases asymptotically, Figure 25. Similar trends are predicted in Goree's analysis also [24]. This phenomenon is in partial agreement with the experimental observation on unidirectional brittle matrix composite coupons containing a central crack, where it is observed that the splitting originates from the crack tip and increases rapidly with increasing applied stress [24]. However, the rate of increase is much more stable than that predicted.

In the case of composites having a linear elastic-perfectly plastic matrix the Lumped Fiber Model predicts a stable and monotonic growth of the inelastic zone with increasing far-field stress, Figure 26. This behavior is attributed to the fact that in the formulation of this model the shear stresses in the bay between the notch and the first intact fiber are not allowed to increase any further once they reach the predefined yield shear stress of the matrix. Thus, any additional increase in the far-field stress must be equilibrated by a proportional increase in the length of inelastic zone.

The elastic SCF obtained form the Lumped Fiber Model is comparable to that obtained in Hedgepeth's infinite array model. For large crack lengths, however, the difference in the SCF according to these two analyses becomes noticeable. For instance, the elastic SCF corresponding to one broken fiber is 3% lower, and the one corresponding to 1000 broken fibers is 20% lower than the SCF's obtained from the infinite array model. After the initiation of the longitudinal damage emanating from the crack tip, the Lumped Fiber Model predicts decreasing SCF's both at the crack tip and at the tip of the inelastic zone with increasing applied stress, Figures 27-28. In the case of a brittle matrix the crack tip SCF decreases very rapidly to unity at a certain applied stress level, Figure 27, whereas, with a ductile matrix the SCF asymptotically approaches unity with increasing applied stress, Figure 28. The change in the SCF with increasing applied stress will be further discussed below. Zweben compared the predicted values of SCF at failure with the experimentally

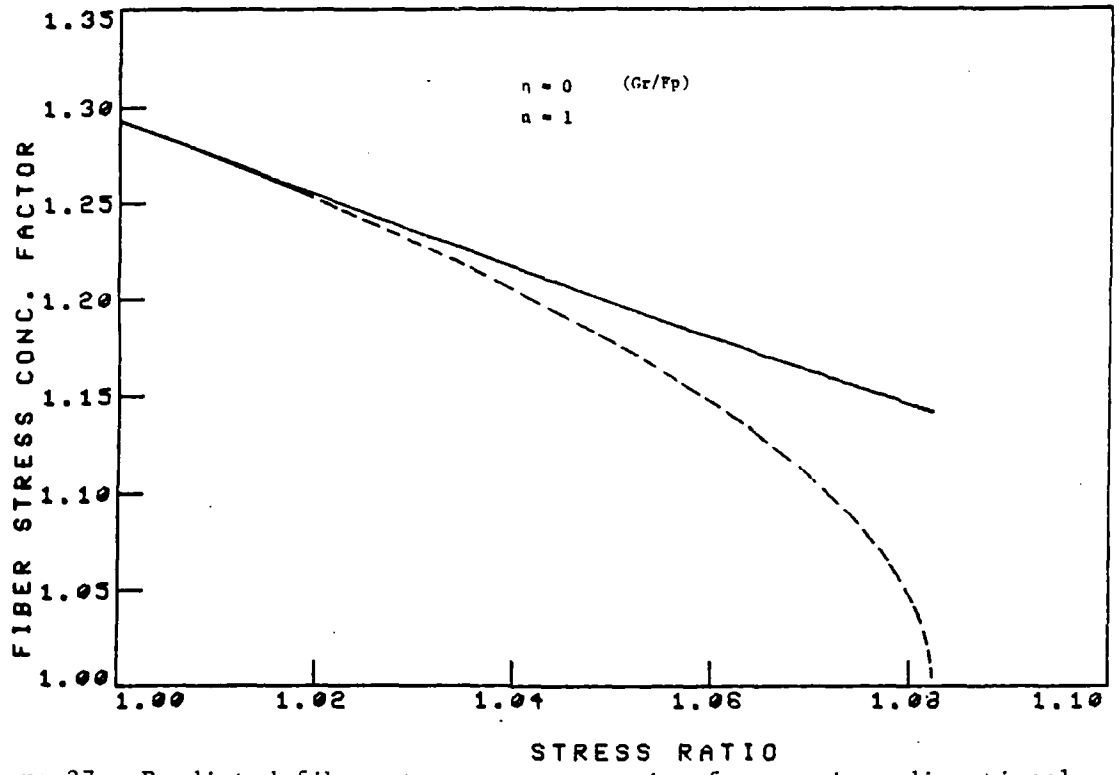

Figure 27. Predicted fiber stress concentration factors in undirectional graphite/epoxy containing a center crack according to the Lumped Fiber Model: - - - at the notch tip; ——— at the tip of the inelastic zone.

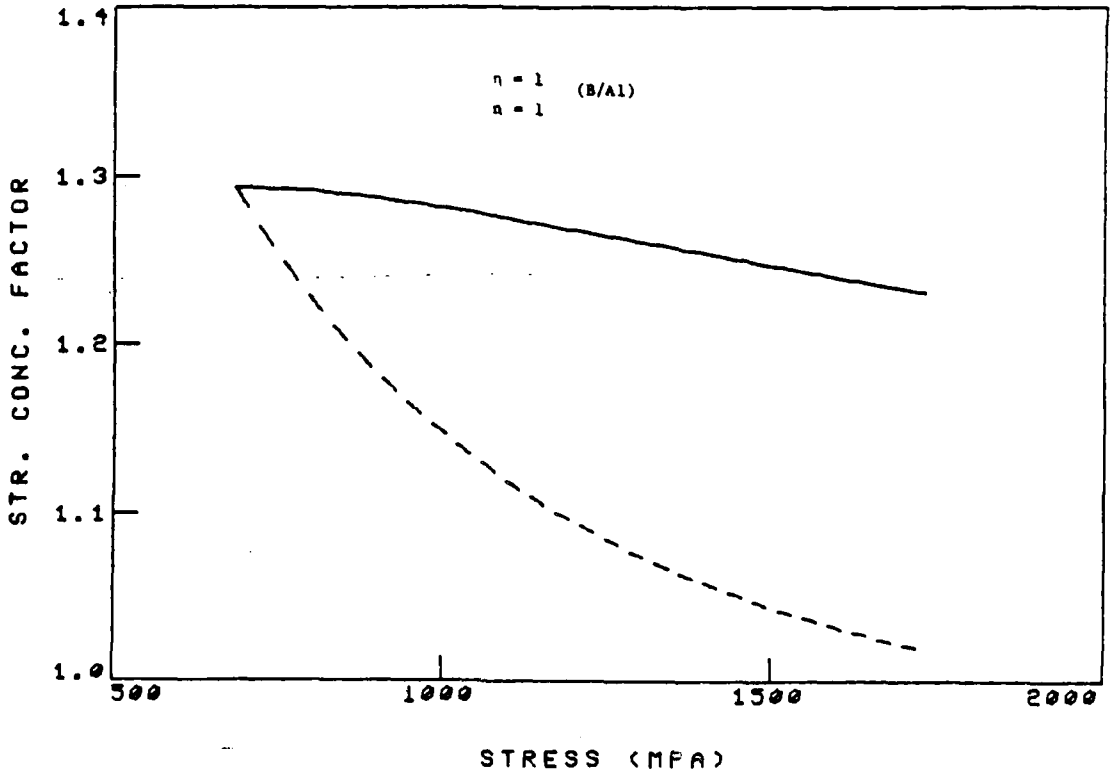

Figure 28. Predicted fiber stress concentration factors in unidirectional boron/aluminum containing a center crack according to the Lumped Fiber Model: - - - at the notch tip; ——— at the tip of the inelastic zone.

AD-A162 352 FRACTURE BEHAVIOR OF BORON ALUMINUM COMPOSITES AT ROOM AND ELEVATED TEMPE (U) DREXEL UNIV PHILADELPHIA PA DEPT OF MECHANICAL ENGINEERING AN J AWERBUCH APR 85 2/3

UNCLASSIFIED AFOSR-TR-85-1099 AFOSR-79-0079 F/G 11/4 NL

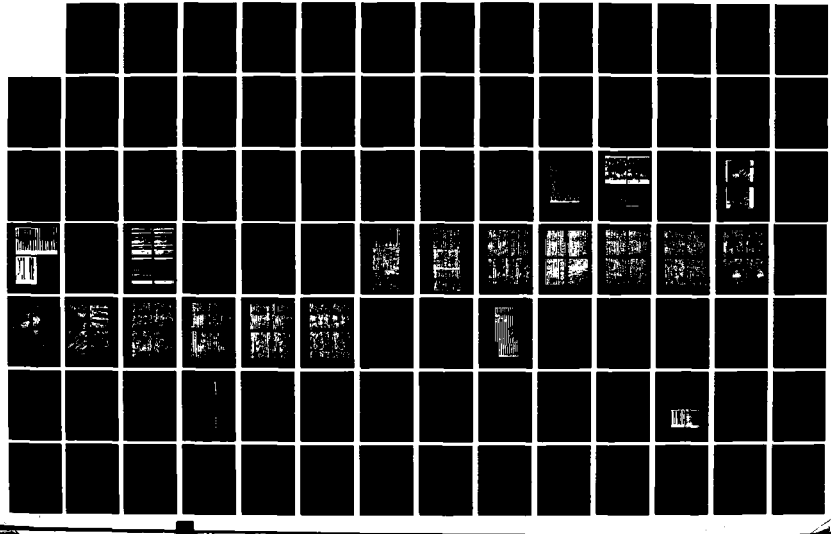

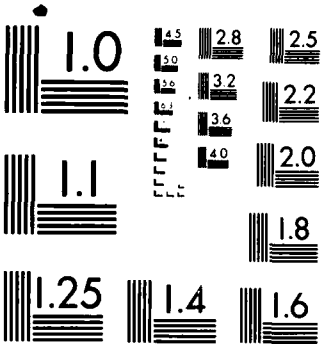

observed values calculated on the basis of the gross failure stress for three different notch sizes in unidirectional carbon fiber/epoxy laminate. It was shown that SCF's at failure determined by the Lumped Fiber Model were approximately 30-40% higher than those obtained experimentally. The corresponding SCF's obtained from elastic analysis of Hedgepeth's infinite array resulted in values which were significantly higher (300-500%) than the experimental values.

5.4.4 Extension of the Lumped Fiber Model

From the preliminary results obtained in the Lumped Fiber Model, it seems that the results are comparable to those obtained in the previously described mechanistic models where every fiber is assigned a unique index. Moreover, the number of equations to be solved in the Lumped Fiber Model are far fewer and less complicated. In the following sections, therefore, a significant amount of effort has been directed to extend the Lumped Fiber Model so that the effect of various model parameters on the predictions can be determined, and more realistic material properties can be included.

The extension of the Lumped Fiber Model has been carried out in two phases. In the first phase the Zweben's model has been extended to predict also the crack opening displacement and notch strength and a comparison between predictions and experiments has been made. In addition, parametric analysis has been performed in which the effects of certain variables, such as matrix yield shear strength, fiber diameter, crack length and specimen width, on the growth of the inelastic zone size, fiber stress and SCF, COD, and notched strength has been analyzed. The basic assumption made by Zweben with regard to the matrix material, i.e. linear elastic-perfectly plastic or brittle, is maintained.

In the second phase, the Zweben's model is reformulated where the assumptions imposed on the matrix are relaxed and a more realistic nonlinear shear stress-strain behavior of the matrix is incorporated. However, the basic shear-lag assumptions,

i.e. the fibers carry longitudinal stresses only and the matrix carries shear stresses only, are still enforced. The following is the development of these two phases.

I. Linear Elastic-Perfectly Plastic Matrix:

A computer code for the Lumped Fiber Model has been developed in such a manner that the model parameters can be varied and their influence on the deformation characteristics can be determined. The matrix is still restricted to be either linear elastic-perfectly plastic or brittle. In the subsequent discussion, however, only the results with linear elastic-perfectly plastic matrix are discussed.

a. Effect of Matrix Ductility

1. Longitudinal Inelastic Zone Size: It has been observed experimentally (see Section VI) that in unidirectional boron/aluminum composites containing a center notch, the first sign of damage appears in the form of a yield zone emanating from the crack tip. In the Lumped Fiber analysis this damage is modeled as a zone where the matrix carries a constant shear stress equal to the yield shear strength of the matrix. Depending on the ductility of the matrix the inelastic zone will attain different lengths at a given applied load. Figure 29* shows the growth of the inelastic zone as a function of applied stress for three different matrices in a unidirectional monolayer of boron/aluminum containing a center notch ($2a/W = 0.3$). The applied stress at which the crack tip yielding initiates increases with increasing yield stress of the matrix. The growth of the inelastic zone is stable, monotonically increasing with the applied stress for all the three matrices, however, with a more ductile matrix the inelastic zone initiates earlier and grows much faster than in a less ductile matrix.

2. Notch Tip Fiber Stress and Stress Concentration Factor (SCF): The effect of matrix yield shear stress on notch tip fiber stress and SCF is shown in Figures 30-31, respectively. A strong influence of matrix on both the longitudinal

* In Figures 29-55 the following material constants were used (unless otherwise stated): $E_f = 400$ GPa, $G_m = 20$ GPa, $\tau_m = 200$ MPa, v/o = 0.5, $d_f = 140$ μm, $W = 25.4$ mm, $2a/W = 0.3$.

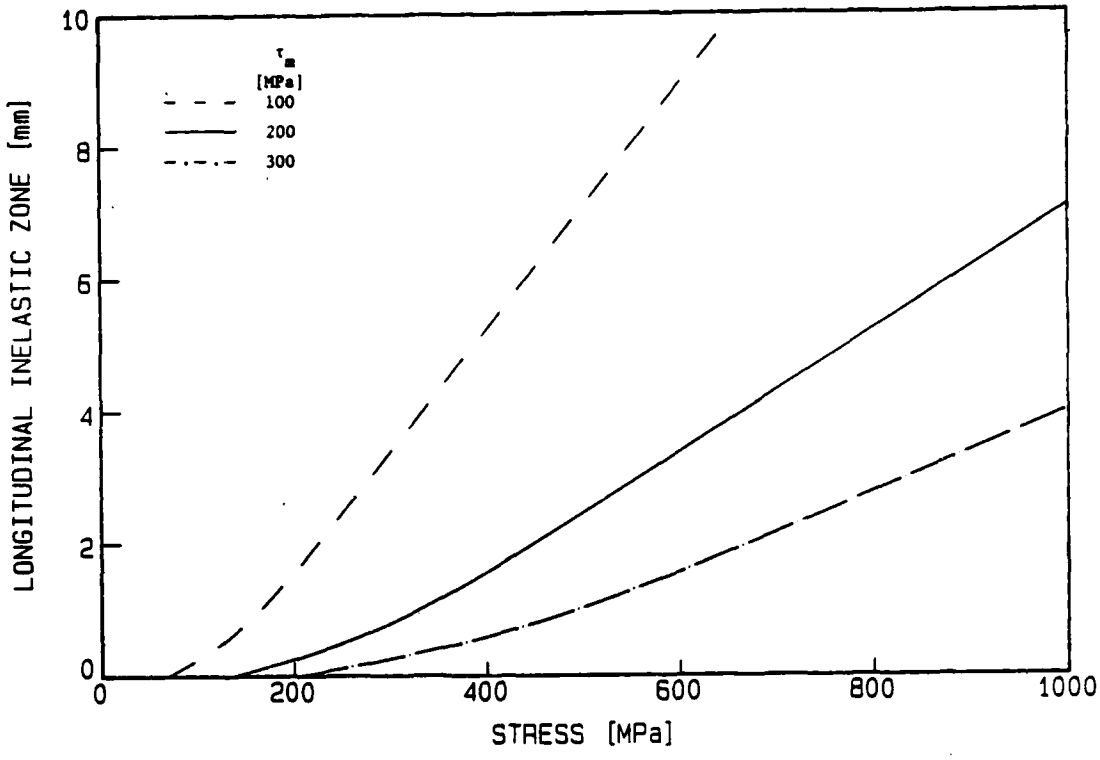

Figure 29. Effect of matrix yield shear stress on the length of the inelastic zone as predicted by the Lumped Fiber Model for unidirectional boron/aluminum.

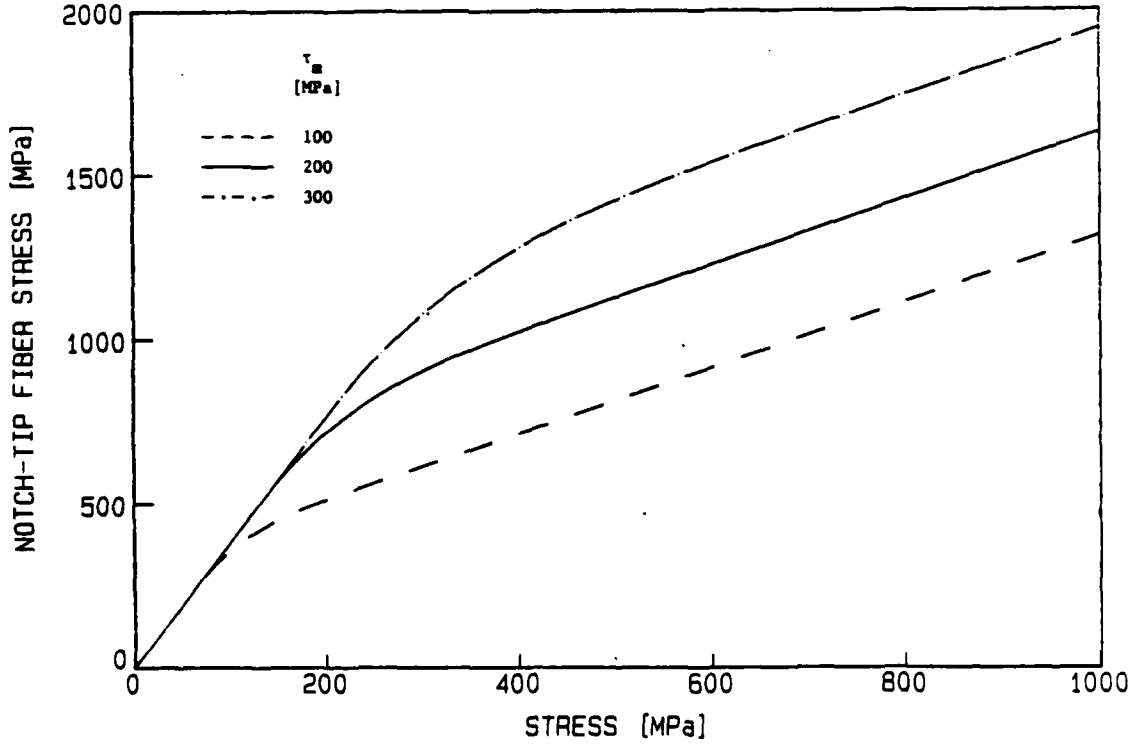

Figure 30. Effect of matrix yield shear stress on the notch tip fiber stress as predicted by the Lumped Fiber Model for unidirectional boron/aluminum.

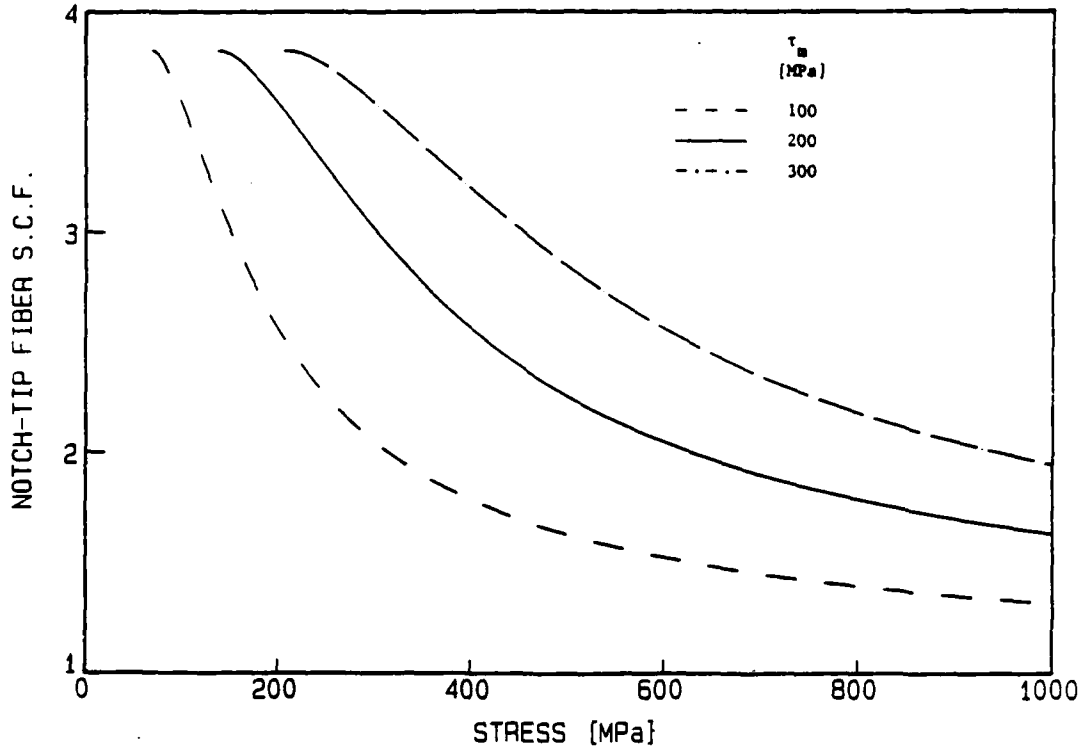

Figure 31. Effect of matrix yield stress on the notch tip fiber stress concentration factor as predicted by the Lumped Fiber Model for unidirectional boron/aluminum.

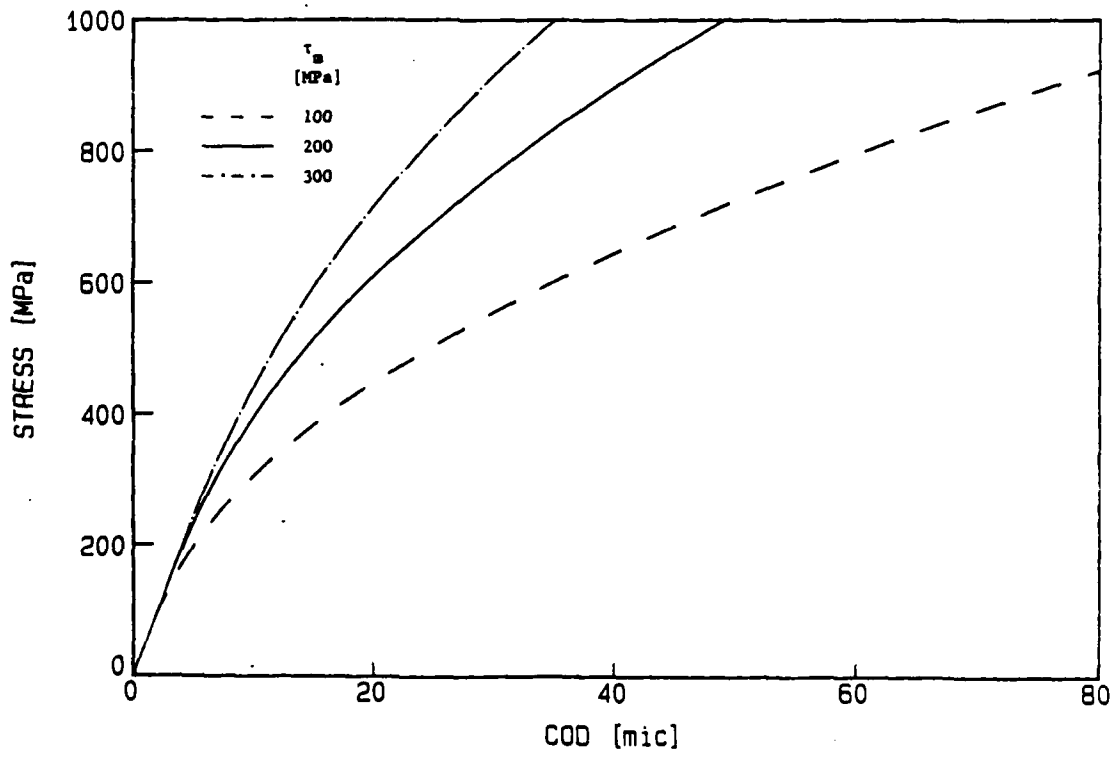

Figure 32. Effect of matrix yield stress on the load-COD curve as predicted by the Lumped Fiber Model for unidirectional boron/aluminum.

stress in the fiber at the notch tip and on SCF is indicated. It is noted that the normal stress in the first intact fiber monotonically increases with applied far-stress, however, for the same applied stress the notch tip fiber stress is much smaller with ductile matrix.

The crack tip SCF decreases with increasing applied stress and asymptotically approaches unity for all three cases. The elastic SCF's (SCF at a stress level when longitudinal damage initiates) are the same for all three matrices, yet the applied stresses at which they occur do depend on matrix yield shear stress. Also, with the ductile matrix the SCF decreases more sharply than with the stronger matrix. The rapid decrease of SCF with a ductile matrix can be explained by the fact that longitudinal damage emanating from the notch tip alleviates the stress concentration at the notch tip [14-15]. The longer the yield zone, the greater would be the stress transfer between the fibers, resulting therefore in a larger reduction in the SCF. The yield zone of the ductile matrix grows faster than that of a stronger matrix, thereby causing a greater reduction in the crack tip SCF.

3. Crack Opening Displacement (COD): The crack opening displacement in the Lumped Fiber Model is defined as the displacement of the "core" at the crack. Figure 32 shows the variation of COD with stress for three matrices. Clearly, the displacements are much higher when the matrix is soft. The comparison of the predictions with the experimentally measured values of COD, Figure 33, through IDG technique (Section 5.3) for center-notched unidirectional boron/aluminum composite indicate that the general trend predicted by the analysis is in agreement with the experiments. It should be noted, however, that the matrix yield shear stress values required to fit the experimental data are substantially low. Also, for the lower loads the analysis predicts the composite to be stiffer than it proved to be experimentally. One possible explanation for this behavior is that in the analysis the inelastic zone emanating from the crack tip is confined to the bay

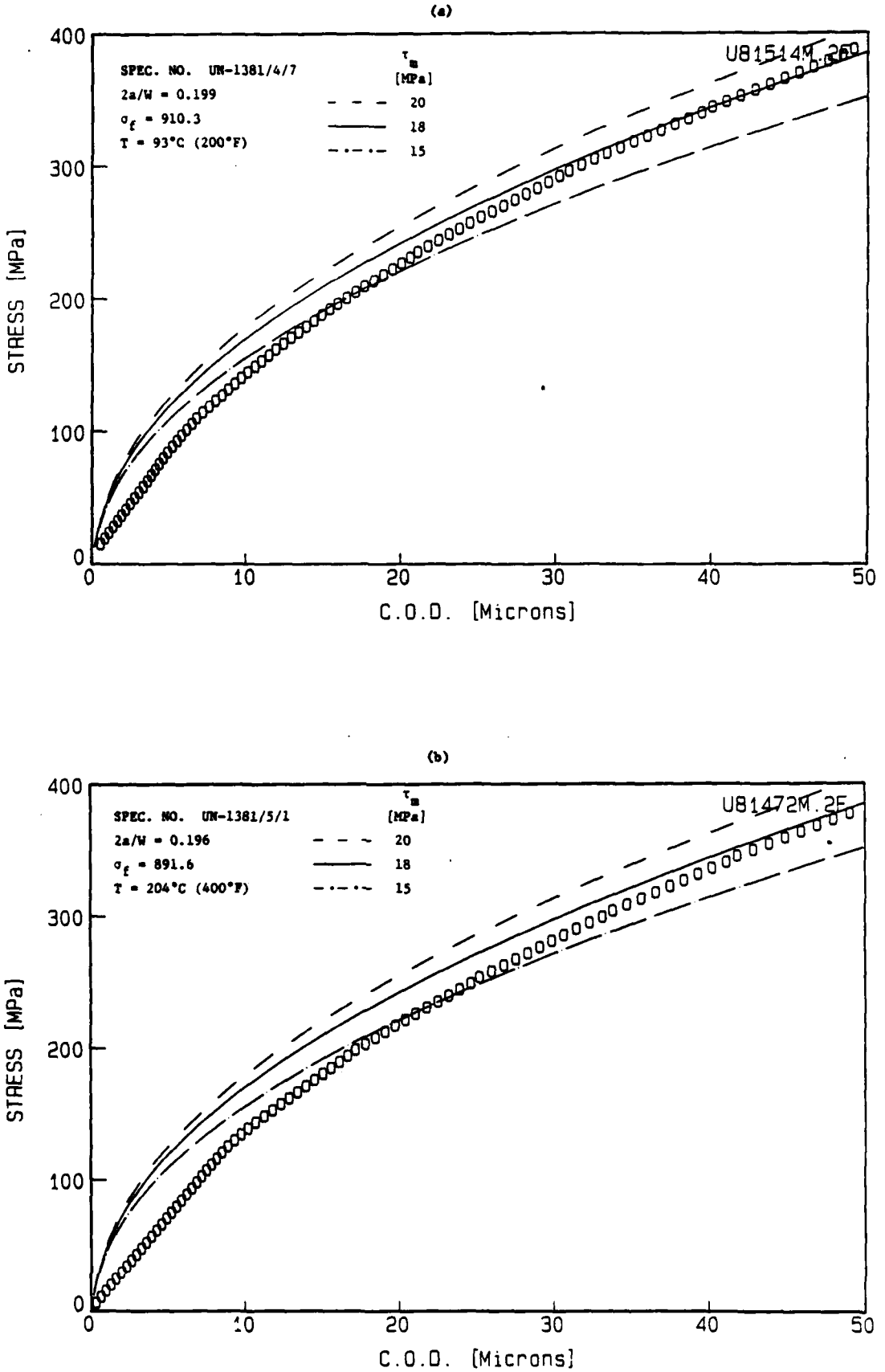

Figure 33. Comparison between predicted (Lumped Fiber Mode) and experimental load-COD curves for unidirectional boron/aluminum specimens.

between the crack and the first intact fiber. Also, the stress field beyond the first intact fiber is assumed to be that of the far-field. This implies that only the first intact fiber experiences the effects of the stress concentration due to the crack, and that the remaining intact fibers behave as if there were no crack. This restriction would make the composite seem stiffer than it actually is.

4. Notched Strength Prediction: The notched strength of center-notched unidirectional boron/aluminum specimens can be predicted providing that an appropriate failure criterion is specified, as discussed below. Since the crack tip elastic SCF increases with crack length (page 74) failure of the first intact fiber (causing an increase of the crack length) will result in an increase in the crack tip elastic SCF in the neighboring fiber. Consequently, an unstable crack extension will occur causing catastrophic fracture of the specimen. In short, the failure criterion used in the Lumped Fiber Model (as in all other shear-lag based models) is that catastrophic fracture occurs when the first intact fiber breaks.

In predicting the notched strength, fiber breakage occurs when the normal stress in the first intact fiber at the notch tip reaches the average fiber strength. The average fiber strenth chosen (2.6 GPa) was calculated from the unnotched strength data determined for the composite using the rule of mixture.

Figure 34 shows the comparison between prediction and experimental notched strength data obtained for center-notched unidirectional boron/aluminum. The predictions are based on three different values of matrix shear yield stress, τ_m. For all three cases the difference between experiments and predictions is quite significant. Moreover the model predicts very high notch sensitivity for short crack lengths and notch insensitivity for the longer crack lengths. It should also be noted that the matrix shear yield stress values chosen in Figure 34 are significantly higher than those used to predict the load-COD , Figure 33.

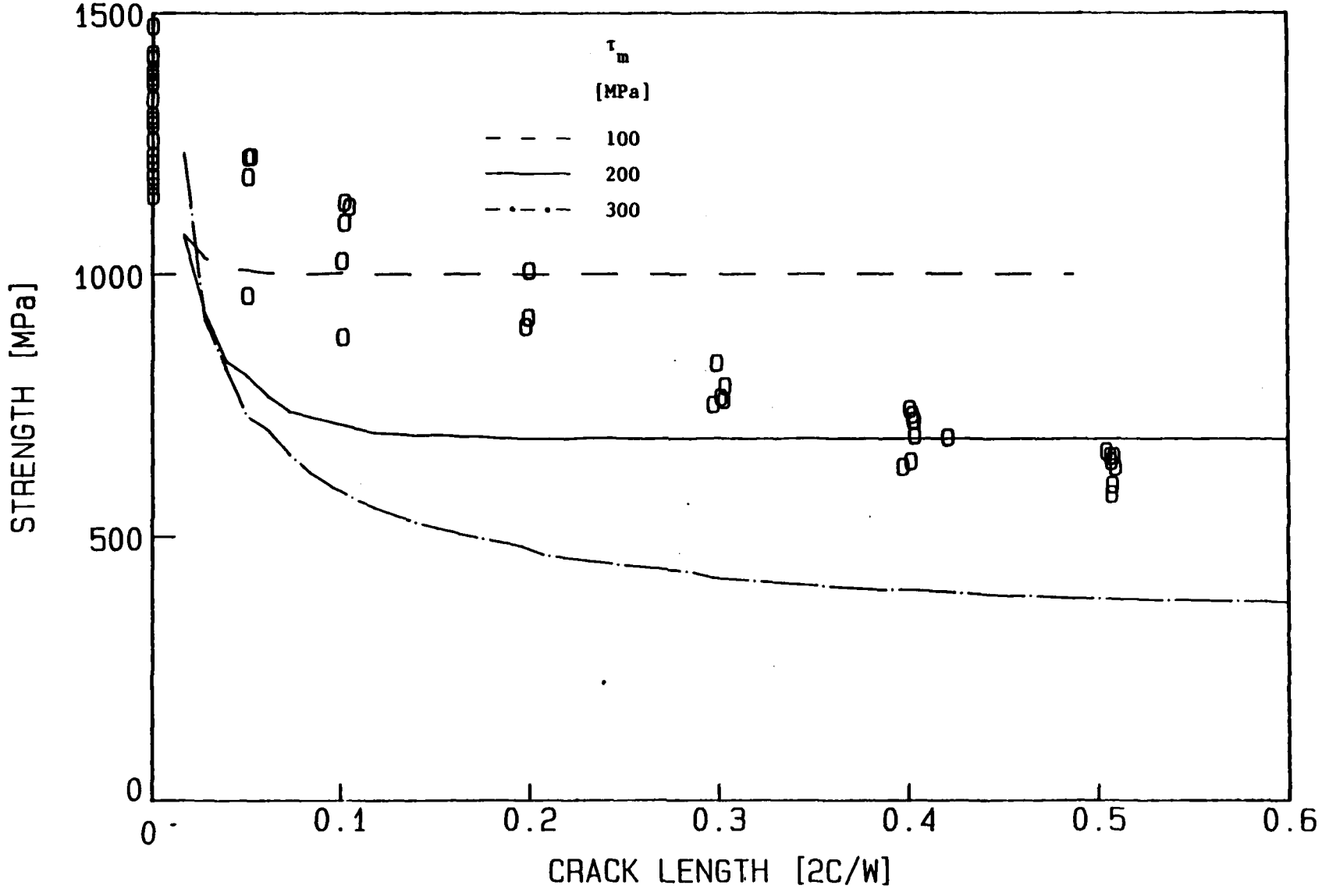

Figure 34. Comparison between predicted (Lumped Fiber Model) and experimental notched strength for unidirectional boron/aluminum.

The lack of agreement between the experimental data and the Lumped Fiber Model is preimarily due to two reasons: 1. the choice of linear elastic-perfectly plastic behavior of the aluminum matrix rather than the actual shear stress strain behavior; and 2. the model predicts catastrophic fracture to follow the breakage of the first intact fiber while actual 6-8 fiber breaks occur prior to catastrophic fracture, as has been discussed in Sections 5.3 and 6.3. The incorporation of these two issues into the model will add significant complexity. In this research program the incorporation of the actual shear stress-strain curve has been attempted, as will be discussed later.

b. Effect of Crack Length

The extent of inelastic deformation in an unidirectional boron/aluminum monolayer is strongly affected by the initial crack size. With larger crack lengths the longitudinal inelastic deformation not only starts earlier but also extends over a greater length, Figure 35. This is expected because the average normal stresses borne by fibers are higher when the initial crack size is large, resulting in higher displacement gradients and longer inelastic zone lengths.

In the previous discussions it was demonstrated that the elastic SCF at the crack tip increases with increasing number of broken fibers or with increasing crack length. Figure 36 shows the SCF as a function of applied stress for two crack sizes. It should be noted that even though the elastic SCF's are higher for longer cracks the increased inelastic deformation associated with longer cracks, Figure 35, results in a rapid reduction in the SCF with increasing applied stress, Figure 36. At sufficiently high applied stress the SCF is independent of crack length and approaches unity.

The load-COD curves shown in Figure 37 clearly indicate that COD is sensitive to crack length, being larger for the longer cracks.

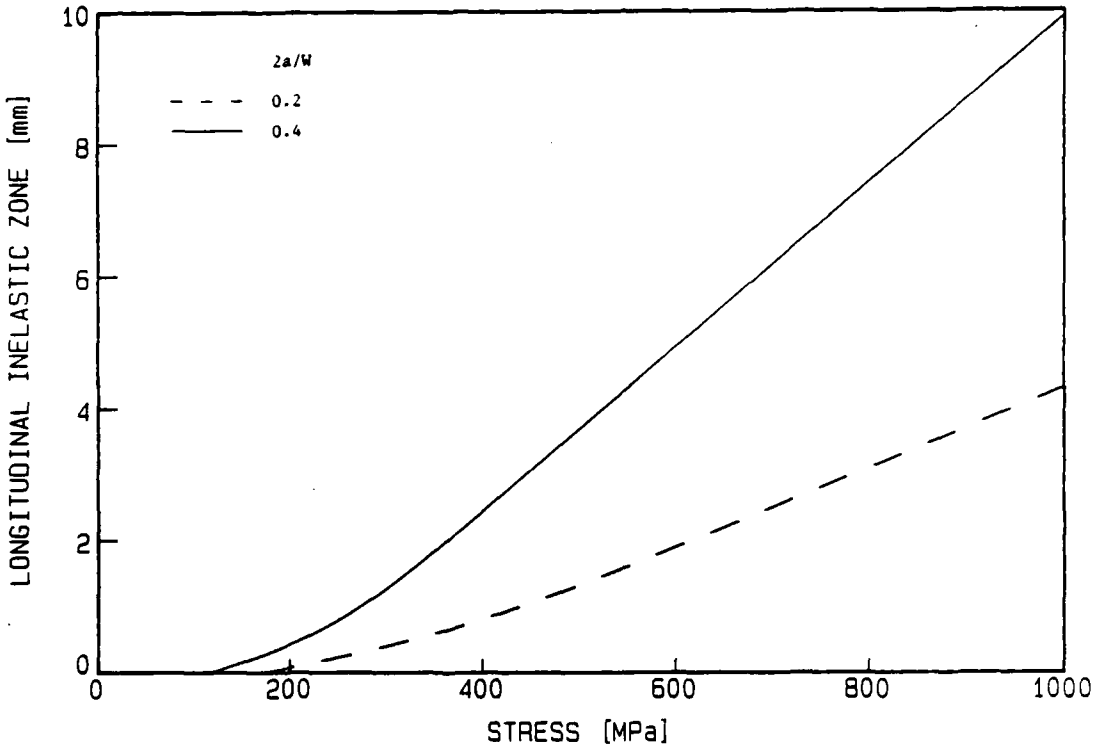

Figure 35. Effect of crack length on length of inelastic zone as predicted by the Lumped Fiber Model for unidirectional boron/aluminum.

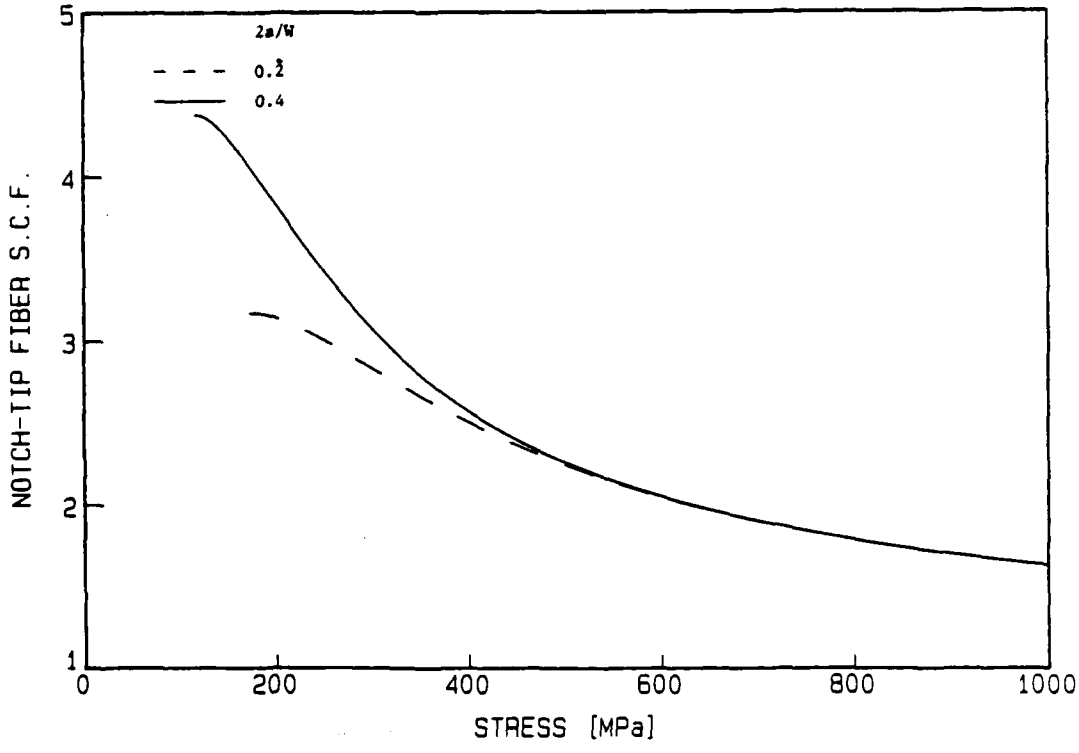

Figure 36. Effect of crack length on notch tip fiber stress concentration factor as predicted by the Lumped Fiber Model for unidirectional boron/aluminum.

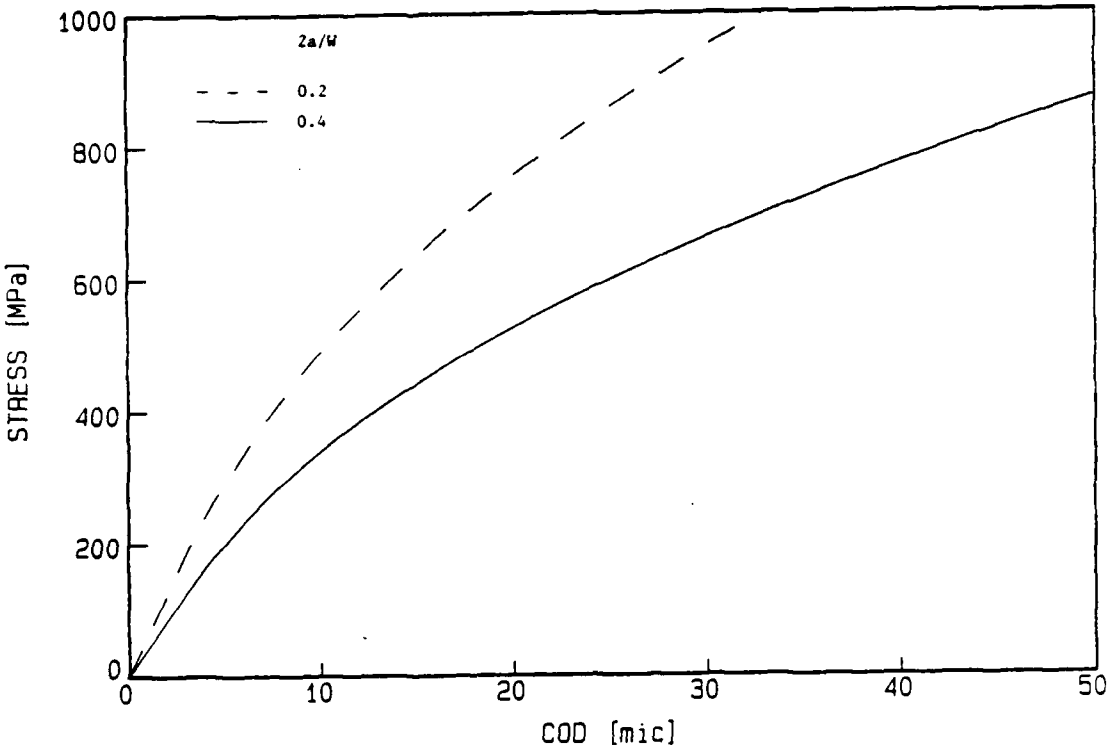

Figure 37. Effect of crack length on load-COD curves as predicted by the Lumped Fiber Model for unidirectional boron/aluminum.

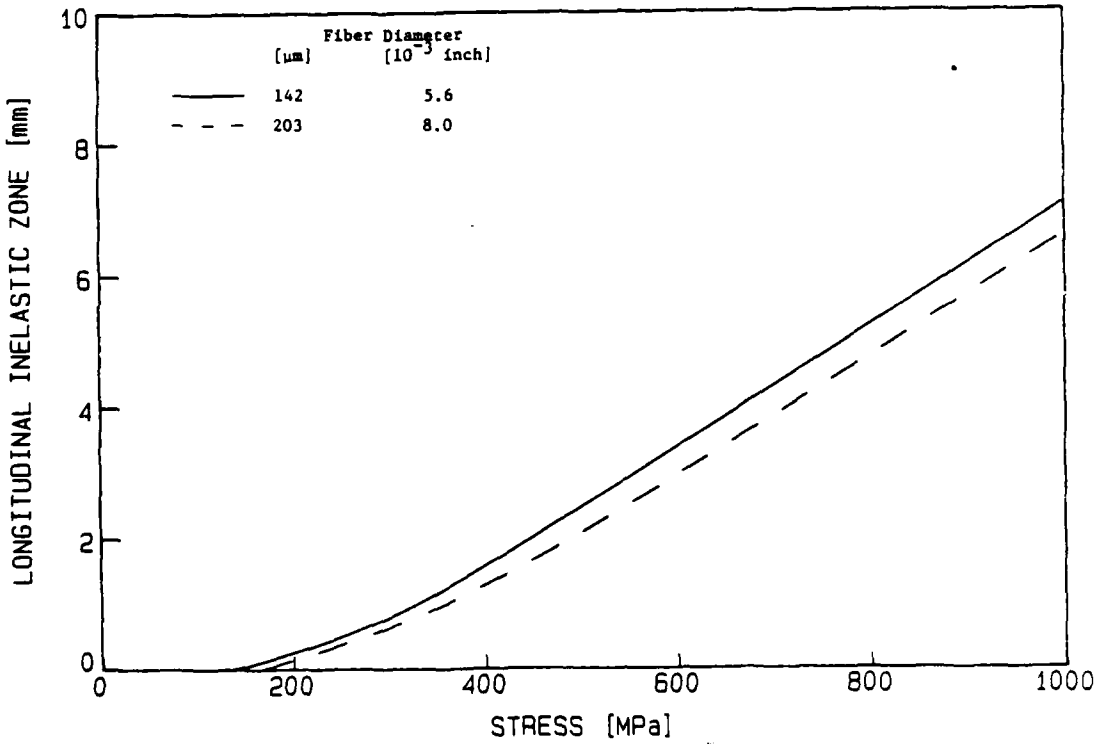

Figure 38. Effect of fiber diameter on length of inelastic zone as predicted by the Lumped Fiber Model for unidirectional boron/aluminum.

c. Effect of Fiber Diameter

In the high performance design with boron/aluminum composites most of the attention has been focused on utilizing 5.6 mil and 8.0 mil boron fibers. The effect of fiber diameter, as predicted by the Lumped Fiber Model on the performance of notched unidirectional boron/aluminum composites is shown in Figures 38-41.

It is seen from Figure 38 that increasing the fiber diameter from 5.6 mil to 8.0 mil results in a reduced inelastic deformation. The differences, however, are not very significant. When the same crack length is maintained in two specimens containing 5.6 mil and 8.0 mil boron fibers, fewer fibers are cut in the specimen containing 8.0 mil boron fibers. Recalling from the previous discussions that the extent of inelastic deformation is directly related to the number of borken fibers contained in the crack, it is therefore expected that the analysis would predict a longer inelastic zone in the specimen containing 5.6 mil boron fibers than in the one containing 8.0 mil boron fibers.

Similar trends are shown in the behavior of crack tip stress and crack tip elastic SCF as a function of applied stress for 5.6 mil and 8.0 mil boron fibers, Figures 39-40. The crack tip fiber stresses and SCF are more severe when utilizing 5.6 mil boron fibers. At sufficiently high applied stresses, however, the differences are insignificant.

The crack opening displacement at a given applied stress demonstrates that for a given crack length the COD is larger when fiber diameter is small, Figure 41. This is expected, once again, because more fibers are cut in a specimen utlizing 5.6 mil boron fibers.

d. Effect of Specimen Width

The effect of specimen width on stress and deformation in a notched unidirectional monolayer is shown in Figures 42-45. It should be noted that, although the specimen width is not included in the formulation of the model, the width effect is nevertheless clearly indicated. This is not surprising because it was shown

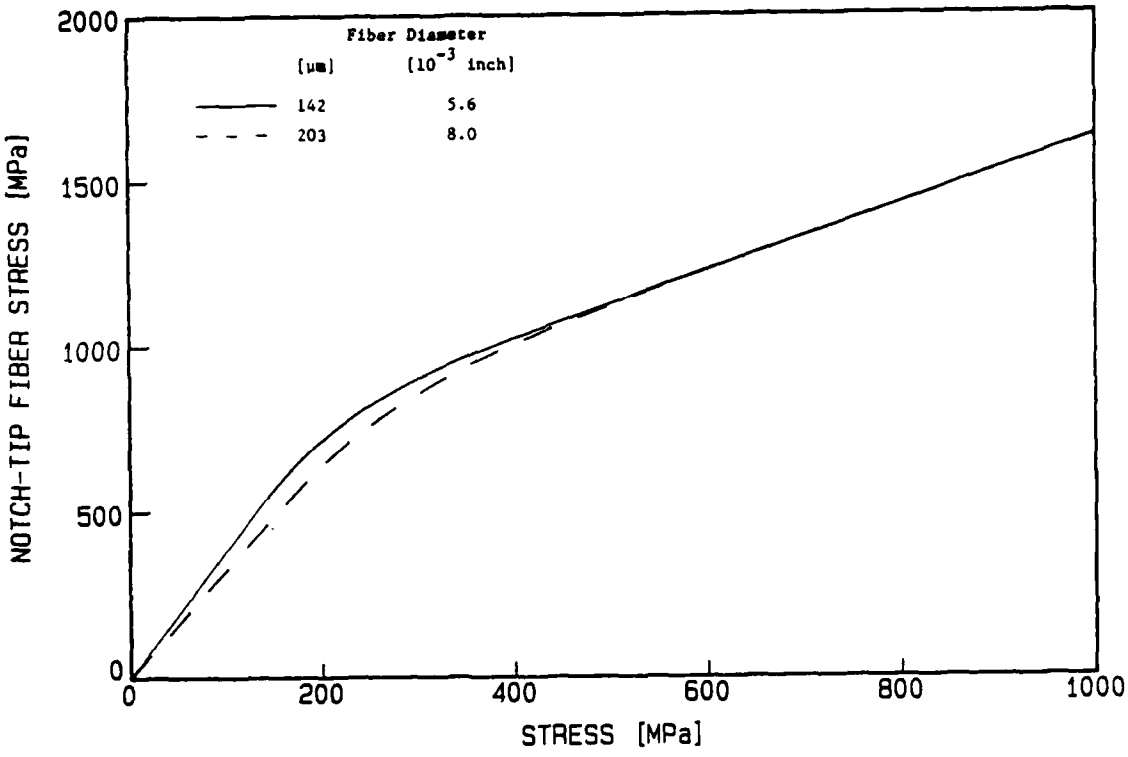

Figure 39. Effect of fiber diameter on notch tip fiber stress as predicted by the Lumped Fiber Model for unidirectional boron/aluminum.

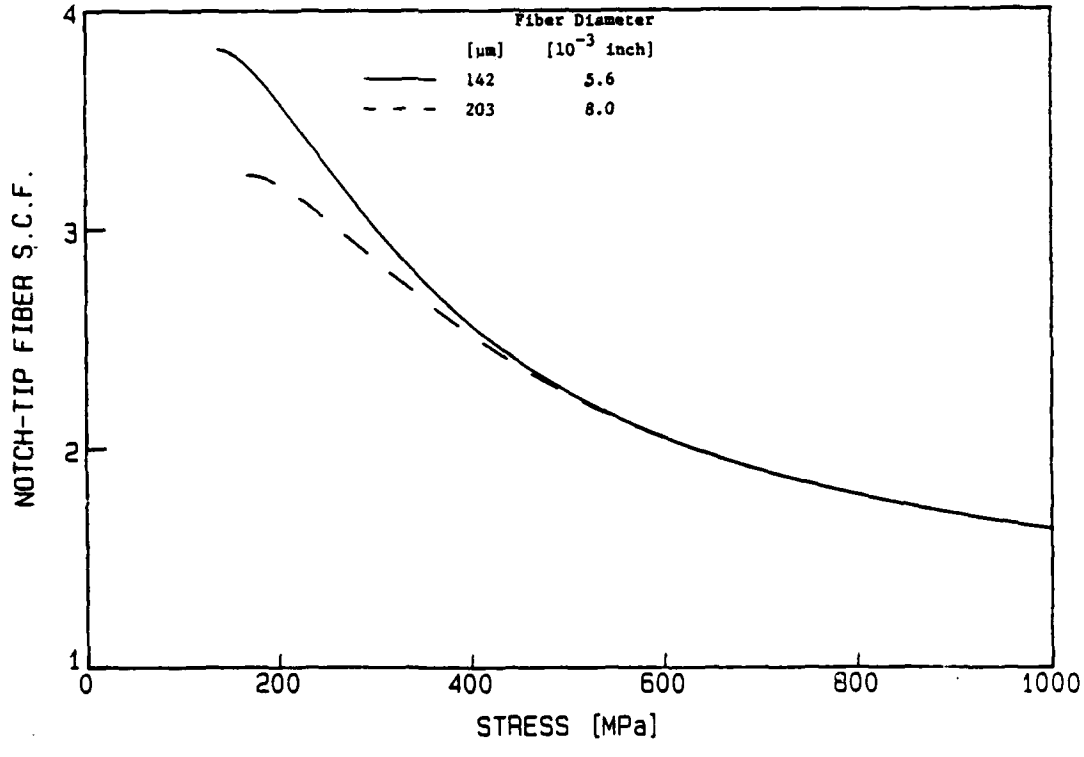

Figure 40. Effect of fiber diameter on notch tip fiber stress concentration factor as predicted by the Lumped Fiber Model for unidirectional boron/aluminum.

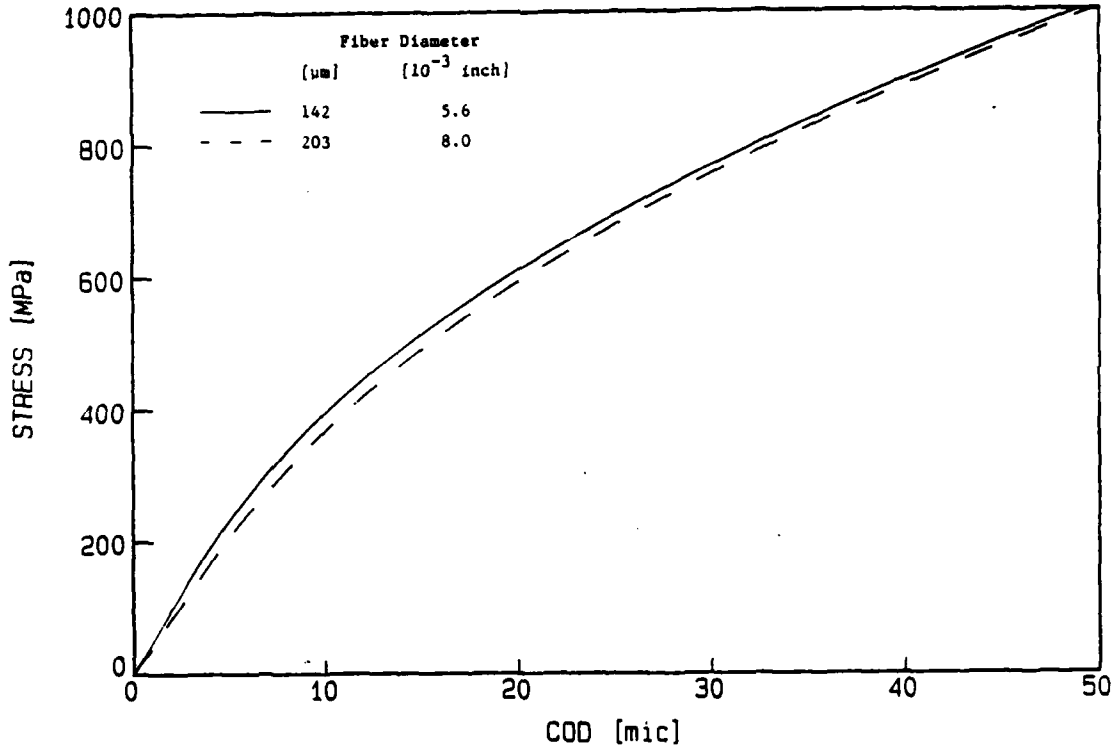

Figure 41. Effect of fiber diameter on load-COD curves as predicted by the Lumped Fiber Model for unidirectional boron/aluminum.

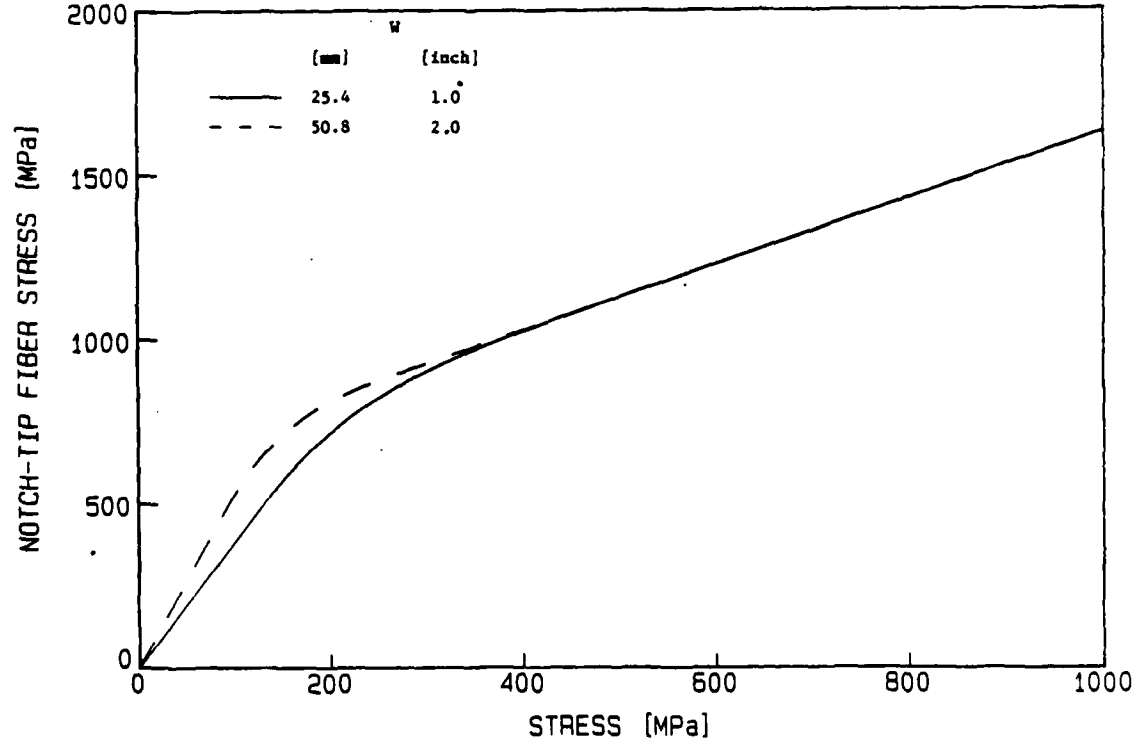

Figure 42. Effect of specimen width on notch tip fiber stress as predicted by the Lumped Fiber Model for unidirectional boron/aluminum.

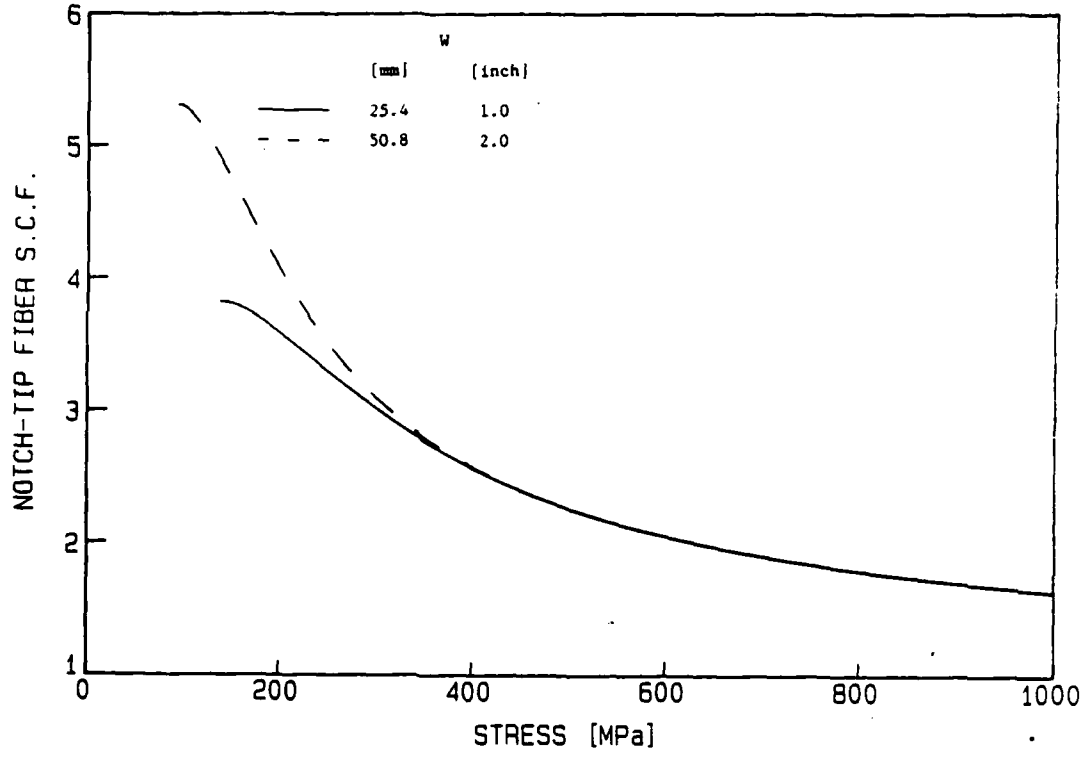

Figure 43. Effect of specimen width on notch tip fiber stress concentration factor as predicted by the Lumped Fiber Model for unidirectional boron/aluminum.

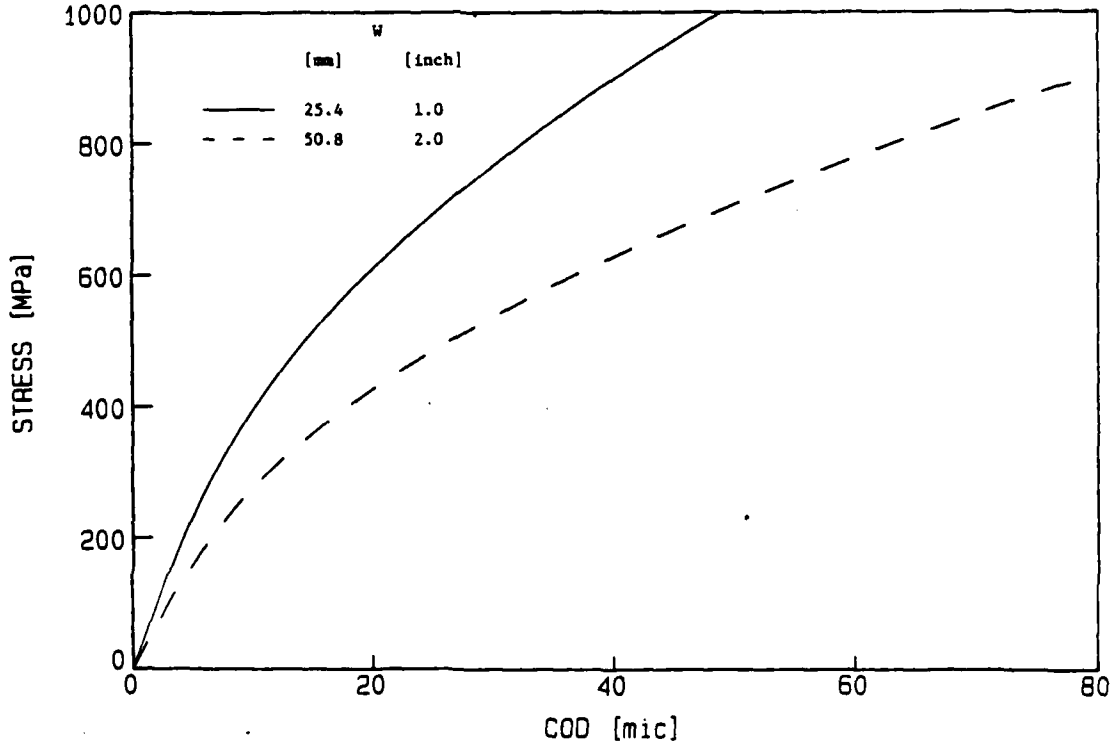

Figure 44. Effect of specimen width on load-COD curves as predicted by the Lumped Fiber Model for unidirectional boron/aluminum.

earlier that notch tip SCF increases with increasing number of initially cut fibers. In order to maintain the same notch to width ratio (2a/W) more fibers would be cut in a wider specimen resulting in higher notch tip fiber stresses (Figure 42), higher SCF (Figure 43) and a larger COD (Figure 44) at a given applied stress.

Due to the higher crack tip stresses in the wider specimen, the predicted notch strength curves when plotted as a function of nondimensional notch length (2a/W) indicate higher notch sensitivity in wider specimens, Figure 45. No experimental data on the notched strength of unidirectional boron/aluminum for two different width specimens is available to verify the higher notch sensitivity of wider specimens. However, the experimental notched strength data for multidirectional boron/aluminum laminates clearly indicated a similar width effect on the notch sensitivity as discussed in Section X.

e. Summary

In the discussion on the Lumped Fiber Model above, it has been demonstrated that results based on this formulation do give a great deal of insight into the basic deformation mechanisms occuring when a notched unidirectional monlayer is subjected to uniaxial tensile loading. Although the comparison between the theory and experiments may not be exact, it is encouraging to note that this simplified approach does predict the correct deformation trends. For example, it was shown earlier that growth of inelastic zone was rapid with a brittle matrix, whereas with a ductile matrix it was stable and unfiorm, and that the yielding was much more extensive with softer matrices. The decreasing notch tip SCF with increasing inealstic length were also in agreement with earlier studies [15]. Experimental results on general multi-directional laminates have indicated increased notch sensitivity with increasing width (See Section X). Predictions by the Lumped Fiber Model on the width effect indicate the similar trends for unidirectional notched composites.

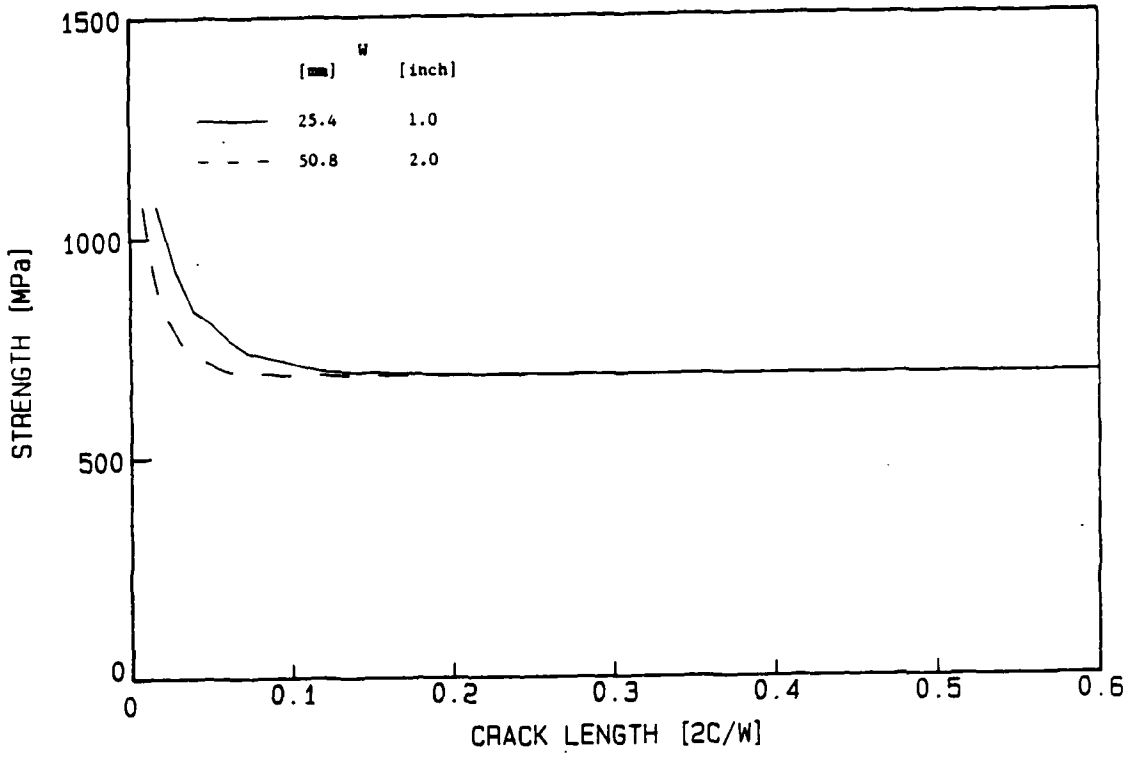

Figure 45. Effect of specimen width on notch sensitivity as predicted by the Lumped Fiber Model for unidirectional boron/aluminum.

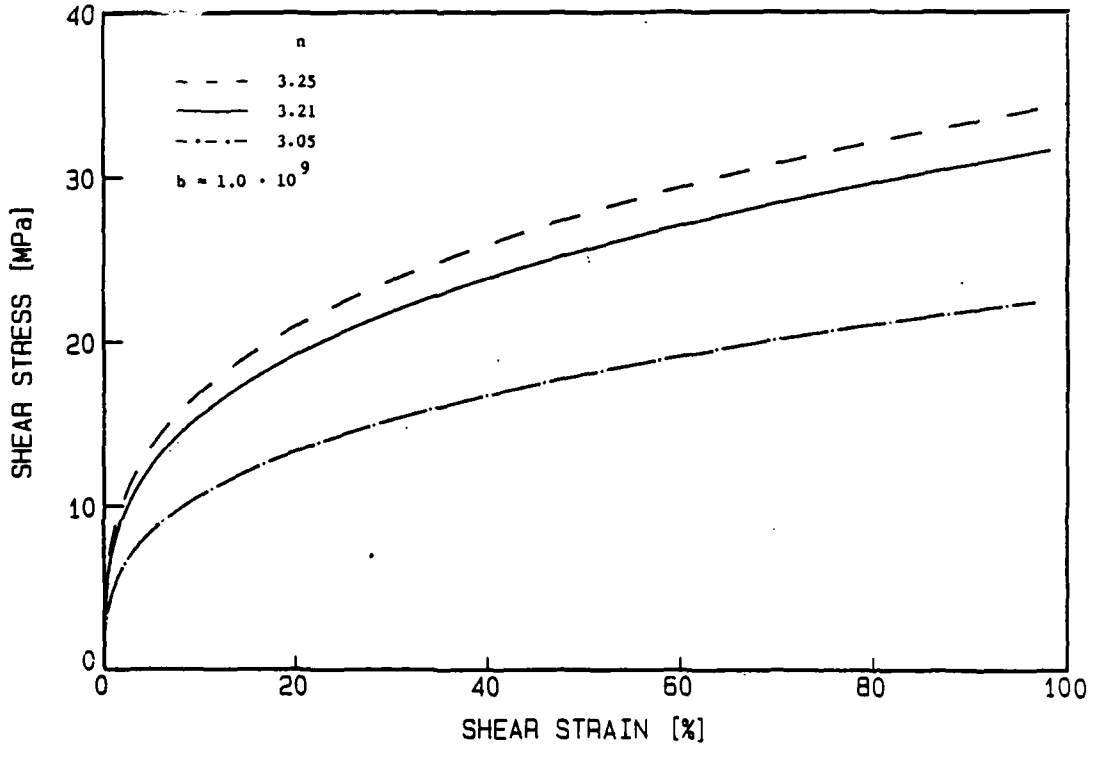

Figure 46. Representative shear stress-strain curves of the aluminum matrix, plotted according to Equation (16), used in the subsequent discussion.

There are, however, several discrepencies in the results obtained from the Lumped Fiber Model. For example, the large difference between the yield shear strength values which best fit the experimental COD and notched strength data. With ductile matrices the model predicts a uniform growth rate of the inelastic zone with increasing applied stress, and when more realistic shear yield strength values are considered, the yield zone can become unrealistically large for nominal values of applied stress. Also, the notch-insensitivity, as predicted by the model for large crack lengths is also subject to scrutiny. In the next phase of development, therefore, an attempt has been made to further modify the Lumped Fiber Model and resolve the aforementioned discrepencies.

II. Nonlinear Lumped Fiber Model

In the second phase of systematic development of the Lumped Fiber Model, the matrix is allowed to deform according to a more realistic non-linear strain-hardening curve instead of in a linear elastic-perfrectly plastic manner. Due to the nonlinearity, however, the calculation schemes involve more complicated algorithms to obtain the solutions. A brief description of the modified model is described below followed by a discussion of the results. Additional details can be found in [26].

a. Formulation of the Governing Equations

Consider a monolayer of infinitely long fibers aligned uniformly and connected by a ductile matrix. The monolayer contains a known number of colinear broken fibers. The monolayer is lumped into three regions, as was done in the original Lumped Fiber Model. The basic shear-lag assumptions are enforced, i.e. that fibers carry all the longitudinal normal stresses and the matrix transfers the normal stresses between the different regions by undergoing shear deformation only. The marix follows a realistic Ramberg-Osgood type of shear stress-strain curve according to:

$$\gamma = b \left(\frac{\tau}{G}\right)^{n} + \frac{\tau}{G} \tag{14}$$

Figure 46 shows three typical shear stress strain curves to be considered in the subsequent discussion. These curves were duplicated from those obtained experimentally in [22,25]. The nonlinear shear stress-strain curves are approximated as a combination of piece-wise linear segments, Figure 47. In order to maintain the overall nonlinearity of these curves they were divided into 500 segments. Thus, each segment is sufficiently small to provide a smooth shear strain-strain curve. The shear modulus of each segment could be determined from:

$$G_i = \frac{\tau_{i+1} - \tau_i}{\gamma_{i+1} - \gamma_i} \tag{15}$$

Based on the calculated value of the shear strain, γ, the instantaneous value of G_i could be detremined. The corresponding shear stress is then calculated from:

$$\tau = \tau_i + G_i (\gamma - \gamma_i) \tag{16}$$

The matrix zones on the left and right hand sides of the first intact fiber are subjected to different shear stress distributions, τ^L and τ^R, respectively. Therefore, different shear moduli should be used in the two zones for any given far-field applied stress. Consequently, the incremental increase in the shear stresses due to an incremental increase in the far-field stress $\Delta\sigma$ will be:

$$\tau^L = \frac{u_o - u_1}{d} \quad G_i \tag{17}$$

$$\tau^R = \frac{u_1 - (\Delta\sigma/E_f)x}{d} \quad G_j \tag{18}$$

The indices i and j denote the different segments of the shear stress-strain curves of the matrix located at the left and right hand sides of the first intact fiber, respectively. u_o and u_1 are the incremental increases in the displacements of the core and first intact fiber, respectively, due to the incremental increase in the

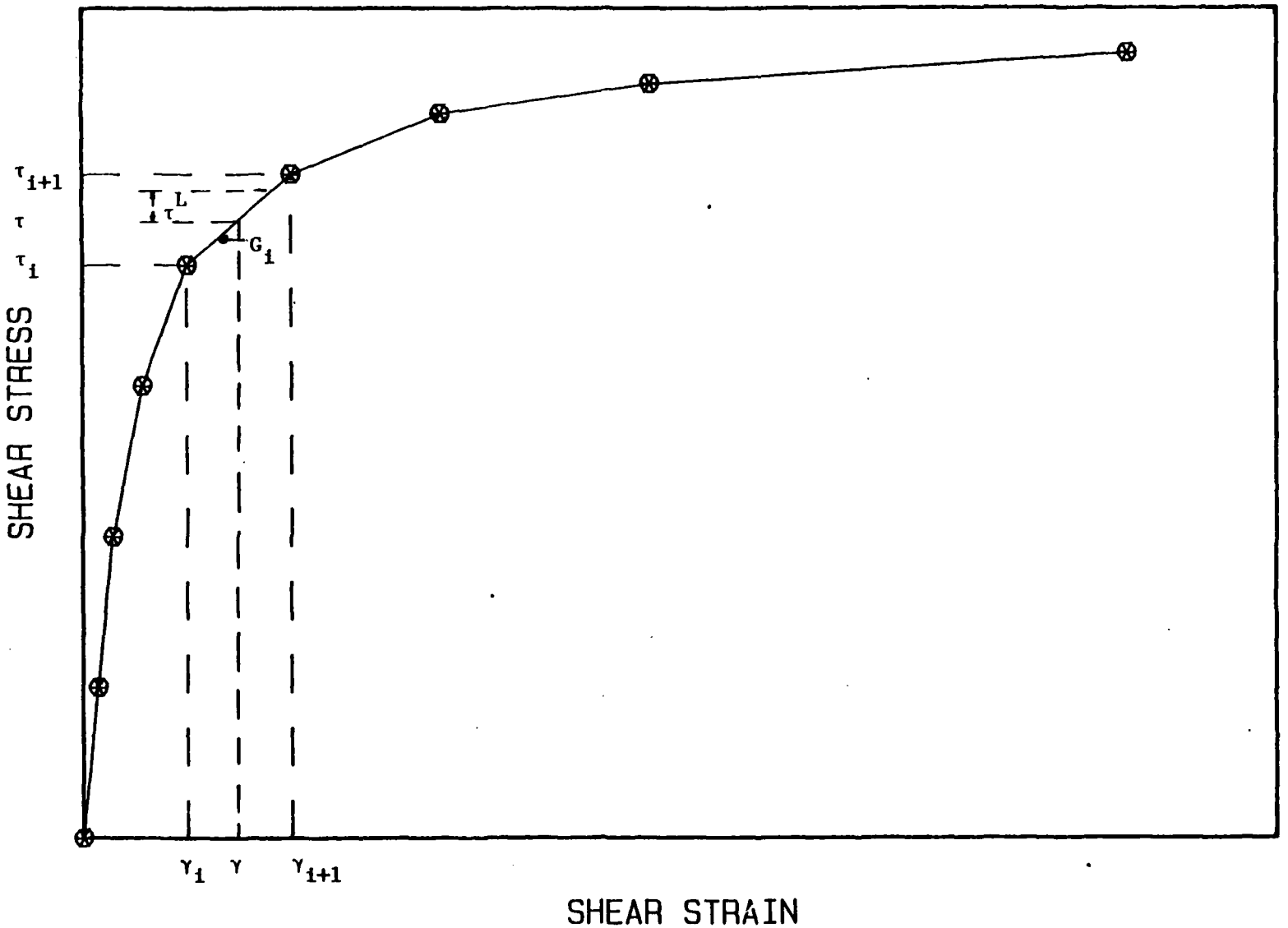

Figure 47. Schematic of discrete shear stress-strain curve used in the numerical calculations of the Nonlinear Lumped Fiber Model.

far-field stress, $\Delta\sigma$. E_f is the fiber stiffness and d is the fiber spacing (assumed to be equal to the fiber diameter).

Equilibrium of forces on the two elements located at the core and at the first intact fiber and located at a distance x results in the following governing differential equations, respectively, in terms of displacements:

$$n E_f A_f \frac{d^2 u_o}{dx^2} - 2 \frac{G_i h}{d} (u_o - u_1) = 0 \tag{19}$$

$$E_f A_f \frac{d^2 u_1}{dx^2} + \frac{h}{d} \{u_o G_i - u_1 (G_i + G_j) + G_j \frac{\sigma}{E_f} x\} = 0 \tag{20}$$

where n is the number of broken fibers (i.e. crack length), A_f is the cross section of the fiber and h is the plate thickness.

The solution of these equations is:

$$\bar{U}_o = Ae^{-\lambda_1 \xi} + Be^{-\lambda_2 \xi} + \xi \tag{21}$$

$$\bar{U}_1 = Ae^{-\lambda_1 \xi} (1 - \frac{n}{2} \frac{G}{G_i} \lambda_1^2) + Be^{-\lambda_2 \xi} (1 - \frac{n}{2} \frac{G}{G_i} \lambda_3^2) \xi \tag{22}$$

where λ_1 and λ_2 are functions of G_i and G_j and $\bar{U}_o$, $\bar{U}_1$ and ξ are the nondimensional values of u_o, u_1 and x, respectively, according to:

$$x = \left(\frac{E_f A_f d_F}{Gh}\right)^{1/2} \xi \tag{23}$$

$$u_{o,1} = \left(\frac{A_f d_f}{G E_f h}\right) \sigma \bar{U}_{o,1} \tag{24}$$

Equations (21-22) automatically satisfy the boundary conditions of Equations (11a and 11b) and the constants of integration, A and B, are obtained from the remaining boundary conditions given in Equations (11c and 11d). The solution for the displacements and stresses at any given location, x, along the fibers in the core and in the first intact fiber are thus defined.

It should be noted, however, that in the formulations given above the deformation (Equations (21-22)) at any point, x, can be determined provided that the indices i and j (i.e. the instantaneous shear moduli) are specified. Along different locations and different far-field applied stress different shear moduli should be applied in the calculation procedures. In other words, at each point x, appropriate shear moduli should be utilized for any given applied far-field stress. Consequently, in order to obtain the complete displacement and stress distributions in the core and first intact fiber the numerical solution requires the application of several iterative procedures, details of which are described in [26]. Such a computer code has been written through which the effects of various intrinsic and extrinsic variables on the deformation characteristics and notch sensitivity of unidirectional boron/aluminum could be analyzed, in a manner similar to that presented previously using the Lumped Fiber Model.

b. Results and Discussion

The Nonlinear Lumped Fiber Model developed above incorporates the actual shear stress-strain curve of the matrix material. This modification of the original Lumped Fiber Model results in a longitudinal shear stress distribution in the yield zone which is no longer constant.

The results obtained form the Nonlinear Lumped Fiber Model include the longitudinal inelastic zone, notch tip fiber stress concentration factors, the crack opening displacements, and notched strength. In the predictions of the longitudinal inelastic zone length, the yield shear stress is taken to be the value corresponding to 0.2% off-set shear strain. A parameteric study has been performed to study the effect of matrix shear stress-strain curve on the predictions. Several nonlinear matrix shear stress-strain curves are considered, Figure 46, and the results corresponding to these different stress-strain curves are shown in Figures 48-50.

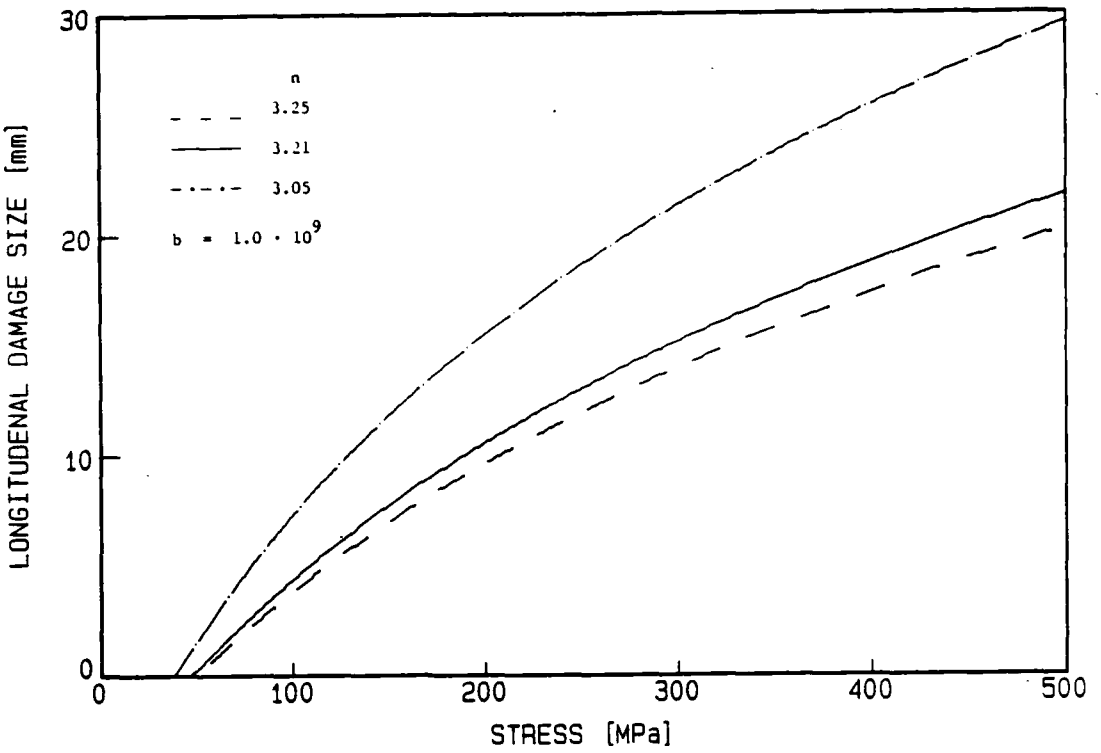

Figure 48. Effect of matrix shear stress-strain behavior on the length of the inelastic zone as predicted by the Nonlinear Lumped Fiber Model for undirectional boron/aluminum.

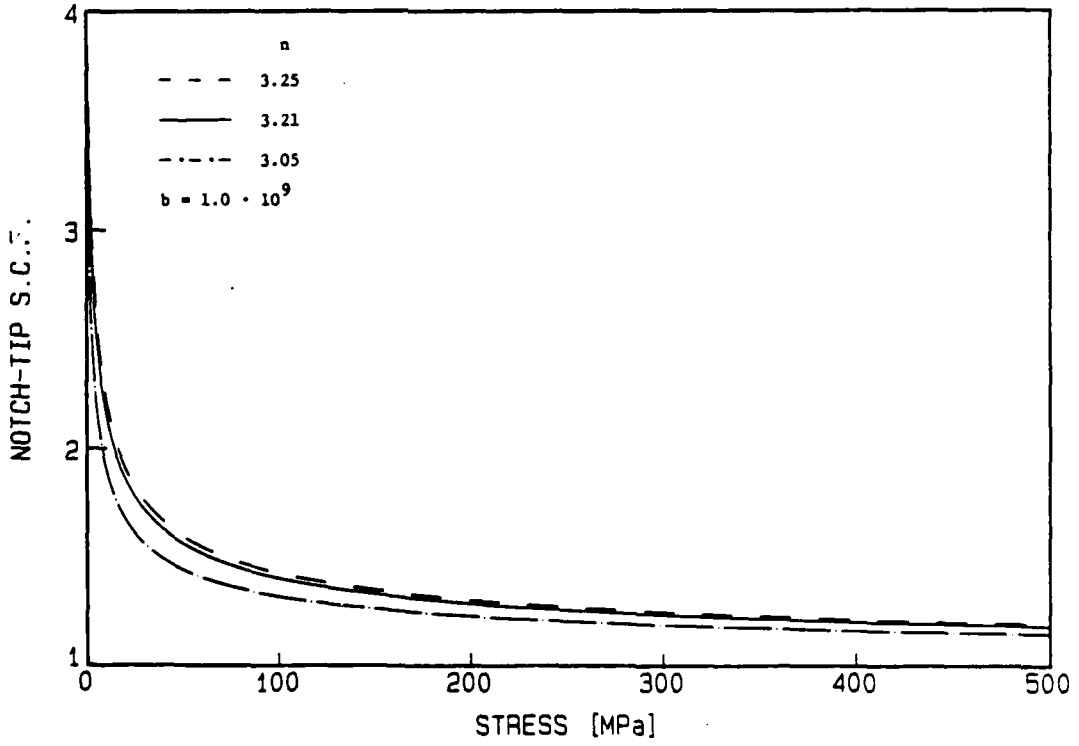

Figure 49. Effect of matrix shear stress-strain curve behavior on the notch tip fiber stress concentration factor as predicted by the Nonlinear Lumped Fiber Model for unidirectional boron/aluminum.

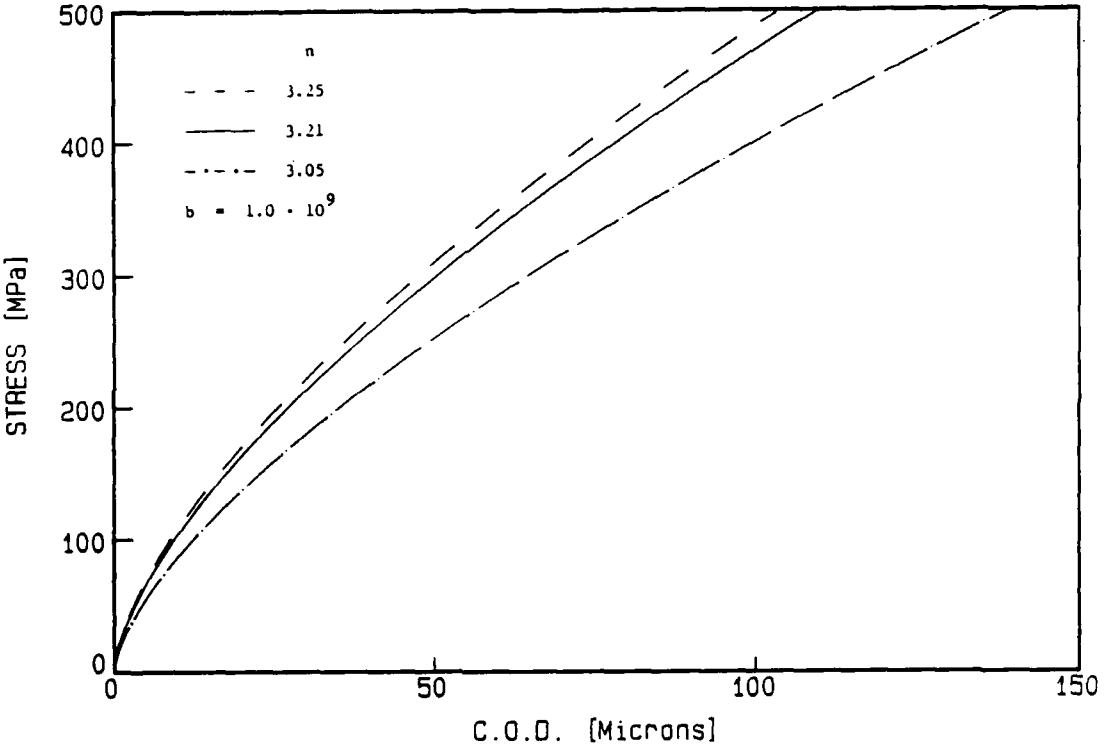

Figure 50. Effect of matrix shear stress-strain curve behavior on the load-COD curve as predicted by the Nonlinear Lumped Fiber Model for unidirectional boron/aluminum.

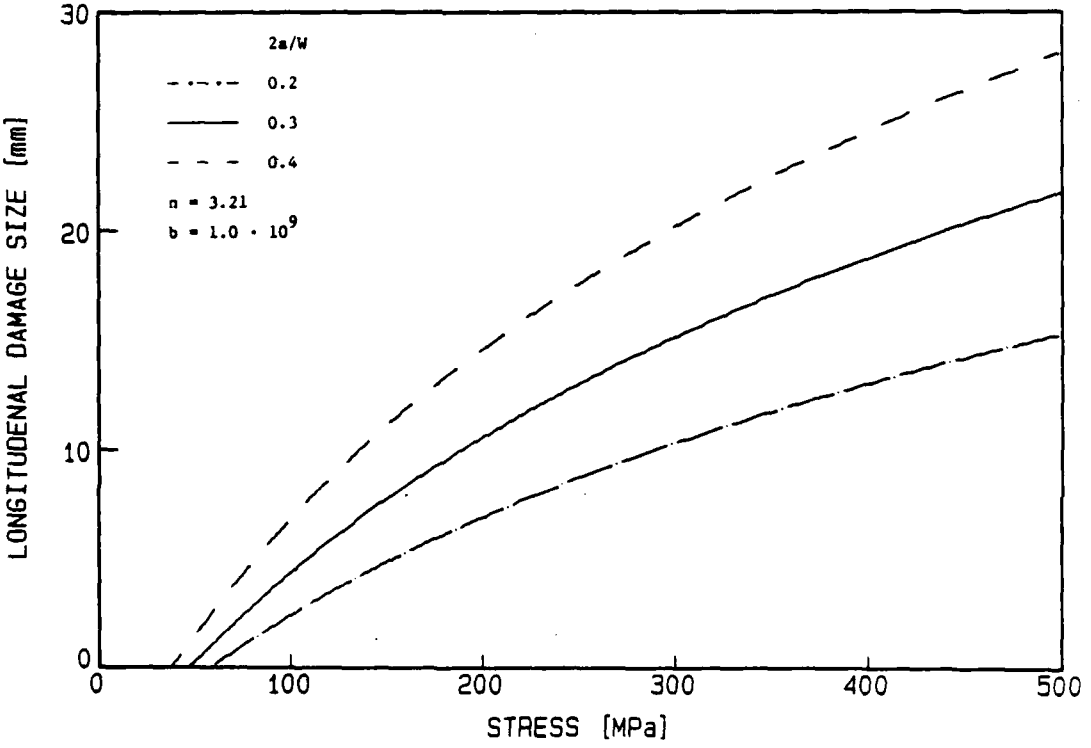

Figure 51. Effect of crack length on the length of the inelastic zone as predicted by the Nonlinear Lumped Fiber Model for unidirectional boron/aluminum.

The trends in the longitudinal inelastic zone length, Figure 48, crack tip SCF, Figure 49, and COD, Figure 50, with increasing applied stress, as predicted by the Nonlinear Lumped Fiber Model are similar to those obtained when the matrix was assumed to be linear elastic-perfectly plastic, Figures 23,31,32. For example, the inelastic deformation increases with increasing applied stress and softer matrices yield longer inelastic zones, Figure 48. As a result of this yielding the stresses in the vicinity of the crack are relieved due to crack tip blunting and due to a greater stress transfer between the first intact fiber and the remaining fibers. The notch tip fiber SCF's, therefore, rapidly approach unity with increasing applied stresses, Figure 44. The initial SCF's, when the applied stress is increased from zero, are the same for all three matrices. However, with increasing matrix ductility, the SCF's approach unity faster with increasing stress, Figure 49. It seems, though, that the effects of matrix ductility on the notch tip SCF are marginal. The predicted COD values for three different matrices are shown in Figure 50. The COD increases with increasing applied stress and a larger crack opening is predicted for the more ductile matrix.

The previous discussion demonstrated that the predictions according to the Nonlinear Lumped Fiber Model are consistent with the material behavior and generally similar to the predictions based on the Linear Lumped Fiber Model. The difference between the two models, however, is clearly manifested in the predicted growth rate of the inelastic zone. While the Linear Lumped Fiber Model predicts a monotonically increasing length of the inelastic zone with increasing far-field stress, the Nonlinear Lumped Fiber Model predicts that the growth rate decreases at higher stress levels. This difference between the two models is expected. In the Linear Lumped Fiber Model the matrix shear stresses are not allowed to increase beyond the pre-determined yield shear strength. Thus, in order to maintain equilibrium any additional increase in the far-field stress must be balanced by a proportional increase of the yield zone. On the other hand, when the actual shear stress-strain

curve is applied (i.e. Nonlinear Lumped Fiber Model), Figure 46, the shear stresses in the matrix are permitted to increase much beyond the yield shear strength. Consequently, a smaller increase in the length of the yield zone is required to maintain equilibrium.

Effect of crack length on the length of the inelastic zone, SCF and COD is shown in Figures 51-53, respectively. As expected, longer crack lengths result in a longer inelastic zone, higher notch tip fiber SCF and longer COD.

The load-COD curves shown in Figures 54-55 indicate a good agreement between prediction and experiments. The predicted load-COD curves were obtained by selecting the matrix shear stress-strain curve which best fit the experimental results. The selected shear stress-strain curve is shown by the solid curve in Figure 46. The validity of the proposed model was verified by demonstrating that the use of the same shear stress-strain curves for all crack lengths, e.g. Figures 54-55, results in good agreement for all cases. Moreover, comparing Figure 33 with Figures 54-55, clearly indicates that the Nonlinear Lumped Fiber Model yields a better agreement between prediction and experimental results. Thus, the modified model can better aid in determining the in-situ properties of the aluminum matrix. This latter issue is of importance, for example, whenever the appropriate fabrication procedure or proper selection of the matrix mateial are of concern.

Finally, it should be noted that for higher applied stresses the experimental COD is larger than the predicted COD. This behavior is expected since the model (as all other models) accounts for a single inelastic zone (between the core and first intact fiber) while experimental observations indicate the occurance of several such zones. Moreover, the formation of these inelastic zones is associated with additional fiber breakage, as discussed in Section 5.3 and 6.3. Consequently, the analytical modeling should be further extended to account for this type of sequential failure process.

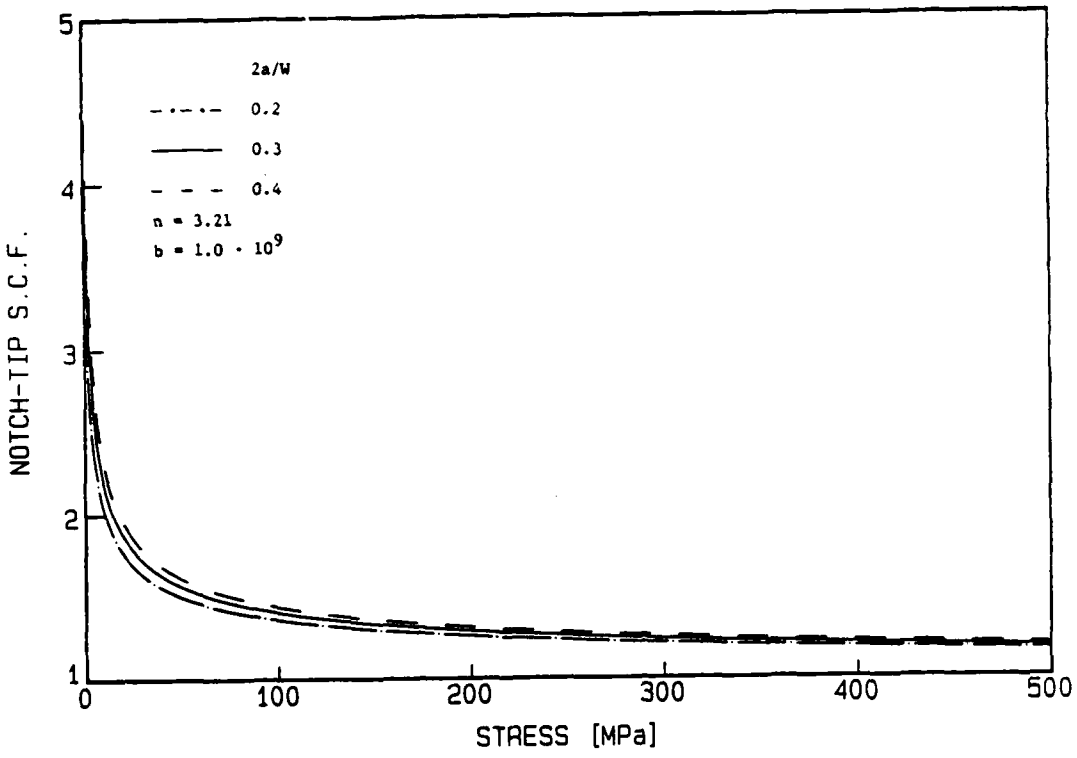

Figure 52. Effect of crack length on notch tip fiber stress concentration factor as predicted by the Nonlinear Lumped Fiber Model for unidirectional boron/aluminum.

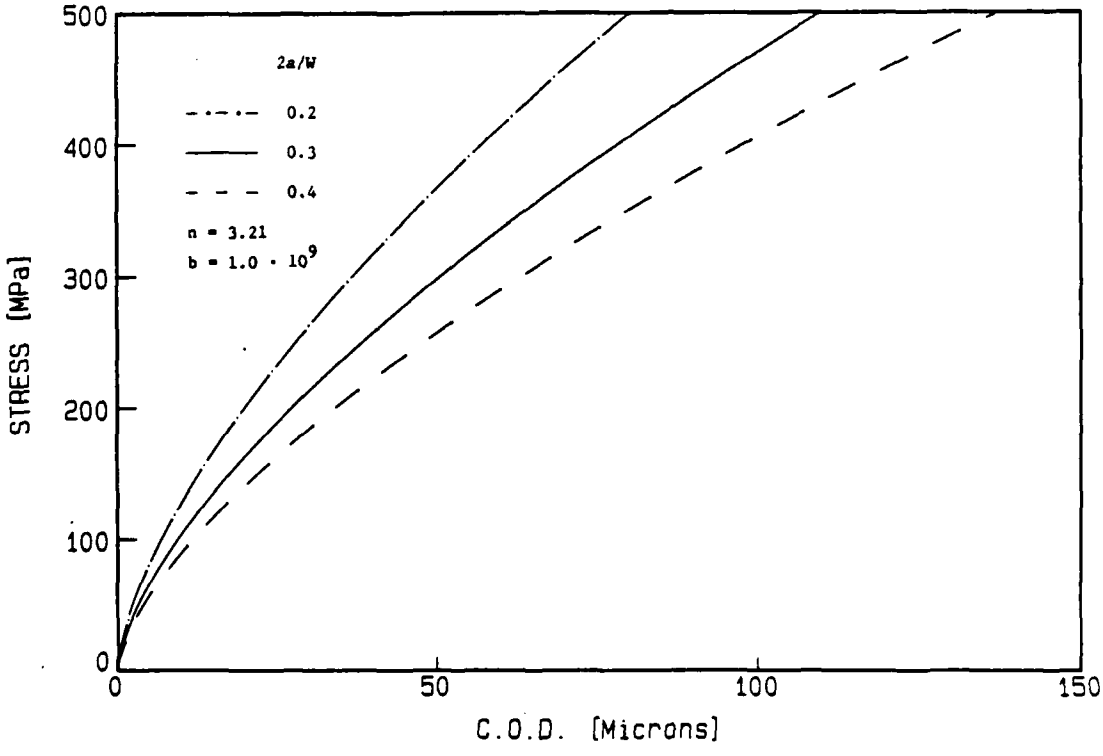

Figure 53. Effect of crack length on load-COD curves as predicted by the Nonlinear Lumped Fiber Model for unidirectional boron/aluminum.

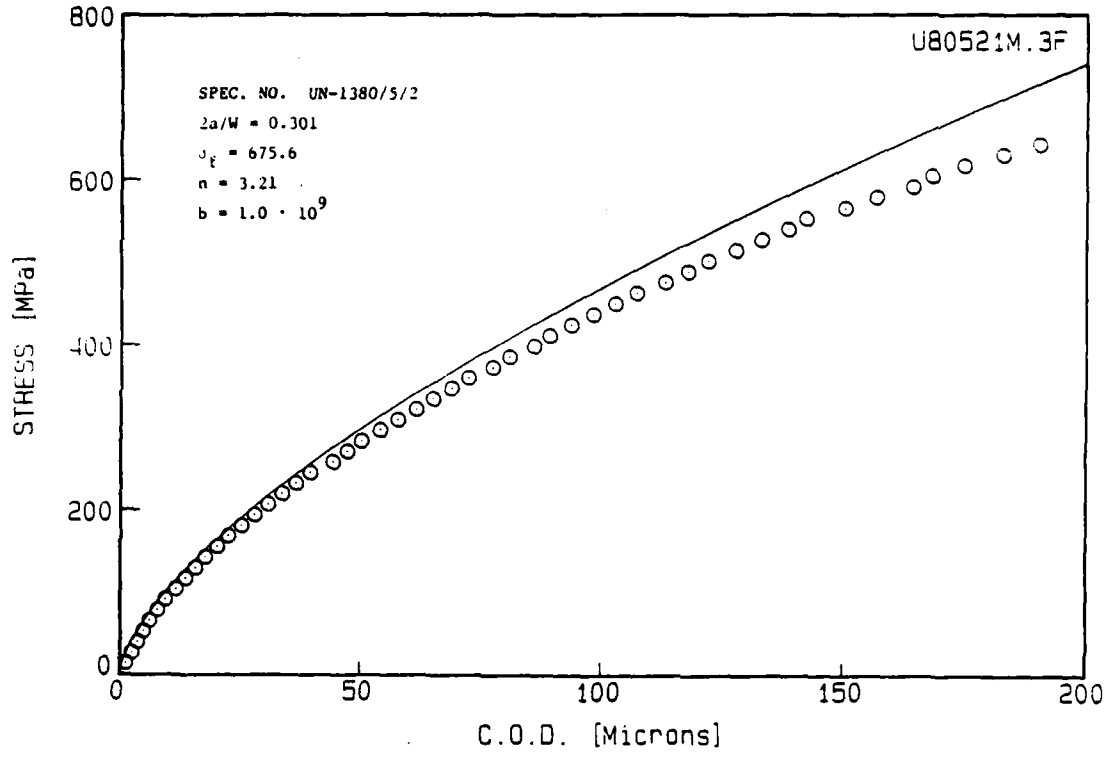

Figure 54. Comparison between predicted (Nonlinear Lumped Fiber Model) and experimental load-COD curves for a unidirectional boron/aluminum specimen, 2a/W = 0.301.

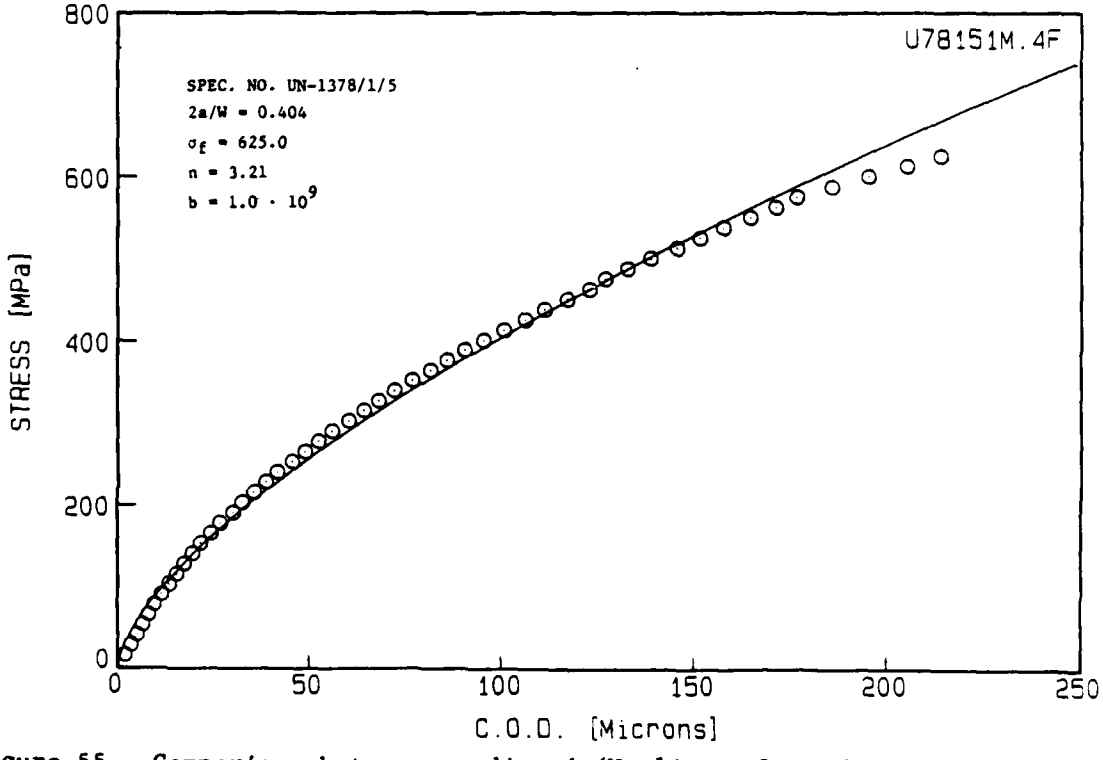

Figure 55. Comparison between predicted (Nonlinear Lumped Fiber Model) and experimental load-COD curves for a unidirectional boron/aluminum specimen, 2a/W = 0.404.

5.5 Conclusions

1. Load-COD curves were obtained for all laminates studied at temperatures up to 315°C (600°F).

2. Load-COD curves are highly nonlinear, with jumps in COD and large deformation remaining upon unloading. Slow crack tip damage growth has been observed, which correlates with acoustic emission results.

3. Load-COD curves are highly dependent on laminate configuration and notch length.

4. Deformation characteristics are less pronounced for multidirectional laminates.

5. At elevated temperatures the nonlinearity of the load-COD curves is much more pronounced, primarily above 204°C (400°F), due to the reduced matrix shear yield strength.

6. Experimental Load-COD curves for unidirectional specimens at room and elevated tempeatures correlate well with predictions based on approximate mechanistic models which are operationally simple to utilize. These models account for the matrix shear deformation along the fiber directions and assume the matrix to be elastic-perfectly plastic.

7. The Lumped Fiber Model has been extended and compared with the experimental load-COD and notch sensitivity curves. The comparison indicates certain differences between prediction and experiments.

8. The Lumped Fiber Model has been modified to incorporate the actual shear stress-strain curve of the matrix material. This modification yields a better agreement between prediction and experiments.

9. Parametric study on the effects of material variables (such as matrix shear stress-strain behavior, fiber diameter, etc.) and specimen geometry indicate their influence on the fracture behavior of unidirectional boron/aluminum.

10. Further modification of the model is warranted to account for a sequential failure process, incorporating the actual crack tip damage extension.

5.6 References

1. J. Awerbuch and M. Madhukar, "Notched Strength of Composite Laminates: Predictions and Experiments - A Review", Journal of Reinforced Plastic and Composites, Vol. 4, No. 1, 1985, pp. 3-160.

2. J.M. Hedgepeth,"Stress Concentrations for Filamentary Structures", NASA TN D-882, 1961.

3. J.M. Hedgepeth and P. Van Dyke, "Local Stress Concentrations in Imperfect Filamentary Composite Materials", J. Comp. Mater., Vol. 1, 1967, pp. 294-309.

4. P. Van Dyke and J.M. Hedgepeth, "Stress Concentrations from Single Filament Failures in Composite Materials", Textile Research, Vol. 39, 1969, pp. 613-626.

5. A.C. Eringen and B.S. Kim, "Stress Concentration in Filamentary Composites With Broken Fibers", Princeton University Tech. Rep. No. 36, Sept. 1973, ONR COntract N-00014-67-A-0151-0004.

6. J.G. Goree and R.S. Gross, "Stresses in a Three-Dimensional Unidirectional Composite Containing Broken Fibers", NASA CR-158986, NSG-1297, 1978.

7. J.G. Goree and R.S. Gross, "Analysis of a Unidirectional Composite Containing Broken Fibers and Matrix Damage", Engineering Fracture Mechanics, Vol. 13, 1979, pp. 563-578.

8. J.G. Goree and R.S. Gross, "Stresses in a Three-Dimensional Unidirectional Composite Containing Broken Fibers", Engineering Fracture Mechanics, Vol. 13, 1980, pp. 395-405.

9. J.G. Goree, L.R. Dharani and W.F. Jones, "Mathematical Modeling of Damage in Unidirectional Composites", NASA CR-3453, 1981.

10. W.F. Jones, "Experimental Determination of Internal Damage Growth in Unidirectional Boron/Aluminum Composites", Ph.D. Dissertation, Clemson University, August 1982.

11. J.G. Goree and W.F. Jones, "Fracture Behavior of Unidirectional Boron/Aluminum Composite Laminates", NASA CR-3753, 1983.

12. L.R. Dharani, W.F. Jones, and J.G. Goree, "Mathematical Modeling of Damage in Unidirectional Composites", Engineering Fracture Mechanics, Vol. 17, 1983, pp. 555-573.

13. W.F. Jones and J.G. Goree, "Fracture Behavior of Unidirectional Boron/Aluminum Composite Laminates" in the Proceedings of ASME-AMD Symposium on Mechanics of Composite Materials, G.J. Dvorak, Ed., Boston, MA., November 13-18, 1983, pp. 171-177.

14. F.A. McClintock, "Problems in Fracture of Composites with Plastic Matrices," presented at the Fourth Symposium on High Performance Composites at St. Louis, MO, Monstanto, Co. and Washington University, 1969.

15. J. Tirosh, "The Effect of Plasticity and Crack Blunting on the Stress Distribution in Orthotropic Composite Materials", J. Appl. Mech., Vol. 40, 1973, p.785.

16. C. Zweben, "Fracture Mechanics and Composite Materials: A Critical Analysis", Special Tech. Publ. 521, A.S.T.M., 1973, pp. 63-97.

17. C. Zweben, "An Approximate Method of Analysis for Notched Unidirectional Composites", Engineering Fracture Mechanics, Vol. 5, 1974, pp. 1-10.

18. C. Zweben, "Failure Analysis of Unidirectional Fiber Composites Under Combined Axial Tension and Shear", J. Mech. Phys. Solids, Vol. 22, 1974, pp. 193-215.

19. E.D. Reedy, Jr., "On the Specimen Dependence of Unidirectional Boron/Aluminum Fracture Toughness", Journal Composite Materials, Vol . 14, 1980, pp. 118-131.

20. E.D. Reedy, Jr., "Analysis of Center-Notched Monolayers with Application to Boron/Aluminum Composites", Journal Mechanics and Physics of Solids, Vol. 28, 1980, pp. 265-286.

21. E.D. Reedy, Jr., "Notched Unidirectional Boron/Aluminum: Effect of Matrix Properties", Journal Composite Materials, Vol. 16, 1982, pp. 495-509.

22. E.D. Reedy, Jr., "Fracture of Notched, Unidirectional Boron/Aluminum: Experiment and Analysis", In the Proceedings of ASME-AMD Symposium on Mechanics of Composite Materials, G.J. Dvorak, Ed., Boston, MA, November 13-18, 1983, pp. 157-170.

23. J. Awerbuch and H.T. Hahn, "Crack-Tip Damage and Toughness of Boron-Aluminum Composite", J. Composite Materials, Vol. 13, 1979, pp. 82-107.

24. J.M. Wolla, "Experimental Determination of the Fracture Behavior of Damaged Graphite/Epoxy Laminates and Comparisons to the Shear Lag Model", M.S. Dissertation, Clemson University, 1984.

25. E.D. Reedy, Jr., "Large Strain Shear Response of Unidirectional Boron/Aluminum", Proceedings of the Joint Japan Society of Mechanical Engineers/Society for Experimental Stress Analysis Conference on Experimental Mechanics, Hawaii, May 22-30, 1982.

26. M. Madhukar, "Fracture Behavior of Boron/Aluminum Laminates at Room and Elevated Temperatures", Ph.D. Dissertation, Drexel University, 1985 (to be published).

VI. FAILURE MODES AND DAMAGE PROGRESSION

6.1 Summary

Fracture surfaces of notched an unnotched specimens subjected to various elevated temperatures were examined through the scanning electron microscope (SEM). Three-dimensional, or stereo, views of the fracture surfaces were prepared from which the different micro-failure modes could be easily identified. Several specimens were loaded to a predetermined load level, unloaded, and the matrix was dissolved. Notch-tip damage extension and the number of broken fibers were inspected through the SEM. Damage progression was also monitored in real-time via a closed-circuit television (CCTV) system which provided a clear view of the notch tip region at the specimen surface at magnifications up to 250X. The observed damage progression (from SEM and CCTV examinations) was also correlated with the acoustic emission results. These procedures enabled verification of the AE and IDG results and the validity of some of the basic assumptions made in the analytical modeling of notch sensitivity and deformation characteristics of metal-matrix composites.

6.2 Introduction

Significant attention has been given during the past two decades to analyzing the micro-failure modes and the metallurgical aspects of failure in metal-matrix composites. These efforts have been necessitated by the strong relationship between the fabrication procedures of metal-matrix composites (MMC) and their performance, e.g. strength and toughness. While the fabrication and curing procedures of advanced resin-matrix composites (e.g. graphite/epoxy) are quite established, the same procedures for MMC are still under continuous development and modification. The strong influence of the fabrication procedures on interface integrity, fiber degradation, etc. are of major concern, and efforts are directed toward optimizing the manufacturing processes of MMC with regard to performance and cost.

The objectives in these studies have therefore been three-fold:

1. determine the quality of the product, i.e. fiber/matrix bonding and matrix/matrix consolidation, interface integrity and characteristics, etc.
2. determine the appropriate fabrication procedures, i.e. nature and role of fiber/matrix interfacial regions, interface degradation (development of reaction zones) due to thermal exposure during processing and service temperatures, relationships between thermal/mechanical processing, interface and mechanical properties, etc.
3. determine the failure mechanisms and processes, i.e. deformation characteristics, crack tip damage growth, etc. in order to support the analytical modeling.

Most of the studies on the development of processing, mechanical characterization and fracture behavior of boron/aluminum do address the first issue and use those findings as background information when reporting on the quality of the material under study, e.g. [1-8]. Such information is obviously of importance in order to validate test results. Extensive studies have also been conducted and reported on the second subject, e.g. [9-13], resulting in a better understanding of the relationships between thermal/mechanical processing, interface and mechanical properties. Finally, studies on the failure mechanisms and processes in boron/aluminum composites, or for that matter in all MMC systems, have concentrated primarily on unidirectional specimens, e.g. [14-18]. Very little research on boron/aluminum laminates has been reported in the literature.

The failure mechanisms and process in metal-matrix composites strongly depend on the fabrication procedures employed. Fiber degradation during processing, fiber/matrix bond quality and matrix/matrix consolidation, chemical compatibility between fiber and matrix, interface integrity (which serves as a vehicle for stress transfer between the constituents), etc., are all affecting

the failure mechanisms and processes and notch sensitivity. The impact of differences in fabrication procedures on failure mechanisms can be seen in the comparison between unidirectional boron/aluminum and borsic/titanium. A detailed study conducted on both material systems indicates significant differences between them [17-18]. While in boron/aluminum crack tip damage appears in the form of shear plastic deformation of the ductile matrix along the fibers [17], borsic/titanium exhibit a plastic zone at the crack tips whose length increases with increasing load, perpendicular to the fibers, and very similar to the Dugdale plastic zone. Weak fiber/matrix bonding and fiber degradation during processing of the borsic/titanium system has resulted in low ultimate tensile strength and an unexpected failure process [18]. The effect of processing on the notch sensitivity of unidirectional boron/aluminum has been reported in [14-15], however without any detailed metallurgical explanation.

The purpose of this phase of the research program was five-fold: 1. identify the material quality under investigation; 2. determine the various micro-failures associated with the catastrophic fracture of boron/aluminum laminates and their correlation with the acoustic emission results; 3. evaluate the effect of elevated temperatures on the characteristics of the fracture surface morphology; 4. determine the effect of laminate configuration on notch tip damage growth; and 5. identify the macro failure process (via visual observations through the CCTV) and directionality of notch tip damage growth during uniaxial quasi-static and tension-tension low cycle fatigue loadings.

6.3 Results and Discussion

6.3.1 Material Qaulity:

The average axial strength data (of 11 specimens) has a surprisingly low value of 1337 MPa (194 ksi). The data shown in the literature give values of 1520-1655 MPa (220-240 ksi), even reaching values as high as 2004 MPa (290.7 ksi) [14]. Moreover, a very large scatter in the data has been observed;

values range between 1187 and 1473 MPa (172.2 -213.7 ksi) with a standard deviation of 87.6 MPa (12.7 ksi), or Weibull shape parameter of 9.7. An attempt has been made to account for this low strength which might be primarily attributable either to poor composite quality or to weak fibers. Both issues are discussed below.

Regarding material quality, the examinations of the fracture surface morphologies (and photomicrographs of the cross-sections) revealed very good fiber/matrix bonding and matrix/matrix consolidation.

The photomicrograph shown in Figure 1 reveal that the fiber volume fraction is approximately 48%. However, fiber distribution throughout the cross-section is not uniform. In some cases the fibers are in contact with each other and in other cases large spacing exists, up to half of a fiber diameter. The cross-section shown in Figure 1 is typical of several specimens examined. These photomicrographs are, however, quite similar to others shown in the literature, therefore it is unlikely that the lack of uniformity in fiber distribution can be the source of the low strength values obtained in this work.

Scanning electron microscope (SEM) photographs were also taken. In order to obtain a better view of the fracture surfaces and better understand the different failure mechanisms, three-dimensional (stereo) views were obtained for all laminates notched and unnotched specimens. Stereo scanning electron micrographs of an unnotched unidirectional B/Al specimen (ultimate strength = 1303 MPa), Figure 2, indicate a very good fiber/matrix bond. The single fiber protruding from the matrix is coated with a substantial residue of aluminum, i.e. the shear strength of the bond exceeds that of the aluminum matrix. The good fiber/matrix bond is also manifested by the fact that many of the wedge-shaped fragments of shattered fibers, shown also in Figure 2a, are still embedded in the aluminum matrix despite the shock and sudden release of elastic energy during fracture. Very little fiber pull-out has been observed.

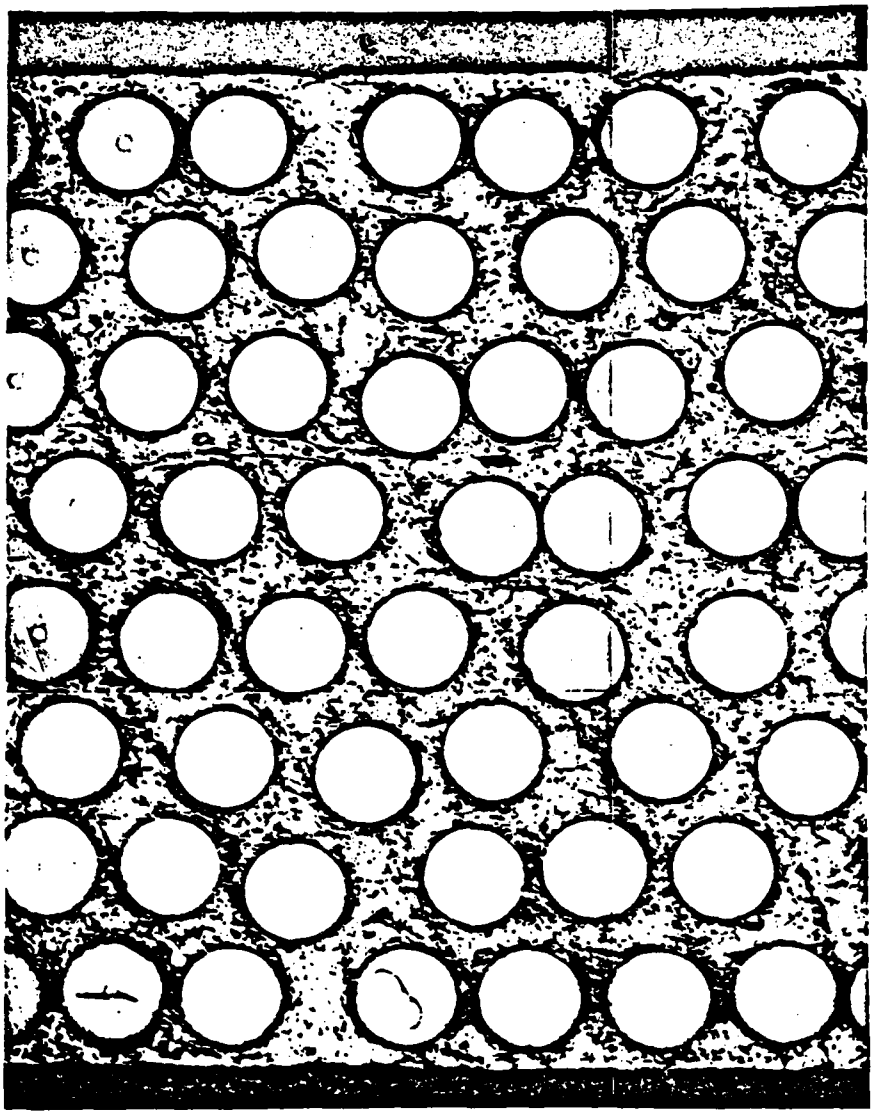

100X

Figure 1. Photomicrograph of unidirectional 5.6 mil boron/aluminum - 6061F specimen.

SPEC. NO. US - 1399/2/1X σ_f = 1303.1 MPa

2a/W = 0.0 T = 21°C

(a)

150X

(b)

30X

Figure 2. Scanning electron microscope micrographs of fracture surface. a. A stereo pair; b. General view of part of the fracture surface. (Ultimate strength = 1303 MPa.)

The few protruding fibers in Figure 2a (and in subsequent Figures) are exceptional and are shown here only to demonstrate the quality of the fiber/matrix bond. No matrix/matrix debonding has been observed, and the large amount of microvoid formation (local yielding of the aluminum matrix) appears to exemplify the increased degree of triaxial restraint which occurs as the matrix/matrix bonding is enhanced [16]. The substantial shattering of the fibers, Figure 2a, and breaking of the tungsten core seems to be limited to a few fiber-diameters along the length of the fibers. Figure 2b shows an overall view of a small section of the fracture surface. The small amount of fiber pull-out and the irregular pattern of the fracture surface are apparent.

The SEM photographs shown in Figure 3 were obtained from a similar unnotched specimen having an ultimate strength of 1469 MPa. Generally, no difference in the fracture surface morphology between the two specimens has been observed and the features described above appear for both the "weaker" and "stronger" specimens. The only difference is that the fracture surface of the "stronger" specimen is more regular. Figure 3 again demonstrates the good fiber/matrix bond; however, to examine the interfacial bond more accurately, an X-ray examination was performed on the fiber surface shown in Figure 3b using an energy dispersive X-ray analyzer on the SEM. The result of this examination, shown in Figure 4, demonstrates the presence of aluminum 6061 on the fiber surface, e.g. Al, Si, Mg lines.

As mentioned earlier, notched unidirectional boron/aluminum specimens were loaded to predetermined levels, approximately 20%, 40% and 60% of the expected ultimate strength, then unloaded and examined under the SEM after dissolving the outer foil of the aluminum matrix, e.g. Figure 5. The crack tip is located at the left side of the photograph in both Figures. Figure 5a shows a general view of the front layer of fibers, demonstrating again the nonuniformity of fiber distribution in the matrix. The broken fiber in the second layer is clearly

(a)

140X

(b)

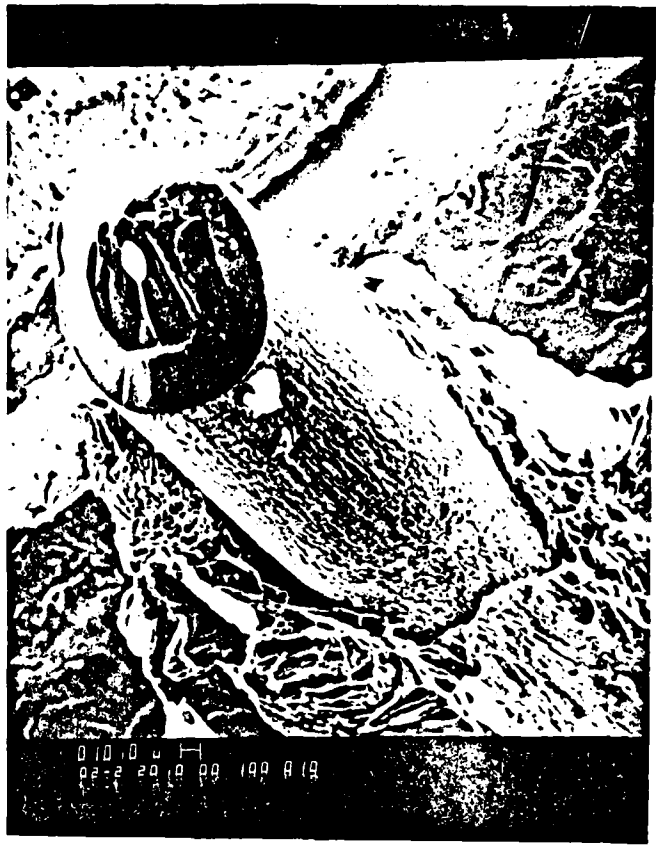

200X

σ_f = 1469 MPa

Figure 3. Scanning electron microscope micrographs of fracture surface: a. General View; b. Individual fiber for X-ray examination of fiber surface. (Ultimate strength = 1469 MPa.)

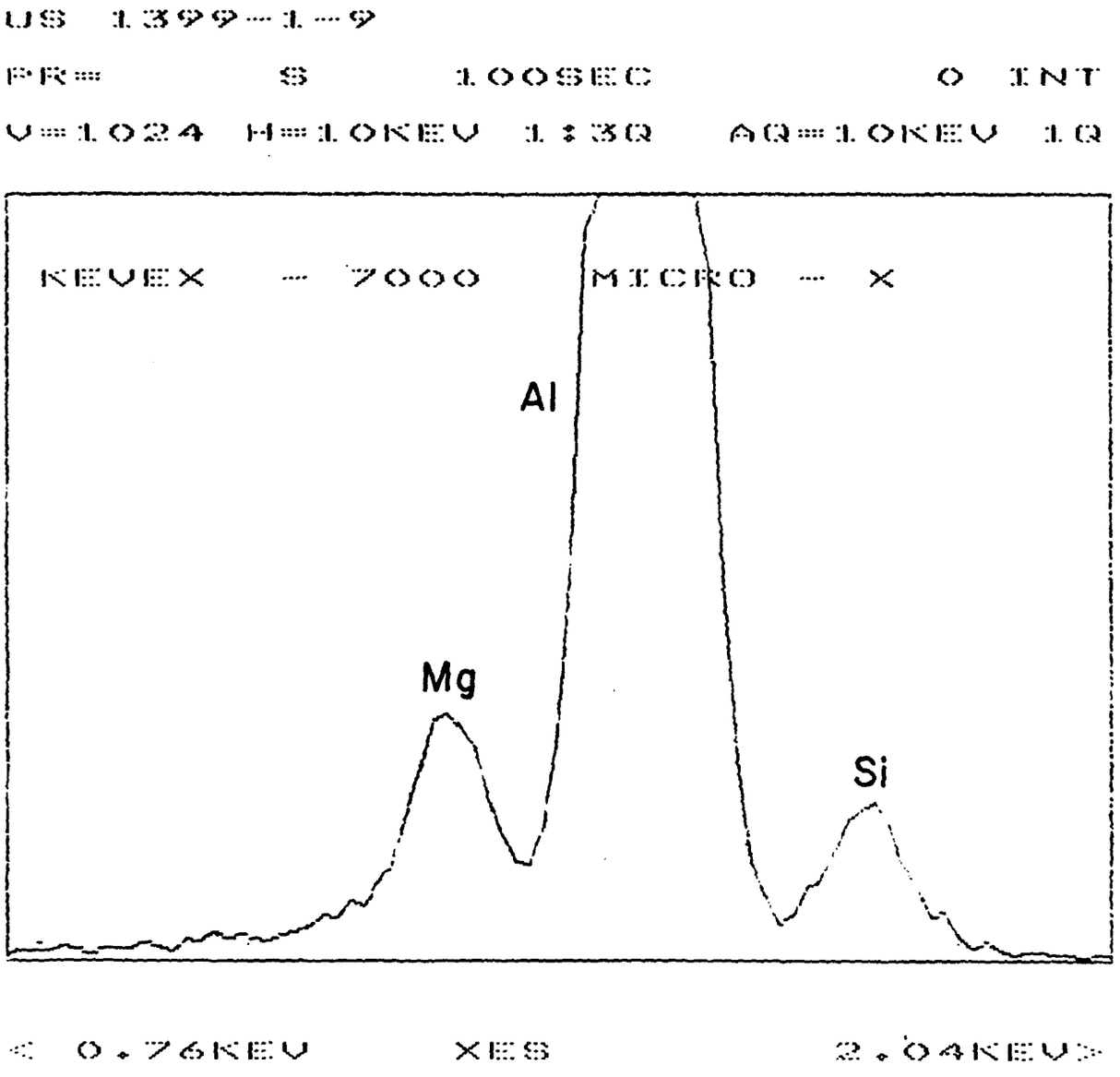

Figure 4. X-ray examination of fiber surface shown in Figure 10 using an energy dispersive X-ray analyzer on the SEM.

SPEC. NO. UN - 1382/3/2 σ_f = 330.9 MPa

2a/W = 0.300 T = 21°C

(a)

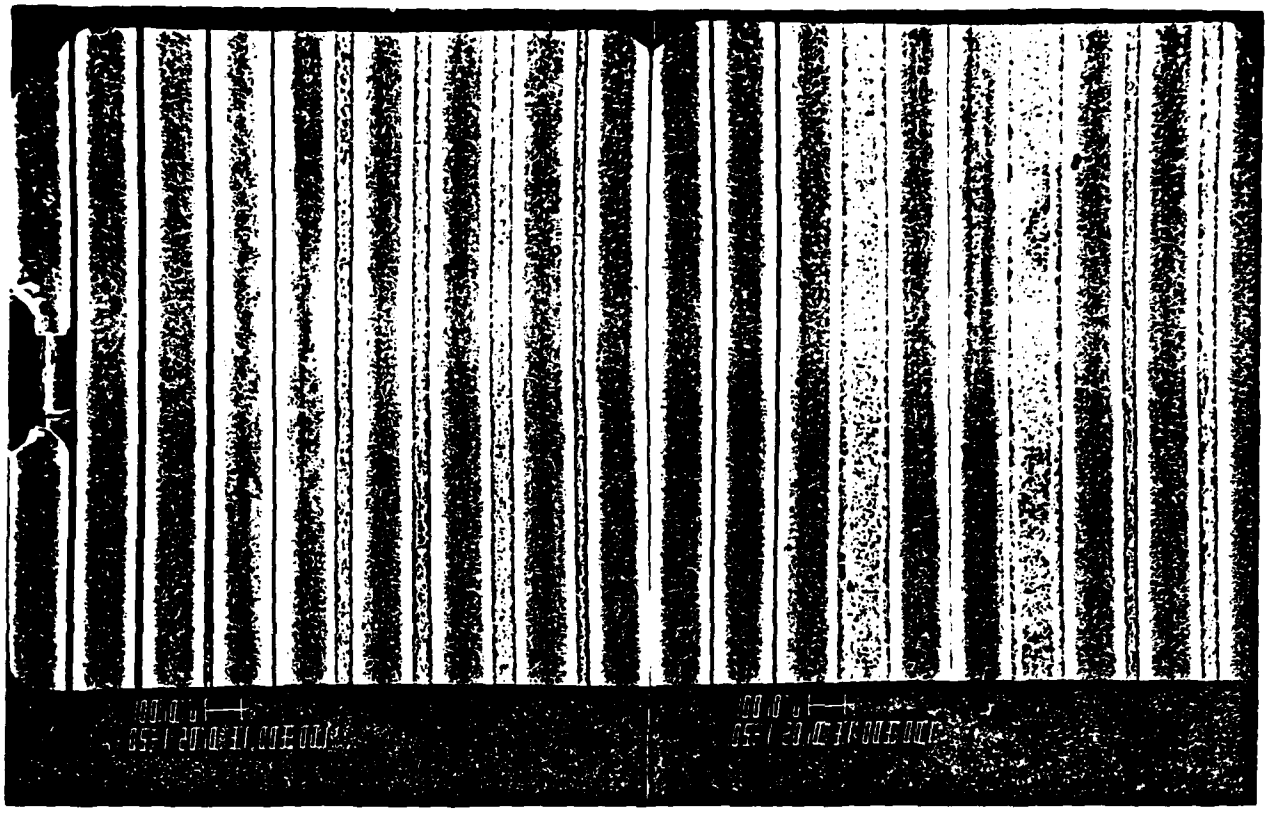

50X

(b)

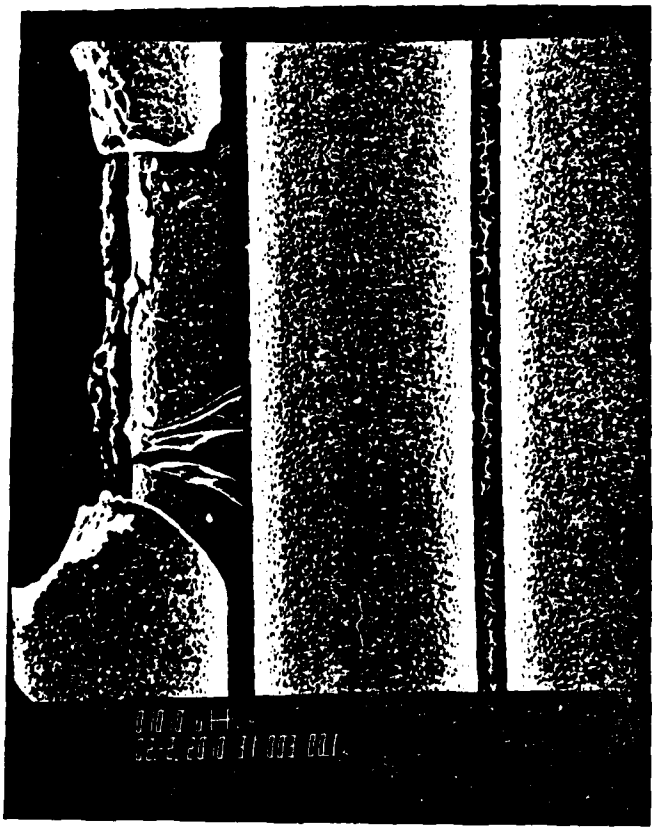

200X

Figure 5. Crack tip damage in unnotched unidirectional 5.6 mil B/Al-6061F specimen after loading to 40% of expected ultimate load (crack length = 7.64 mm). a. General view; b. Detail of crack tip damage.

seen, a detail of which is shown in Figure 5b. Note the typical pattern of wedge-shaped fragments with their apexes pointing toward the original crack tip. The uppermost left fiber on the front layer shown in Figure 5a is broken due to the burn-out resulting from the electrical discharge machining process of the slit, and is also detailed in Figure 5b.

SEM photographs of notched and unnotched $[90]_8$ B/Al specimens are shown in Figure 6. Careful examination of the fracture surface of both specimens show some irregularity in the specimen thickness direction, however it is limited to no more than one fiber diameter. The fibers shown in Figure 6a are practically clean of aluminum residue, indicating significant interfacial failure. Throughout the fracture surface only one split fiber has been found, and this was at the edge of the specimen where a complex state of stress exists just prior to fracture. The split fiber shown in the photograph for the unnotched specimen, Figure 6b, is also the only one found throughout the fracture surface.

From the results obtained so far, no clear answer can be given in regard to the low strength values obtained for the material system studied in this program. The manufacturing process of this material seems to be adequate. Consequently, attention has been placed on the important aspect of the strength and scatter in strength of individual fibers. For this purpose, representative fibers used in the fabrication of each plate were purchased and tested.

The scatter in strength has been characterized by the two-parameter Weibull distribution for the 5.6 mil and 8.0 mil diameter boron fibers and unidirectional composite, Figures 7-10. Note the very large scatter and low average fiber strength as indicated by the very low shape, α, and scale, $\hat{X}_s$ parameters shown in Figures 7-8. The comparison between the strength distributions of the individual fibers and the unidirectional boron/aluminum, Figure 10 explains the relatively low strength of the composite tested in this program. The same conclusion can also be shown by applying the elementary rule of mixtures using 45% volume fraction of the fibers in the composite plates.

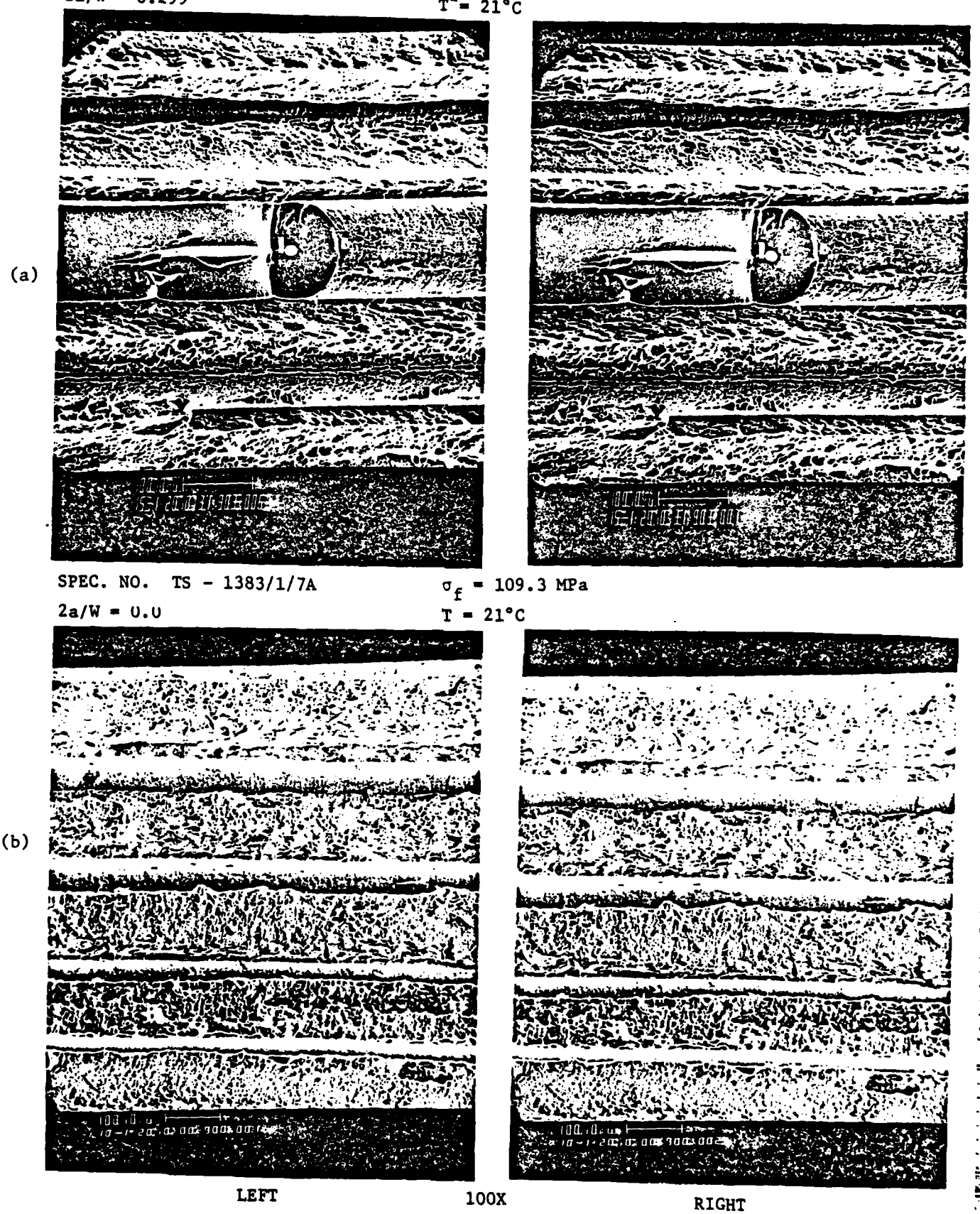

Figure 6. Scanning electron microscope micrographs of the fracture surface of $[90]_8$ boron/aluminum.

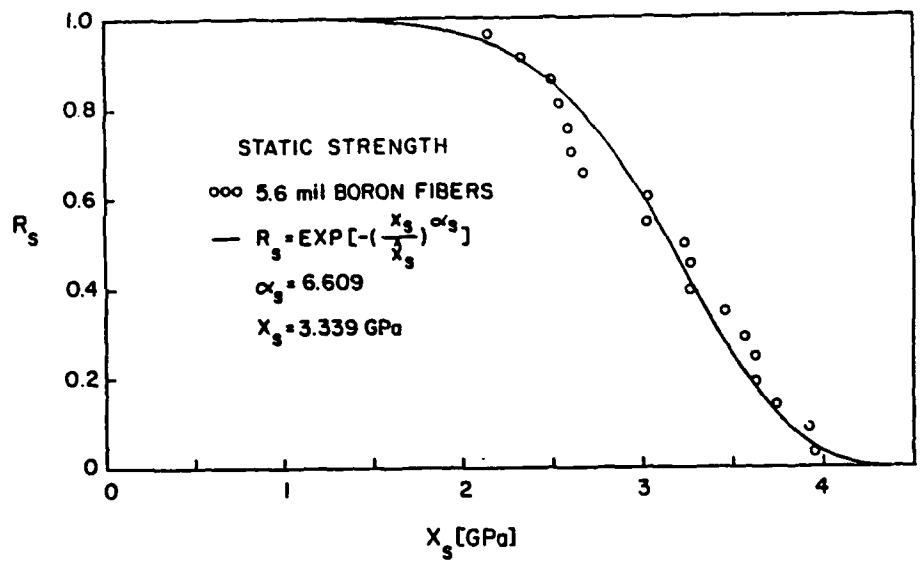

Figure 7. Static strength distribution of individual 142 μm (5.6 mil) diameter boron fibers.

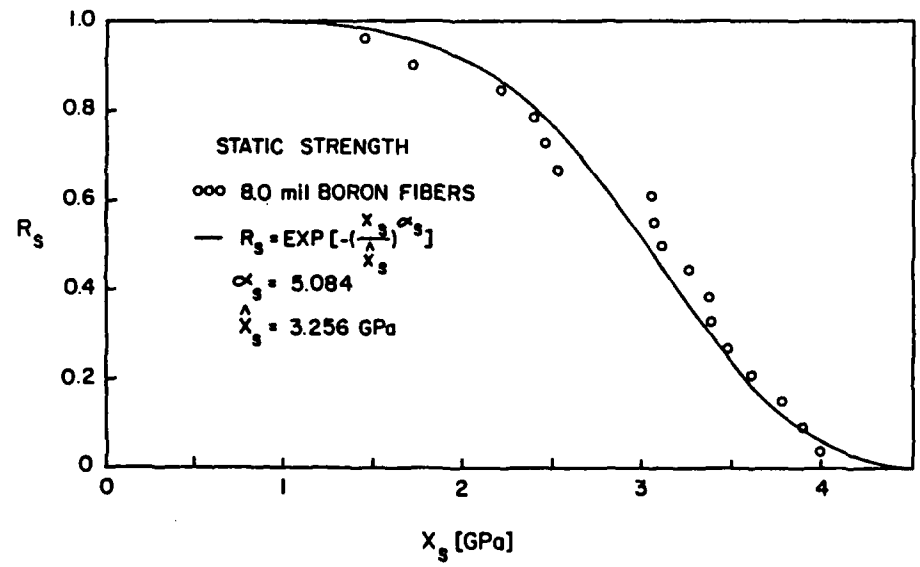

Figure 8. Static strength distribution of individual 203 μm (8.0 mil) diameter boron fibers.

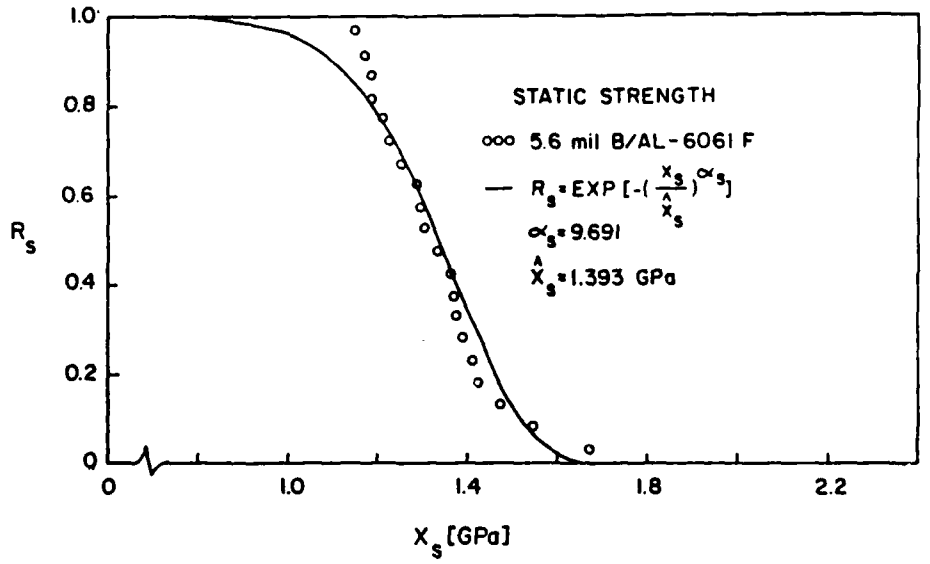

Figure 9. Static strength distribution of unidirectional 5.6 mil boron/aluminum - 6061F.

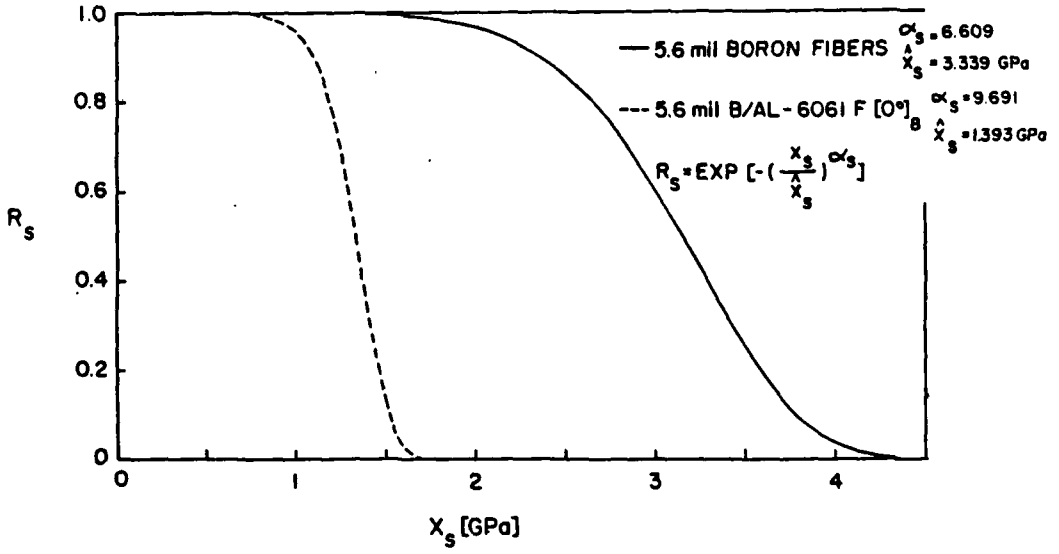

Figure 10. Comparison between static strength distributions of unidirectional 5.6 mil boron/aluminum specimens and 5.6 mil diameter boron fibers.

It should be noted that all fibers were obtained from the same batch of material and that no correlation could be established between individual fiber strength and the specimen strength, both depicted from the same plate. In other words, the scatter in fiber strength was inherent in each of the plates purchased. Consequently, when the mechanical performance of boron/aluminum composites are evaluated it is essential that data on consitituent properties be available so that proper interpretation of the tests results can be made and meaningful conclusions can be drawn.

6.3.2 Fracture Surface Morphologies of Multidirectional Laminates at Room Temperature

A general view of the fracture surface morphologies for the six different lay-ups tested in this program are shown in Figure 11. The detailed SEM examinations revealed various micro-failure modes associated with the fracture of the various laminates. In all laminates containing 0° fibers, those fibers are shattered into wedge-shaped fragments. Exposing the fibers through matrix dissolution revealed that this fiber shattering does not extend to a depth greater than two fiber diameters from the fracture surface. The extent of the fiber fragmentation was also confirmed by observation through the stereo viewer.

Extensive fiber splitting in the 90° and 45° plies occurred in all multi-direction laminates, Figures 12-15. The split surfaces of the 45° fibers are quite rugged. In most cases one half of the split surface is striated along its length while the other half is more smooth; however, transverse cracks can be easily seen, Figures 12-16. The source of this pattern in the split surface is unclear. One possible explanation is that the striation resulted from shear stress along the 45° plies while the transverse cracks indicate possible intermittent progression of splitting. In the 90° fibers very little striation is detected and only a few transverse cracks are present. It should be recalled that very little fiber splitting has been detected in the $[90]_8$ specimens,

SPEC. NO. UN-1401/4/4
LAY UP: $[0]_8$
2a/W = 0.422
σ_f = 625.4 MPa

SPEC. NO. GN-1385/5/9
LAY UP: $[\pm 45]_{2s}$
2a/W = 0.405
σ_u = 83.1 MPa

SPEC. NO. TN-1384/1/3
LAY UP: $[90]_{2s}$
2a/W = 0.293
σ_u = 89.0 MPa

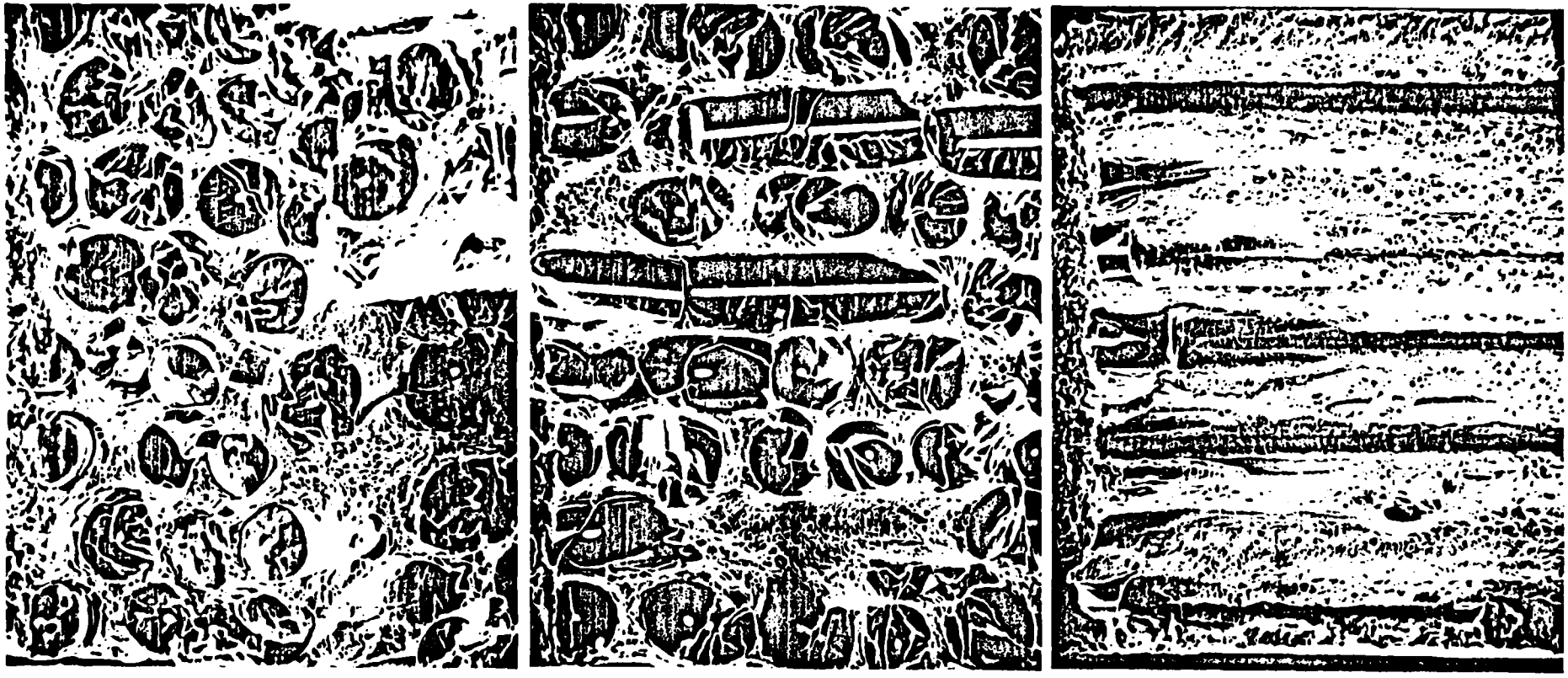

Figure 11. Scanning electron microscope micrographs of fracture surfaces of six boron/aluminum laminates showing the various micro-failure modes.

SPEC. NO. CPN-1393/5/5
LAY UP: $[0/90]_{2s}$
2a/W = 0.402
σ_f = 236.3 MPa

SPEC. NO. LAN-1520/9
LAY UP: $[0/\pm45/0]_s$
2a/W = 0.502
σ_f = 272.3 MPa

SPEC. NO. QIN-1522/8
LAY UP: $[0/\pm45/90]_s$
2a/W = 0.406
σ_f = 202.1 MPa

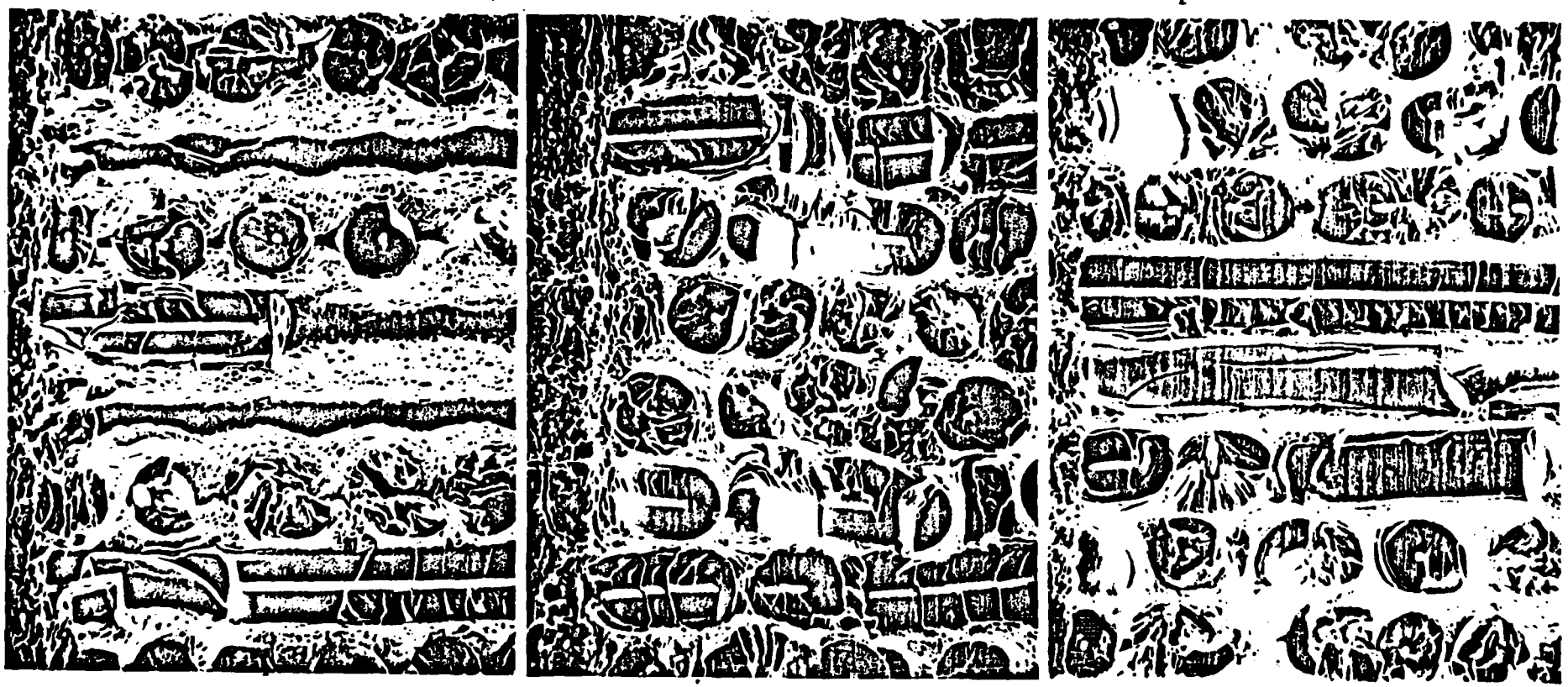

Figure 11. Continued.

SPEC. NO. GN = 1385/6A/1 σ_f = 97.2 MPa

2a/W = 0.301 T = 21°C

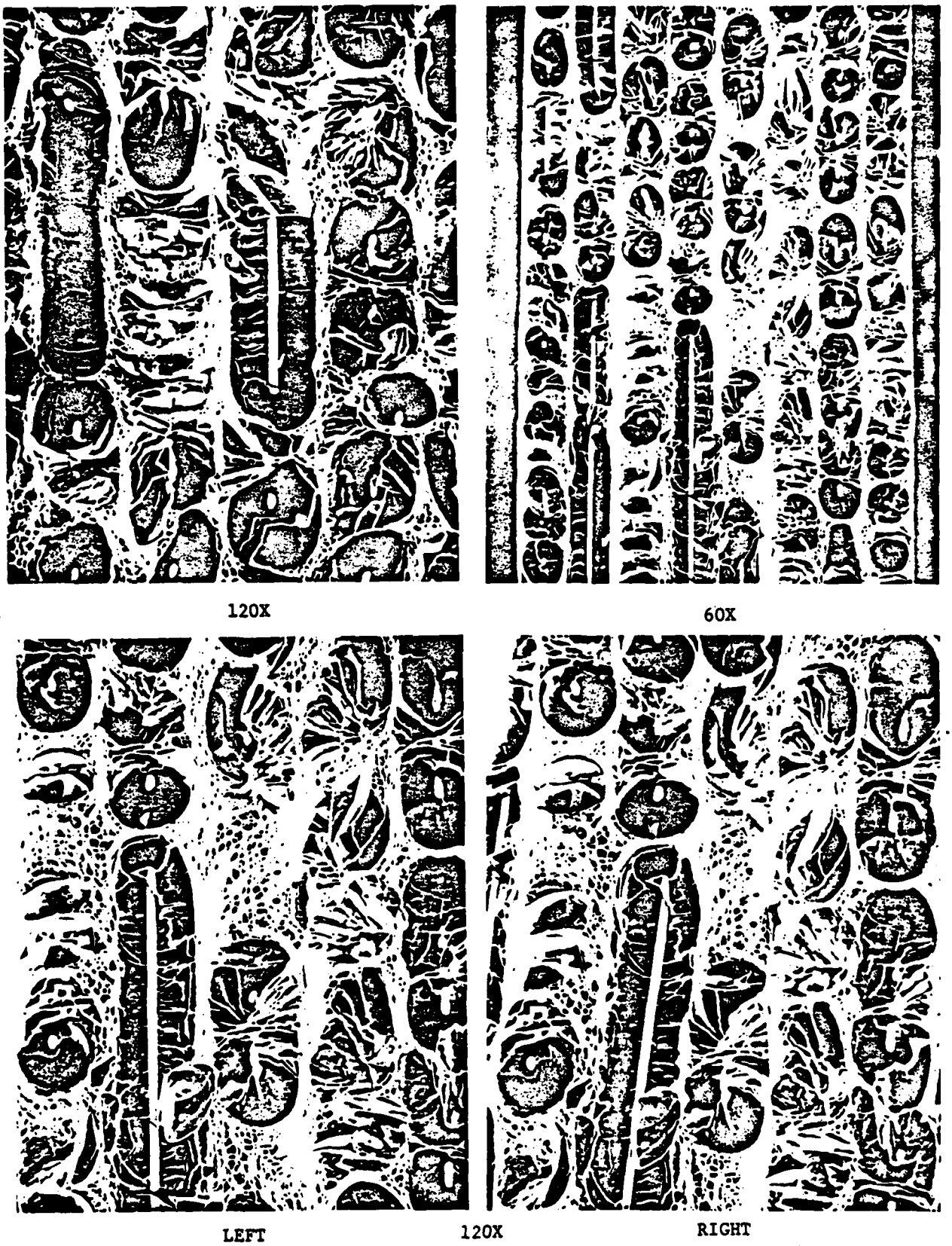

Figure 12. Scanning electron microscope micrographs of the fracture surface of $[\pm 45]_{2s}$ boron/aluminum laminate at room temperature.

SPEC. NO. CPN - 1394/5/1 σ_f = 270.6 MPa

2a/W = 0.305 T = 21°C

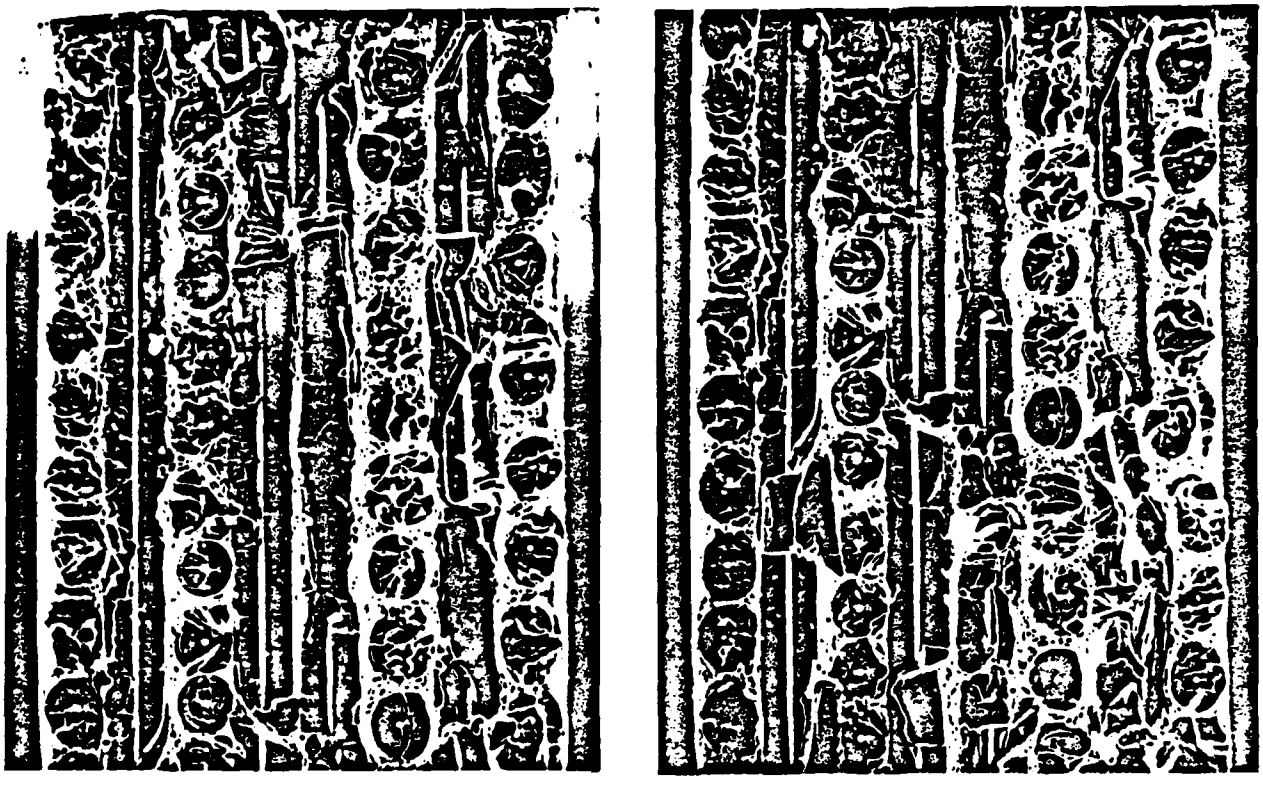

60X

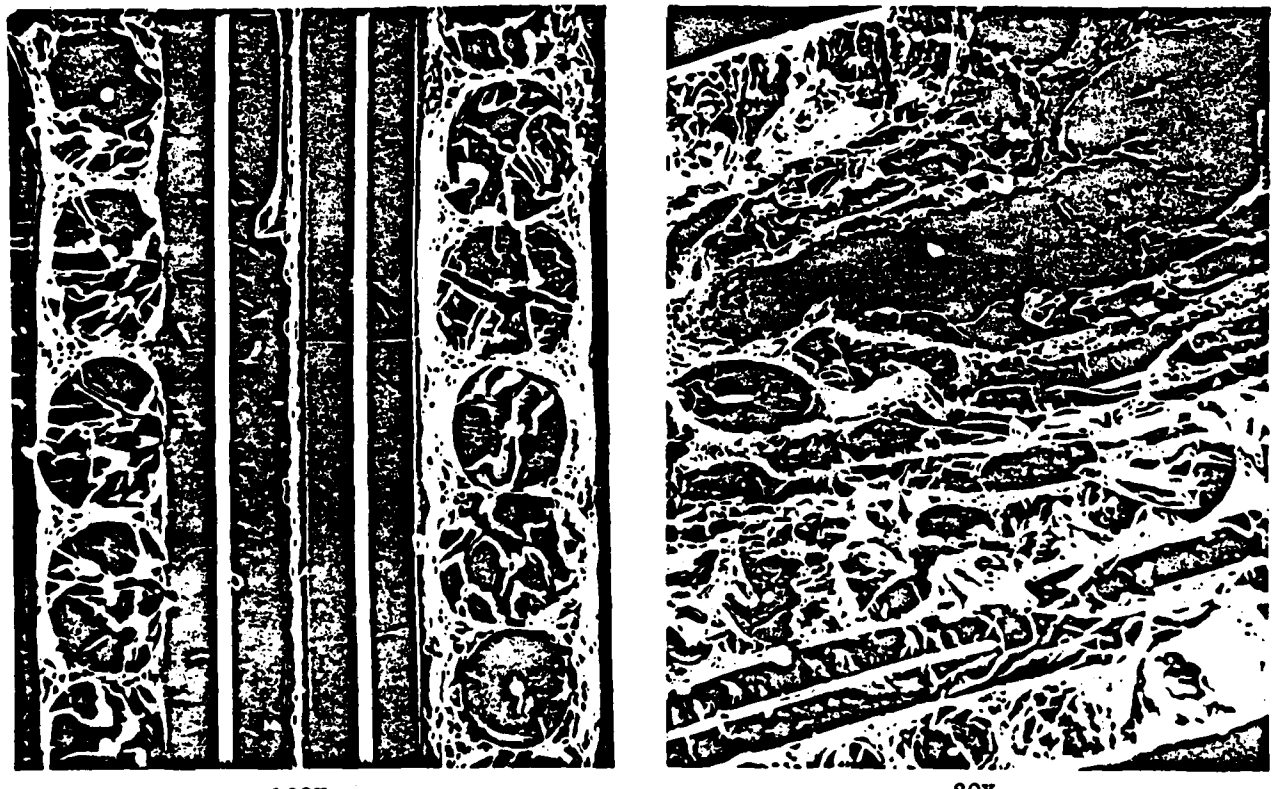

120X 80X

Figure 13. Scanning electron microscope micrographs of the fracture surface of $[0/90]_{2s}$ boron/aluminum laminate at room temperature.

SPEC. NO. QIN - 1522/6 σ_f = 223.8 MPa

2a/W = 0.307 T = 21°C

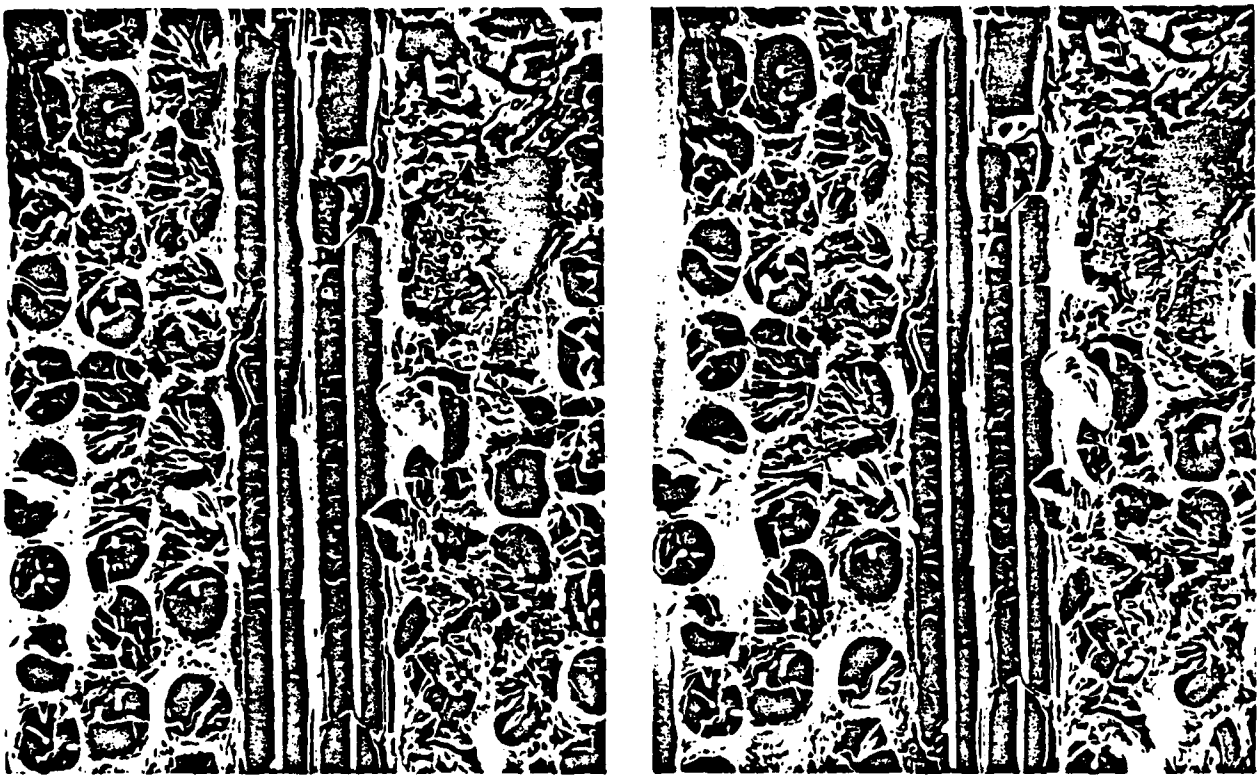

LEFT 68X RIGHT

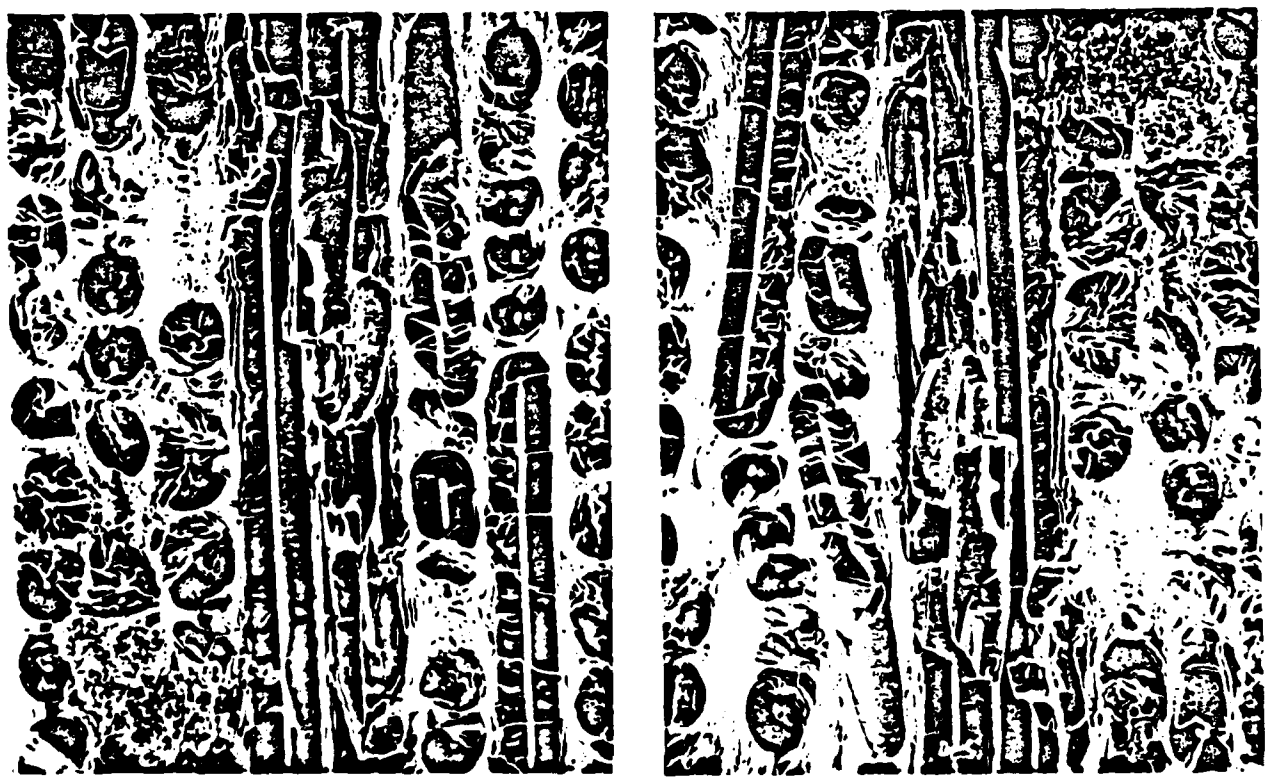

LEFT 68X RIGHT

Figure 14. Scanning electron microscope micrographs of the fracture surface of $[0/\pm45/90]_s$ boron/aluminum laminate at room temperature.

SPEC. NO. LAN - 1520/28 σ_f = 379.7 MPa

2a/W = 0.305 T = 21°C

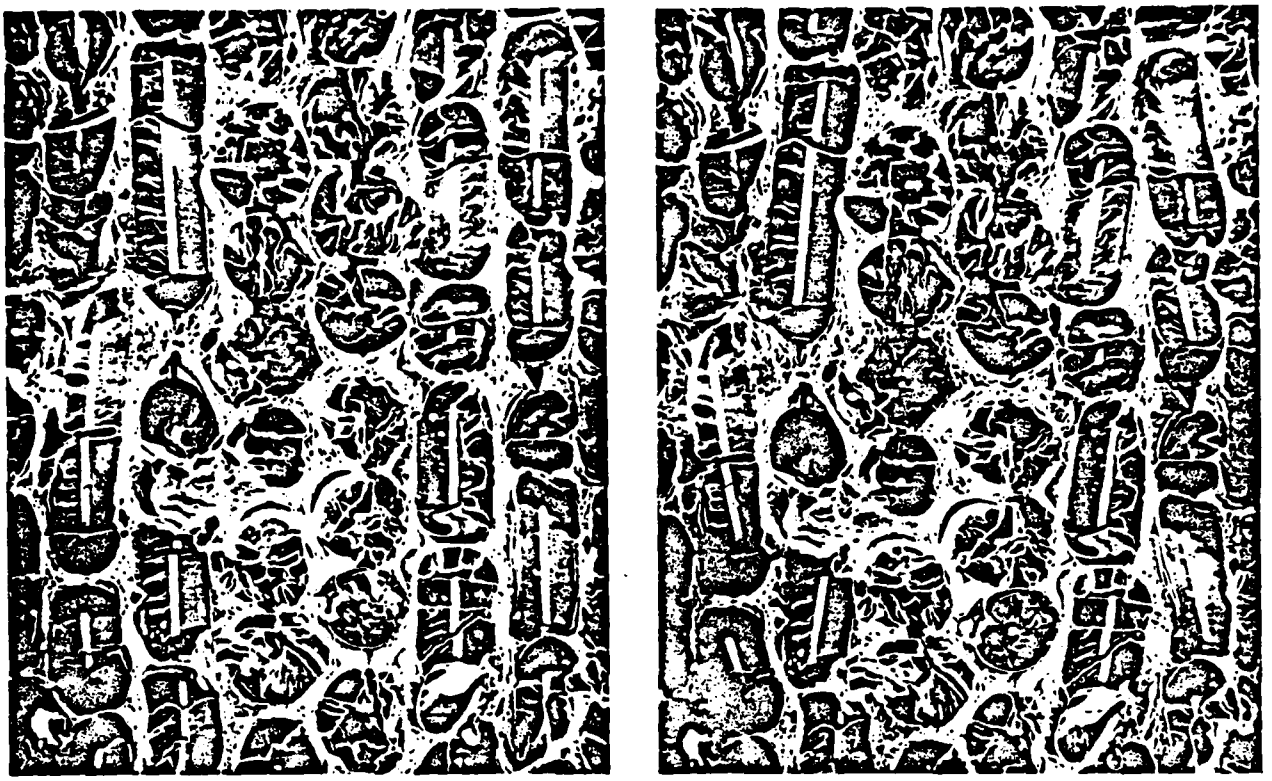

LEFT 80X RIGHT

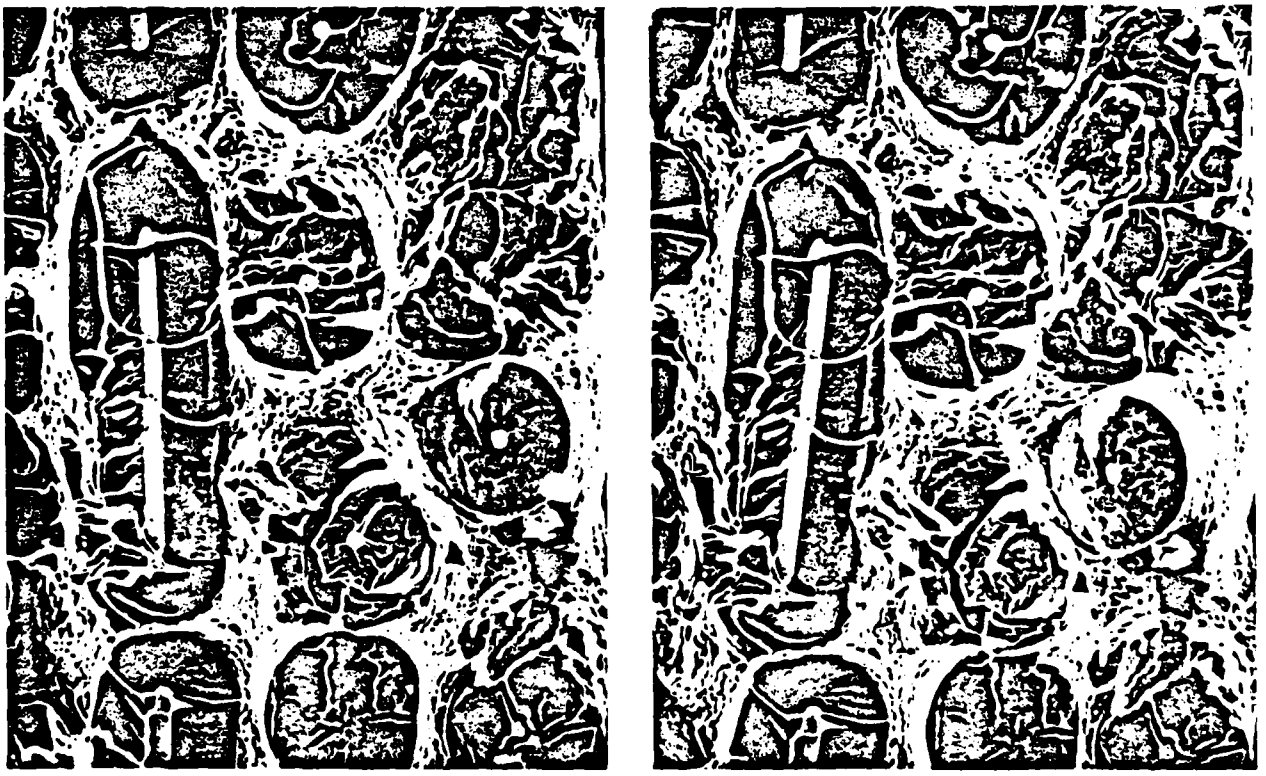

LEFT 160X RIGHT

Figure 15. Scanning electron microscope micrographs of the fracture surface of $[0/\pm45/0]_s$ boron/aluminum laminate at room temperature.

SPEC. NO. LAN - 1520/28 σ_f = 379.7 MPa

2a/W = 0.305 T = 21°C

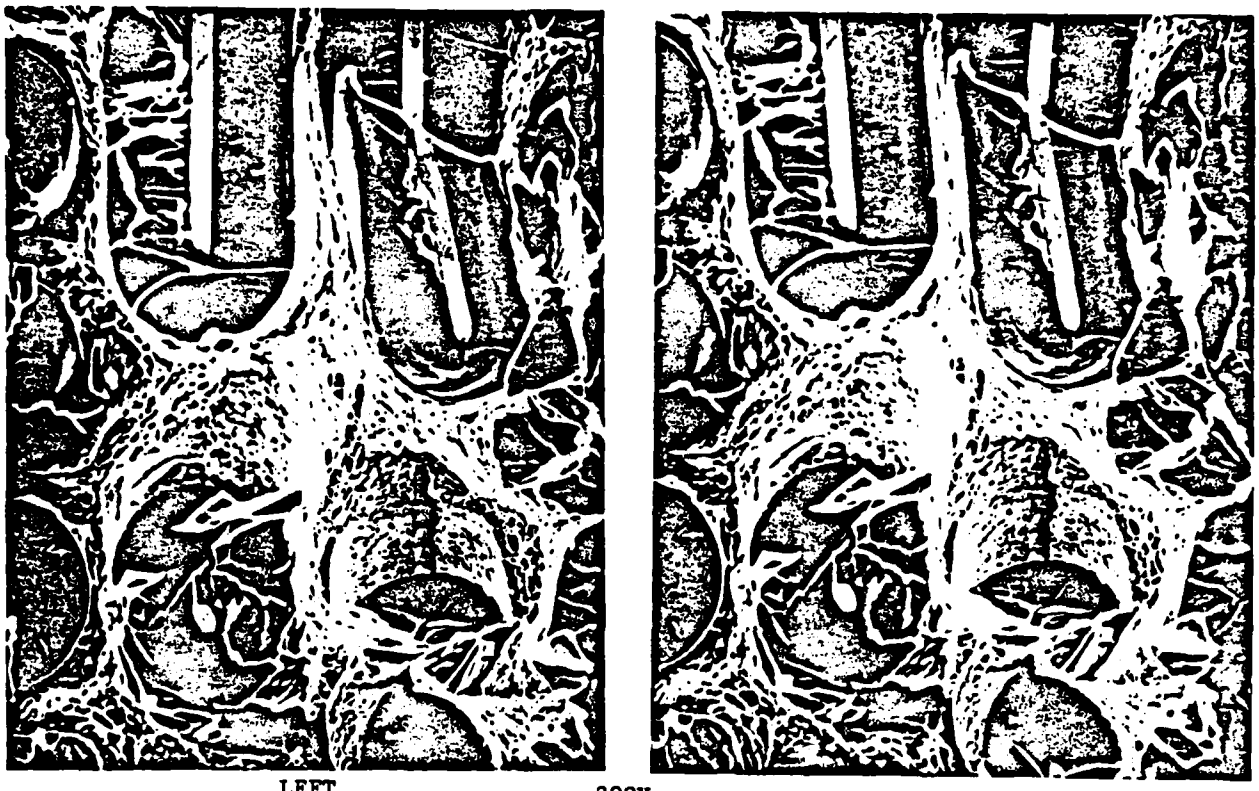

LEFT 200X RIGHT

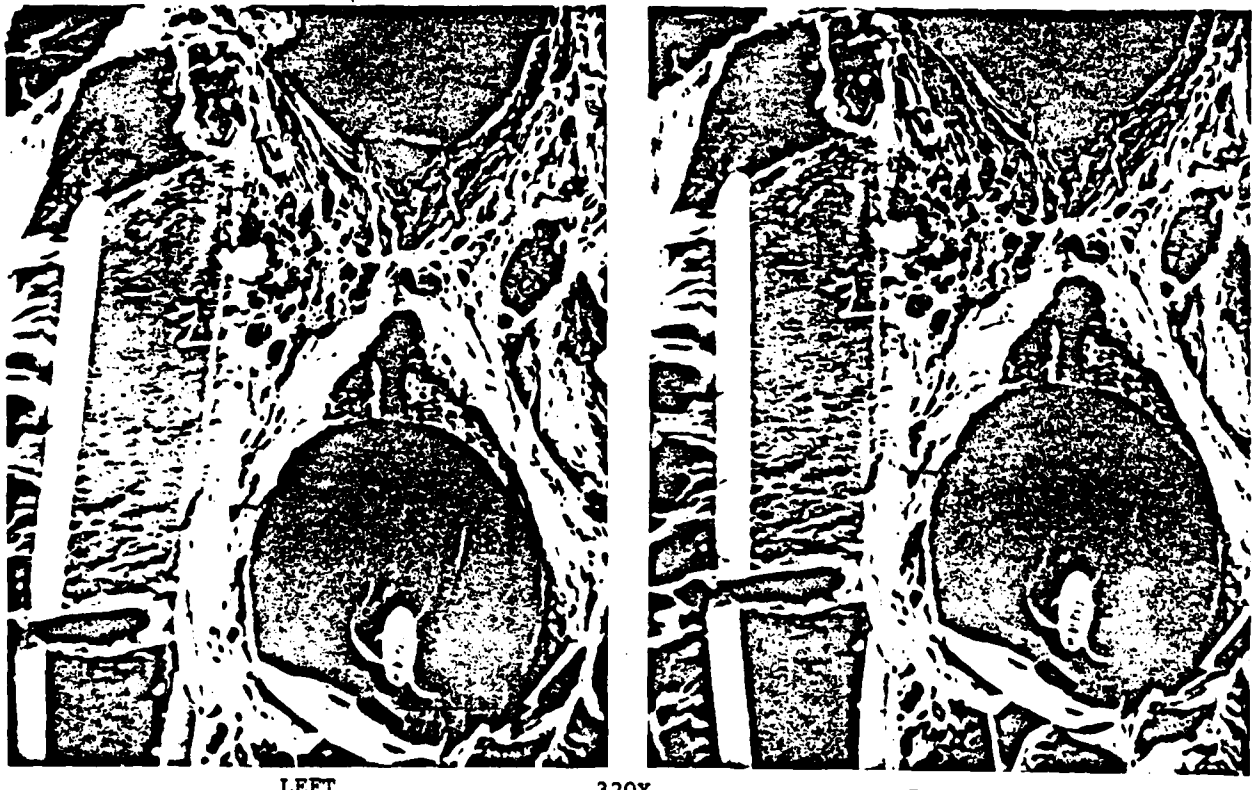

LEFT 320X RIGHT

Figure 16. Scanning electron microscope micrographs of the fracture surface of $[0/\pm45/0]_s$ boron/aluminum laminate at room temperature, showing details of fiber splitting and interfacial failure.

except in the vicinity of the notch tip, Figure 11.

Interfacial failure in the multidirectional laminates was noticeable in all 90° layers and to a lesser degree along the 45° layers. Little if any interfacial failure could be detected in the $[0]_8$ specimens, as previously discussed.

Significant matrix yielding has been noticed in all laminates, manifested by the large amount of micro-void coalescence. Matrix plastic shear deformation along the split surfaces of the $[0]_8$ specimens could also be identified. There was little if any evidence of shear deformation along the 0° and 45° fibers in the multidirectional laminates, however, this issue has not been addressed in sufficient detail to reach definite conclusions. Fiber pull-out occurred randomly throughout the fracture surfaces of all multidirectional laminates, primarily for the 0° fibers. In most cases the pull-out length extended to approximately 2-3 fiber diameters.

6.3.3 Effect of Elevated Temperatures on Fracture Surface Morphology:

No significant effect of elevated temperatures (up to 315°C, 600°F) on the fracture surface morphologies has been noticed. For all laminates tested, the SEM examinations reveal no distinction between the micro-failure modes of specimens tested at room temperature, Figures 12-15, and those tested at 315°C (600°F) Figures 17-22. The SEM examinations were directed toward the amount of fiber pull-out, fracture surfaces of the broken fibers, amount of fiber shattering, fiber/matrix and matrix/matrix bonding, plastic deformation and local yielding of the aluminum matrix, etc.

The only distinction which appeared between the room and elevated temperature morphologies was in the amount of micro-void coalescence noticed at room temperature, while at elevated temperatures specimens exhibited a much higher degree of matrix plastic deformation, as expected and as the load-COD curves obtained with

UN-1381/4/7 320X T = 93°C (200°F) 2a/W = 0.199 σ_f = 910.3 MPa

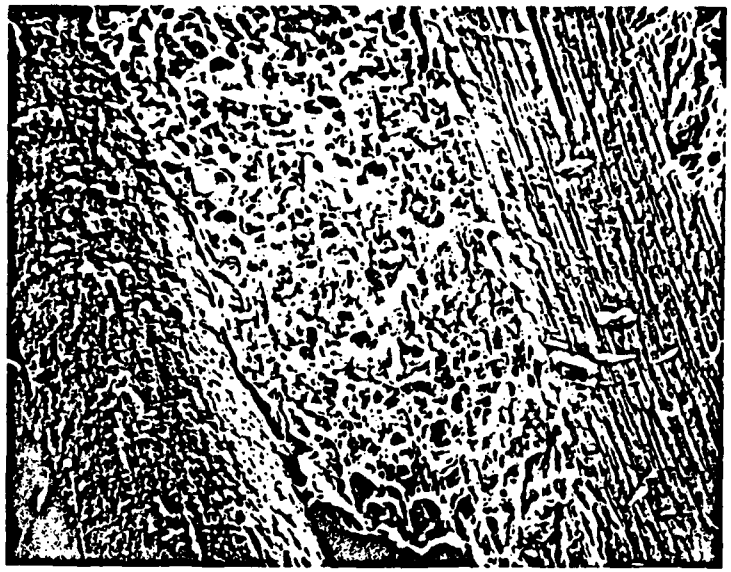

UN-1380/3/4 320X T = 21°C (70°F) 2a/W = 0.199 σ_f = 893.9 MPa

UN-1401/4/1A 320X T = 316°C (600°F) 2a/W = 0.200 σ_f = 811.0 MPa

UN-1381/5/1A 320X T = 204°C (400°F) 2a/W = 0.196 σ_f = 892 MPa

Figure 17. Scanning electron microscope micrographs of the split surface in unidirectional boron/aluminum at room and elevated temperatures, showing excessive matrix yielding at higher temperatures.

TN-1381/1/1 160X T = 21°C (70°F) 2a/W = 0.300 σ_f = 77.8 MPa

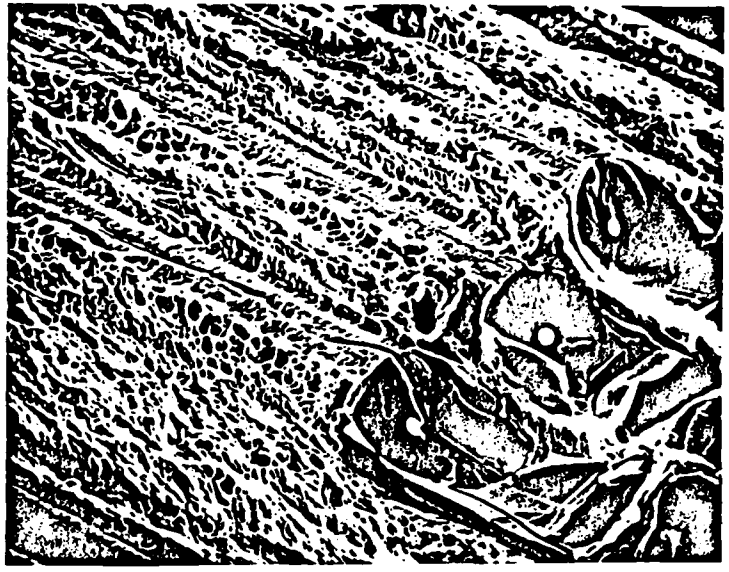

TN-1381/1/1 160X T = 21°C (70°F) 2a/W = 0.300 σ_f = 77.8 MPa

TN-1383/2/5 160X T = 316°C (600°F) 2a/W = 0.508 σ_f = 21.6 MPa

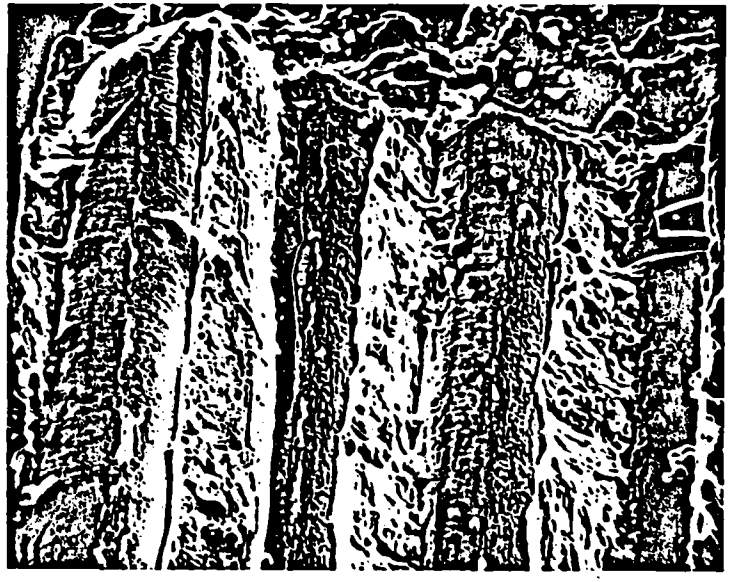

TN-1384/2/8 T = 204°C (400°F) 160X

Figure 18. Scanning electron microscope micrographs of the fracture surface of $[90]_8$ boron/aluminum at room and elevated temperatures, showing excessive matrix yielding and interfacial failure at higher temperatures.

SPEC. NO. GN - 1385/3/7 σ_f = 59.0 MPa

2a/W = 0.301 T = 315°C

LEFT 120X RIGHT

LEFT 120X RIGHT

Figure 19. Scanning electron microscope micrographs of the fracture surface of $[\pm 45]_{2s}$ boron/aluminum laminate at elevated temperature.

SPEC. NO. CPN - 1393/2/3 σ_f = 285.9 MPa

2a/W - 0.303 T = 315°C

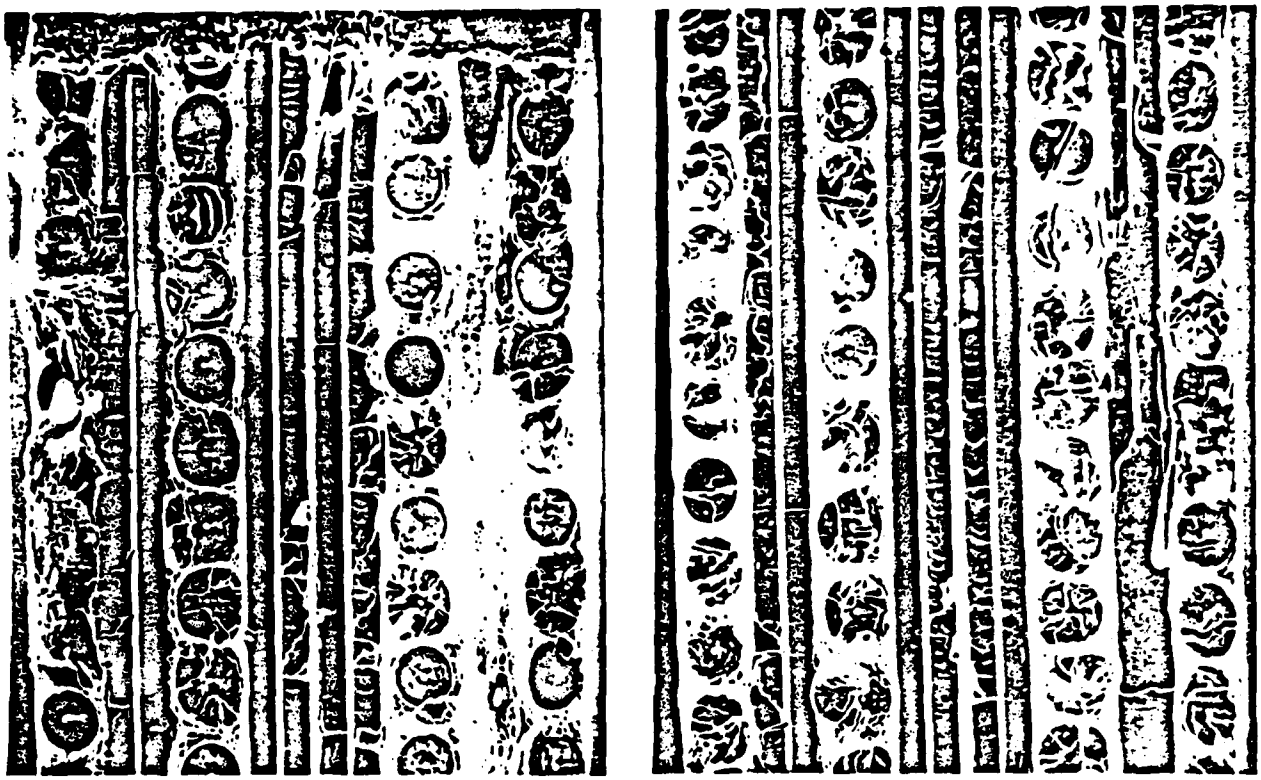

60X

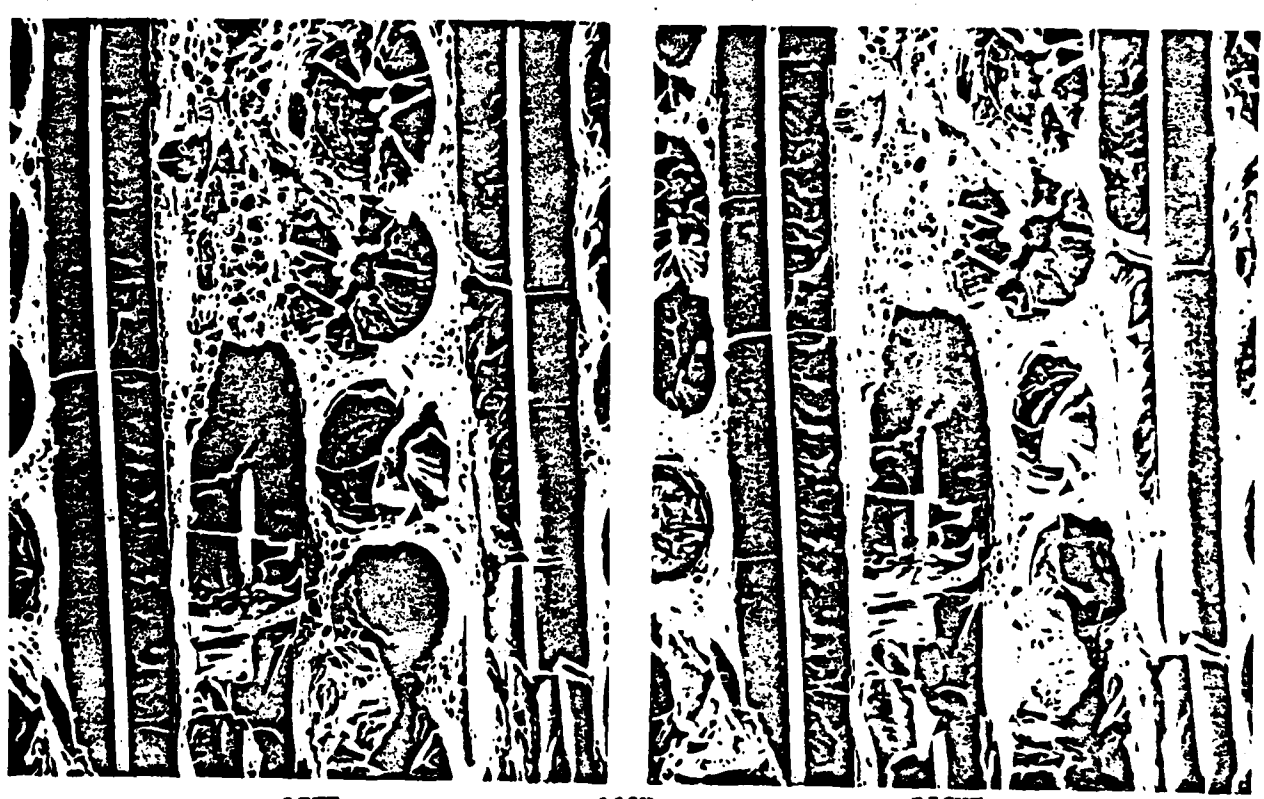

LEFT 120X RIGHT

Figure 20. Scanning electron microscope micrographs of the fracture surface of $[0/90]_{2s}$ boron/aluminum laminate at elevated temperature.

SPEC. NO. QIN - 1523/4 σ_f = 219.4 MPa

2a/W = 0.305 T = 315°C

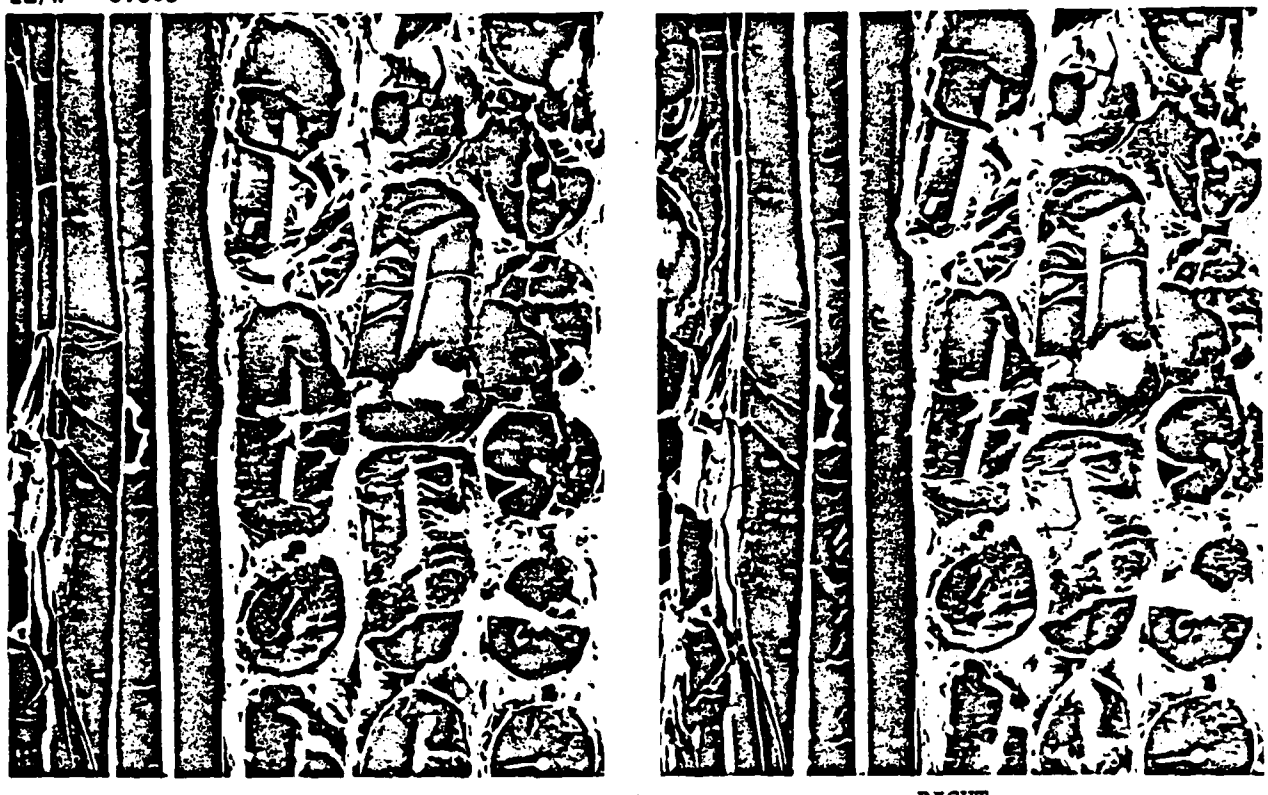

LEFT 120X RIGHT

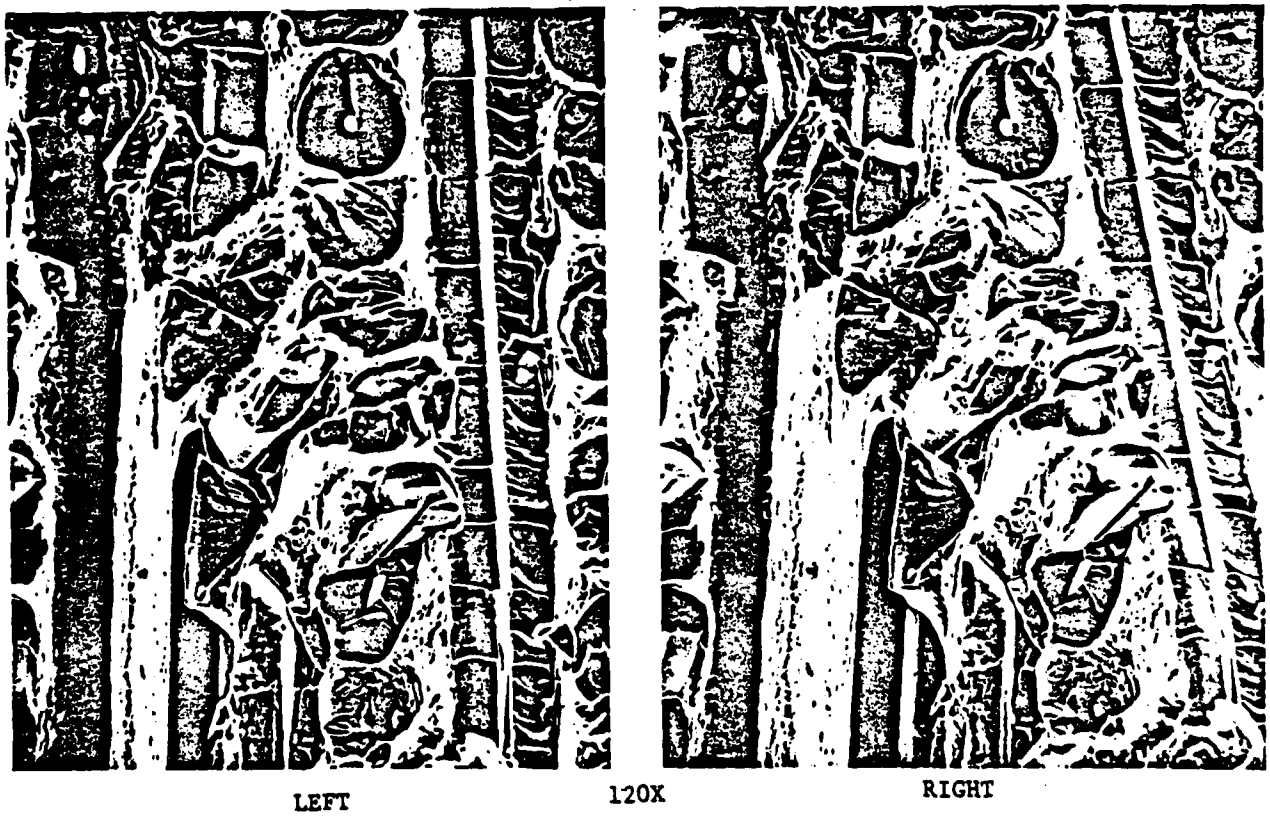

LEFT 120X RIGHT

Figure 21. Scanning electron microscope micrographs of the fracture surface of $[0/\pm45/90]_s$ boron/aluminum laminate at elevated temperature.

SPEC. NO. LAN - 1519/5 σ_f = 375.7 MPa

2a/W = 0.306 T = 315°C

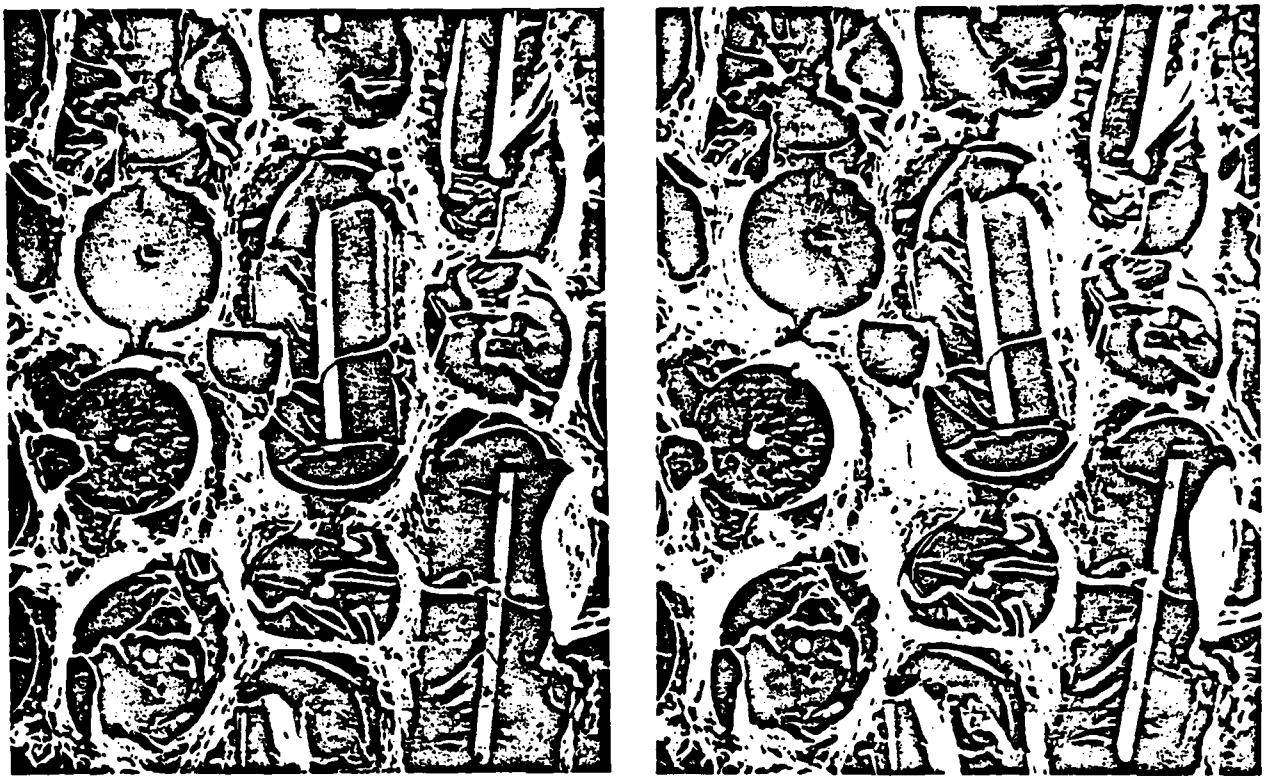

LEFT 160X RIGHT

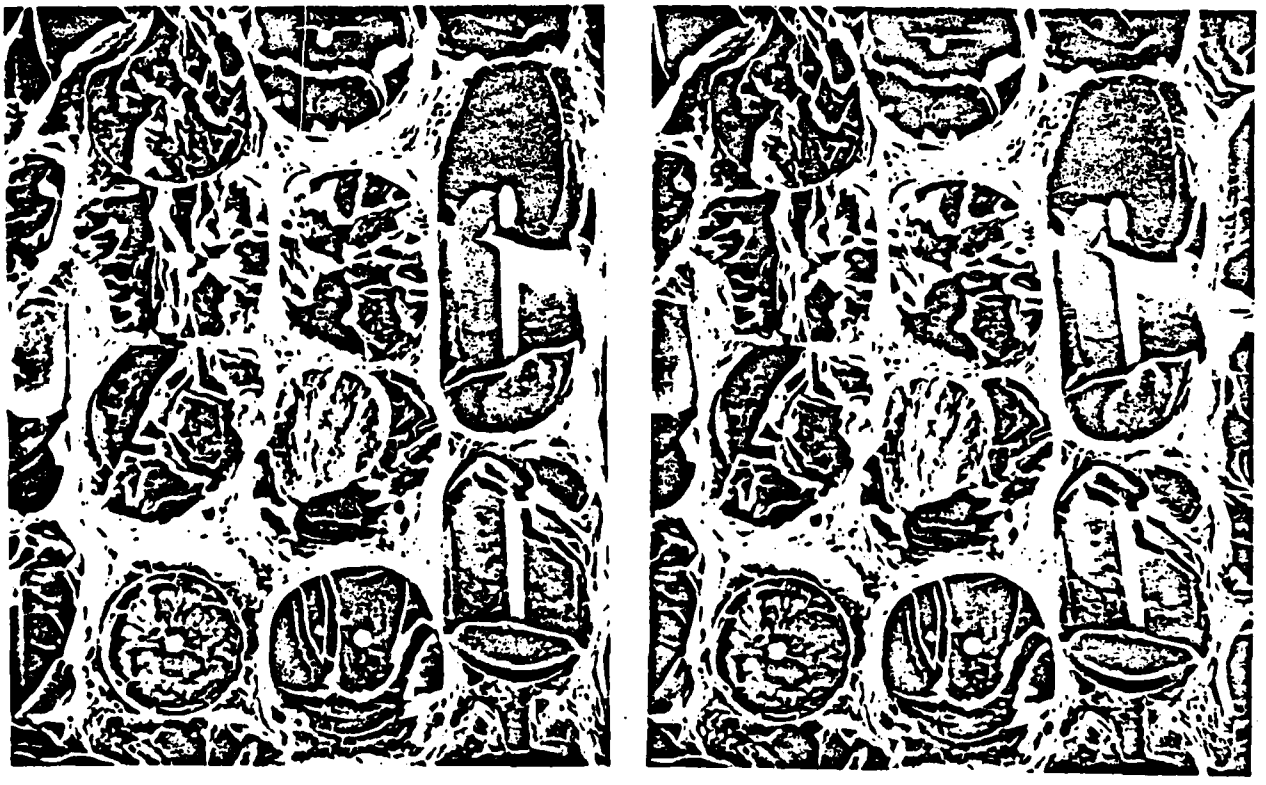

LEFT 160X RIGHT

Figure 22. Scanning electron microscope micrographs of the fracture surface of $[0/\pm45/0]_s$ boron/aluminum laminate at elevated temperature.

the IDG, Section IV, indicated. The effect of elevated temperatures on fiber/matrix interface integrity, fiber degradation, etc. has not been addressed in this study. It is felt however, that this issue deserves special attention. Results on the notched strength of the various laminates, Section XI, indicate that elevated temperatures do affect the notch sensitivity of the subject material. A detailed study on the effect of temperature on interface integrity may shed more light on this issue.

6.3.4 Crack Tip Damage Progression:

For a selected number of specimens crack tip damage progression has been visually monitored in real-time via a closed-circuit television system (CCTV) with an attached microscope which allows magnification up to 250X. Results were recorded on a tape-recorder for the purpose of demonstration and illustrations.

Visual observation is frequently used in monitoring fatigue crack tip damage progression in metals. In composites, however, the results of such an examination procedure cannot be directly related to the "effective" crack tip damage growth since only surface damage can be detected visually. The observed matrix cracking will not necessarily mean significant degradation in performance, while breakage of fibers (which are the load carrying constituent) cannot be visually detected. An alternative test procedure for determining "effective" crack tip damage progression can be the compliance matching procedure, provided that a sufficiently sensitive technique such as the IDG discussed in Section III is applied in measuring crack opening displacement.

Monitoring damage progression in composites via visual observation can, however, indicate qualitatively the sequence of internal failure, i.e. the failure process, and the rate of failure progression. In this study primary emphasis has been placed on determining the approximate number of broken fibers

and the occurrence of matrix plastic deformation and cracking prior to catastrophic fracture. For this purpose, the front layer of fibers has been slightly exposed by carefully sanding and polishing the surface aluminum foil.

Visual observations clearly indicated slow crack tip damage growth in all laminates studied. In $[0°]_8$ specimens, approximately 6-8 broken fibers have been counted prior to catastrophic failure. This indicates that the assumption made in several of the recently developed analytical models (discussed in Section V) is inappropriate, i.e. that catastrophic fracture occurs when the first intact fiber at the front of the notch breaks. In fact, a sequential failure has been observed. Fiber breakage is associated with matrix plastic shear deformation along the fibers and occasional splitting in the matrix. This procedure repeats itself 6-8 times prior to catastrophic fracture. Fiber breakage occurs randomly at some weak spot along the fiber's length, Figure 23, resulting in a final irregular fracture surface. A more detailed description of this failure process in unidirectional boron/aluminum is given in [17].

The failure process of the $[90]_8$ specimen is much simpler; in fact, a self-similar crack extension is observed. The failure progression is relatively slow, along the fiber/matrix interface, for 4-6 fiber diameters prior to rapid catastrophic fracture.

Slow notch tip damage progression has been observed in all multidirectional laminates as well, except in the cross-ply laminate. In the latter laminate no more than 1-2 broken fibers have been detected prior to catastrophic fracture, while in the $[0/\pm45/90]_s$ and $[0/\pm45/0]_s$ laminates notch tip damage extended to approximately 4-8 fiber diameters, and it propagated primarily along the ±45° direction, however, it was much more localized compared with the $[0°]_8$ specimen. These observations could be correlated with the notch sensitivity results (discussed in Section X), i.e. the more localized the notch tip damage zone is prior to catastrophic failure, the more notch sensitive the subject material is.

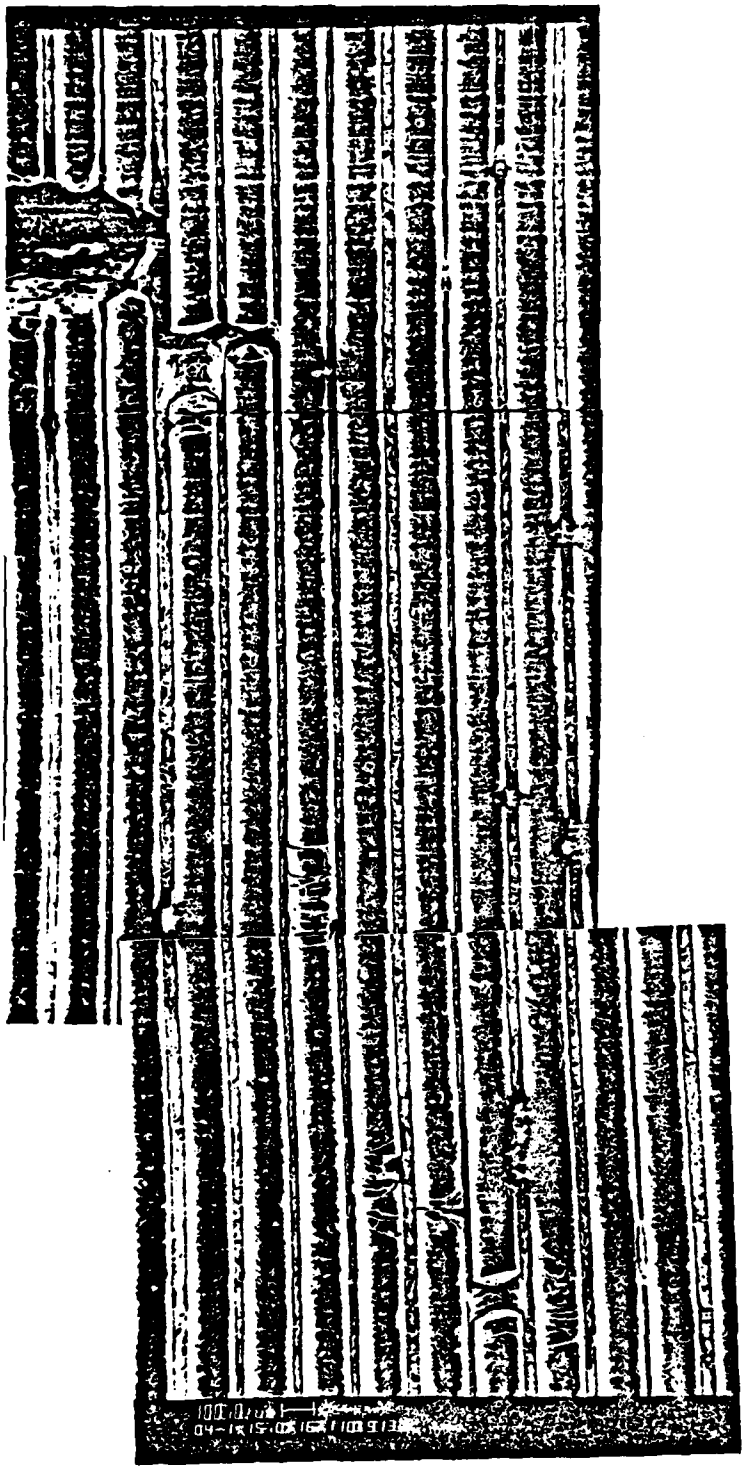

Figure 23. Crack tip damage extension; aluminum matrix is dissolved exposing broken fiber.

6.4 Conclusions

A summary of the major conclusions is listed below:

1. In unidirectional specimens, crack tip damage appears in the form of plastic deformation in the longitudinal direction and fiber breakage. Prior to catastrophic fracture, multiple longitudinal plastic zones appear, accompanied by fiber fracture, both of which result in an irregular fracture surface for both unnotched and notched specimens. These plastic zones serve as a crack arrest mechanism. No matrix cracking or interfacial splitting has been observed prior to catastrophic fracture.

2. In $[90]_8$ specimens a self-similar crack extension was observed; the fracture surface is fairly regular and coplanar.

3. In multidirectional laminates crack tip damage is quite localized. In $[0/90]_{2s}$ laminate a self-similar crack extension was observed. In $[\pm 45]_s$, $[0/\pm 45/90]_s$, and $[0/\pm 45/0]_s$ laminates crack extension propagates primarily along the ±45° direction. The fracture surface is quite irregular.

4. The fabrication procedure employed proved to be adequate, providing for strong fiber/matrix interfacial bond and a very good matrix consolidation. However, irregular fiber spacing has been observed.

5. The micro failure examinations revealed:
   a. little fiber pull-out;
   b. practically no fiber splitting in either unidirectional or transverse specimens.
   c. significant fiber splitting in the 90° and 45° layers of all multidirectional laminates.
   d. a significant amount of fiber shattering in the 0° fibers in all laminates.

e. fiber breakage occurring at load levels below 40 percent of ultimate.

f. significant micro-void coalescence in the aluminum matrix.

g. interfacial failure in the 90° and 45° fibers in all multi-directional laminates.

6. No significant effect of elevated temperatures (up to 315°C) on the observed micro-failure has been noticed. However, a lesser degree of fiber shattering has been observed, possibly indicating a weaker fiber/matrix interfacial bond. Also, a high degree of matrix plastic deformation has been observed. The effect of temperature on fiber/matrix bond and interface integrity deserve addditional attention.

7. From the microstructural point of view the fiber strength dominates the composite performance. An assessment of fiber damage as a function of loading would be useful in analyzing the weak link in the structure.

6.5 References

1. E.L. Foster, Jr., "Technology Development of Metal Matrix Composites for DOD Application Requirements," proceedings of First MMC Workshop, Institute of Defense Analysis, Paper P-1144, September 1975.

2. K.M. Prewo, "Exploratory Development of Low-Cost Primary Fabrication Processes for Boron-Aluminum Composites," AFML-TR-74-40 Air Force Materials Laboratory, March 1974.

3. I.J. Toth, "An Exploratory Investigation of the Time Dependent Mechanical Behavior of Composite Materials," AFML-TR-69-9, Air Force Materials Laboratory, April 1969.

4. G.D. Menke, I.J. Toth, "The Time Dependent Mechanical Behavior of Metal Matrix Composites," AFML-TR-71-102, Air Force Materials Laboratory, September 1971.

5. R.C. Jones and J.L. Christian, "Analysis of an Improved Boron/Aluminum Composite," Composite Materials: Testing and Design (Second Conference), ASTM STP 497, American Society for Testing and Materials, 1972, p. 439.

6. R.C. Jones, "Fractography of Aluminum-Boron Composites," Composite Materials: Testing and Design (Second Conference), ASTM STP 497, American Society for Testing and Materials, 1972, pp. 439-468.

7. K.G. Kreider, L. Dardi, and K. Prewo, "Metal Matrix Composite Technology", AFML-TR-71-204, Air Force Materials Laboratory, December, 1971.

8. B.R. Collins, W.D. Brentnall, and I. J. Toth, "Properties and Fracture Modes of Borsic/Titanium", in Failure Modes in Composites, I.J. Toth Ed., The Metallurgical Society of the AIME, Vol. I, New York, New York, 1972, pp. 103-128.

9. M.J. Klein and A.G. Metcalfe, "Effect of Interfaces in Metal Matrix Composites on Mechanical Properties", AFML-TR-71-189, Air Force Materials Laboratory, October 1971.

10. M.J. Klein, A.G. Metcalfe, and M.E. Gulden, "Effect of Interface in Metal Matrix Composites on Mechanical Properties", AFML-TR-72-226, Air Force Materials Laboratory, November 1972.

11. A. Skinner, M.J. Koczak and A. Lawley, "Tensile Properties of SiC/Aluminum Filamentary Composites: Thermal Degradation Effects", Powder Metallurgy International, Vol. 14, 1982, p. 3.

12. A. Skinner, M.J. Koczak and A. Lawley, "Work of Fracture in Aluminum Metal Matrix Composites", Met. Trans. A, Vol. 13A, 1982, p. 289.

13. K. Prewo, "Fabrication and Evaluation of Low Cost Alumina Fiber Reinforced Metal Matrices", AFML Final Report, R79-912245, United Technologies, East Hartford, Conn., 1979.

14. J.R. Hancock, "The Initiation and Growth of Fatigue Cracks in Filament-Reinforced Aluminum Alloys", AFML-TR-71-82, Air Force Materials Laboratory, March 1971.

15. J.A. Steele and H.W. Herring, "Tensile Fracture of Unidirectional B-Al Composite", in Failure Modes in Composites, I.Y. Toth Ed., The Metallurgical Society of the AIME, Vol. I, New York, New York, 1972, pp. 343-356.

16. K.M. Prewo and K.G. Kreider, "Fatigue Failure Mechanism in Boron Aluminum", in Failure Modes in Composites, I.J. Toth Ed., The Metallurgical Society of the AIME, Vol. I, New York, New York, 1972, pp. 395-413.

17. J. Awerbuch and H.T. Hahn, "Crack Tip Damage and Fracture Toughness of Boron/Aluminum Composites," J. Composite Materials, Vol. 13, 1979, pp. 82-107.

18. J. Awerbuch and H.T. Hahn, "Crack Tip Damage and Fracture Toughness of Borsic/Titanium Composites", Experimental Mechanics, October 1980, pp. 334-344.

VII. MONITORING DAMAGE PROGRESSION THROUGH ACOUSTIC EMISSION

7.1 Summary

This study concentrated on monitoring damage initiation and progression through acoustic emission in center-notched boron/aluminum laminates subjected to quasi-static tensile loading. The objective of this study was to investigate the potential of the acoustic emission technique for locating existing damage, detecting and tracking damage initiation and progression, identifying potential fracture sites and distinguishing among the major failure mechanisms of the different laminates. Emphasis was placed on developing the proper test methodology for characterizing a new composite material system through acoustic emission. For base-line data, mechanical properties, fracture behavior, and deformation characteristics were studied and acoustic emission was recorded for the composite constituents (i.e. fiber and matrix) as well. A good degree of reproducibility has been established. Acoustic emission results could be correlated with the deformation characteristics of the subject material, and failure modes and processes for the various laminates could be identified. This Section summarizes results published in [1].

7.2 Introduction

A wide range of non-destructive inspection techniques are used to detect and locate internal damage and damage progression in composites, to identify failure modes, and to evaluate material quality. In resin matrix composites, the delamination and matrix cracking that usually precede fiber fracture are of major concern. The ultrasonic C-scan and X-ray radiography techniques have demonstrated their viability for identifying these types of failure in numerous investigations. In metal-matrix composites, however, delamination and matrix cracking are seldom of

concern. Fiber fracture, the associated matrix plastic deformation, and interfacial failure are the types of failure that must be detected and identified. For these failure mechanisms, the ultrasonic C-scan and X-ray radiography examination techniques are not always satisfactory, primarily when multidirectional laminates are being studied.

The acoustic emission (AE) technique appears to offer a very practical procedure for monitoring failure processes in filamentary metal-matrix composites. Moreover, this technique is more readily used under actual service conditions. This is important because the composite systems are, in many instances, fabricated during the manufacturing of the complete structure. A non-destructive inspection of the complete component is frequently required to locate non-visual damage and indicate its criticality.

An important aspect of the AE technique is that the information is obtained in real-time. Also, once the instrumentation settings have been properly selected for a given problem, the technique is very simple to utilize. On the other hand, acoustic emission by its nature is applicable only during proof-loading. This may limit its usage in certain aeronautical and aerospace applications, although it is already widely applied to assess the integrity of composite structures in the chemical and automotive industries. For small scale laboratory testing on well-defined specimens, however, the AE technique can serve as a supportive test procedure for research into the failure process of new composite systems subjected to external stimulation.

A significant amount of research during the past decade has addressed the viability of acoustic emission as a non-destructive test technique for composite materials. Most of the work has been directed toward resin-matrix systems, primarily glass/epoxy and graphite/epoxy, with some scattered efforts directed toward composite structures. Very few works have been directed toward metal-matrix composites, e.g. [2-6]. They could be considered as preliminary studies, however,

all have demonstrated the viability of the AE technique for metal-matrix systems as well.

In this study, the validity of the AE technique for detecting and locating existing damage, determining damage criticality, and identifying the major failure mechanisms in center-notched boron/aluminum laminates has been investigated. Damage initiation and accumulation have been monitored during quasi-static uniaxial tensile loading. Six different laminates were studied: $[0°]_8$, $[90°]_8$, $[\pm45]_{2s}$, $[0/90]_{2s}$, $[0/\pm45/0]_s$ and $[0/\pm45/90]_s$ 5.6 mil boron aluminum 6061-F having six different notch length-to-width ratios ranging from 0.05 to 0.5. Constituents, i.e. individual fibers and matrix, were tested as well. Results indicated that the failure process in the different laminates can potentially be identified through amplitude analysis of the acoustic emission events. Other issues addressed in this paper include: the effect of crack length and laminate configuration on damage initiation and accumulation; the applicability of acoustic emission for locating damage and determining damage criticality; correlation of AE results with the actual deformation characteristics; the reproducibility of AE results; and a comparison between failure mechanisms identified through acoustic emission and those observed visually and via the scanning electron microscope.

7.3 Results and Discussion

7.3.1 Introduction

The features and characteristics of the acoustic emission events and the interpretation of AE results depend upon the type of composite systems studied, the laminate configuration, quality of fabrication, mechanical properties, fracture behavior, and failure modes. Therefore, it is imperative that such information be available before the AE data can be properly assessed. Accordingly, the discussion on the fracture behavior of center-notched boron/aluminum laminates given in the other sections is briefly summarized here.

a. Boron aluminum laminates demonstrate significant notch sensitivity.

b. The notch sensitivity depends on laminate configuration, fabrication, procedure, constituents, scatter in properties, etc.

c. load-COD curves are highly non-linear; crack tip damage is manifested by jumps in COD and by significant deformation remaining upon unloading.

d. examination of fracture surface morphologies reveal significant shattering of the 0° fibers and splitting of the 90° and ±45° fibers, interfacial failure in the 90° and ±45° plies, significant matrix yielding, micro void coalescence, and plastic shear deformation along the 0° fibers.

All these deformation characteristics and failure mechanisms will affect the acoustic emission results and their interpretation.

7.3.2 Accumulative Counts and Events

The most straightforward AE measurement is count-rate as a function of applied load and its correlation with the far-field load-displacement curves, e.g. Figures 1 and 2. The AE results repeatedly showed that emission initiates at load levels for which the load-displacement curves deviate from linearity, as indicated by the arrows in Figures 1 and 2. Also, increased AE activity is associated with higher non-linearity in load-displacement curves, i.e. increased inelastic deformation with increasing load. In most cases, whenever jumps in displacement occur, a suden surge in AE activity is recorded, Figure 3. Therefore, distinctly different count-rate results were recorded for each of the different laminates as they exhibit different deformation characteristics. It should be noted that the emission initiation load can be as low as 20% of ultimate load. It should be recalled that the IDG results also indicated inelastic deformation at approximately 15-20% of ultimate load. In summary, the AE results can be easily and directly correlated

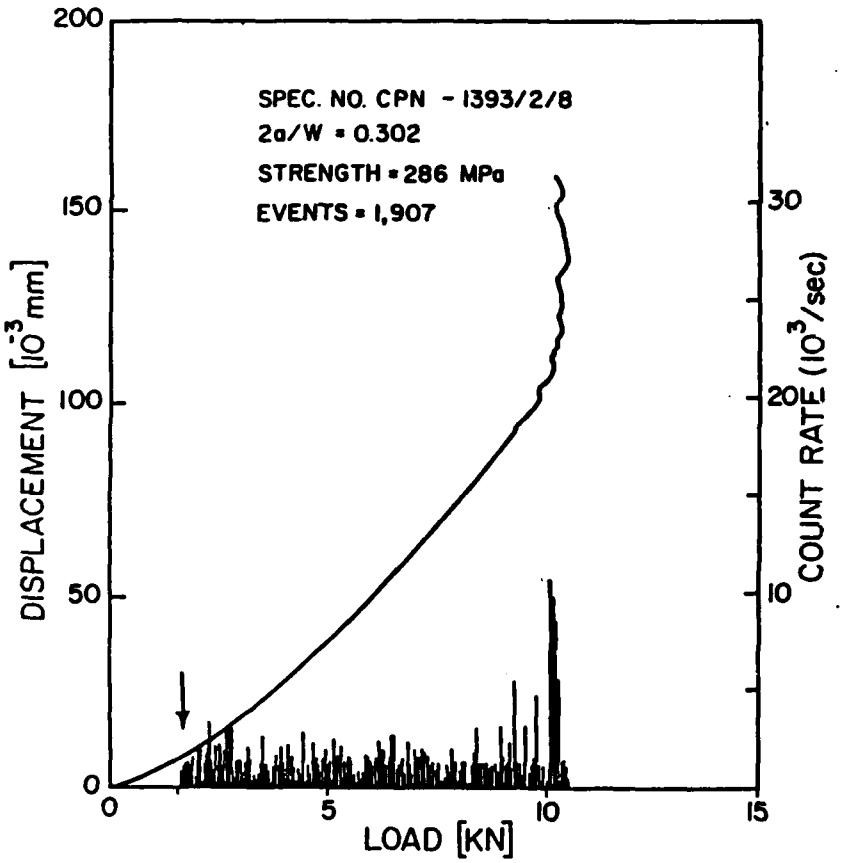

Figure 1. Far-field displacement and AE count rate as a function of load for $[0/90]_{2s}$ laminate.

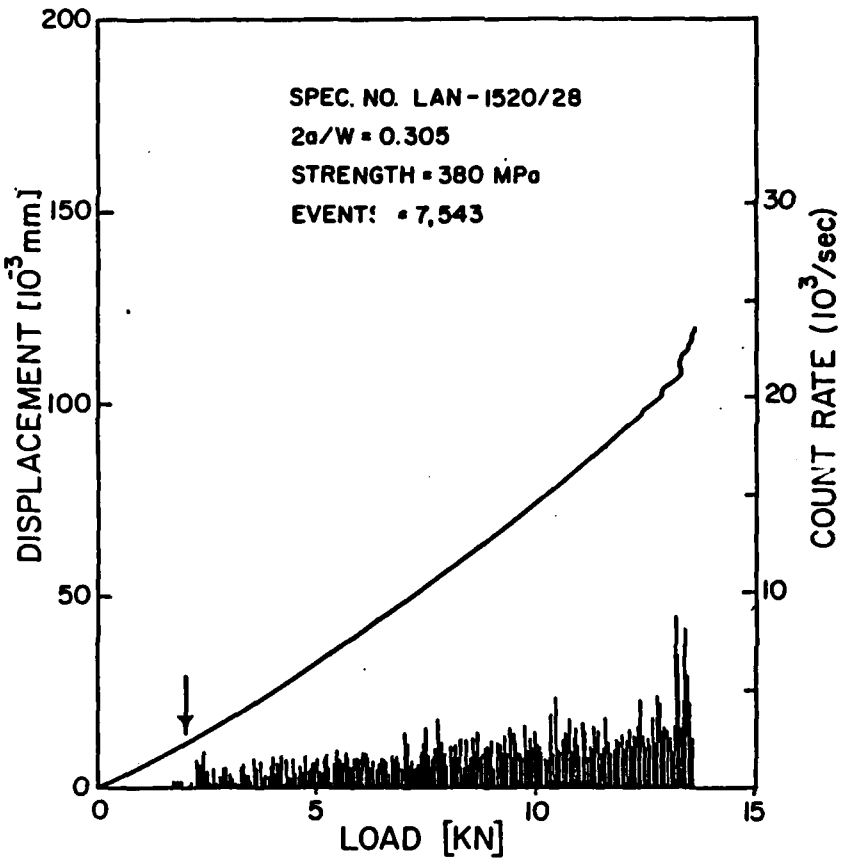

Figure 2. Far-field displacement and AE count-rate as a function of load for $[0/\pm45/0]_s$ laminate.

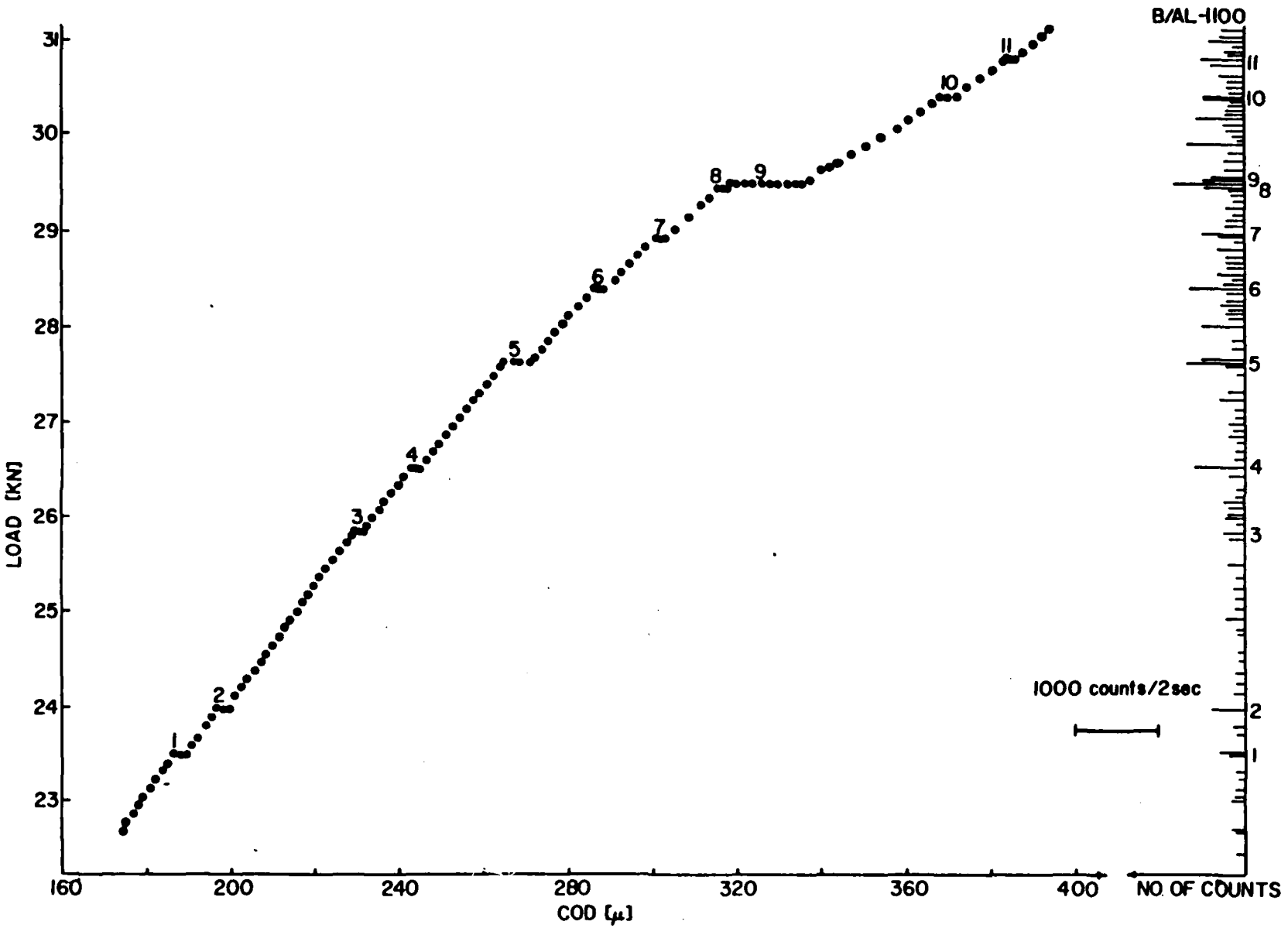

Figure 3. Detail of load-COD curve for unidirectional 8.0 mil B/Al-1100F (crack length = 5.16 mm) showing jumps in COD as load approaches its ultimate level. Results indicate good correlation between COD and acoustic emission counts.

with the deformation characteristics and can furnish information on damage/deformation initiation at a relatively early stage of loading.

The potential of the AE technique for distinguishing among specimens with different notch sizes (or notch length-to-width ratios, 2a/W) has been addressed as well. The results for different 2a/W ratios are shown in Figures 4 and 5 in an events-versus-applied load format. It seems that for all boron/aluminum laminates studied, no distinction could be made among the various notch lengths. In other words, notch length does not affect either the emission initiation load or the rate of increase in emission with increasing load. This lack of sensitivity of AE to notch length is surprising considering the significant notch sensitivity of boron/aluminum laminates, Section X. It seems, however, that the extensive matrix plastic deformation which takes place all along the specimen length (to be discussed later) emit significantly more AE than do the localized regions of the notch tip. The accumulative emission generated from the matrix deformation and probably from the interfacial failure overwhelms the emission associated with the local damage growth at the tip of the artificial notch.

7.3.3 Location Distrubition Histograms of Events

The location at which damage occurs is obtained by placing the two AE transducers a known distance apart. From the time difference between stimulation of each transducer by an AE event (i.e. occurrance of damage) and a priori knowledge of the surface wave speed of the subject material (usually obtained by proper calibration of the AE instrumentation), the location at which the AE event occurs can be determined in real-time. With increasing load, AE events will emanate from throughout the specimen length, yielding location distribution histograms of events at various load levels. It is expected that the AE activity will be more pronounced at the location of stress raisers (e.g. notches, impact damage, etc.) and thus existing damage could be detected and located and its progression could be tracked.

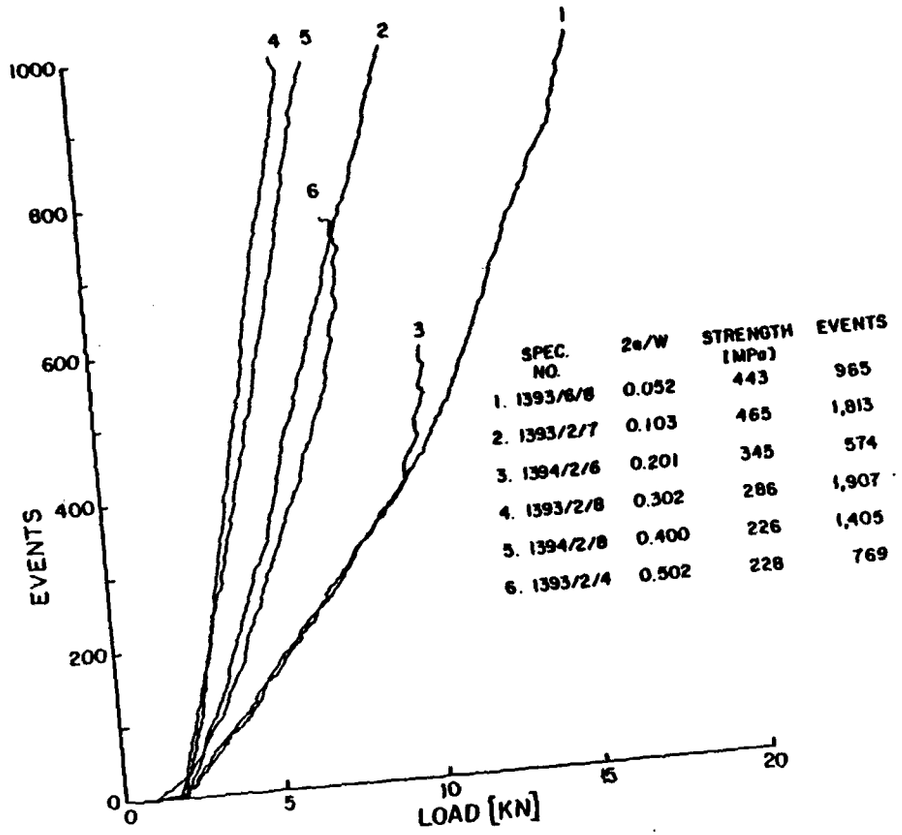

SPEC. NO.	2a/W	STRENGTH (MPa)	EVENTS
1. 1393/6/8	0.052	443	965
2. 1393/2/7	0.103	465	1,813
3. 1394/2/6	0.201	345	574
4. 1393/2/8	0.302	286	1,907
5. 1394/2/8	0.400	226	1,405
6. 1393/2/4	0.502	228	769

Figure 4. Accumulative events as a function of load for various notch lengths for $[0/90]_{2s}$ laminate.

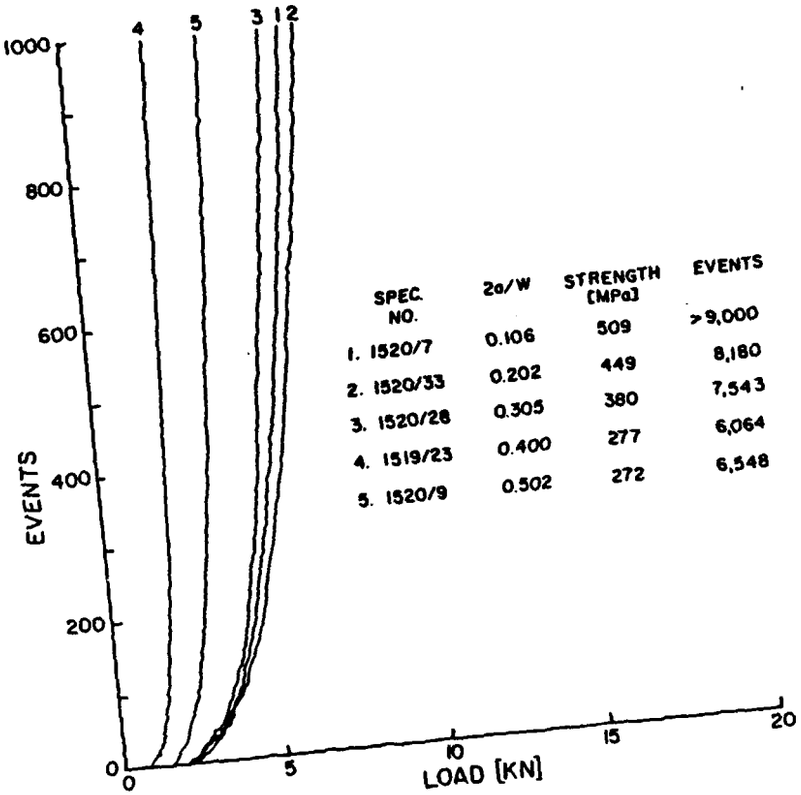

SPEC. NO.	2a/W	STRENGTH (MPa)	EVENTS
1. 1520/7	0.106	509	>9,000
2. 1520/33	0.202	449	8,180
3. 1520/28	0.305	380	7,543
4. 1519/23	0.400	277	6,064
5. 1520/9	0.502	272	6,548

Figure 5. Accumulative events as a function of load for various notch lengths for $[0/\pm45/0]_s$ laminate.

Location distribution histograms of events at various load levels for a notched (2a/W = 0.3) $[0/\pm45/0]_s$ laminate are shown in Figure 6. For the sake of clarity, the distributions recorded at various load levels have been separated in the Figure. The applied stress and associated accumulated number of AE events within the pre-selected "window" of 40-60 are given for each distribution. The results shown in Figure 6 indicate that the artificially induced notch could be easily detected and located (location "50" at the center of the specimen), i.e. increased AE activity has been recorded at that location. Moreover, the existing notch could be located at a relatively low load level, within less than 20% of ultimate load. With increasing load, significant AE activity has been recorded also at location "45", Figure 6. This increased AE activity can be attributed to either damage progression along the 45° direction, as has been repeatedly observed visually through the CCTV, or it may be due to damage progression at the other notch-tip and the failure of the AE instrumentation to accurately distinguish between two sources of emission (both notch tips) generating simultaneously.

The results shown in Figure also indicate that emission occurs practically throughout the specimen length, and increases with increasing load. It seems that this emission is due primarily to the significant matrix plastic deformation and interfacial failure typical to boron/aluminum laminates. In fact, the number of AE events occurring in the notch region (i.e. location "50") amounts to less than 20% of the total number of events occurring throughout loading. Obviously, this ratio will depend on "window" limits, specimen dimensions (being lower for longer specimens), and on laminate configuration, fabrication procedure, material quality, and constituent properties. Because of the relatively large amount of emission generated throughout the specimen length, no clear distinction could be made among various notch lengths in the events-versus-load curves shown in Figures 4 and 5, even though the events recorded are generated within a relatively narrow, pre-selected "window" of 40-60.

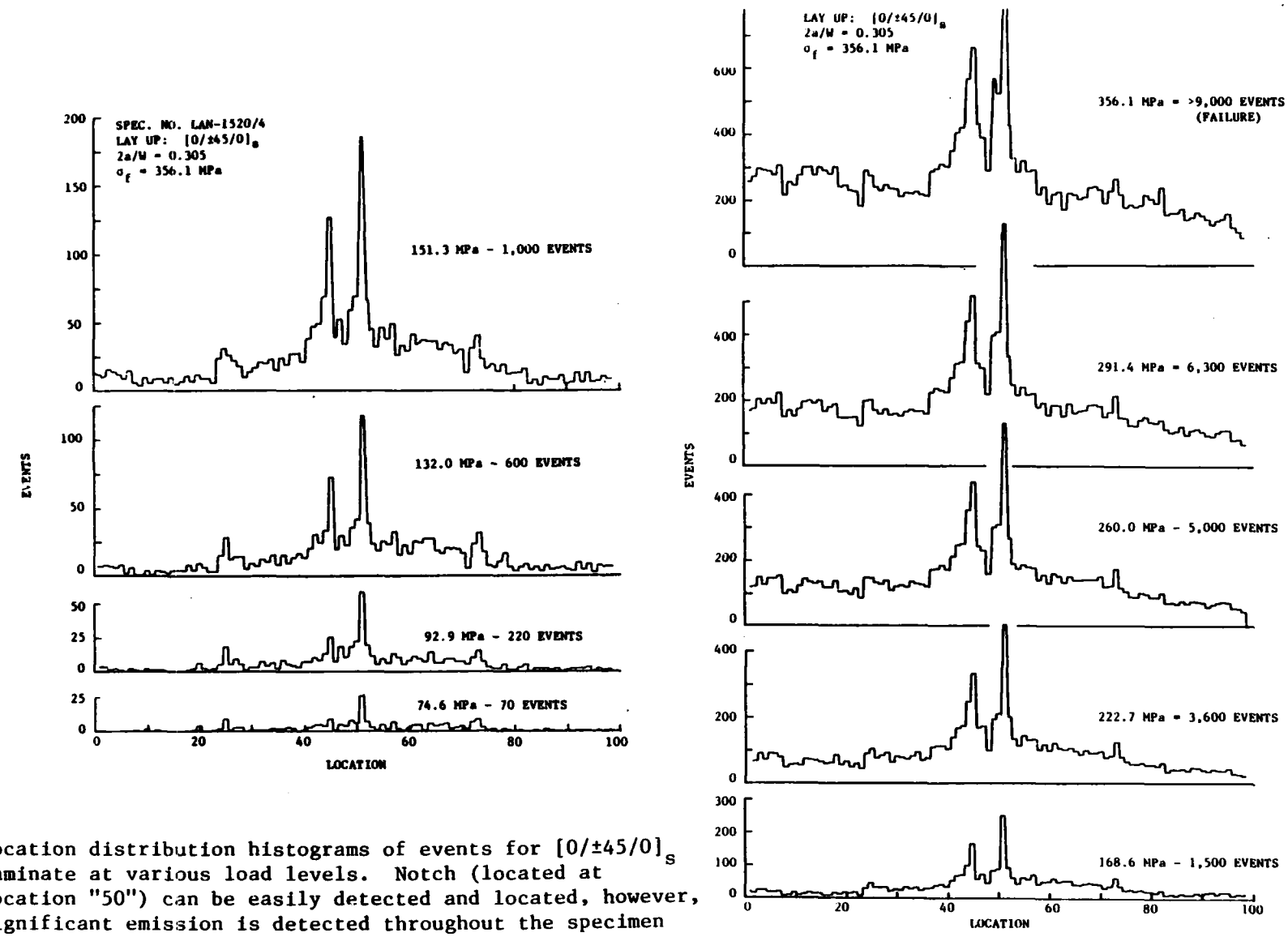

Figure 6. Location distribution histograms of events for $[0/\pm45/0]_S$ laminate at various load levels. Notch (located at location "50") can be easily detected and located, however, significant emission is detected throughout the specimen length and increases with increasing load.

Another important issue is to determine the smallest notch size the AE technique can detect and locate. From results for $[0/\pm45/0]_s$ laminate with various 2a/W values, such as those shown in Figure 6, it has been determined that a damage size of 2a/W = 0.1 could be easily located. For smaller notch sizes, determination of location was more difficult. The reason is that notch tip damage growth for small notch lengths only occurs at relatively high load levels. At these levels, the rate of emission generated from throughout the specimen gage length is too high for the AE instrumentation to record, i.e. the system becomes saturated or "locked-out". Generally, when damage progression occurs at relatively low load levels (for which case the rate of emission is sufficiently slow for accurate data acquisition by the AE instrumentation), detection and location of existing damage was easily and repeatedly obtained. On the other hand, when damage progression emanating from an existing notch occurs at higher load levels, the AE instrumentation fails to detect its location. Consequently, detection and location of the artifiicially induced notches in $[0°]_8$, $[\pm45]_{2s}$, $[0/90]_{2s}$, and $[0/\pm45/90]_s$ laminates could not be made unless $2a/W \gtrsim 0.2$.

7.3.4 Detection of Failure Mechanisms

Determination of the major failure mechanisms using acoustic emission can be based upon a variety of AE source intensity analyses such as events amplitude, duration, energy, counts per event, frequency spectrum, rise-time, etc. In this study, emphasis has been placed on analyzing the amplitude distribution histograms of events to determine the dominant failure mechanisms and processes in the various laminates.

A special concern in boron/aluminum laminates is the detection of fiber breakage and determining the load at which it occurs. For this purpose, as a first stage, individual 5.6 mil and 8.0 mil diameter fibers were loaded to failure. Ultimate strength and event amplitudes were recorded. The results show that practically all

fiber failures generated high amplitude events of 95 dB and 98 dB for the two fiber types, respectively.

As a second stage, in order to identify fiber breakage within the composite, several unidirectional boron/aluminum specimens were loaded to a predetermined load level at which high amplitude events were recorded, the specimens were removed from the testing fixture, the aluminum matrix was dissolved, and the number of broken fibers was recorded. A representative result is shown in Figures 7 and 8, for which a unidirectional specimen with a notch length of $2a/W = 0.30$ has been loaded to approximately 12% of ultimate load. At this load level, the amplitude distribution histogram, Figure 7 (shown for clarity on a logarithmic scale), includes several high amplitude events, indicating the possible occurrance of broken fibers. The scanning electron microscope photographs, Figure 8, obtained after dissolving the outer layer of the aluminum matrix do reveal the existence of broken fibers. In summary, it could be concluded with confidence that the occurrance of high amplitude events is associated with fiber breakage.
events is associated with fiber breakage.

In the third stage, amplitude distribution histograms of events were recorded for all six boron/aluminum laminates with all six notch length-to-width ratios, Figures 9 to 14. These histograms are for all the events accumulated during quasi-static loading to failure that occur within the location window of 40 to 60. It is of interest to note that different amplitude histograms were obtained for the different laminates, while within each given laminate configuration the amplitude histograms were consistent and independent of notch length. In other words, the results were highly reproducible.

It should be noted that the amplitude distribution histograms of events shown in Figures 9 to 14 indicate several event amplitudes below the AE system threshold, i.e. 1 Volt (40 dB). The measured and actual amplitudes agree very well within the approximate range of 45 dB to 90 dB. However, for event amplitudes below 45 dB the

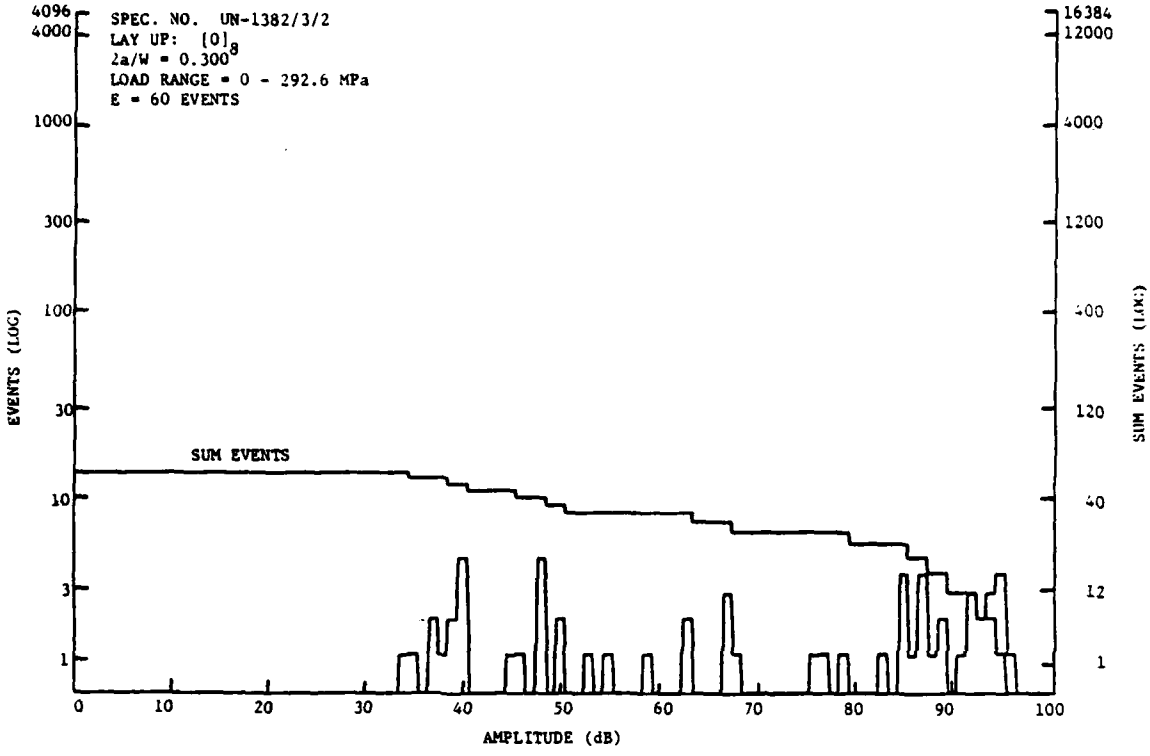

Figure 7. Amplitude distribution histogram and cumulative event amplitude distribution (CEAD) for unidirectional specimen loaded to approximately 12% of expected ultimate load, showing high amplitude events..

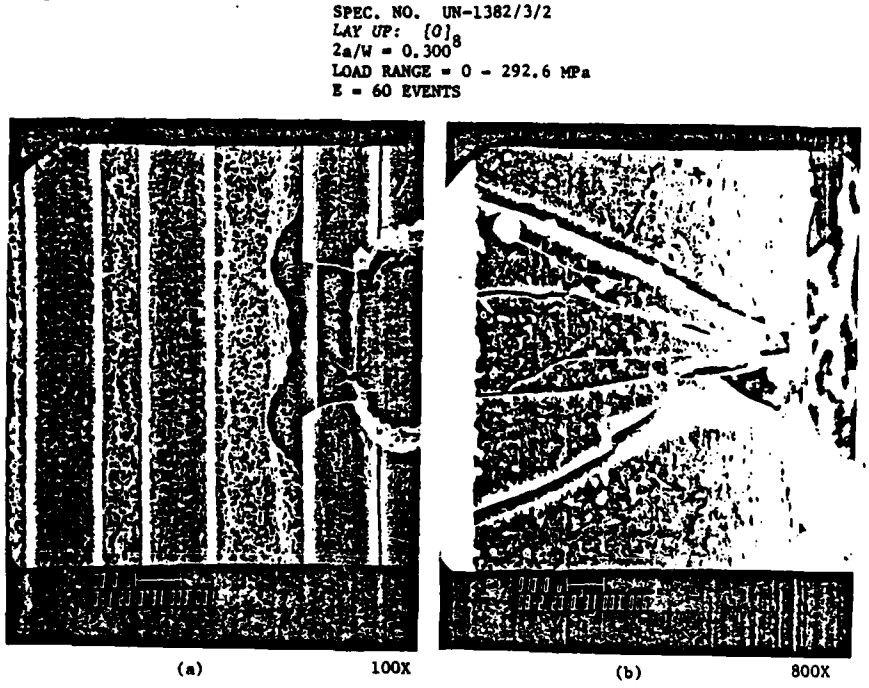

Figure 8. Scanning electron microscope photographs of broken fibers at notch-tip (after dissolving surface layer of aluminum matrix) for a unidirectional specimen loaded to 12% of expected ultimate load (same specimen as shown in Figure 7): a. notch-tip damage, broken fiber seen in third layer; b. detail of broken fiber in third layer.

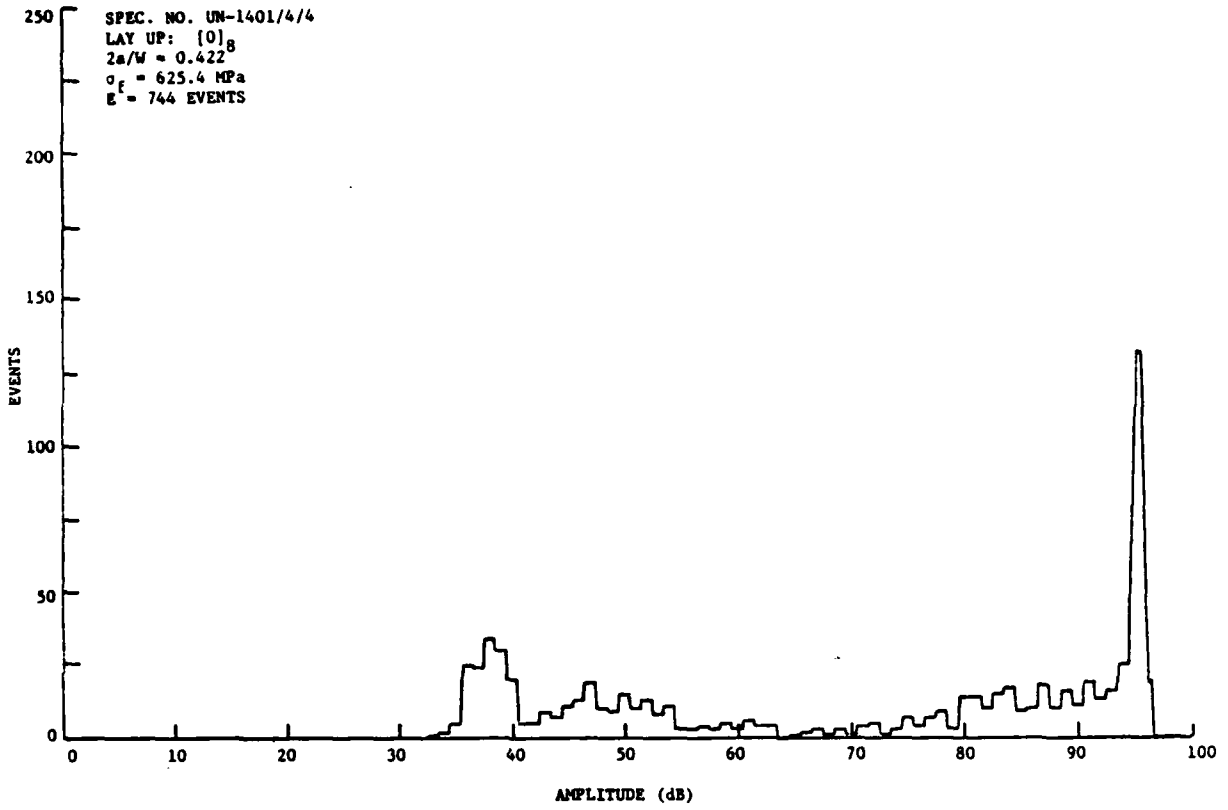

Figure 9. Amplitude distribution histogram of events accumulated throughout loading to failure for $[0]_8$ laminate showing primarily high range amplitude events.

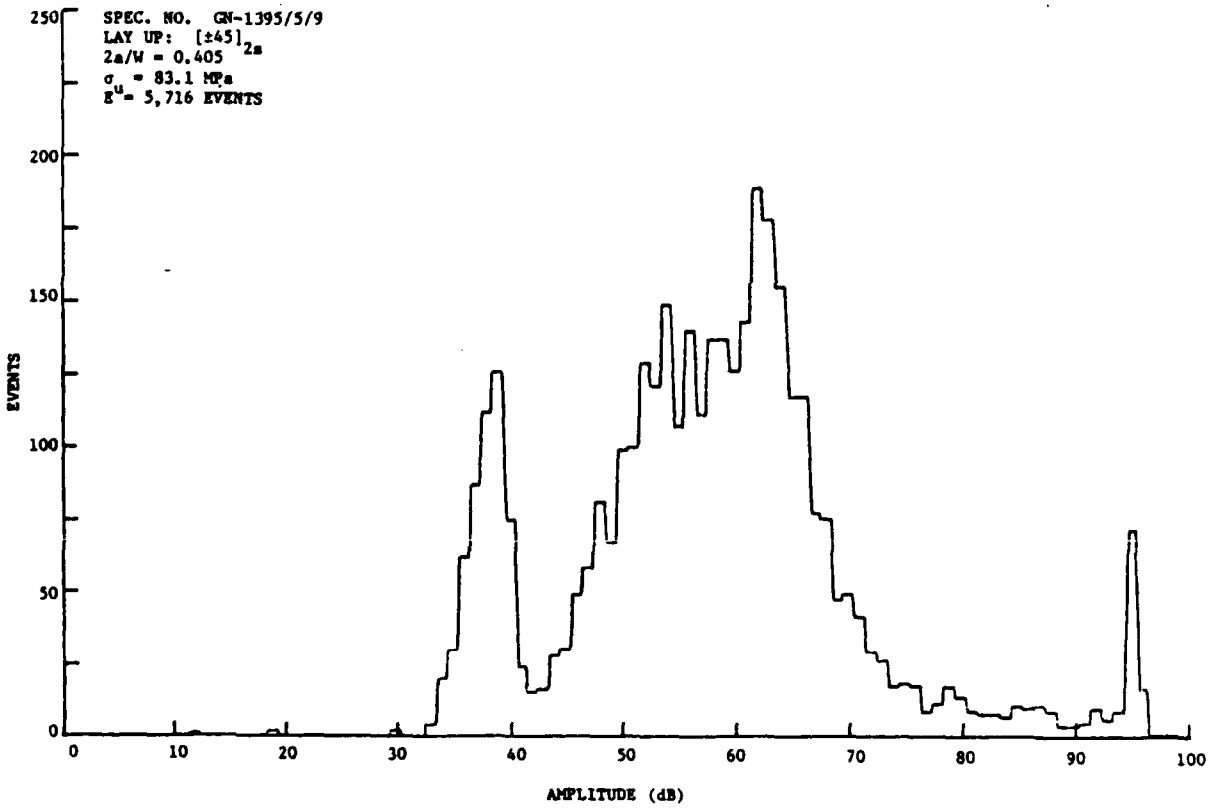

Figure 10. Amplitude distribution histogram of events accumulated throughout loading to failure for $[\pm 45]_{2s}$ laminate, showing primarily low and middle range amplitude events.

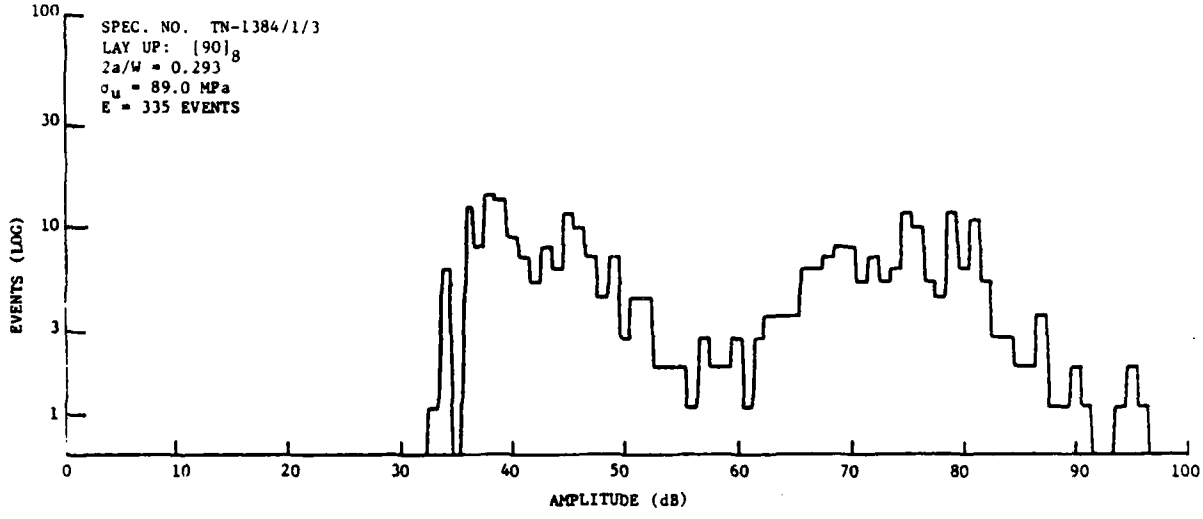

Figure 11. Amplitude distribution histogram of events accumulated throughout loading to failure for $[90]_8$ laminate, showing primarily low and middle range amplitude events.

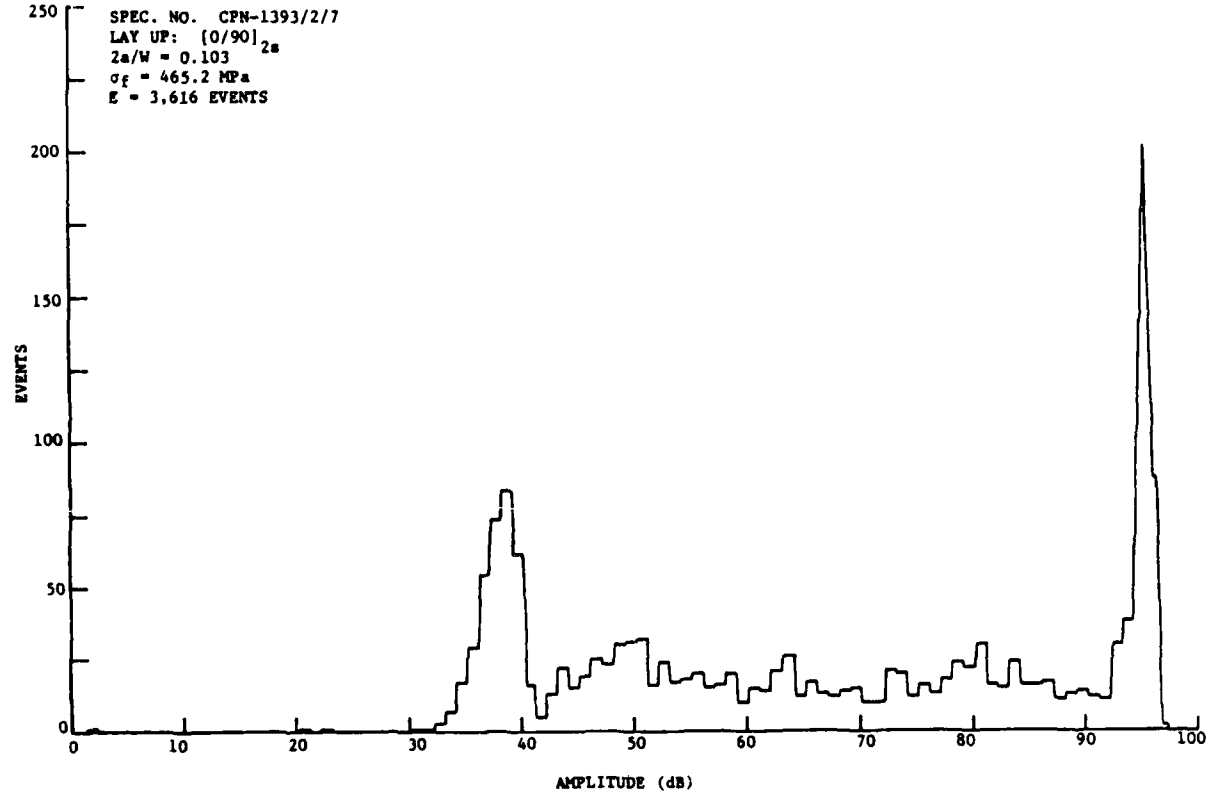

Figure 12. Amplitude distribution histogram of events accumulated throughout loading to failure for $[0/90]_{2s}$ laminate, showing primarily low and high range amplitude events.

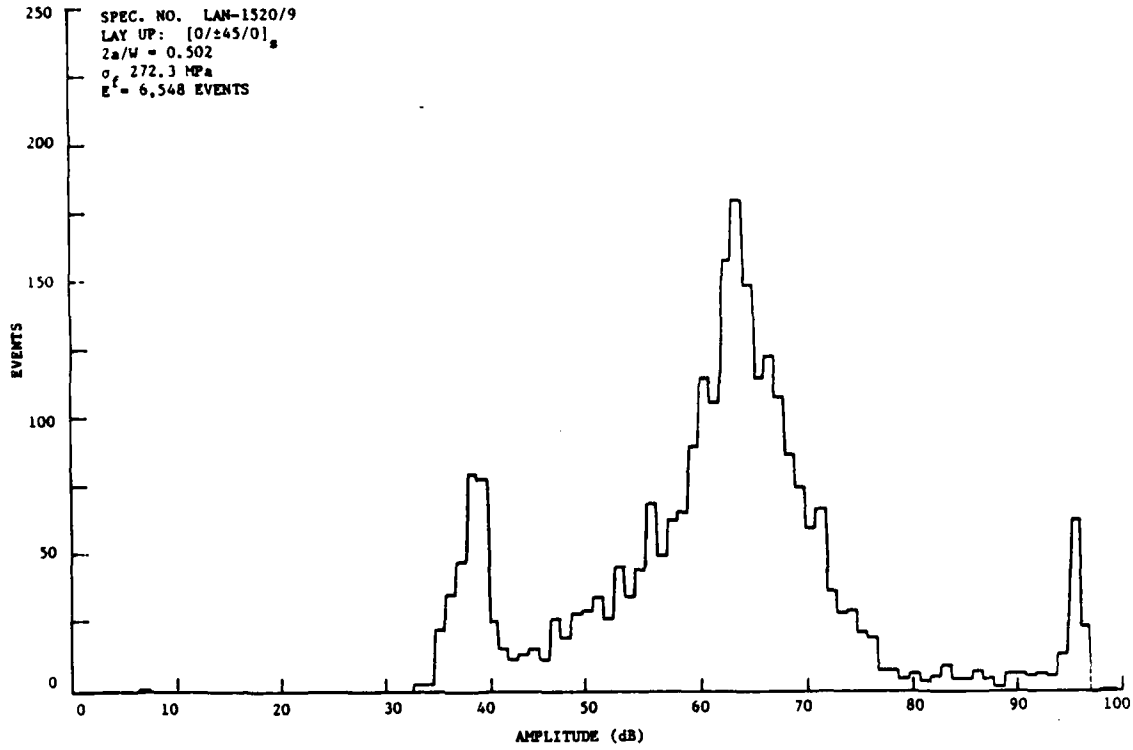

Figure 13. Amplitude distribution histogram of events accumulated throughout loading to failure for $[0/\pm45/0]_s$ laminate showing all three ranges of amplitude events.

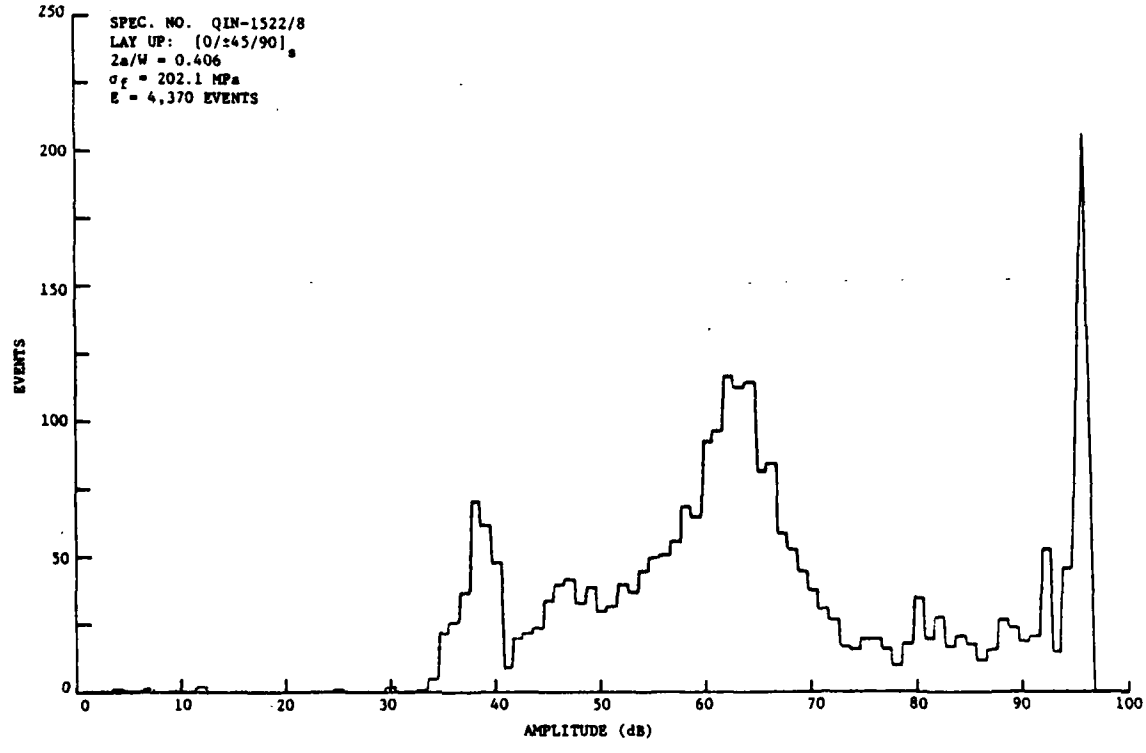

Figure 14. Amplitude distribution histogram of events accumulated throughout loading to failure for $[0/\pm45/90]_s$ laminate showing all three ranges of amplitude events.

margin of error increases dramatically on the low side. Consequently, all the event amplitude below 40 dB shown in the amplitude distribution histograms of events should be considered to be in the 40 dB to 45 dB range. The error between the actual and measured peak amplitude is due to the specific hardware and data processing design of the AE instrumentation, a technical explanation of which is beyond the scope of this report. It should be noted, however, that for the purpose of this discussion the precise dB level of the event amplitudes is not critical. Rather, the purpose is to determine whether the distinct amplitude ranges can be associated with specific failure modes.

The amplitude distribution histogram of events for the $[0]_8$ specimen, Figure 9, includes a large number of events in the 94 dB to 96 dB range which can be attributed to fiber breakage, as previously discussed. Some increased activity in the 40 dB range and a few events in the middle range, 50 dB to 70 dB, were recorded as well. Completely different amplitude distribution histograms were recorded for the $[\pm 45]_{2s}$ laminate, Figure 10, for which a larger number of events were in the lower (40 dB) range and a significant amount of emission occurred in the middle (50 dB to 70 dB) amplitude range. Since significant matrix plastic deformation is expected to occur in the $[\pm 45]_{2s}$ laminate, it could be concluded that the middle range amplitude events are associated with this plastic deformation. This conclusion is also supported by a comparison among the AE results for all the laminates, as discussed below. It seems that the lower amplitude range is associated with either interfacial failure or significant shear deformation of the matrix along the fibers, or a combination thereof, depending upon the laminate configuration. The precise nature is difficult to distinguish due to the complex inter- and intra-ply states of stress.

In the $[90]_8$ specimens, Figure 11 (shown for clarity on a logarithmic scale), a relatively large number of events occur in both the lower and middle amplitude ranges. These two amplitude ranges seem to be associated with interfacial failure and matrix plastic deformation, respectively. These two failure modes are expected

to occur in $[90]_8$ specimens. The high amplitude events (94 dB to 96 dB) shown in Figures 10 and 11 were generated when the specimens approached their ultimate tensile strength (UTS), which will be discussed later.

Based on the amplitude distribution histograms obtained for these laminate "building blocks", it should be expected that the amplitude distribution histograms for multidirectional laminates would include all three amplitude ranges, associated with interfacial failure or matrix shear deformation along the fibers, matrix plastic deformation, and fiber breakage. The results shown in Figures 12 to 14 for $[0/90]_{2s}$, $[0/\pm45/0]_s$, and $[0/\pm45/90]_s$ laminates, respectively, confirm this. For the $[0/90]_{2s}$ laminate, Figure 12, the amplitude distribution histogram is similar to that recorded for the $[0]_8$ specimen, Figure 9, i.e. a large number of high amplitude events with limited activity in the middle amplitude range. However, compared with the $[0]_8$ specimen the amplitude distribution histogram of the $[0/90]_{2s}$ laminate also includes a larger number of low amplitude events which might be contributed by the presence of the 90° plies. The results obtained for the other two multidirectional laminates, Figures 13 and 14, clearly show all three amplitude ranges.

The issue of identifying the precise failure modes associated with the lower (40 dB) and middle (50 dB to 70 dB) event amplitude ranges cannot be resolved conclusively at this stage. Based on a comparison between the amplitude distribution histograms shown in Figures 9 to 12 it is plausible to associate the middle range event amplitudes with matrix plastic deformation. Actually, a variety of mechanisms are associated with the inelastic deformation of the aluminum matrix, e.g. the relative motion between adjacent layers, particulate fracture, microcracking, etc. No attempt was made in this study to distinguish among the various mechanisms, and for the sake of brevity they are generally defined here as plastic deformation. The low amplitude events could also be due to a variety of failure mechanisms, e.g. interfacial failure, extensive shear deformation of the matrix along the 0° and 45° fibers, matrix-matrix bond failure, etc. Based on the examinations

of the fracture surface morphologies of multidirectional laminates, recalling that interfacial failures were noticed in the 90° and 45° plies, it seems that this failure mode dominates the low amplitude events. The amplitude distribution histograms recorded for the $[90]_8$ specimens, Figure 11, do correlate with this assumption. An additional study currently underway on selected unidirectional off-axis boron/aluminum monolayers may resolve this issue.

Virtually no emission has been recorded for the unreinforced aluminum 6061-F matrix. In other words, using the preselected AE instrumentation settings of threshold, gain, etc. as applied in this study, the neat matrix was practically silent. Similar results were also reported elsewhere, e.g. [3]. It seems that the increased local plastic deformation, caused by the presence of the fibers, and the complex state of stress in the composite laminate generate significantly more emission than the unreinforced aluminum. The issue of correlating the number of high amplitude events with the actual number of broken fibers was not addressed in this study. Such attempts were made in [4,6] with partial success and additional study into this issue is warranted.

Finally, an important issue is the applicability of the AE technique to monitor the failure processes discussed above in real-time. For this purpose, amplitude distribution histograms of events were recorded during loading at different load levels. Representative results for all laminates studied are shown in Figures 15 to 20. The amplitude distribution histograms shown for the $[0]_8$ and $[0/90]_{2s}$ laminates, Figures 15 and 16, respectively, indicate that high amplitude events (i.e. fiber breakage) occur at relatively low load levels, at approximately 20% of ultimate load. In most cases, fiber breakage is followed by low amplitude events which seem to be associated with interfacial failure and whose number increases with the number of broken fibers. Similar results were repeatedly obtained for the $[0/\pm45/0]_s$ and $[0/\pm45/90]_s$ laminates, Figures 17 and 18, respectively. High amplitude events were recorded at approximately 20% of ultimate load, followed by

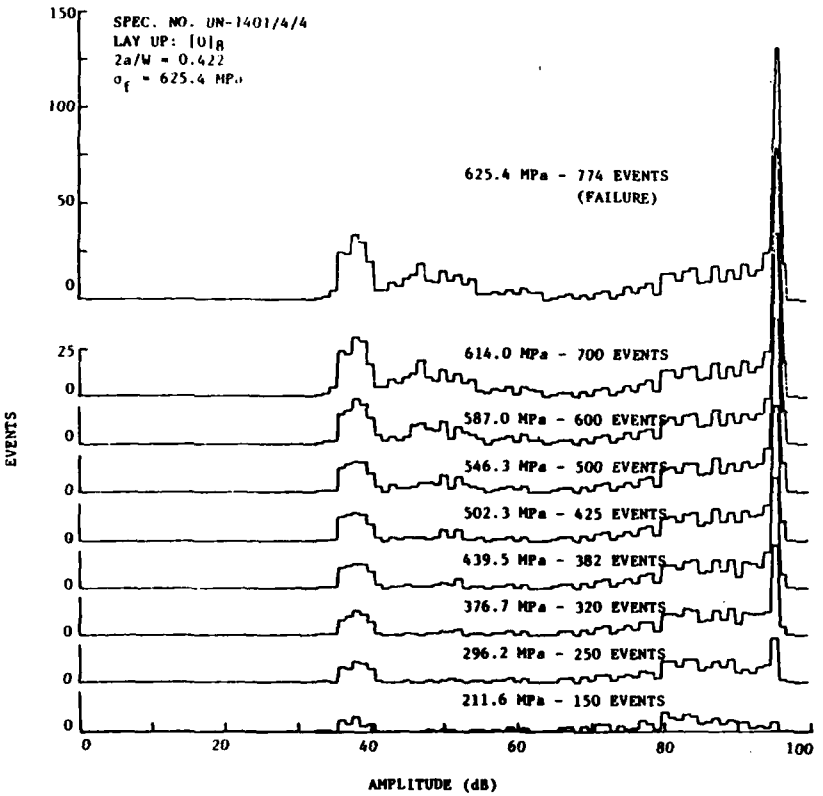

Figure 15. Amplitude distribution histograms of events for $[0]_8$ specimens at different load levels. High amplitude events are detected at relatively low load levels.

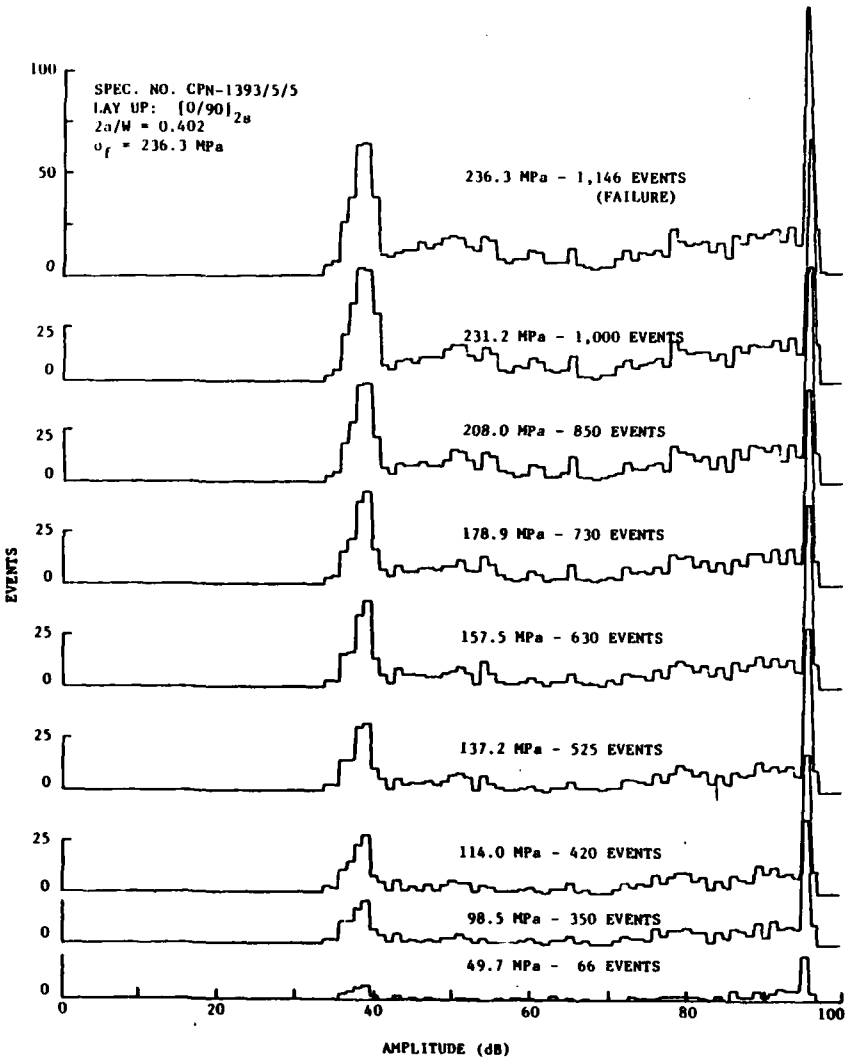

Figure 16. Amplitude distribution histograms of events for $[0/90]_{2s}$ laminate at different load levels. High amplitude events are detected at relatively low load levels.

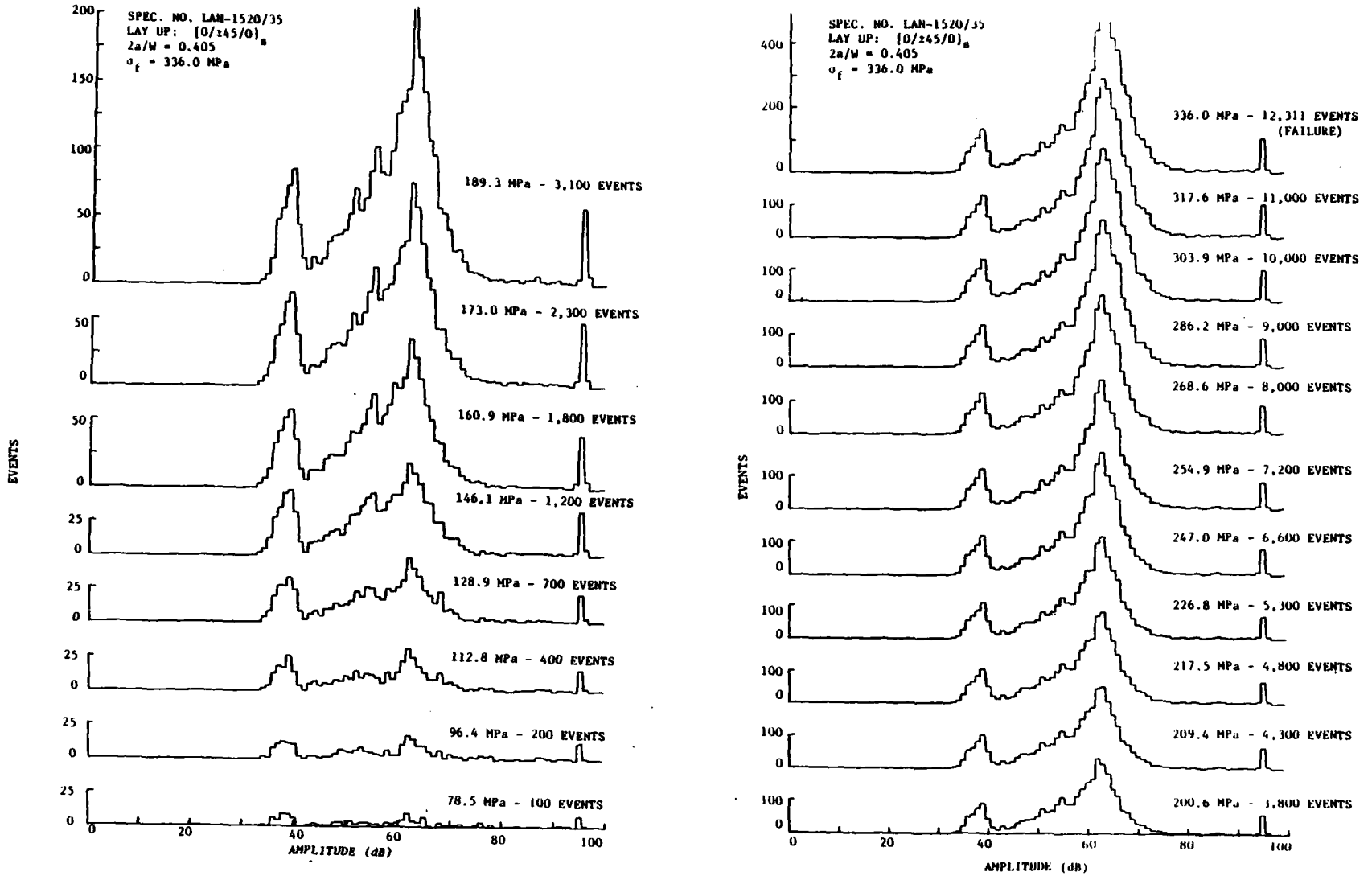

Figure 17. Amplitude distribution histograms of events for $[0/\pm45/0]_s$ laminate at different load levels. The low, middle and high range amplitude events seem to indicate interfacial failure, matrix deformation and fiber breakage, respectively. Note that fiber breakage is detected at less than 20% of ultimate load.

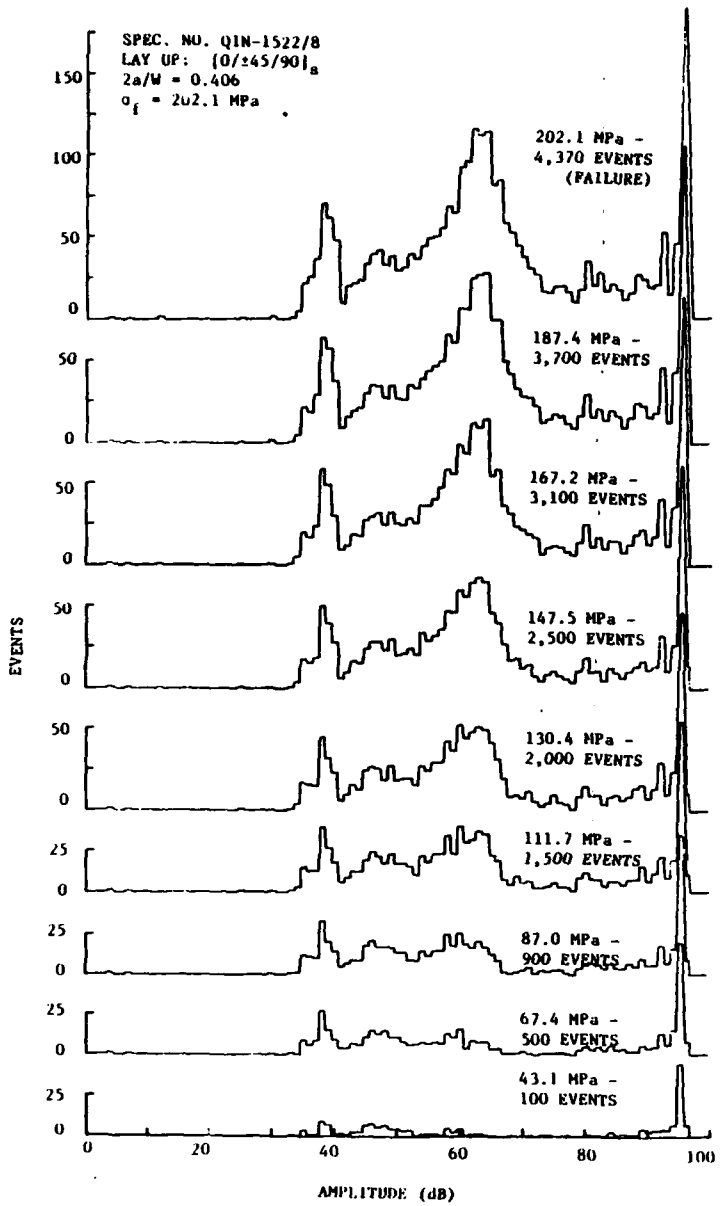

Figure 18. Amplitude distribtuion histograms of events for $[0/\pm45/90]_s$ laminate at different load levels. High amplitude events are detected at relatively low load levels.

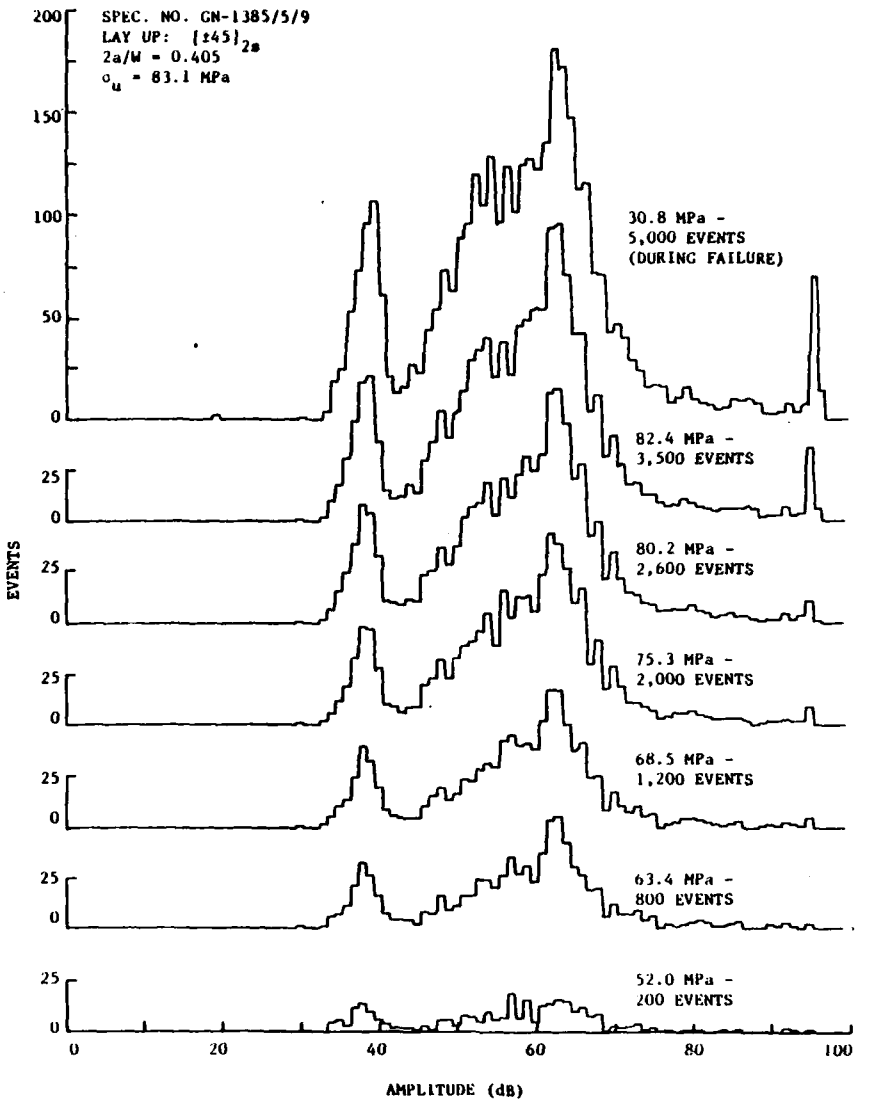

Figure 19. Amplitude distribution histograms of events for $[\pm45]_{2s}$ laminate at different load levels. High amplitude events are detected at load levels approaching ultimate, preceded by low and middle range amplitude events.

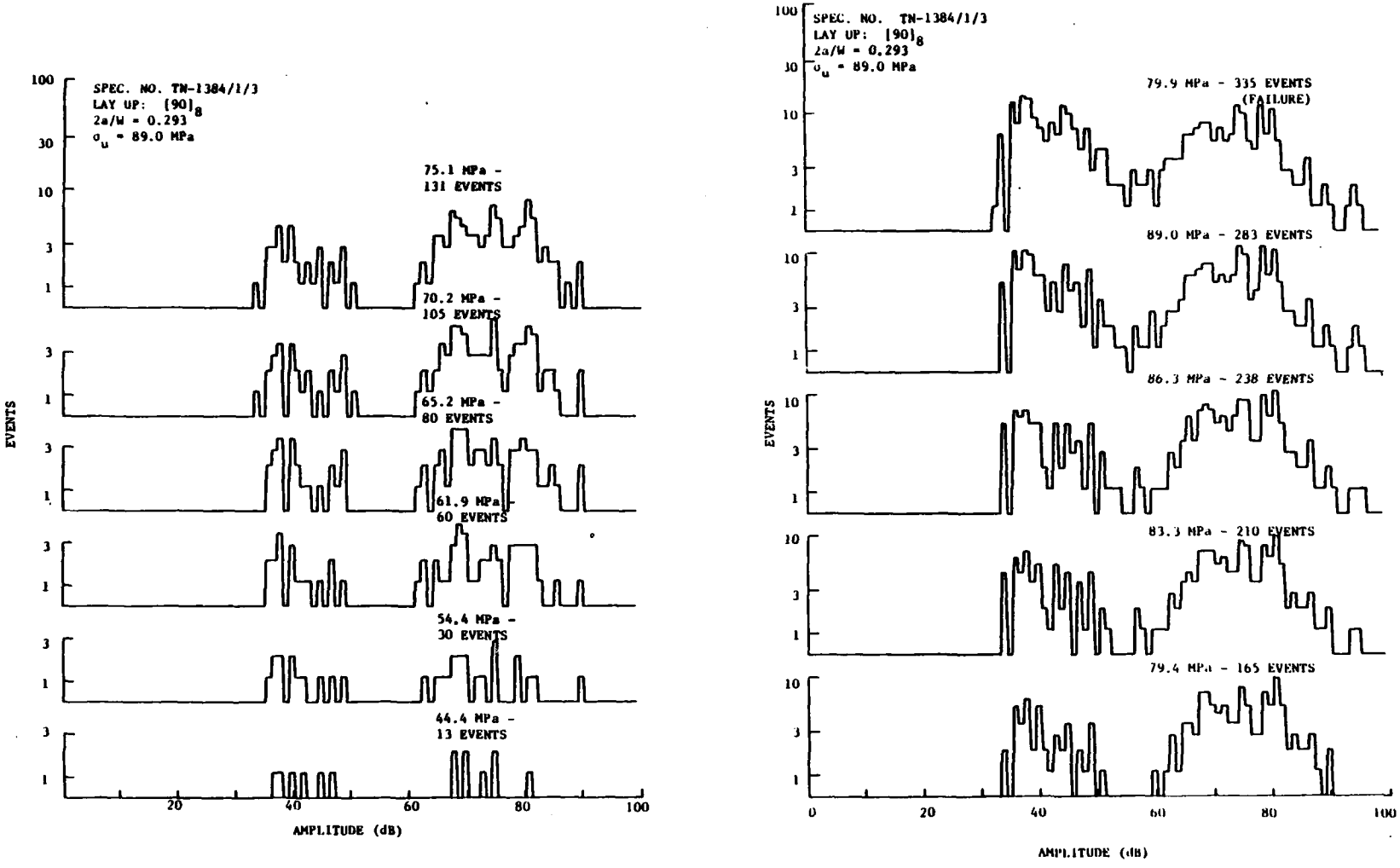

Figure 20. Amplitude distribution histograms of events for $[90]_8$ specimen at different load levels. Low and middle range amplitude events seem to be indicative of interfacial failure and matrix deformation, respectively. High amplitude events (i.e. fiber breakage/splitting) occur at relatively high load levels.

an increased number of low (40 dB) and middle (50 dB to 70 dB) range amplitude events. For the $[\pm 45]_{2s}$ and $[90]_8$ laminates, Figures 19 and 20, respectively, events in the low and middle amplitude ranges initiated first, while the high amplitude events were detected at very high load levels, primarily when the load approached UTS. For the $[\pm 45]_{2s}$ laminate, the number of high amplitude events increased beyond the UTS when significant necking of the specimen occurs, resulting ultimately in the specimen fracture, at which stage fiber breakage occurs. For the $[90]_8$ laminate only a few number of high amplitude events were detected which occur at relatively high load levels and which are most probably associated with fiber splitting. Such fiber splitting has been observed through the SEM, as discussed in Section VI.

In summary, the representative results shown in Figures 15 to 20 indicated that for boron/aluminum laminates containing 0° plies, fiber breakage may occur at relatively low load levels, followed by significant matrix plastic deformation. Both of these failure modes can be easily detected in real-time through acoustic emission.

It should be emphasized that the acoustic emission results strongly depend on extrinsic (loading rate, gripping procedure, etc.) and intrinsic (laminate configuration, material system, etc.) parameters and on the AE instrumentation, e.g. transducers, filters, data acquisition rate, etc. For example, using different types of fibers, or different aluminum alloys as matrix material may result in different AE characteristics, e.g. [3]. Also, the use of different AE instrumentation settings, transducers, etc. [5] will also yield different results.

7.4 Conclusions

This study addressed several issues regarding the viability of the acoustic emission technique as a non-destructive test method for detecting and locating existing notches, tracking damage progression, indicating damage criticality and identifying the major failure mechanisms in center-notched boron/aluminum laminates.

The significant notch sensitivity of the subject material and its specific deformation characteristics and failure mechanisms suggest the need for an NDT tool that can identify failure processes in real-time. The extensive experimental results obtained indicate that the AE technique does have the potential as a supporting tool in laboratory studies to characterize the failure processes in a new composite system. The major conclusions of this study are summarized below.

1. Emission initiation load was found to be relatively low, approximately 20% of ultimate strength, primarily due to matrix plastic deformation.

2. A qualitative correlation could be established between AE activity and deformation characteristics, e.g. count-rate and COD.

3. Location distribution histograms of events revealed that emission occurs throughout the specimen length, resulting from extensive matrix and interface deformation in all laminates studied.

4. Location distribution histograms of events could detect and locate existing notches provided that they exceeded a minimum length.

5. The fracture of individual fibers resulted in high amplitude events. These results are reproducible and distinctly higher than event amplitudes generated by matrix dominated failures.

6. Amplitude distribution histograms of events were distinctly different for the various laminates studied. The results indicate that they are associated with three failure modes: $[0]_8$ and $[0/90]_{2s}$ laminates demonstrate primarily fiber fracture; $[90]_8$ and $[\pm 45]_{2s}$ laminates demonstrate primarily matrix deformation and interfacial failure; $[0/\pm 45/0]_s$ and $[0/\pm 45/90]_s$ laminates demonstrate all three modes of failure. However, additional investigation is warranted for a more accurate and definitive distinction between matrix plastic deformation and interfacial failure.

7. AE results indicated fiber fracture at approximately 20% of ultimate load.

8. Amplitude distribution histograms of events indicated that for multidirectional laminates containing 0° plies, fiber fracture precedes the significant accumulation of matrix dominated failure, as expected.

9. It is imperative that a prior understanding of the fracture behavior and deformation characteristics of the subject material be available for a proper interpretation of AE results.

10. Certain issues regarding the selection of AE instrumentation settings, analyses of other AE parameters such as event energy, duration, etc., and primarily a clearer identification of the matrix dominated failure mechanism in boron/aluminum laminates deserve additional investigation.

7.5 References

1. M. Madhukar and J. Awerbuch, "Monitoring Damage Progression in Center Notched Boron Aluminum Laminates Through Acoustic Emission", Composite Materials; Testing and Design (Seventh Conference), American Society of Testing and Materials, STP , 1985, to be published.

2. E.G. Henneke, II and H.W. Herring, "Spectrum Analysis of Acoustic Emissions from Boron Aluminum Composites", Composite Reliability, ASTM STP 580, American Society for Testing and Materials, 1975, pp. 202-214.

3. A.F. Grenis and A.P. Levitt, "Fracture Characteristics of Different Fibers in Fiber Reinforced Aluminum as Detected by Acoustic Emission", Proceedings of the 1975 International Conference on Composite Materials (ICCM), Vol. 2, 1975, pp. 1019-1050.

4. J.M. Grandemange and K.N. Street, "The Effect of Notch Root Radius and Thickness on the Static Fracture Toughness of B-Al Composites", Proceedings of the 1975 International Conference on Composite Materials (ICCM), Vol. 2, 1975, pp. 1019-1050.

5. R.B. Pipes, N.J. Ballintyn, W.R. Scott and J.M. Carlyle, "Acoustic Emission Response Characteristics of Metal Matrix Composites", Composite Materials: Testing and Design (Fourth Conference) ASTM STP 617, American Society for Testing and Materials, 1977, pp. 153-169.

6. W.S. Johnson, C.A. Bigelow and Y.A. Bahei-El-Din, "Experimental and Analytical Investigation of the Fracture Process of Boron/Aluminum Laminates Containing Notches", NASA Technical Paper 2187, September 1983.

VIII. MONITORING ACOUSTIC EMISSION DURING LOW CYCLE FATIGUE LOADING

8.1 Summary

The objective of this study was to determine the potential of the acoustic emission (AE) technique for monitoring damage initiation and progression in boron/aluminum laminates during low cycle fatigue loading. In particular, the acoustic emission technique has been applied to determine the effect of fatigue loading on crack tip damage growth, to locate fatigue damage initiation and progression, and to identify the major failure mechanisms, specifically the occurrence of fiber breakage during fatigue loading. Special attention has been placed on distinguishing between friction generated emission (from newly created fracture surfaces) and emission generated from actual damage initiation and progression. Other issues addressed in this study include: effect(s) of fatigue loading, fatigue load level and loading frequency on AE results, e.g. post fatigue emission initiation load; correlating between fatigue damage progression and mechanical properties such as post-fatigue global compliance and strength; and correlating between AE results and actual damage progression observed visually.

8.2 Introduction

Significant efforts have been devoted in recent years to studying damage initiation and accumulation in composite laminates during fatigue loading. Most studies, experimental and analytical, have been directed toward resin-matrix composites, and the graphite/epoxy system has received most of the attention. Various non-destructive examination (NDE) techniques have been employed for this purpose, the most common being the ultrasonic C-scan and X-ray radiography. The primary interest in these studies was the determination of initiation, progression, and accumulation of matrix cracking and delamination. Fiber fracture during fatigue loading of graphite/epoxy laminates has received less attention for three main reasons: 1) the complex analytical methodology required in predicting fiber breakage;

2) the difficulties in non-destructively detecting broken fibers; and 3) the current design criteria of composite structures, e.g. design limits are set in many instances for less than 4,000 micro-strain, with little if any concern for fiber fracture. Those studies which have addressed the issue of fiber fracture in graphite/epoxy laminates have used destructive detection techniques, e.g. the deplying technique.

In filamentary metal-matrix composites (e.g. boron/aluminum), however, fiber-matrix interfacial failure, matrix plastic deformation and fiber breakages are the types of failure dominating the fatigue behavior, and the initiation of matrix cracking and delamination during fatigue loading is seldom of concern. The issue of detecting fiber breakage in metal-matrix composites is especially important since these material systems are considered for primary structural applications. While the interfacial failure mode, i.e. splitting, can be easily detected (visually, in many cases) the detection and identification of the other two failure modes in multi-directional metal-matrix laminates through ultrasonic C-scan and/or X-ray radiography involve many difficulties. Also, these NDT techniques are usually not appropriate for real-time applications.

It could be concluded therefore that an NDT technique which enables the monitoring of the failure process in filamentary metal-matrix composites in real-time is needed. Based on earlier investigations, it seems that the acoustic emission (AE) technique can offer a very practical examination procedure for monitoring damage in composites. The potential for using the acoustic emission technique to monitor damage progression in composite laminates during fatigue loading has been studied extensively by the Principal Investigator for different resin-matrix composite systems. It has been determined that the AE technique can serve both as an early warning device and as a supportive tool in the laboratory for characterizing the failure processes in new composite systems.

This study concentrates on the applicability of the AE technique for monitoring damage in center-notched boron/aluminum laminates during fatigue loading. Emphasis is placed on distinguishing between friction generated emission and emission generated from actual damage initiation and progression. Other issues addressed in this study include: identifying the typical failure modes (occurring during fatigue loading); effect(s) of fatigue loading, fatigue load level and loading frequency on AE results, e.g. post-fatigue emission initiation load; locating fatigue damage initiation and progression; correlating between fatigue damage progression and mechanical properties such as post-fatigue compliance and strength, and correlating between AE results and actual damage progression observed visually.

8.3 Experimental Procedure

The problem of eliminating unwanted information when monitoring acoustic emission during fatigue loading has been recognized for a long time. It is known that emission is generated by friction in metals during crack closure under fatigue loading. In composites the problem is much more complex. There is the multiplicity of types of damage (e.g. cracking, delamination, interfacial failure, crack directionality, etc.) to contend with and also the large amount of non-critical damage and/or micro-failure which nevertheless generates emission when fracture surfaces are continuously grated together by the cyclic loading.

Several methods have been developed to screen this "unwanted" emission. The most common is the use of Voltage Controlled Gating (VCG). Acoustic Emission data recording is controlled by an external signal such as the output of a load-cell, strain gage, etc. The VCG allows the system to operate only during a pre-selected portion of the load cycle, determined by high and/or low pre-set limits of the VCG which deactivate the data procurement system, thus eliminating the recording of unwanted information. In composites, however, it may be more useful to distinguish this friction emission from emission generated by actual damage progression.

AD-A162 352 FRACTURE BEHAVIOR OF BORON ALUMINUM COMPOSITES AT ROOM AND ELEVATED TEMPE (U) DREXEL UNIV PHILADELPHIA PA DEPT OF MECHANICAL ENGINEERING AN J AWERBUCH APR 85

3/3

UNCLASSIFIED AFOSR-TR-85-1099 AFOSR-79-0079 F/G 11/4 NL

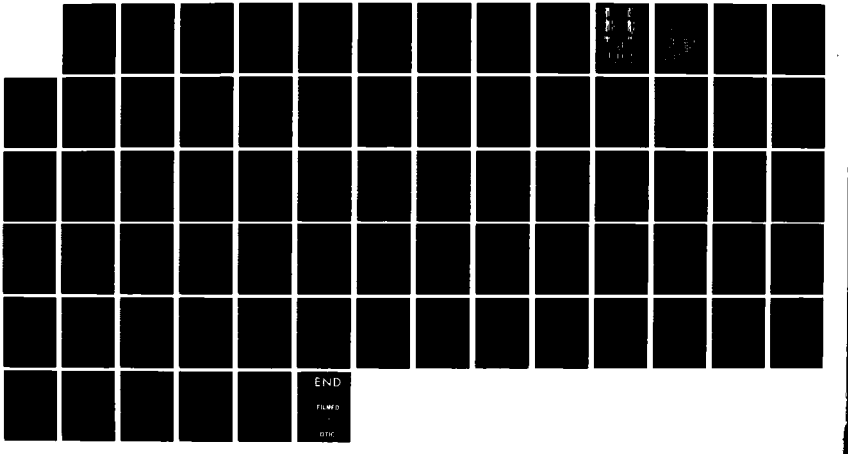

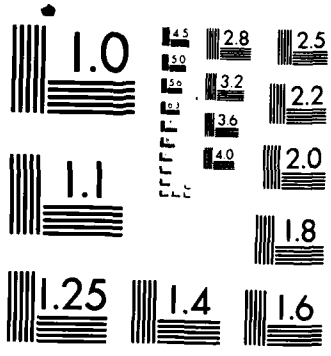

than eliminating it altogether. It is also useful to allow monitoring of emission throughout the load cycle, since the load level at which "unwanted" emission may be generated is not established.

The simplest way of satisfying these constraints is to use a data acquisition system which is interfaced with the AE instrumentation and through which the AE parameters (e.g. events) are recorded throughout each load cycle of the fatigue loading. In post-test analyses, the amount of emission generated within several pre-determined load ranges of each load cycle can be extracted and a more complete picture can be obtained as to the distribution between significant and insignificant AE information.

For this purpose, a special computer program has been developed during the course of various research programs in which the data acquisition system (DEC-MINC 11) recorded events occurring within pre-selected load ranges. The pre-determined levels were set arbitrarily at 60%, 80% and 95% of the maximum fatigue load, P_d, (see Figure 1) to allow the recording of events falling within the following load ranges: 10-100%, 60-100%, 80-100% and 95-100% of P_d. To emphasize the amount of emission occurring at the low load ranges (and attributed to friction), the events accumulated within 10-60%, 10-80% and 10-95% of P_d were recorded as well. The data recorded were then plotted in two formats: Events as a function of number of cycles, called E.-N. curves; and Events per cycle, or "event-rate", as a function of the number of cycles, called E.R.-N. curves. These plots were prepared for all seven load ranges: those accumulated during the entire load cycle (10-100% of P_d), those accumulated in the low load ranges (10-60%, 10-80% and 10-95% of P_d) attributed to friction and called here the "friction side" of the load cycle, and those accumulated in the upper part of the load cycle (60-100%, 80-100% and 95-100% of P_d). Again, these three load levels were pre-determined arbitrarily. Whether all the emission generated within the 95-100% P_d load range is due to actual damage progression is questionable, and most probably the recorded events are partially generated by friction. However, the random nature of the events accumulated in this load range during each load cycle do indicate that this emission can be attributed primarily to new damage progression.

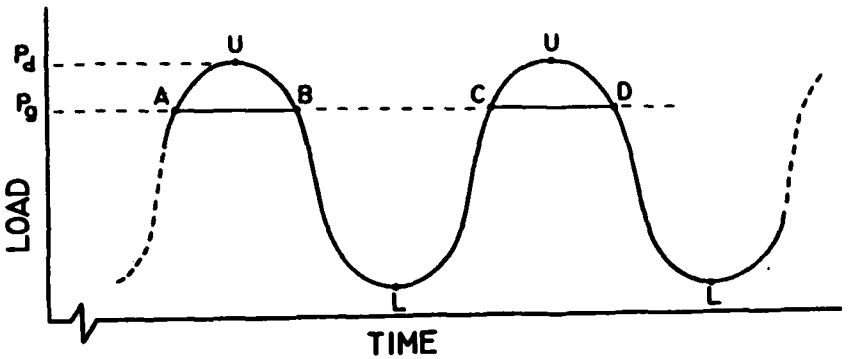

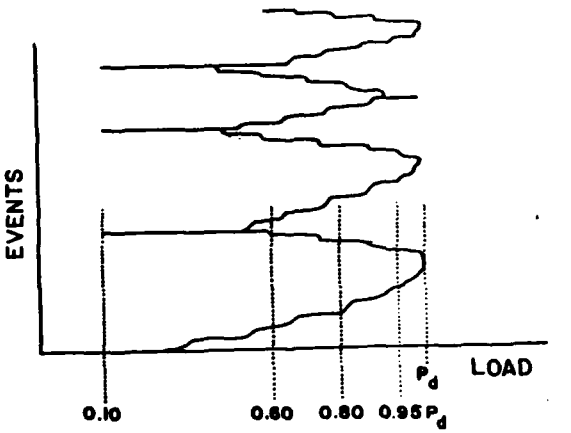

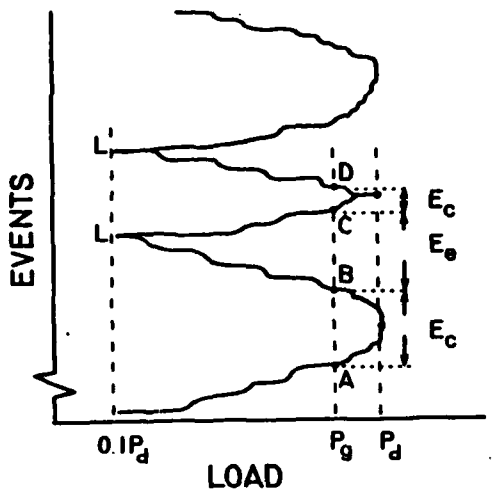

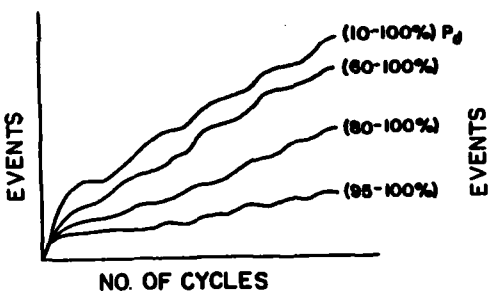

"DAMAGE SIDE"

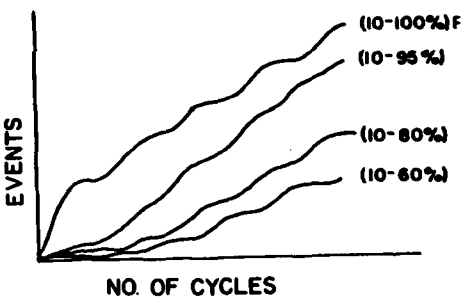

"FRICTION SIDE"

E_c----COUNTED EVENTS DURING THE PRE-SELECTED PORTION OF THE LOAD CYCLE

E_e----EVENTS ELIMINATED DURING A PRE-SELECTED PORTION OF THE LOAD CYCLE

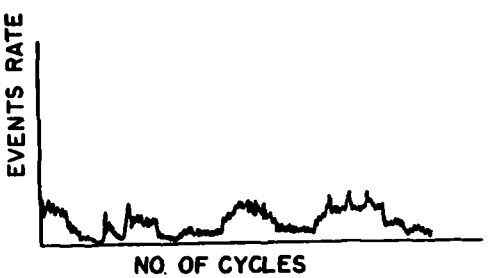

Figure 1. Schematic of acoustic emission data reduction during fatigue loading.

The identification of the actual type of damage can be achieved through a detailed analysis of the acoustic emission event. A variety of source intensity signatures could be analyzed such as events amplitude, duration, energy, count per event, frequency spectrum, etc. In this study, emphasis has been placed on analyzing amplitude distribution histograms of events to determine the dominant failure mechanisms. In metal-matrix composites the primary modes of failures are fiber breakage, matrix inelastic deformation and interfacial failure. These three different failure modes generate emission of different event characteristics, and their detection and identification is usually determined through histograms of the event intensity, e.g. amplitude,energy, duration, rise time, etc. The increased activity in the low, middle and upper events amplitude ranges indicates three different failure modes. It has been shown in Section VII that these three amplitude ranges are correlated with the three different types of failures occurring in boron/aluminum laminates.

Similar data analysis could be done for all other AE events characteristics, both during quasi-static and fatigue loading. Preliminary results have shown that such analysis can also more accurately identify the friction generated emission. These results are discussed below.

8.4 Results and Discussion

8.4.1 Event Accumulation During Fatigue Loading

The number of events emitted at each load cycle is completely random and may vary from load cycle to load cycle. In other words, specimens may be fatigued for several load cycles without any events being generated, followed by load cycles in which the number of events emitted per cycle can be as high as several hundred (depending on fatigue stress level, material, specimen geometry, etc.) seemingly without warning or consistency. The random nature of the number of events emitted can be clearly seen in the plot shown in Figure 2a obtained on an X-Y recorder during the fatigue test. Furthermore, most of the events shown in this Figure occur at the higher dynamic load levels, i.e. between approximately 22.0 KN and 23.0 KN, or

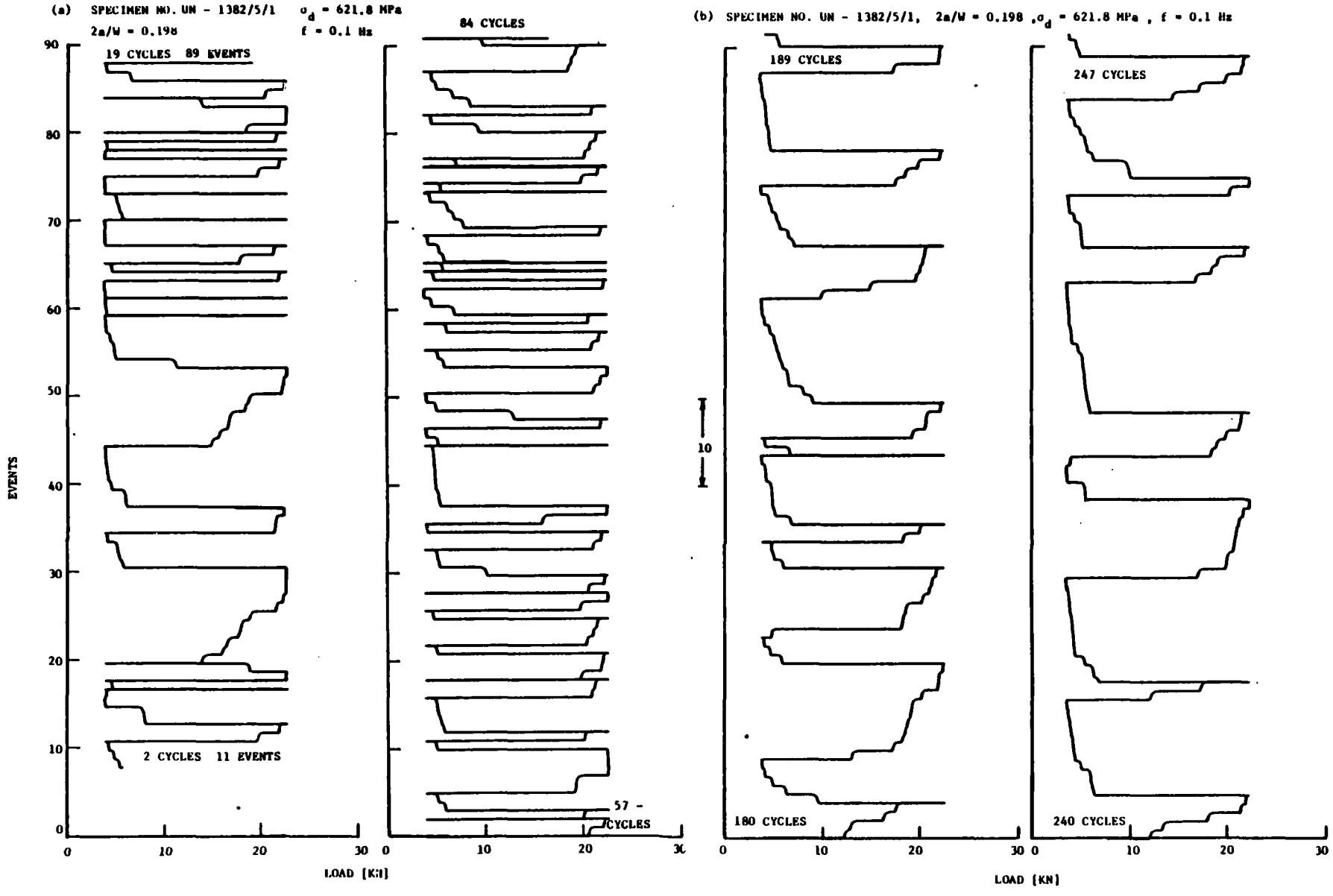

Figure 2. Accumulative events as a function of load during fatigue loading of notched unidirectional boron/aluminum specimen.

the 95th percentile of the dynamic load range.

However, as the fatigue loading progresses, a relatively significant amount of emission is generated at load levels much below the maximum fatigue level, P_d. In fact, as shown in Figure 2b, very few events occur at the upper dynamic load level. Moreover, most of the emission generated in the 2.3 to 14.0 KN load range (10-60% of P_d) is emitted during the unloading stage of each load cycle. This emission is most probably caused by friction among fracture surfaces (i.e. crack tip damage) during crack closure.

The friction between fracture surfaces developed during fatigue loading could also be seen visually through the closed-circuit television system (CCTV) which was magnified by a microscope attached to the CCTV. The relative motion between fracture surfaces, i.e. opening and closure of cracks, could be easily correlated with the rhythm of the audible levels of emission recorded by the audio monitor of the AE system. The correspondence between emission and crack closure was immediately and unmistakably recognized. This phenomenon of emission generated at load levels much below P_d has been observed for all specimens tested.

The general shape of the load-versus-event curves obtained during fatigue loading varies as the fatigue loading progresses and varies among different specimens as well. Figure 2a, for example, shows that a significant amount of emission occurs during the unloading phase of each load cycle, and much below the maximum fatigue load. It can be verified through the visual observation made with the CCTV system that crack closure can occur also during the loading phase, Figure 2b, depending upon the directionality of the damage. Matrix/fiber splitting in unidirectional specimens and crack progression in multidirectional laminates are quite rugged, and fracture surfaces do come in contact also during loading. Note that in this case, events also occur repeatedly and quite precisely at the same load level, Figure 2b, both during the loading and unloading phases of most load cycles.

Although the phenomenon described was observed repeatedly for all specimens tested, the details and shape of the events-versus-load curves will vary from specimen to specimen, depending on material quality, laminate configuration, specimen geometry, stress amplitude, load level, test frequency, typical damage size, etc. Therefore no attempt is made here to deduce any quantitative information but rather to illustrate the phenomenon that significant amounts of emission might be generated by friction among fracture surfaces developed during the cyclic loading, and that such emission is not necessarily due to new damage progression. In fact, the amount of emission generated by friction can be significantly greater than the amount of emission generated by damage progression.

8.4.2 Crack Tip Damage Growth

The pattern of the crack tip damage growth during fatigue loading has been carefully monitored in real-time through a closed circuit television system with an attached microscope which allows magnifications up to 250X. Post-fatigue fracture surface morphologies were examined through the scanning electron microscope (SEM). The following is a brief discussion of representative results.

During fatigue loading, significant differences occur in the crack tip damage growth among different laminates, and in some cases they might be different from damage occurring during quasi-static uniaxial loading. Representative examples are shown schematically in Figure 3. In unidirectional specimens, significant splitting (matrix/fiber interfacial failure) occurs, and at dynamic stress levels of 60% of ultimate static, splitting occurs within a few loading cycles. This splitting does not appear in both notch tips simultaneously, neither is the growth rate of the four splits equal. Consequently, the loading rapidly ceases to be symmetric, and the resulting in-plane bending causes crack (split) closure during the fatigue loading. This crack closure generates significant emission due to friction. With an increasing number of cycles, fibers may fail at some weak spot along their length causing a new

SCHEMATIC OF FAILURE IN $[0]_8$ B/Al SPECIMEN

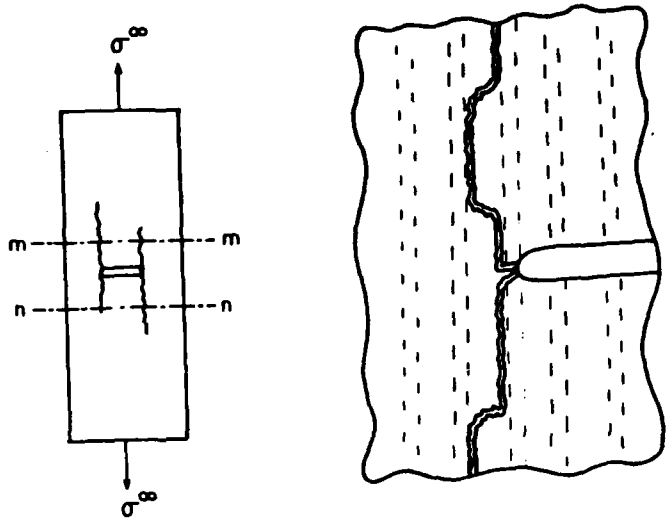

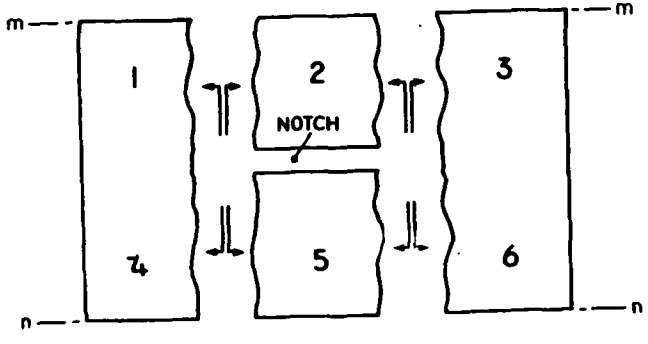

SCHEMATIC OF FAILURE IN $[0/\pm45/0]_s$ B/Al LAMINATE

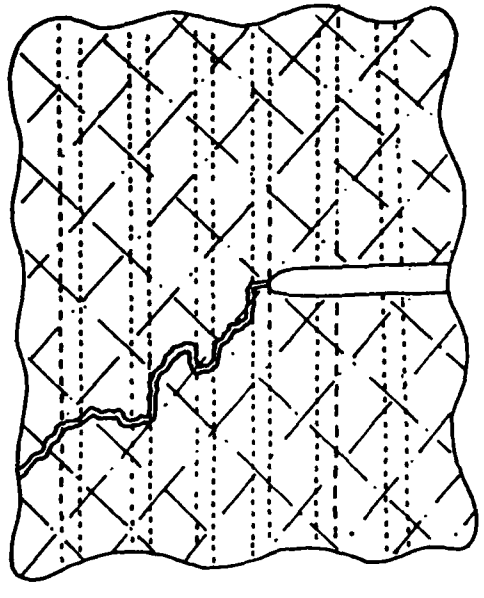

Figure 3. Schematic of damage progression in boron/aluminum during fatigue loading.

split in the neighboring interface. The splits do not necessarily progress along the same interface but rather they progress between two neighboring interfaces as shown in the schematic of Figure 3. This pattern of the split progression further increases the friction generated emission. It should be noted here that no such splitting has been observed during quasi-static uniaxial loading.

In order to verify the occurrence of friction and the extent of fatigue damage progression the fracture surfaces of the surviving specimens were examined via the scanning electron microscope (SEM) following post-fatigue loading to failure. From each region of the fracture surfaces a pair of photographs were taken, e.g. Figure 4, so that a three-dimensional view could be obtained. Examination of the fracture surfaces of the split areas (see arrows in Figure 3) through the SEM clearly reveals that they were subjected to grating. The fracture surfaces shown in Figure 4 seem to have been rubbed together during the fatigue loading. The fiber surfaces are coated with a thin layer of aluminum. The SEM photographs in Figure 4 also show a broken fiber which occurred at some distance away from the tip of the original crack, as previously discussed.

In boron/aluminum multidirectional laminates the directionality of the crack tip damage growth depends on laminate configuration. For a cross-ply laminate the damage progresses along the 90° layer, i.e. a coplanar and self-similar crack growth has been observed. When ±45° layers are included in the laminate, e.g. $[0/\pm45/90]_s$ or $[0/\pm45/0]_s$ the crack tip damage progresses along the ±45° direction as shown schematically in Figure 3. Examination of the fracture surfaces clearly indicate the extent of fatigue crack progression. The specimen shown in Figure 5 was subjected to 10,000 load cycles, followed by post-fatigue quasi-static loading to failure. The top photographs in Figure 5 were taken in the region of fatigue crack progression (as observed through the CCTV). The extensive rubbing and smashed fibers caused by the repeated crack closure during the fatigue loading are clearly seen. The bottom photographs in Figure 5 were taken in the region of crack propagation during the

SPEC. NO. UN - 1384/5/1

2a/W = 0.301 SURFACE 1/2

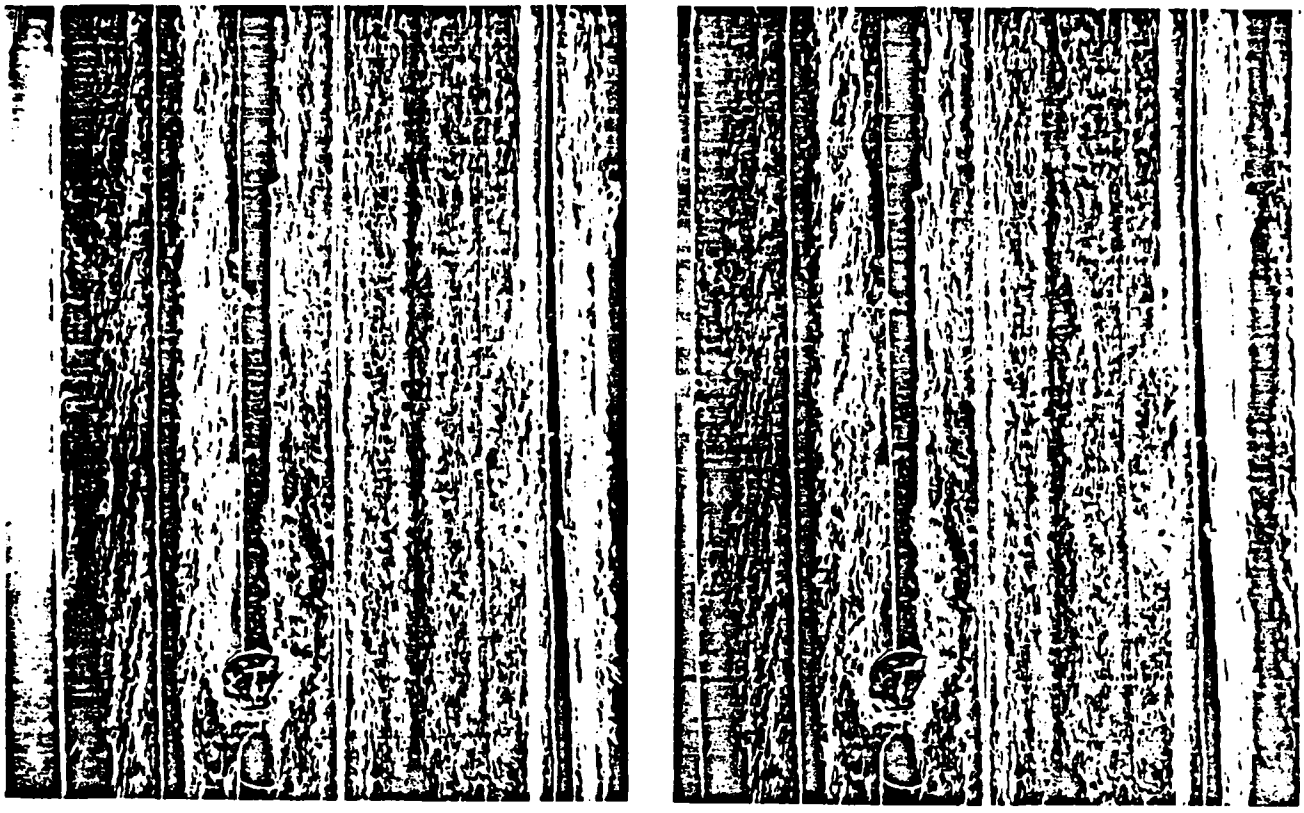

LEFT 80X RIGHT

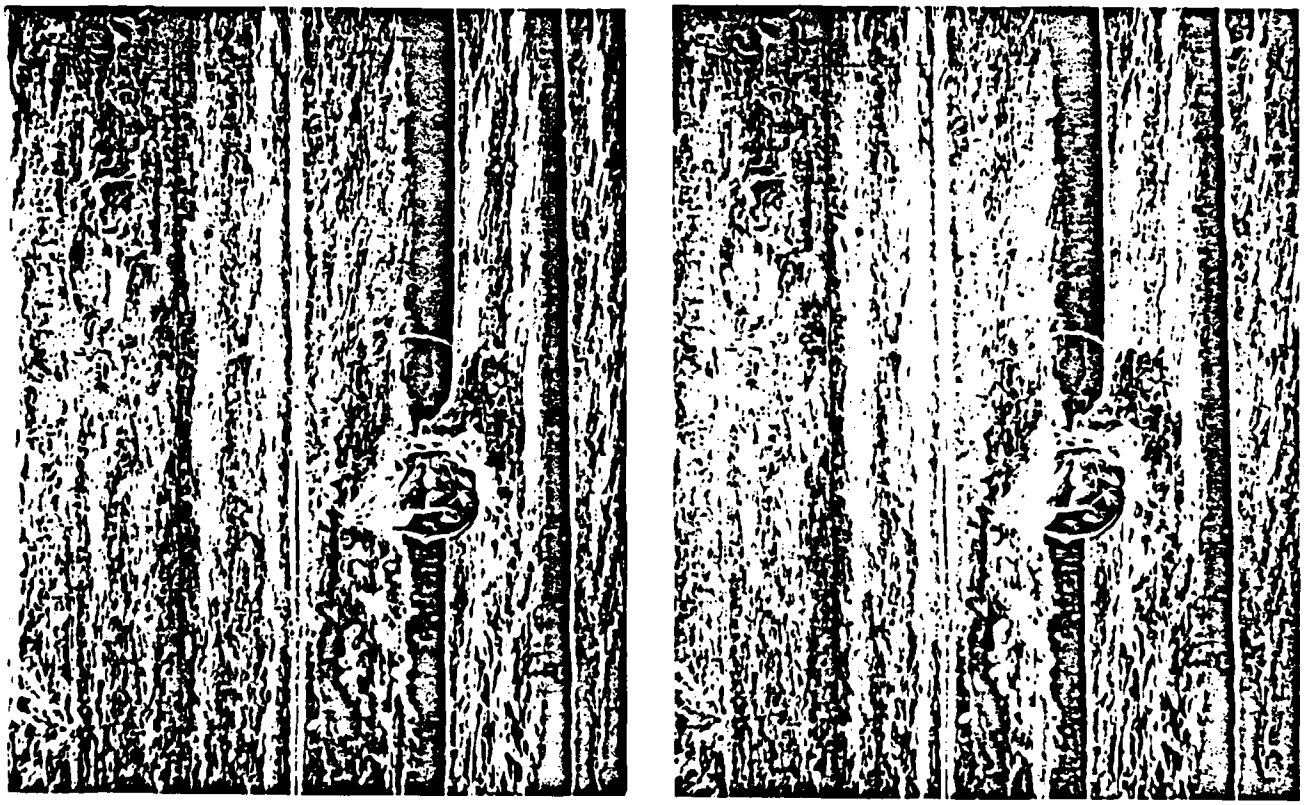

LEFT 120X RIGHT

Figure 4. Pairs of scanning electron microscope micrographs of unidirectional boron/aluminum showing the fracture surface of the split surface. Friction among newly created fracture surfaces is evident.

SPEC. NO. QIN - 1523/48 σ_d = 112.8 MPa N = 10,000 CYCLES

2a/W = 0.305 σ_f = 182.3 MPa f = 1.0 Hz

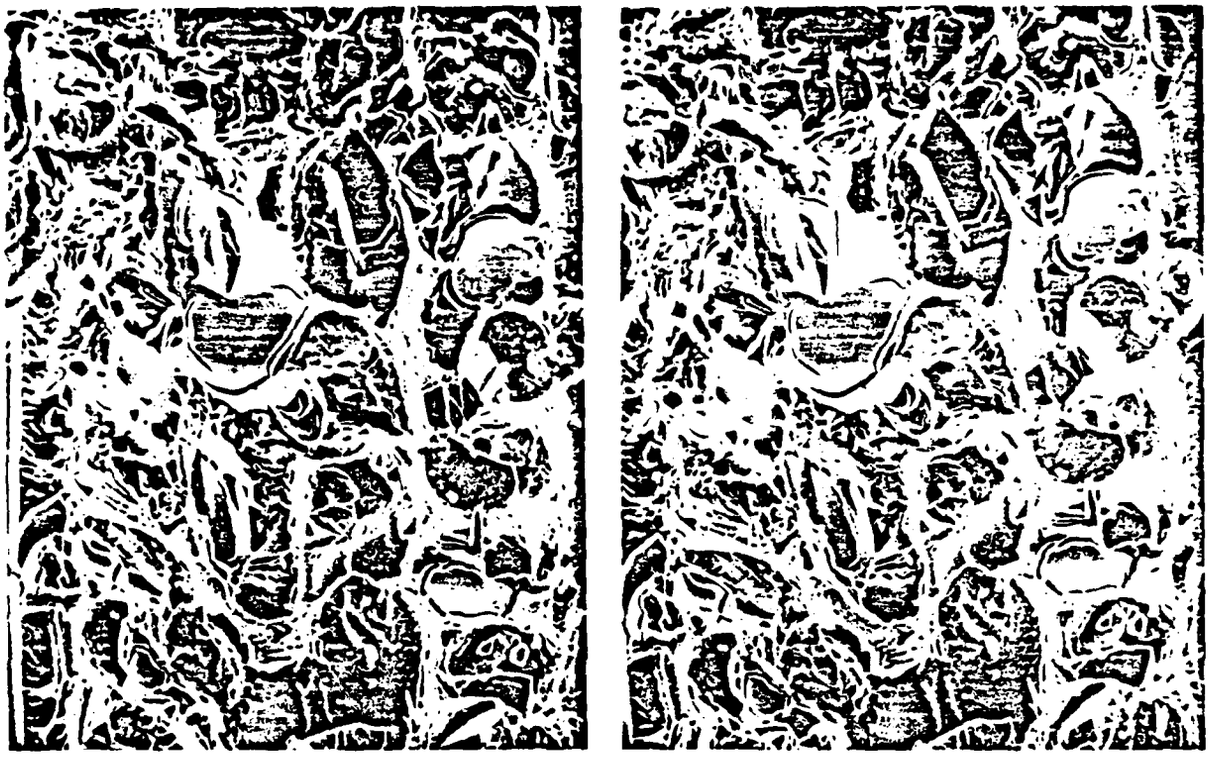

LEFT 120X RIGHT

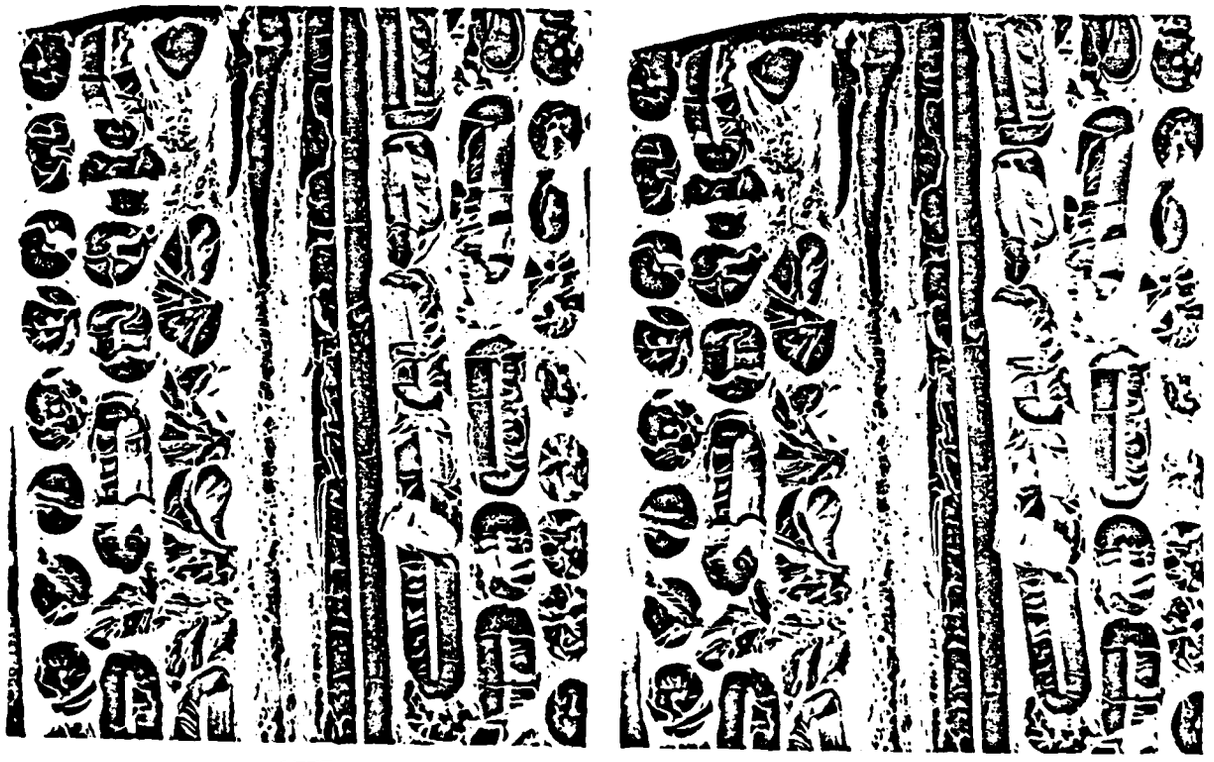

LEFT 80X RIGHT

Figure 5. Pairs of electron microscope micrographs of $[0/\pm45/90]_s$ boron/aluminum laminate. The grated fracture surfaces (top) were created during the fatigue crack propagation, while during post-fatigue loading to failure (bottom photographs) the fracture surfaces are similar to those obtained during quasi-static loading as shown in Figure 14.

post-fatigue static loading. Here, the fracture surface is practically identical to that shown in Figure 11 of Section VI. From the examination of the entire fracture surface the differences between fatigue and static crack propagation are clearly distinguishable.

In summary, from both the acoustic emission results and from the fracture surface morphologies it could be concluded that significant friction and grating occurs during fatigue loading, as expected. Therefore, when the acoustic emission technique is applied for monitoring damage progression during fatigue loading the emission generated due to friction should be separated from that generated due to new damage. A simplified approach applied in this research program has been discussed in Section 8.3, the results of which are discussed below.

8.4.3 Detection of Damage Initiation and Progression

Damage initiation and progression during fatigue loading strongly depend on laminate configuration, notch length, dynamic stress level, loading frequency, state of initial damage (e.g. generated during initial loading) etc. Consequently, the recorded emissions will also be affected by the variety of intrinsic and extrinsic variables. Also, the significant inherent scatter in material properties, quality, and state of initial damage are such that for each specimen the recorded AE will be different. Below, only representative results, depicted from the entire test matrix conducted in this program, are discussed.

Figure 6 shows E.-N. plots for a center-notched unidirectional boron/aluminum specimen subjected to tension-tension (R=0.1) fatigue loading at a loading frequency of 1.0 Hz. The E.-N. curves (and the E.R.-N. curves shown in Figure 7 for the same specimen) show events generated at seven different load ranges (see Section 8.3). Several conclusions could be drawn: First, the amount of emission generated due to damage (in the upper load range, 95-100% of the maximum dynamic load, P_d) is, by order of magnitude, smaller than the total amount of emission recorded. In other words,

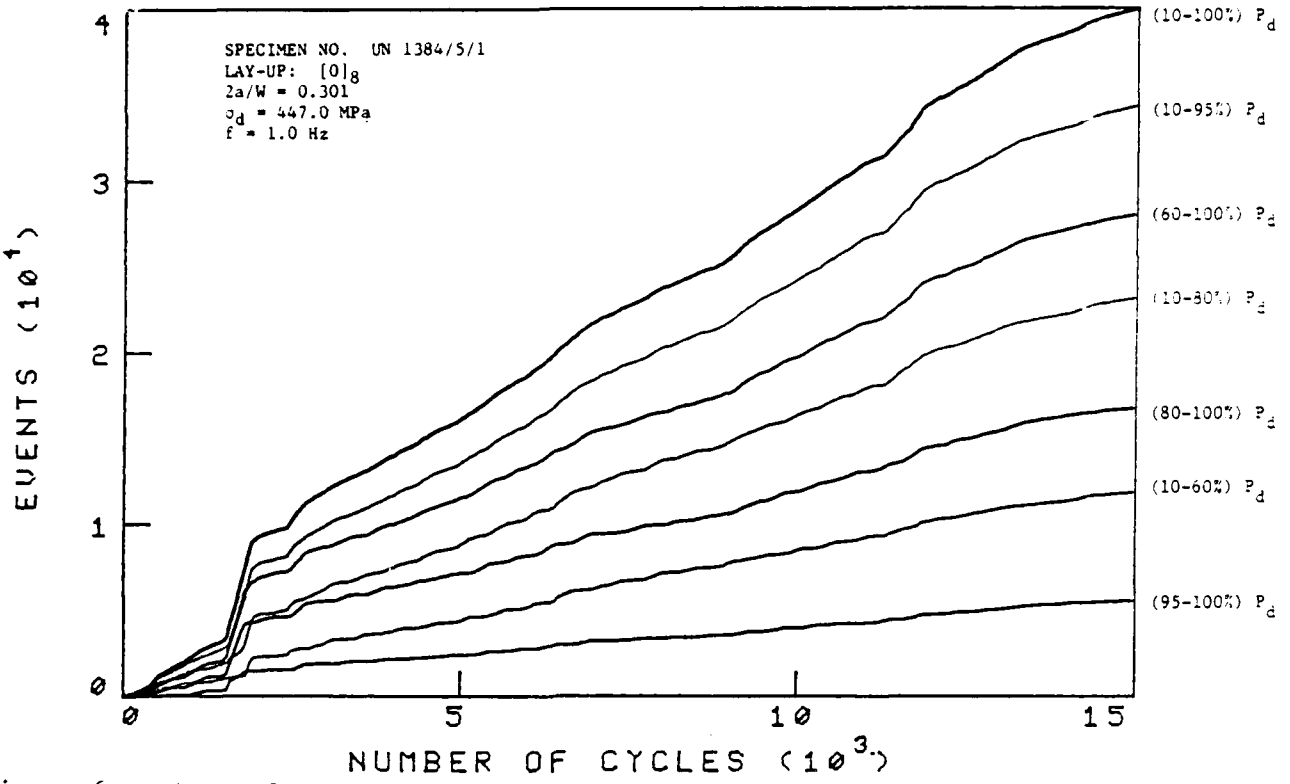

Figure 6. Accumulative events as a function of number of cycles for a notched boron/aluminum specimen (notch length-to-width ratio = 0.30), distinguishing emission generated in different load ranges.

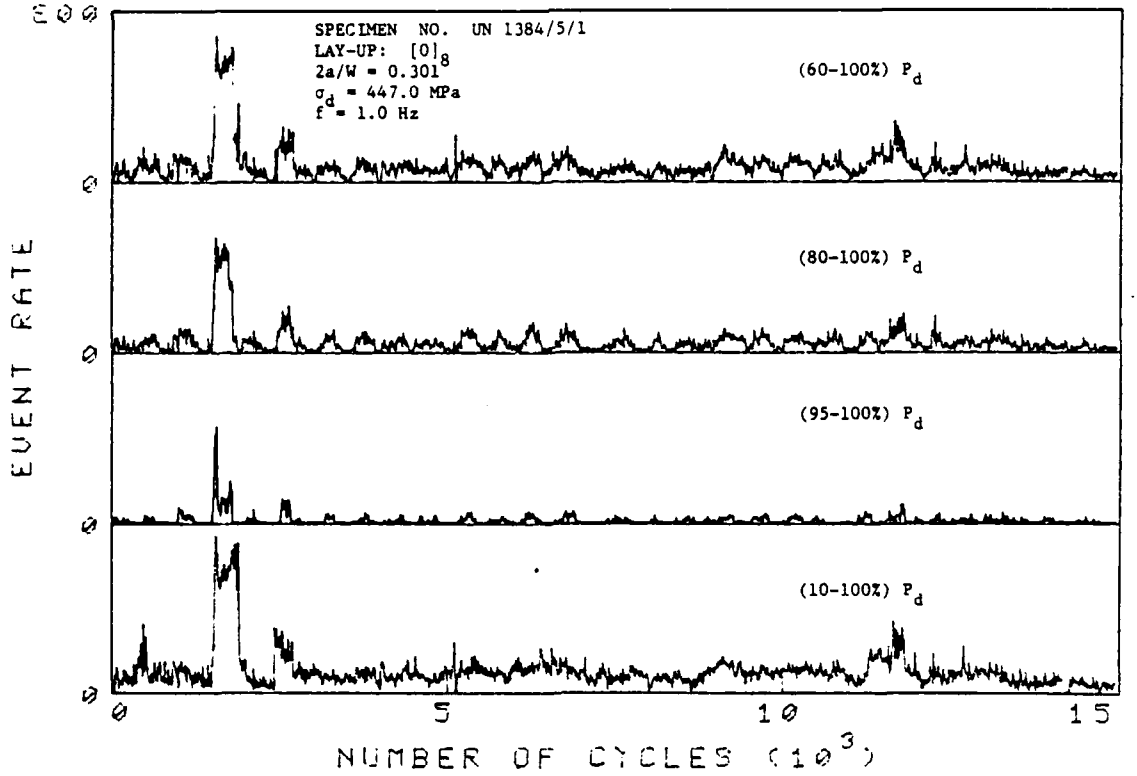

Figure 7. Number of events per ten cycles as a function of number of cycles for the same specimen shown in Figure 6 (notch length-to-width ratio = 0.30) distinguishing emission generated in different load ranges, recorded on the "damage side".

most of the emission was generated due to friction among the newly created fracture surfaces. Second, in this particular case, practically all the emission was initially generated at the low load range, i.e.it is due primarily to friction. This indicates that significant crack tip damage has occurred already during the first quasi-static cycle. (It should be noted that the emission recorded during this first load cycle was eliminated from the E.-N. curves). In other cases, where no damage has occurred during the first load cycle, most of the emission generated in the initial fatigue cycles is in the upper load range, indicating damage progression. With increasing load cycles friction generated emission is recorded which accumulates continuously throughout the entire fatigue loading. Third, damage progression as detected through the acoustic emission is intermittent (see Figure 7 at 95-100% P_d). Fourth, as indicated in Figures 6-7 (details of which are shown in Figures 8-9), a sudden surge in emission occurred at 1650 cycles. Visual observations of the specimen in real-time, using a closed circuit television system, revealed the occurrence of significant damage in the form of matrix splitting all along the specimen length. At this stage, due to the large newly created fracture surface, significant emission was generated in the low load range, i.e. indicating friction generated emission.

Similar results were obtained also for multidirectional laminates, examples of which are shown in Figures 10-13. The intermittent nature of damage progression as detailed from the acoustic emission is clearly seen, and in most cases it is accompanied by a significant surge of friction generated emission. It could be that when damage progression is very rapid, as is usually the case with composite laminates, the AE system may fail to respond; however, the occurrence of this damage can be inferred from the subsequent increase in friction-generated emission. Similar results were obtained for many other specimens as well. All the E.-N. curves evidence the same emission pattern: emission accumulated in the upper load ranges is discontinuous and followed by sudden increases in friction-generated emission.

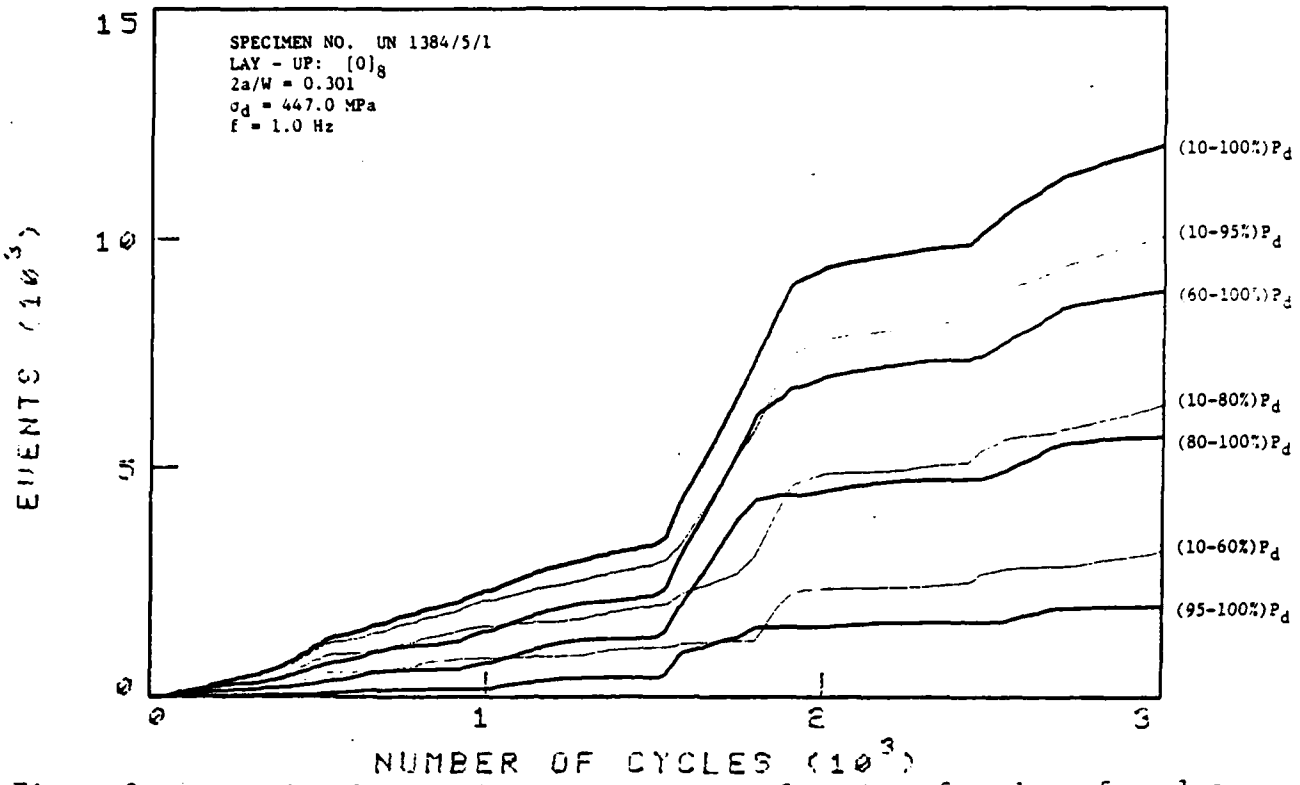

Figure 8. Details of accumulative events as a function of number of cycles for the same specimen shown in Figure 6 (notch length-to-width ratio = 0.30), distinguishing emission generated in different load ranges.

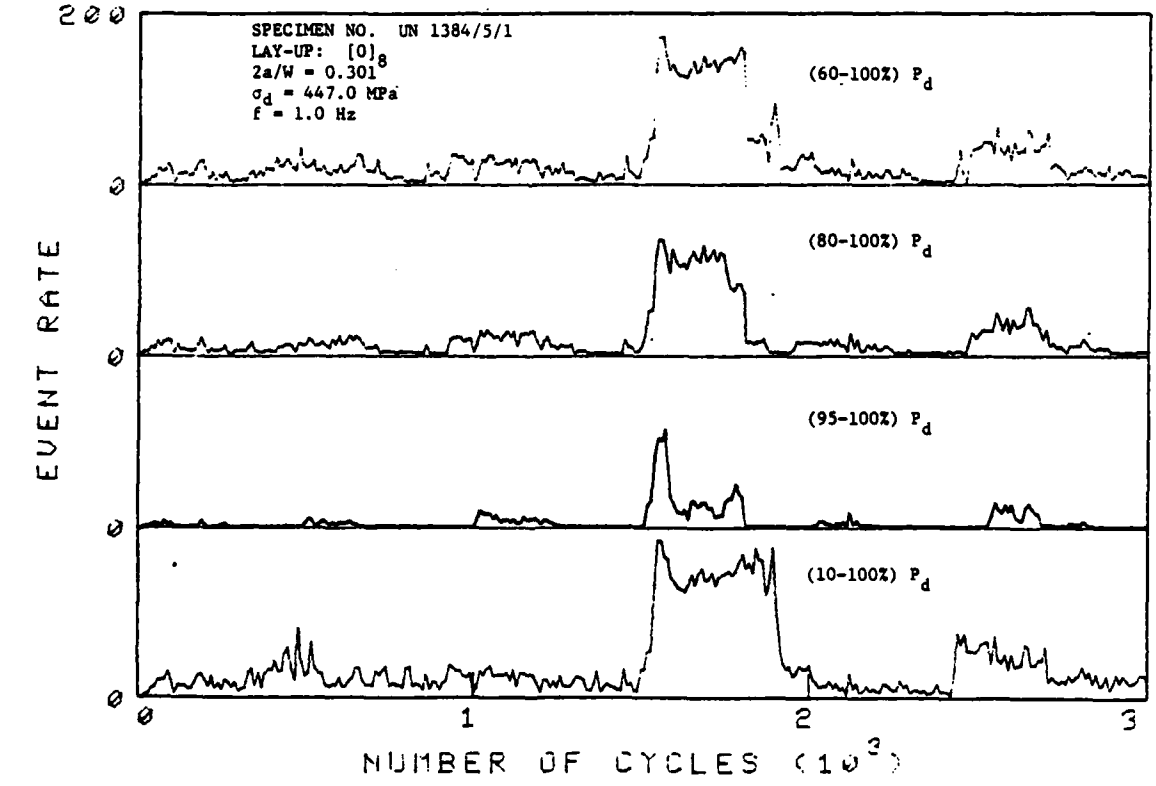

Figure 9. Number of events per ten cycles as a function of number of cycles for the same specimen shown in Figure 8 (notch length-to-width ratio - 0.30) distinguishing emission generated in different load ranges, recorded on the "damage side".

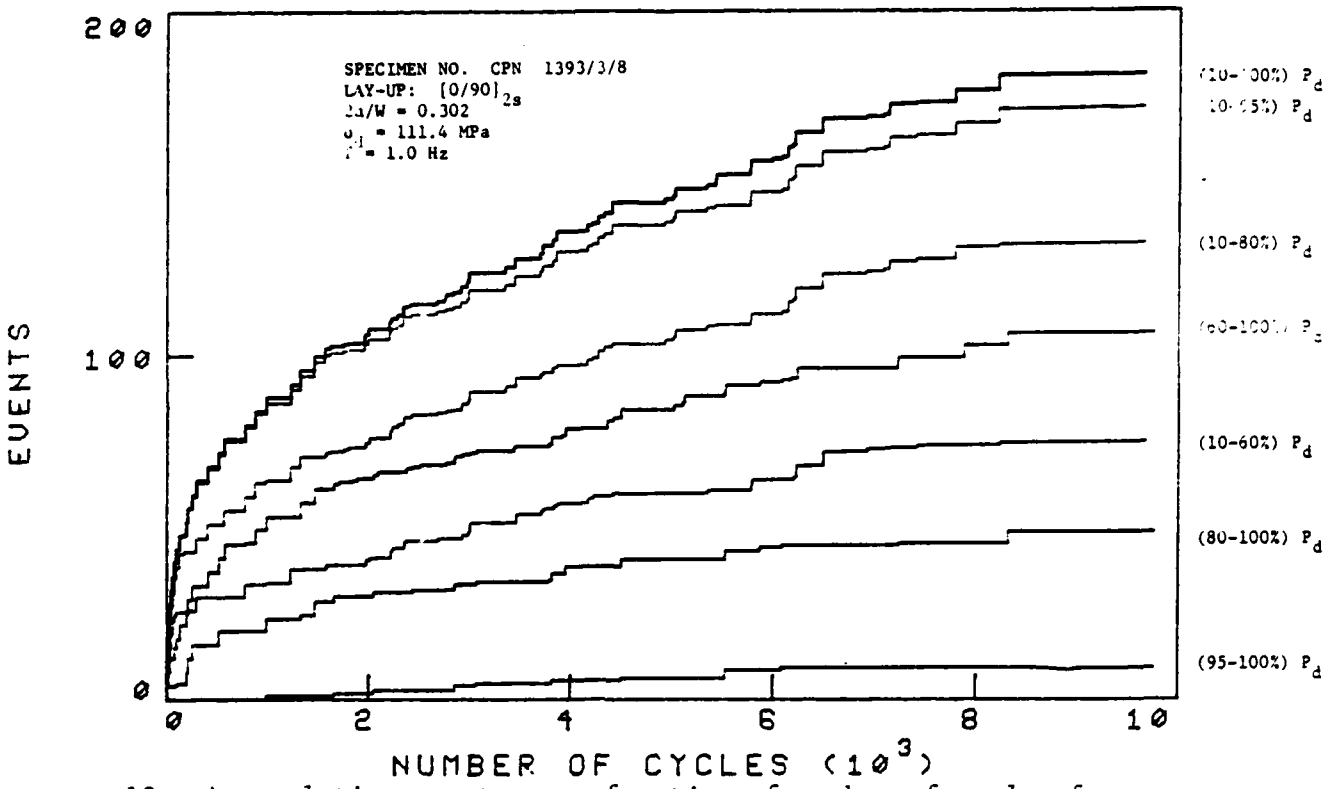

Figure 10. Accumulative events as a function of number of cycles for a notched $[0/90]_{2s}$ boron/aluminum laminate (notch length-to-width ratio = 0.30), distinguishing emission generated in different load ranges.

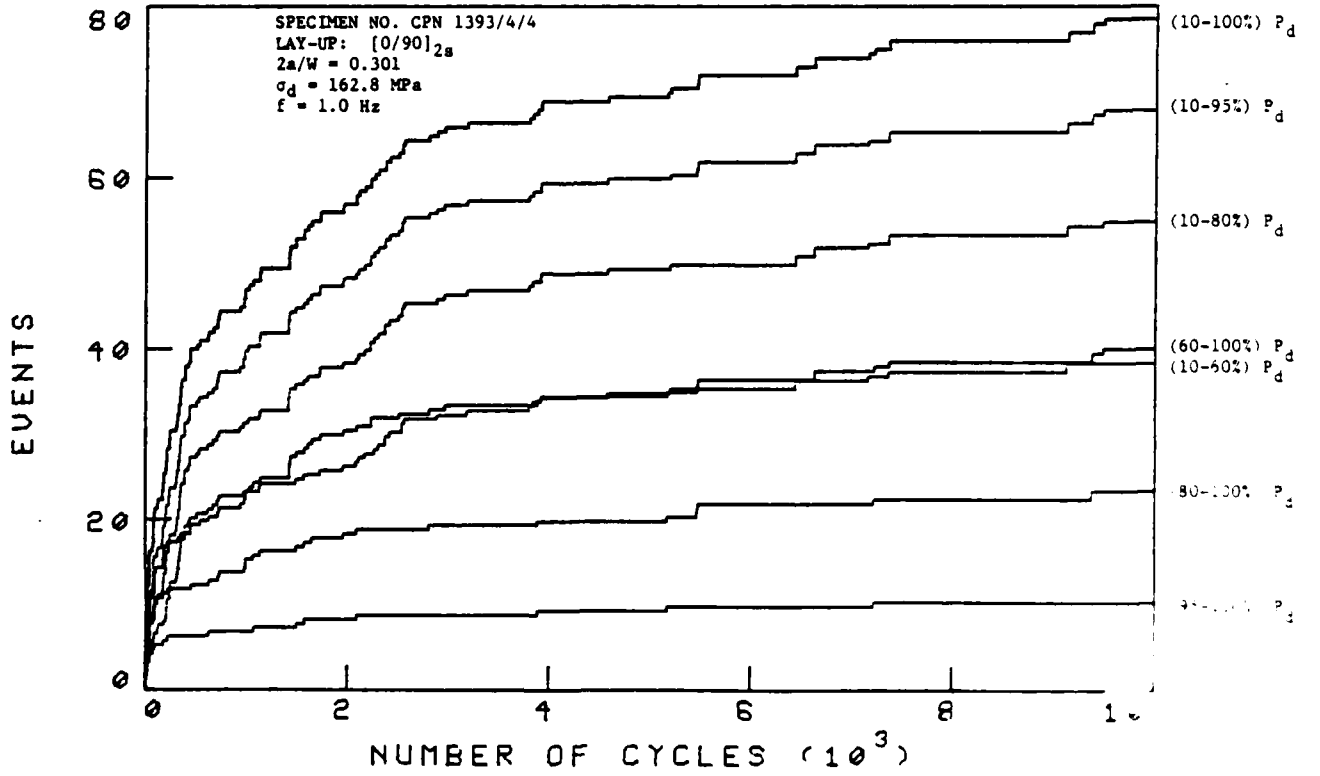

Figure 11. Accumulative events as a function of number of cycles for a notched boron/aluminum laminate (notch length-to-width ratio = 0.30), distinguishing emission generated in different load ranges.

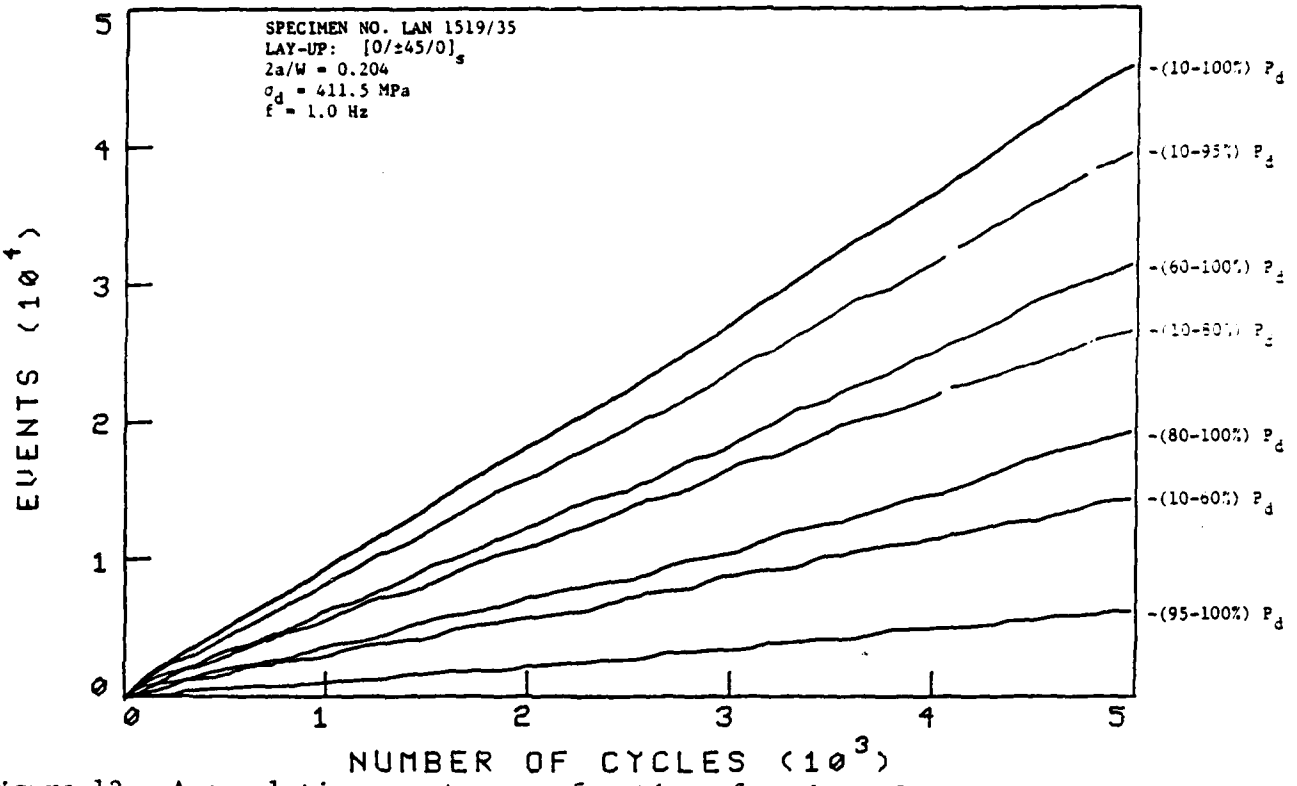

Figure 12. Accumulative events as a function of number of cycles for a notched boron/aluminum laminate (notch length-to-width ratio = 0.20), distinguishing emission generated in different load ranges.

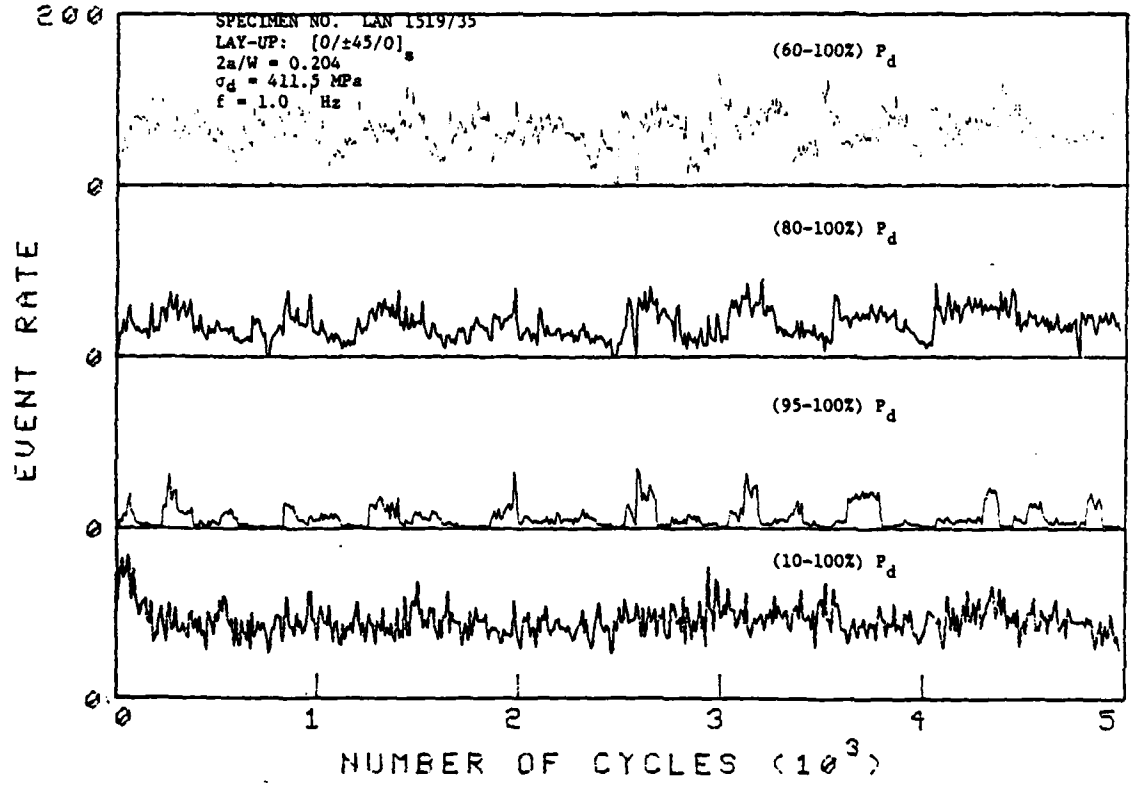

Figure 13. Number of events per ten cycles for the same laminate shown in Figure 12 (notch length-to-width ratio = 0.20) distinguishing emission generated in different load ranges, recorded on the "damage side".

Generally, in composite laminates damage progression is frequently found to be discontinuous. In all cases the amount of emission attributable to new damage is significantly lower than that attributable to friction. However, from the E.-N. plots and even more so from the E.R.-N. plots, the cycle number at which new damage progresses can be readily and precisely determined.

The issue mentioned previously regarding the effect of the inherent scatter in properties and initial state of damage on acoustic emission results can be clearly seen in the comparison between Figures 10 and 11. Although the two cross-ply specimens are seemingly identical it is surprising that the total number of emissions recorded for the specimen loaded at the lower dynamic stress level, σ_d, Figure 10, is higher than that recorded for the specimen subjected to the higher stress level, Figure 11. However, it should be noted that the number of events generated in the 95-100% range of the dynamic stress is lower for the specimen subjected to the lower dyanmic stress level. Also, damage initiation (determined from the emission generated in the upper load range) occurred at a much later stage for that specimen (at approximately 1000 cycles), while for the specimen subjected to the higher dynamic stress level damage initiation appeared immediately upon load application.

When a multidirectional laminate includes also ±45° plies, e.g. Figures 12-13, the amount of emission is significantly higher. This should be attributable to the significant inelastic deformation in the ±45° plies, as discussed in Section VII, and it is much higher than the emission recorded for the unidirectional specimen, Figure 6. Significant crack tip damage progression has been observed for this specimen through the CCTV, resulting in a large amount of friction generated emission during crack closure.

8.4.4 Location Distribution Histogram of Events

During fatigue loading, location distribution histograms of events were recorded at predetermined cycle number. The purpose of this procedure was to verify the results of event-versus-load plots shown in Figure 2, the results of event-versus

cycle number (E.N.) plots shown in Figures 6 to 13 and to compare with visual observation through the CCTV.

The location distribution histograms for two laminates shown in Figures 14-15 indicate that emission has been generated throughout the specimen length. From the results shown in Figure 14 for the cross-ply laminate (same specimen as in Figure 10) it could be concluded that no significant crack tip damage progression (location "52") has occurred. An increased activity in the crack tip regions occurred after approximately 5000 load cycles. In the case of $[0/\pm45/0]_s$ laminate, Figure 15, the significant emission was generated from the crack tip regions and also throughout the specimen length. In such cases crack tip damage progression could be easily seen visually through the CCTV. It should be recalled (see Section 3.5) that the number of events indicated in Figures 14-15 and in the E.N. plots are for those events generated from within the location window of "40"-"60".

8.4.5 Detection of Failure Mechanisms

The definition of damage vis a vis friction generated emission, as discussed previously, is obviously incomplete. A more detailed study into the distinction between damage and friction generated emission can be made by analyzing the acoustic emission events. Determination of the major failure mechanisms using acoustic emission can be based upon a variety of AE source intensity analyses such as events amplitude, duration, energy, counts per event, frequency spectrum, rise-time, etc. As discussed in Section VII, a comprehensive study on the detection of the major failure mechanisms during quasi-static loading has been conducted in which emphasis has been placed on analyzing the amplitude distribution histograms of events. Preliminary study on analyzing the other AE event source intensities was also initiated.

Based on the base-line information obtained during quasi-static loading, Section VII, a clearer understanding of the failure processes during fatigue loading

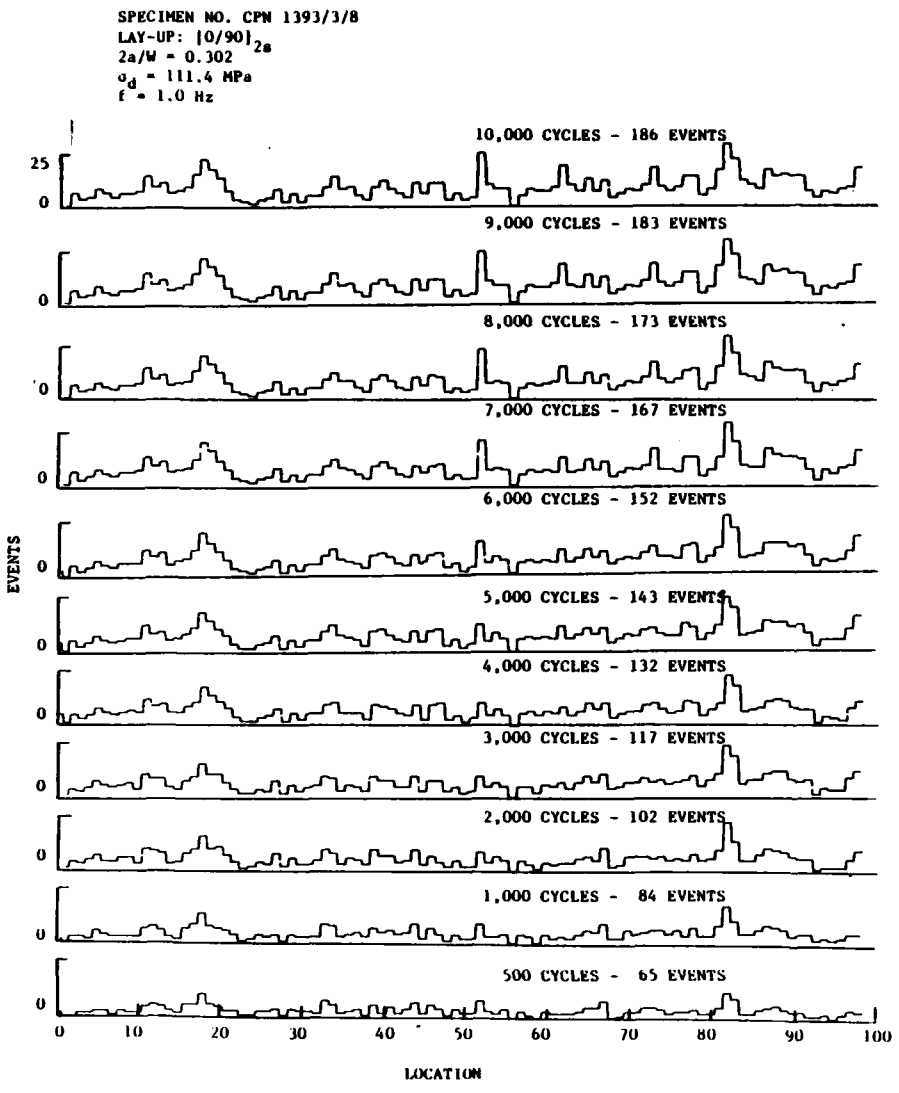

Figure 14. Location distribution histograms of events for notched $[0/90]_{2s}$ boron/aluminum laminate at different cycle numbers.

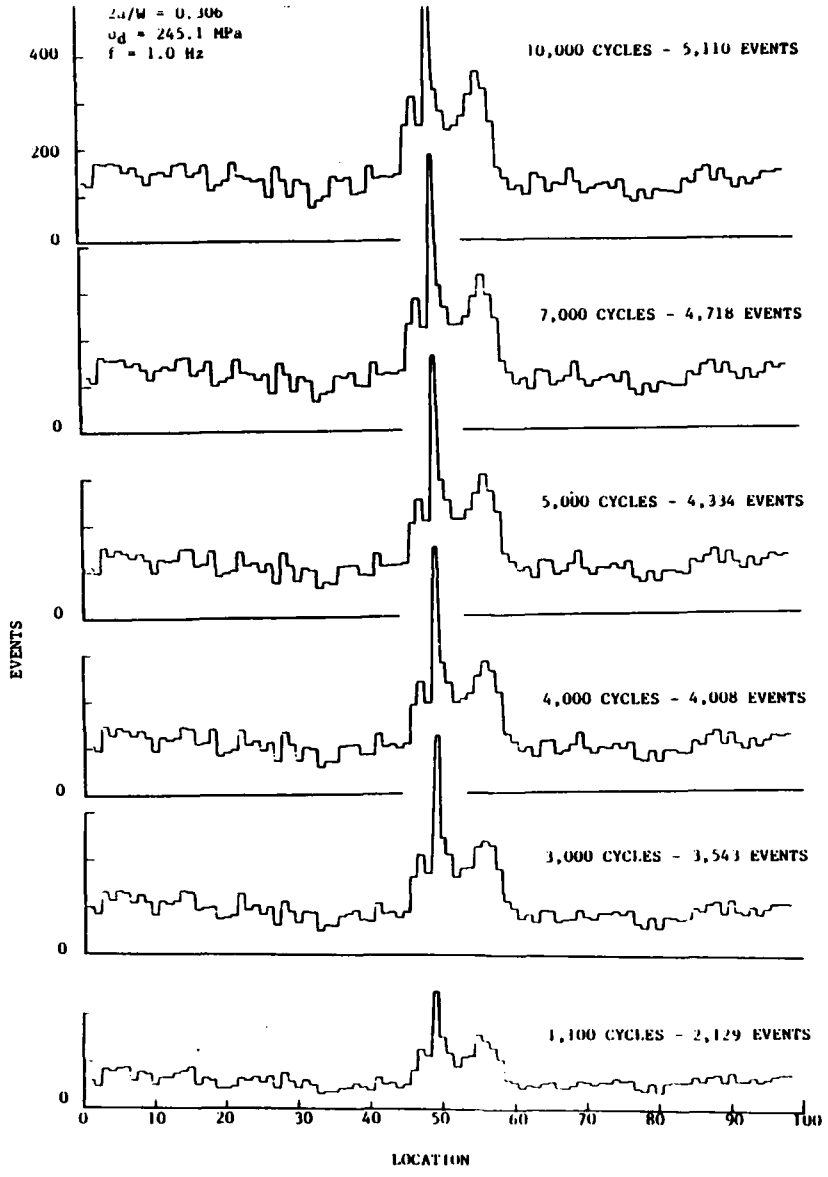

Figure 15. Location distribution histograms of events for notched $[0/\pm45/0]_{s}$ boron/aluminum laminate at different cycle numbers.

can be obtained. For example, it is expected that friction-generated emission will display different acoustic emission signatures than emission caused by damage progression, and that the occurrence of fiber breakage (i.e. crack tip damage initiation and progression) can be detected.

An example of amplitude distribution histograms of events obtained for two notched $[0/\pm45/0]_s$ specimens are shown in Figure 16. Three histograms are shown, representing the three phases of the loading sequence; initial quasi-static loading to a predetermined maximum fatigue load; fatigue loading; and post-fatigue quasi-static loading to failure. Note that the amplitude distribution histograms in these Figures are for those events accumulated only during each separate phase of the loading sequence.

As expected, all amplitude distribution histograms obtained during the initial quasi-static loading phase are similar to those obtained during quasi-static loading to failure at corresponding load levels (see Section VII). However, during fatigue loading, the number of high amplitude events (i.e. fiber breakage) strongly depend on the dynamic stress level (and number of cycles, not shown here). For the lower dynamic stress level (145.1 MPa) no high amplitude events were generated, while for the higher applied load (up to 185.7 MPa) a few high amplitude events were generated.

The type of damage occurring within different load ranges during fatigue loading could also be determined by analyzing other AE event source intensities. Figure 17 shows the events' rise-time, duration, energy, counts and amplitude as a function of load obtained during fatigue loading of unidirectional boron/aluminum specimen. Each point in Figure 17 indicates an event occurring at a given load level and having a specific source intensity. The results indicate that during the first 150 cycles practically all high source intensity levels occur at or close to the maximum load levels, while the low source intensities may occur throughout the load cycle. Also, all events are lumped in either the upper or the lower load ranges,

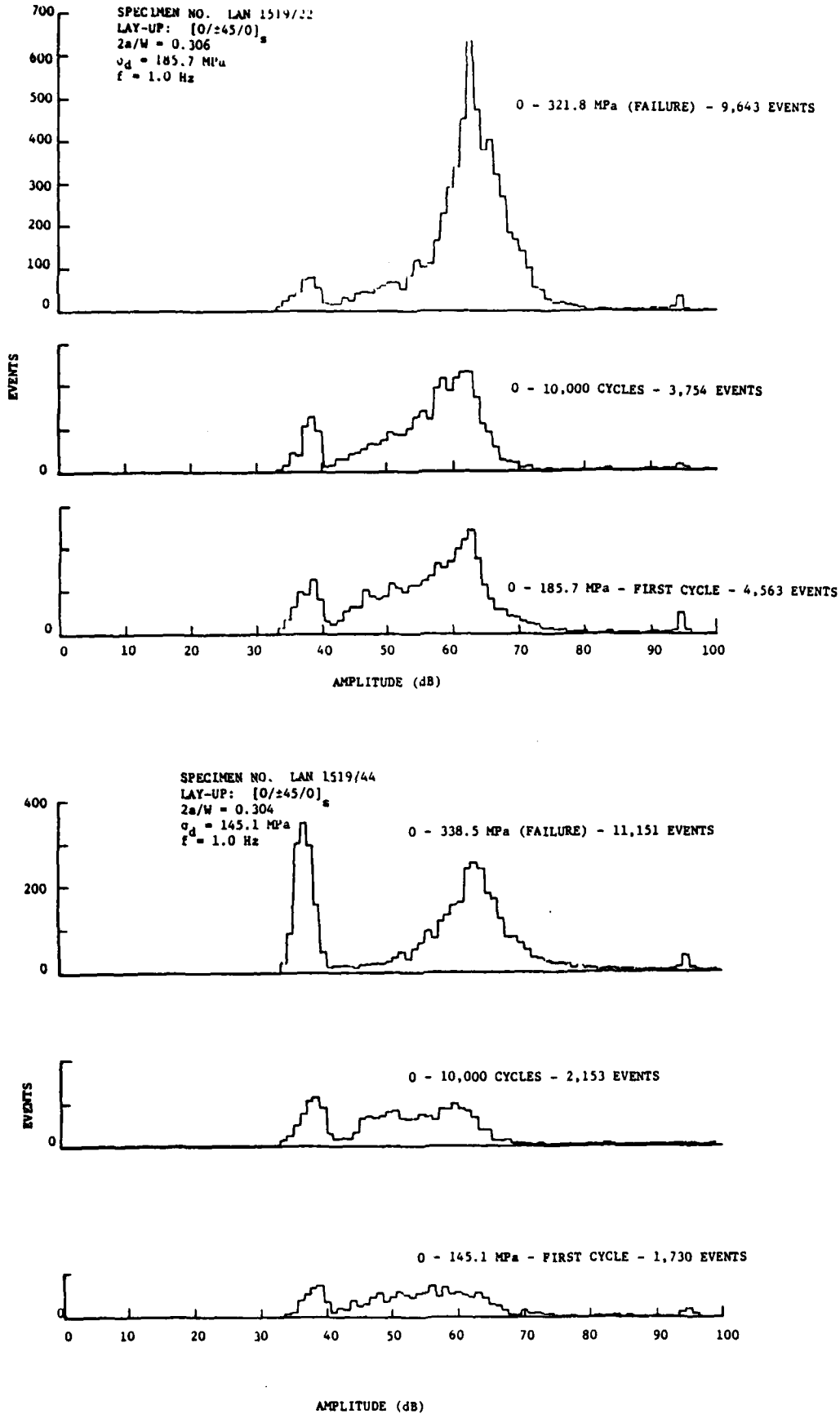

Figure 16. Amplitude distribution histograms of events for a notched $[0/\pm45/0]_s$ boron/aluminum laminate (2a/W = 0.30). Histograms are for events accumulated during: a) initial quasi-static loading; b) fatigue loading; c) quasi-static loading to failure.

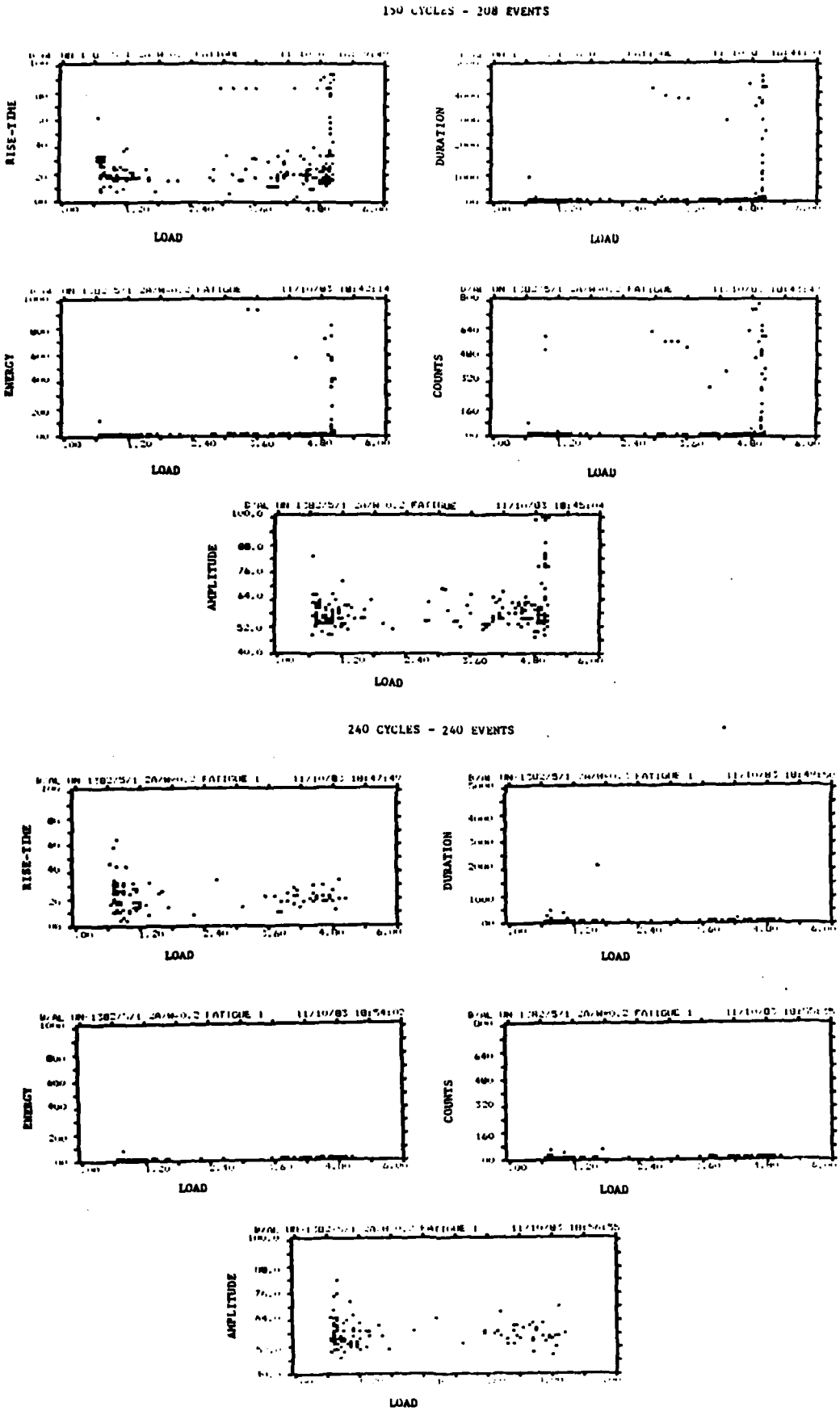

Figure 17. Effect of fatigue loading on acoustic emission events source intensities. The higher intensities occur primarily at the upper dynamic stress level.

indicating possible emission generated from new damage and crack closure (friction), respectively. Finally, damage progression during fatigue loading is not necessarily continuous. The results shown in Figure 17 for the emission generated during the subsequent 240 cycles (i.e. 151-391 cycles) indicate no high event source intensities.

It should be noted that these results are only preliminary and an additional detailed study into discriminating different types of acoustic emission source intensities and their correlation with the actual type of damage and failure processes during fatigue loading is warranted.

8.4.6 Fatigue Degradation in Mechanical Performance

Post-fatigue global compliance and residual strength were recorded for all specimens and data were compared with the corresponding values obtained during quasi-static loading. The comparison indicates, as expected, a slight increase in global compliance resulting from crack tip damage growth during fatigue loading. This change in global compliance could indicate the "effective" crack tip damage growth (applying the compliance matching data reduction procedure) during fatigue loading. However, recalling from the discussions given in Section IV, the global compliance curves are not sufficiently sensitive to yield accurate evaluation of changes in crack length. A better test procedure would have been to apply the IDG technique (to determine the local compliance) and compare the results with the local compliance claibration curve of the subject material. Recent attempts, on a preliminary basis, indicated that such a test procedure can in fact accurately determine the "effective" crack tip damage growth during fatigue loading.

Post-fatigue residual strength data did not reveal a specific trend in the effect of fatigue loading. Although strength degradation (of up to 10%) has been recorded for most specimens, a slight increase in strength (of up to 5%) has also been recorded for a relatively large number of specimens. Such post-fatigue increase in the strength of composite laminates, particularly for a low number of fatigue cycles, has been reported and analyzed in numerous publications.

It should be recalled that in this program specimens were subjected to no more than 15,000 cycles with emphasis on the monitoring of damage initiation and progression during fatigue loading through acoustic emission. Thus, insufficient data are available to draw definite conclusions regarding strength degradation of boron/aluminum laminates during fatigue loading.

8.5 Conclusions

Fatigue damage progression and accumulation in center-notched boron/aluminum laminates has been monitored through acoustic emission during low cycle tension-tension fatigue loading. Special efforts have been placed on differentiating between emission generated by actual damage and that seemingly generated by friction among fracture surfaces created during the fatigue loading. The results of this study can be summarized as follows.

1. A significant amount of emission is generated by friction among fracture surfaces which have been created during the fatigue loading, e.g. matrix cracking. It is essential to differentiate between this type of emission and emission generated by actual damage progression.

2. Friction-generated emission should not be eliminated from the recorded information because it can serve as an important indicator of damage progression. Matrix damage progresses so rapidly that the AE instrumentation may fail to register the associated events; however, the sudden resulting increases in friction-generated emission indicate that damage progression has occurred.

3. A direct correlation has been clearly established between the AE results which indicate friction-generated emission and the visual observations of damage progression made through the CCTV.

4. Damage progression is intermittent and the cycle number at which a sudden damage growth has occurred can be easily and precisely determined and can

also indicate the location at which the damage has occurred as well as the dominant failure modes.

5. During the initial fatigue loading most of the emission seems to be generated by damage progression; with increasing number of cycles, most of the emission is primarily due to friction. However, when significant damage has been introduced during initial loading, friction generated emission can also be emitted at the beginning of the fatigue loading.

6. There is a large scatter in the events-versus-number-of-cycles plots among the different specimens, indicating a large variation in rate of damage progression and/or material quality.

7. Location distribution histograms of events reveal that emission occurs throughout the specimen length, resulting from the extensive matrix and interface deformation in all laminates tested.

8. A direct correlation could be established between location distribution histograms of events and the events-versus-number-of-cycles plot and with the visual observations through the CCTV.

9. Post-fatigue emission initiation load is slightly higher than the maximum fatigue stress.

10. Post-fatigue emission initiation load is significantly higher than pre-fatigue initiation load, and depends strongly on fatigue stress level. Consequently, load history is a significant parameter in evaluating material quality and/or damage progression through acoustic emission.

IX. NOTCHED STRENGTH OF COMPOSITE LAMINATES: PREDICTIONS AND EXPERIMENTS - A REVIEW*

9.1 Summary

In this study several of the recent and commonly used fracture models for predicting the notched strength of composite laminates have been reviewed. Emphasis has been placed on semi-empirical fracture models which are operationally simple to utilize.

Representative experimental results on the notched strength of composite laminates containing a circular hole or straight crack and subjected to quasi-static uniaxial tensile loading have been collected from the open literature. Notched strength data for graphite/epoxy, boron/aluminum and graphite/polyimide were analyzed. Over 2800 notched strength data for seventy different laminate configurations and twenty material systems have been collected and filed into a computer data bank for subsequent analysis.

The various parameters associated with all the fracture models have been determined for all laminates and their correlation with the actual notch sensitivity of the subject laminate has been identified. All notched strength data sets were compared with all fracture models and the applicability of the different fracture models in predicting the notched strength of composite laminates has been reviewed and evaluated.

A self-contained review of the fracture models along with a detailed discussion of the variables affecting the notch sensitivity of composite laminates and the parametric analyses are given in [1,2]. The actual notched strength data collected,

* This extensive review was also partially supported by NASA Langley Research Center and the Institute of Structural Mechanics, the German Aerospace Research Establishment (DFVLR). The program monitors were C.C. Poe of NASA LaRC and H.W. Bergmann of the DFVLR.

test procedures, major conclusions of the various publications reported, etc. are all given in detail in [2].

9.2 Introduction

Extensive research has been performed in recent years on the fracture behavior and toughness of composite systems containing artificially induced circular holes or cracks. These studies focus on subjects such as initiation of crack tip damage growth, critical crack tip damage zone size, notch sensitivity, fracture toughness, failure modes on the micro and macro scales, crack arrest mechanisms, etc., using various theoretical and experimental techniques. Due to the multiplicity of failure modes and the corresponding complexity of failure processes and damage progression in laminated composites, a variety of analytical techniques have been developed ranging from comprehensive numerical methods to simplified semi-empirical fracture models.

The purpose of this study was to investigate the notch sensitivity of composite laminates containing circular holes and straight cracks when subjected to uniaxial tensile loading. Several of the most commonly used semi-empirical fracture models proposed to predict the notched strength of composites were critically reviewed. The review is sufficiently detailed so as to be self-contained [1]. Experimental results were reviewed in detail [2] including all the relevant available information regarding material system, laminate configuration and geometry, testing procedure, fracture strength data, material mechanical properties, etc. This information formed the basis for the correlations performed in this study. All notched strength data were compared with all the fracture models reviewed and the various parameters associated with these fracture models were determined. For this purpose, special computer programs were developed by which all data could be analyzed through a variety of procedures. Notched strength data for graphite/epoxy, boron/aluminum and graphite/polyimide were analysed and the effect of intrinsic and extrinsic variables such as laminate configuration, stracking sequence, material system,

notch geometry, test temperature, etc. on the notch sensitivity were discussed. The model parameters were correlated with the notch sensitivity of composite laminates and their applicability as measures of notch sensitivity has been evaluated.

9.3 Fracture Models

Due to the complexity of analyzing the fracture behavior of notched composite laminates, several simplified fracture models have been proposed in recent years. The review laid the ground-work for applying them in the analysis of the published fracture data for various material systems and for the data obtained for boron/aluminum in this research study.

The fracture models reviewed and applied throughout this study are listed in Table I.

TABLE I: LIST OF FRACTURE MODELS REVIEWED

Authors	Ref.	Abbrv.	Criterion	Hole	Slits
M.E. Waddoups J.R. Eisenmann B.E. Kaminski	3	WEK	LEFM	✓	✓
J.M. Whitney R.Y. Nuismer	4,5	WN	Point Stress Average Stress	✓ ✓	✓ ✓
R.F. Karlak	6	K	Point Stress	✓	-
R.B. Pipes R.C. Wetherhold J.W. Gillespie	7,8,9	PWG	Point Stress	✓	✓
J.W. Mar K.Y. Lin	10,11	ML	$N \neq 0.5$	✓	✓
C.C. Poe J.A. Sova	12,13	PS	Strain	-	✓

A highly detailed review [1,2] was deemed necessary for several reasons. First, since the models were compared with a large body of experimental data, it was felt that the reader should not have to refer to the original works in order

to understand the analyses and follow the discussion. Second, not all of the original works are equally accessible in the literature. Third, the review was also intended to serve as a point of departure for those who wish to pursue the subject matter, therefore it was designed to offer as comprehensive a coverage as possible of the current state-of-the-arts in the subject of notched strength of composite laminates.

A total of eleven of the commonly used fracture models have been reviewed, by which the notched strength of composite laminates containing circular holes and straight cracks can be predicted. The application of these models to composite laminates requires that certain parameters associated with each fracture model be known a priori, Table II. These parameters can be determined from preliminary experiments on notched laminates, and the number of tests that must be conducted depends upon the model itself and the level of accuracy required. Consequently, these models can be considered as semi-empirical fracture models, and it should be expected that they would all compare favorably with the actual experimental results. The only model that might be applied without preliminary testing is the PS-fracture model, and then only providing that the "general fracture toughness parameter" can in fact be considered sufficiently general as to be common to all laminate configurations.

Most of the models (WEK, WN, K and PWG fracture models) are based upon determination of a characteristic distance ahead of the notch tip at failure. The issue of whether or not this parameter is a material constant has been addressed in detail by each of these investigators and by numerous other experimental investigations as well. Exhaustive studies have been conducted in regard to this subject.

The first two models (WEK and WN) assumed that this parameter is a material constant, and Whitney and Nuismer even hypothesized that it might be independent of material system and/or laminate configuration. Several experimental investigations subsequently attempted to apply the values of the characteristic distances determined

TABLE II. SUMMARY OF PARAMETERS ASSOCIATED WITH THE FRACTURE MODELS

Fracture	Criterion	Parameters		No. of Tests Required[a]
		Hole	Crack	
WEK	LEFM	a_c	a_c	2
WN	Point Stress	d_o[b]	d_o	2
	Average Stress	a_o[b]	a_o	2
K	Point Stress	k_o[b]	-	2
PWG	Point Stress	m,C[b]	m,K	3
ML	$n \neq -0.5$	n,H_C	n,H_C	2
PS	Strain	-	ε_{tuf}[b]	-

(a) Includes unnotched strength.

(b) Lamina elastic properties are required.

by Whitney and Nuismer for certain material systems to the experimental data of different material systems and laminate configurations, however with mixed results. The correlation between the fracture models and the experimental notched strength data reviewed in this study demonstrate that the characteristic distances do depend strongly on material system and laminate configuration and possibly on other parameters as well, such as loading procedures, environment, fabrication procedures, etc. However, for a given type of laminate and test conditions, most if not all of the experimental results indicate that the notched strength can be predicted assuming that these characteristic distances are independent of notch size.

Several investigators, however, have concluded that the characteristic distances cannot even be considered as independent of notch size. Consequently, the WN-fracture models ("point-stress" criterion) have been modified and an exponential relationship between the characteristic distances and the notch size has been proposed (K and PWG-fracture models). This assumption led to the introduction of two additional parameters, i.e., the notch sensitivity factor and an exponential

parameter which are also to be determined empirically. It may be suggested that these are material parameters, however, they also vary significantly for different material systems and laminate configurations. When the pertinent parameters are determined from preliminary testing, these proposed fracture models compare favorably with all experimental results. No attempt has yet been made to generalize these parameters for all types of materials. Instead, a relative notch sensitivity parameter has been introduced (PWG-fracture model) which depends directly on the notch sensitivity factor and the exponential parameter, and from which the relative notch sensitivity of any given laminate can be determined.

A fracture model which does not take into account such characteristic distance ahead of the notch tip has been proposed as well. This model (ML-fracture model) developed an exponential relationship between the notched strength and the size of the discontinuity. The exponential parameter in this model can be determined analytically, depending only on the constituent elastic properties; however, experimental results indicate that it may also depend on the laminate configuration and stacking sequence. Therefore, when this model is applied the exponential parameter is also determined experimentally from testing of notched laminates.

Clearly, all these models should agree with the experimental results, however, the dependence of the various parameters on the type of laminate is of interest. In this study, therefore, all these models were compared with a large volume of notched strength data and conclusions regarding the range of their applicability are discussed in [1,2] and summarized below.

Finally, it should be emphasized that in the formulation of the fracture models it was suggested that they be applied only to the case of laminates subjected to uniaxial loading. Also, the application of the models should be restricted to laminates which exhibit essentially linear stress-strain curves, e.g. [5], and that notch tip damage zone size should be small, e.g. [12,13], relative to notch length. However, due to the curve fitting procedure employed with all the models reviewed it is not surprising that they could all be fit with all sets of experimental data. The

graphite/epoxy $[0]_6$ and $[90]_4$ lay-ups were the only exception. Consequently, in the various comparisons and correlations discussed in the following sections, all laminate configuration and material systems were compared and correlated with these models.

9.4 Factors Affecting Notch Sensitivity

It is well established that the fracture behavior of composite laminates depends on a variety of intrinsic and extrinsic variables. Among the former are lamiante configuration, stacking sequence, constituent properties, fiber volume fracture, fiber-matrix interface characteristics, fabrication procedure, etc., and all may affect to varying degrees the fracture behavior of the subject laminate. The most important extrinsic parameters affecting the notch sensitivity are specimen geometry, shape of discontinuity, test temperature, moisture content, loading function and history, loading rate, etc. A comprehensive evaluation is still lacking regarding the effects of all these variables on the notch sensitivity of composite laminates. Because of the very complex nature of the subject matter, most of the investigations have studied the fracture behavior and notched strength under very specific intrinsic and extrinsic parameters. The only exceptions were the experimental data published for graphite/epoxy in Refs. [14-18]* where comprehensive experimental programs were conducted under seemingly identical loading and environmental conditions with the same constituents and fabrication procedures, the same procedure of specimen preparation, etc., and in which the only variables were the lamination angles and stacking sequences.

* The authors are indebted to P. A. Lagace of the Department of Aeronautics and Astronautics, Massachusetts Institute of Technology, for providing us with the data generated at the Technology Laboratory for Advanced Composites, MIT.

There is sufficient evidence that any or all of the variables mentioned above may affect the fracture behavior and notch sensitivity of composite laminates. In addition to the effect of stacking sequence, e.g. [6,19], the effect of constituents, varying fiber and matrix, may improve the material toughness [20-22] and therefore the notch sensitivity. The effect of matrix toughness on impact damage and post-impact residual (i.e. notched) strength was studied extensively in [23-26]. In Ref. [23], for example, twenty-four different matrices (all with identical graphite fibers) were examined, demonstrating that a proper choice of resin can improve the susceptibility to impact damage and improve the fracture toughness of the composite laminate. The use of hybrid laminates has also been studied extensively in recent years. Most of the results indicate that hybrid systems have higher fracture toughness than all-graphite laminates, e.g. [27], without necessarily sacrificing structural efficiency. The effects of fabrication procedure has been addressed primarily for metal-matrix composites, and was found to have significant effect on the notch sensitivity, e.g. [7,28]. Since most of the composite laminates are highly notch sensitive, which limits their utilization in several important structural applications, it seems that the effects of as many intrinsic and extrinsic variables as possible should be examined further.

Despite the recognized importance of these variables on the notch sensitivity of composite laminates, it is worth noting here that in most studies key information such as fiber volume fraction (except metal-matrix composites), constituent (fibers) properties, fabrication procedures, environmental test conditions, etc. are not reported. Consequently, unnotched and notched strength data may vary significantly among different publications even for seemingly identical laminate configurations and material systems. Thus, any comparison of notch sensitivity among different laminates obtained from different sources is of questionable value.

In the studies on the notch sensitivity of composite laminates, attention has been placed primarily on the notched strength of the subject laminate. Relatively

very few works attempted to correlate the fracture behavior with notch tip damage progression and the failure processes prior to catastrophic fracture. The limited efforts in this latter area were directed primarily toward X-ray radiography, thermography (graphite/epoxy) and brittle coating (boron/aluminum). Since the applicability of the fracture models reviewed depends on the failure process, e.g. delamination, splitting, size of damage zone, etc. this issue also deserves additional attention. It seems that additional research on the applicability of various available non-destructive examinations (e.g. ultrasonics, acoustic emission, on-line X-ray radiography, etc.) is warranated as well for determining the fracture behavior and damage criticality of composite laminates. Also, it seems that more detailed studies on the failure process, both on the micro and macro scales, will aid in better understanding the major factors affecting the notch sensitivity of a given material system.

9.5 Comparison Between the Fracture Models and Experimental Results

The fracture models reviewed have each been compared with all the sets of experimental notched strength data reviewed. These comparisons* clearly established an excellent agreement between predictions and experiments. Consequently, when all models are compared with each other they should all yield similar predictions. Such a comparison is shown in Figure 1 for a given set of notched strength data for boron/aluminum laminates containing a circular hole and a straight crack. Considering the curve fitting procedure employed it is not surprising that they all agree with the experimental data and with each other.

The application of the different fracture models to composite laminates requires that certain parameters associated with each fracture model be known a priori. These parameters can be determined from preliminary testing on notched laminates, and the number of tests that must be conducted depends upon the model itself and the level of

---

* The actual Figures can be obtained from the Principal Investigator upon request.

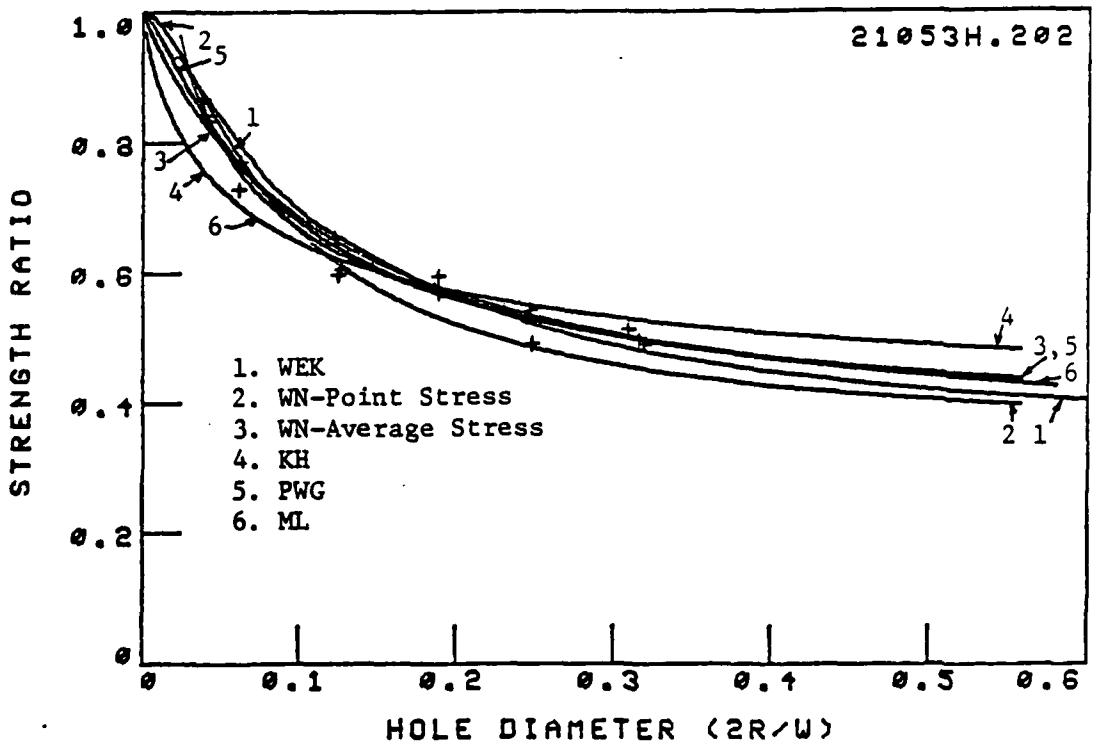

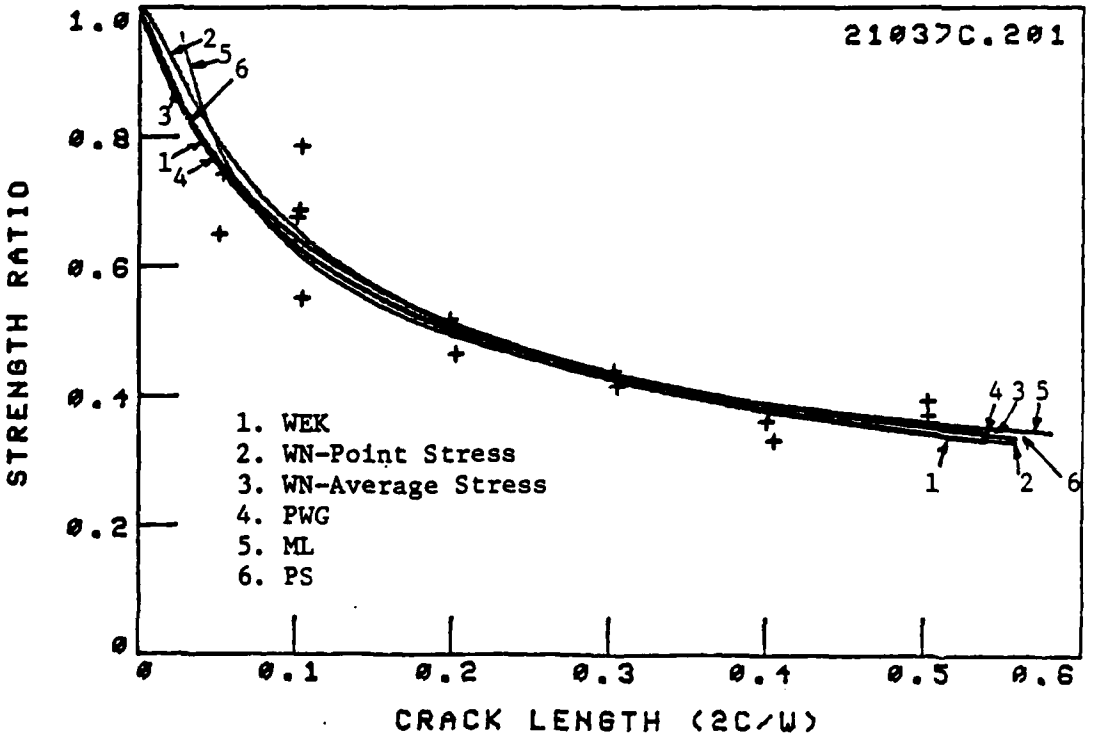

Figure 1. Comparison among the various fracture models reviewed with boron/aluminum laminates containing: a. a circular hole, $[\pm 45/0_2]_s$, b. a center crack, $[0/90]_{2s}$.

accuracy required. Generally, a minimum 2-3 specimens must be tested: one test to determine the unnotched strength and one to two tests with notched specimens, having different notch sizes, to determine the parameters listed in Table II. In the comparisons between predictions and experiments performed here, the different parameters obtained have been determined using the complete set of notched strength data reported for each investigation. Error analyses resulted in values for these parameters that yield the best fit between predictions and experiments. This procedure led to a more accurate determination of the various parameters and, in turn, to an exceelent agreement between predicted notched strength and the experimental results. For all cases in which the effective elastic moduli are necessary for applying a specific fracture model, they have been calculated based upon the lamina properties rather than by using the experimental data. This procedure has been adopted for the sake of consistency since not all publications report this information or else they report only selected moduli.

As mentioned previously, the various parameters associated with the different fracture models to depend upon laminate configuration, material system, etc. An example is shown in Table III in which the characteristic dimensions d_o and a_o of WN-fracture models are listed for all laminates and material systems analyzed in this study.* Clearly, these two parameters vary significantly with ply orientation, material system, etc.

The effect of other intrinsic material variables on the notch sensitivity is manifested by the significant differences among values of the characteristic dimensions for identical lay-ups obtained from different sources, suggesting significant influence of constituent properties, fiber volume fraction, fabrication procedures, etc. Because these variations in the characteristic dimensions strongly affect the

---

* Similar Tables were prepared for all other fracture models and are not shown here for reasons of space. They can be obtained from the Principal Investigator upon request.

Table III. Summary of Parameters for WN-Fracture Model, Boron/Aluminum Laminates

a. Circular Holes

File Name *	Lay-Up	σ_o [MPa]	K_T^∞	d_o [mm]	a_o [mm]
25001H.208	$[0]_8$	1013.6	3.50	1.25	3.83
21001H.256	$[0]_8$	1672.0	3.61	0.69	2.23
21004H.202	$[\pm 45]_s$	360.2	2.70	0.77	2.13
21004H.256	$[\pm 45]_s$	277.4	2.71	1.29	3.32
21012H.256	$[0/\pm 45]_s$	581.4	2.99	1.63	4.85
21052H.256	$[0_2/\pm 45]_s$	800.0	2.46	0.78	2.38
21053H.202	$[\pm 45/0_2]_s$	844.6	3.13	0.64	2.20

b. Straight Cracks

File Name *	Lay-Up	σ_o [MPa]	d_o [mm]	$K_Q^{(1)}$ [MPa$\sqrt{m}$]	a_o [mm]	$K_Q^{(2)}$ [MPa$\sqrt{m}$]
21001C.201	$[0]_8$	1313.7	0.95	101.5	4.23	107.1
21001C.204	$[0]_6$	1672.0	0.71	91.2	3.00	93.7
22001C.256	$[0]_5$	1272.6	1.06	103.9	4.74	109.8
21001C.206	$[0]_8$	1573.3	0.32	70.5	1.40	73.8
2X001C.207	$[0]_{16}$	1144.1	0.72	68.2	3.25	75.4
25001C.208	$[0]_8$	1013.6	0.60	70.2	2.51	71.8
26001C.208	$[0]_8$	1048.0	0.45	55.7	2.46	65.1
27001C.208	$[0]_8$	1454.7	0.35	68.2	1.53	71.3
21001C.209	$[0]_8$	2012.4	0.45	107.0	2.03	113.6
21H01C.201	$[0]_8$	1578.3	0.57	94.5	2.52	99.3
21L01C.201	$[0]_8$	1578.3	0.52	90.2	2.39	96.7
21001I.210	$[0]_8$	2004.8	0.42	102.5	1.88	108.9
21004C.201	$[\pm 45]_s$	171.4	0.94	13.2	4.24	14.0
21004C.204	$[\pm 45]_s$	277.4	0.76	19.2	3.28	19.9
21007C.201	$[90]_8$	105.4	2.09	12.1	10.68	13.7

Table III. Continued

File Name*	Lay-Up	σ_o [MPa]	d_o [mm]	$K_Q^{(1)}$ [MPa$\sqrt{m}$]	a_o [mm]	$K_Q^{(2)}$ [MPa$\sqrt{m}$]
21007C.206	$[90]_8$	139.3	1.61	14.0	7.83	15.5
25007C.208	$[90]_4$	104.8	4.55	17.7	29.44	22.5
27007C.208	$[90]_4$	160.0	0.49	9.8	2.66	10.3
21H07C.201	$[90]_8$	84.9	1.48	8.2	6.60	8.6
21012C.204	$[0/\pm45]_s$	581.4	1.16	49.6	5.16	52.3
2X036C.207	$[0/90]_s$	755.2	0.48	41.5	2.26	45.0
21037C.201	$[0/90]_{2s}$	684.7	0.42	35.2	1.81	37.0
21L37C.201	$[0/90]_{2s}$	678.4	0.41	34.4	1.71	35.2
21039C.201	$[0/\pm45/90]_s$	347.7	1.60	34.9	7.32	37.3
21L39C.201	$[0/\pm45/90]_s$	408.5	0.76	28.2	3.66	31.1
2X044C.207	$[0/90/\pm45]_s$	697.5	0.36	33.2	1.53	34.2
21052C.204	$[0_2/\pm45]_s$	800.0	0.65	51.1	2.96	54.6
21053C.202	$[\pm45/0_2]_s$	844.6	0.52	48.3	2.24	50.1
21053S.202	$[\pm45/0_2]_s$	844.6	0.46	45.4	2.06	48.0
21053C.204	$[\pm45/0_2]_s$	910.5	0.54	53.0	2.26	54.2
21058C.201	$[0/\pm45/0]_s$	774.8	0.61	48.0	2.68	50.3
21L58C.201	$[0/\pm45/0]_s$	814.0	0.50	45.6	2.37	49.7
21060C.206	$[0/\pm22]_s$	1283.2	0.38	62.7	1.74	67.1
21060I.206	$[0/\pm22]_s$	1283.2	0.38	62.7	1.62	64.7
21061C.206	$[90/\pm68]_s$	187.5	0.73	12.7	3.20	13.3
21061I.206	$[90/\pm68]_s$	187.5	1.48	18.1	8.54	21.7
21062C.203	$[0/\pm22/0]_s$	1335.3	0.26	54.0	1.10	55.5

* Each set of notched strength data collected from the literature was assigned a number for the purpose of storing the data in the computer data bank in the form of data files. This number, or File Name, is comprised of nine digits which represent five types of information, namely: material system, test temperature, lay-up, shape of discontinuity and reference source. Details are given in Ref. [1]. This File Name appears in all Figures in this Section and Section X in the upper right corner (for a single set of data) or in tabular form (when comparison between several sets of data is made).

the notch sensitivity predictions for a given laminate, the applicability of a given fracture model parameter is restricted to the specific laminate for which it has been determined.

For illustrating this issue, Figure 2 shows a representative notched strength data for a boron/aluminum laminate containing a center crack. These data are compared with the WN-fracture model using relatively small and large values of d_o and a_o within the range of values determined from the different sets of experimental notched strength data reviewed, and also those values which best fit the experiments. The best fit of the characteristic dimensions have intermediate values. The comparison clearly indicates the degree of error which can result by choosing arbitrary values for d_o and a_o and applying them to all laminate configurations, material systems, shapes of discontinuity, etc. In summary, values determined for previous data are not sufficiently reliable, even for identical laminates. However, when the parameters are determined individually for each new data set, the fracture model prediction agrees very well with experiments, e.g. Figure 1.

The previous discussion applied the WN-fracture model for the purpose of illustration. However, the conclusions mentioned above apply to all other fracture models as well.

Finally, the issue of scatter in strength of composite laminates has been of concern and this subject has received significant attention in the research and application studies during the past decade. Although the fracture models call for only 2-3 tests in order to determine their associated parameters, scatter in unnotched and notched strength should be kept in mind when any of the fracture models are applied. Since larger scatter is expected for small notch sizes it seems most appropriate that the preliminary tests be carried out with specimens having a relatively large notch size-to-width ratio, e.g. 0.3. With such notch size the error in determining the fracture model parameter is somewhat reduced as illustrated

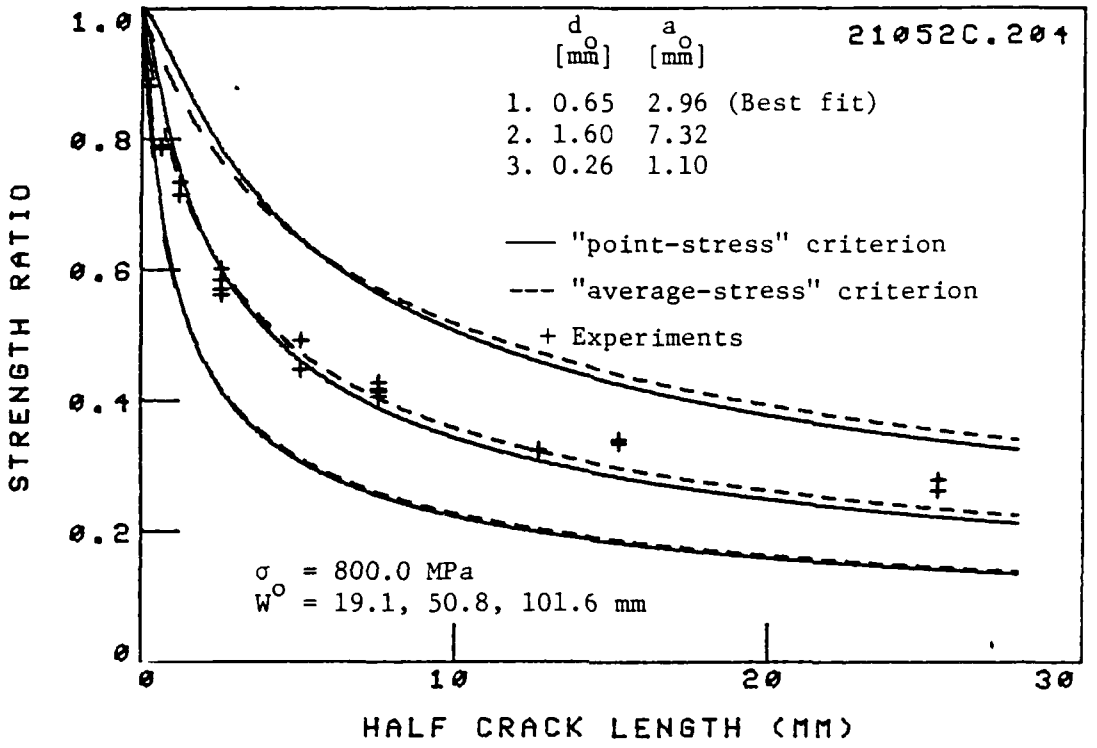

Figure 2. Effect of the characteristic dimensions (WN-fracture model) on notched strength of a boron/aluminum $[0_2/\pm45]_s$ laminate containing a center crack.

in Figure 3. The experimental results are shown for boron/aluminum $[0/90]_{2s}$ laminate containing a center crack according to the WN-fracture model, "point-stress" criterion, where the slope is the value of d_o. The solid and dashed lines represent the best fit using the absolute error minimization and linear regression procedures, respectively, in which all notched strength data in the given data set have been used. The dash-dot and long/short dash lines represent the values of d_o determined from the smallest and medium crack sizes. The error invoked by using the smallest crack size is significant, as can be clearly seen by comparing the notched strength prediction using all four data reduction procedures, Figure 3. Note that when a large number of notched strength data is available, both error analysis procedures yield similar results. Based on this discussion

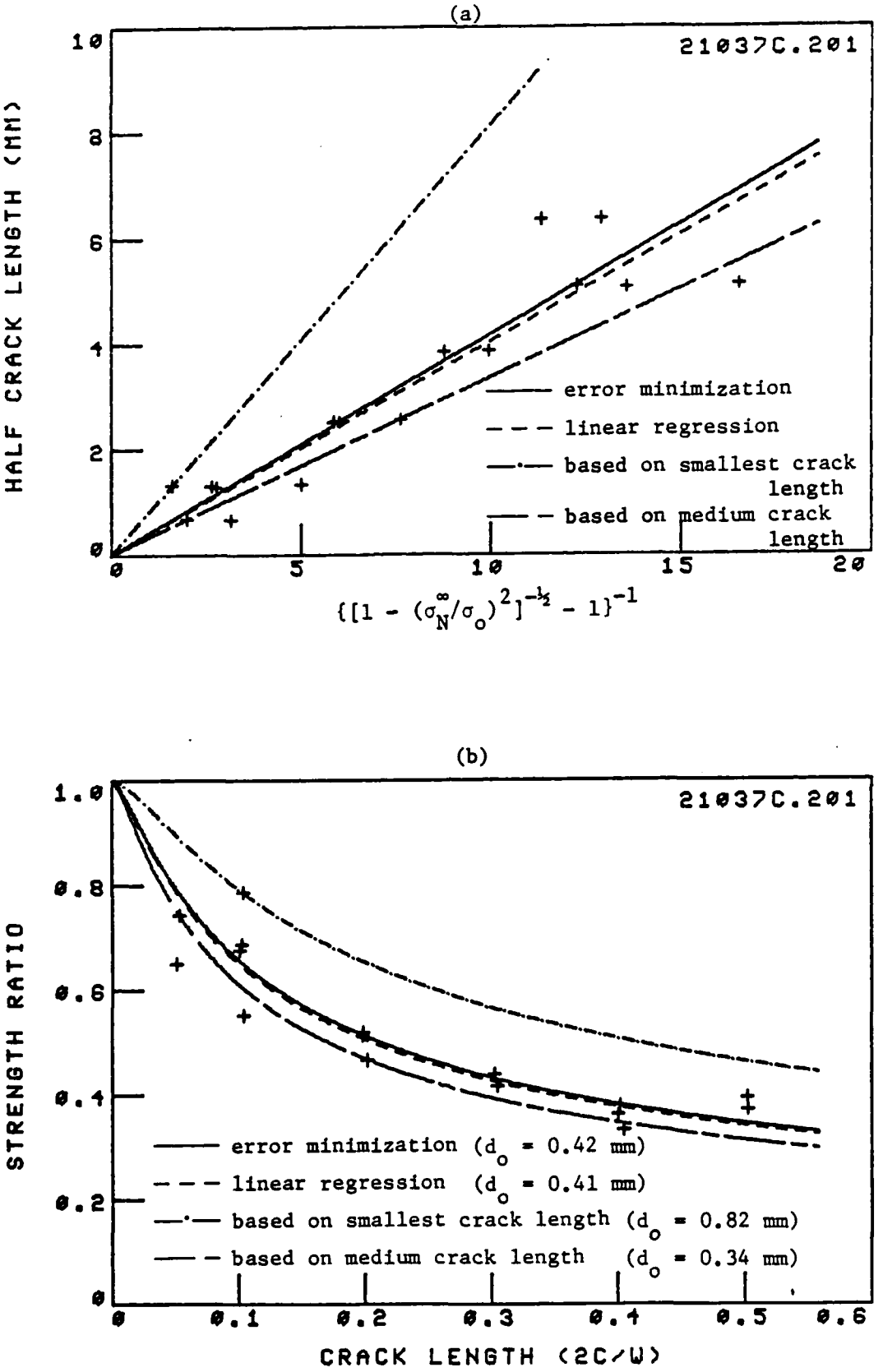

Figure 3. Effect of scatter and test procedure in determining the characteristic distance, d_o, (WN-fracture model, "point-stress" criterion) for boron/aluminum laminate: a. characteristic distance (slope of lines); b. notched strength predictions.

the parameters associated with the various fracture models, Table II, were determined using the complete set of notched strength data for each laminate. The correlation among these parameters and notch sensitivity of composite laminates is discussed in detail in [1,2], a brief discussion of which is given below.

9.6 Correlation Between Notch Sensitivity and Fracture Model Parameters

The different fracture models reviewed in this study utilize a variety of parameters associated with each model and which must be determined experimentally. In all the models it is assumed that these parameters are constant, i.e. independent of notch size, and are to be considered as material parameters. It is of interest to identify which of these parameters can be correlated to the notch sensitivity of composite laminates containing circular holes and straight cracks. For this purpose, the ratio of notched to unnotched strength (σ_N^∞/σ_o) at various notch sizes has been recorded from all the data analyzed, e.g. Table IV, and it has been correlated with the various parameters associated with the different fracture models. The specific notch size for which the σ_N^∞/σ_o is correlated with the various parameters are: $2R/W = 0.23\text{-}0.27$ for laminates containing a circular hole; and $2c/W = 0.28\text{-}0.32$ for laminates containing a straight crack.* The correlation between the strength ratio, σ_N^∞/σ_o, and several of the parameters is shown in Figure 4. Each point in these Figures corresponds to a different set of notched strength data such as those shown in Table IV. In other words, the values of σ_N^∞/σ_o for a specific notch size, i.e. $2R/W = 0.25$ and $2c/W = 0.3$) were plotted against the values of the different parameters determined for the given set of data, e.g. Table IV. If more than one notched strength data was available for the preselected notch size ($2R/W = 0.25 \pm 0.2$, $2c/W = 0.3 \pm 0.2$) the average value of σ_N^∞/σ_o for that notch size was plotted. This

*The reason for choosing a range (± 0.2) of notch size is two fold: First, in order to establish the correlation for as many data as are available and second, the reported values of notch size are usually rounded off. Also, the notch edge roughness due to machining should be taken into account.

Table IV. Experimental Notched Strength Data

Material: Boron/Aluminum 5.6/6061

Lay-Up: $[0/90]_{2s}$

Ref. [29]

File Name: 21037C.201

2c [mm]	2c/W	Strength [MPa]	Strength Ratio
0.00	0.00	709.4	1.036
0.00	0.00	679.8	0.993
0.00	0.00	664.8	0.971
1.36	0.05	509.2	0.744
1.32	0.05	445.2	0.650
2.64	0.10	538.5	0.786
2.56	0.10	463.6	0.677
2.61	0.10	470.7	0.687
2.67	0.10	377.8	0.552
5.14	0.20	319.6	0.467
5.04	0.20	352.0	0.514
5.05	0.20	355.7	0.520
7.75	0.31	285.6	0.417
7.69	0.30	301.5	0.440
10.26	0.40	228.0	0.333
10.16	0.40	249.3	0.364
10.20	0.40	260.7	0.381
12.76	0.50	255.0	0.372
12.74	0.50	270.1	0.394

Fracture Model Parameters:

WEK: a_c = 0.85 mm, K_{IC} = 35.4 MPa $\sqrt{m}$

WN: d_o = 0.41 mm, K_Q = 34.4 MPa $\sqrt{m}$

a_o = 1.71 mm, K_Q = 35.2 MPa $\sqrt{m}$

PWG: m = 0.113, K = 1.91, a_m = 1.77, a_K = 22.68, $\hat{a}_{Km}$ = 62.83

ML: n = 0.286, H_C/σ_o = 0.772 $[(mm)^n]$

PS: Q_C = 5.05 10^{-3} $\sqrt{mm}$, K_Q = 36.68 MPa $\sqrt{m}$

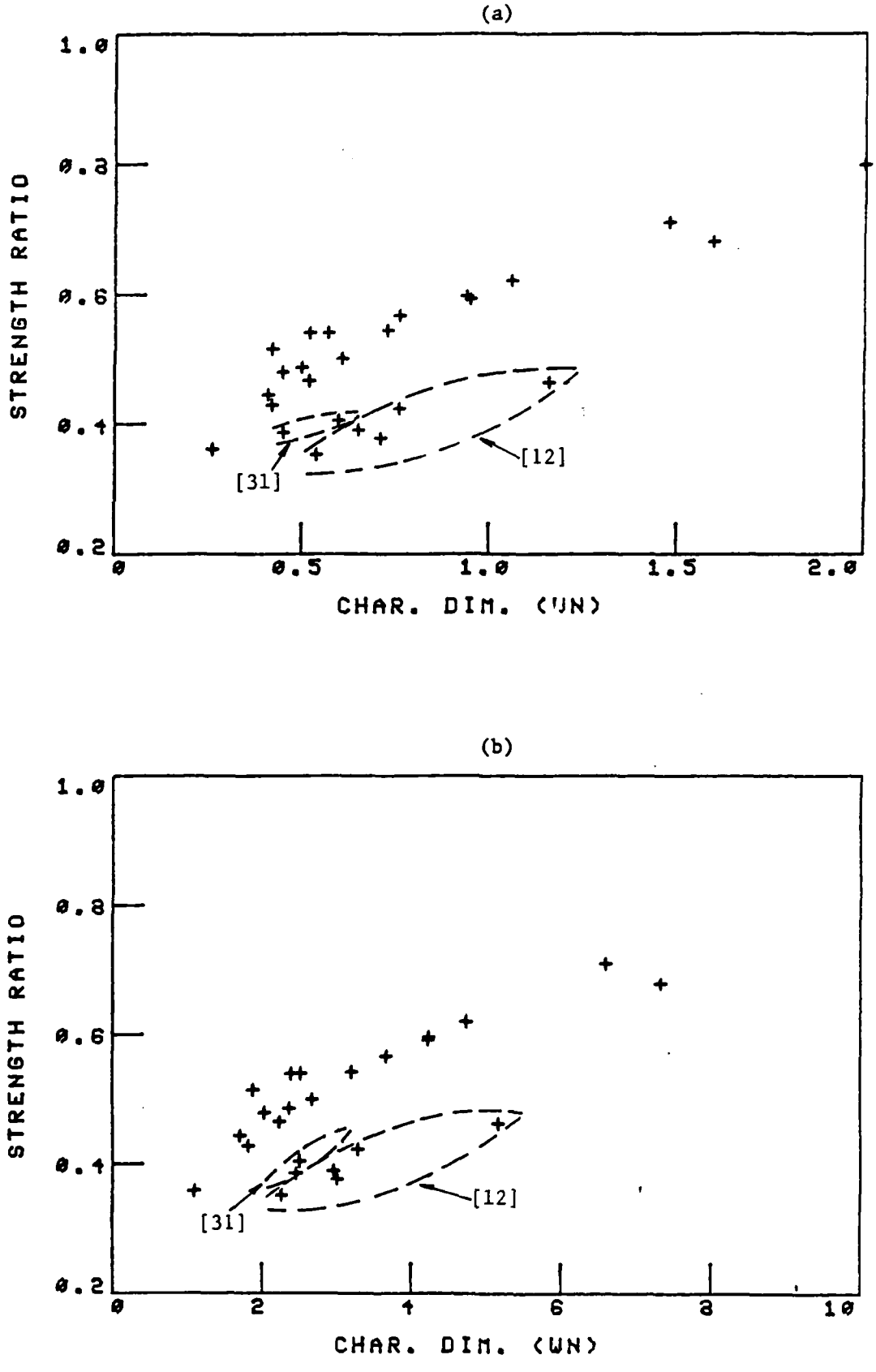

Figure 4. Correlation between notched strength ratio and the characteristic dimension (WN-fracture model) for boron/aluminum laminates containing a center crack, 2c/W = 0.3: a. d_o ("point-stress" criterion); b. a_o ("average-stress" criterion).

correlation was plotted for all the data sets. Thus, the "point plots" shown in Figure 4 lump all data for all material systems and laminate configurations irrespective of lay-up, stacking sequence, etc. Consequently, significant scatter exists in the values of all the parameters, and it is emphasized that conclusions regarding the presence or absence of correlation can only be qualitative, i.e. restricted to the specific specimen geometry, loading function, etc. which are analyzed in this study. No definitive conclusions can be drawn without additional data on all the different laminates.

The results indicate that the notch sensitivity of composite laminates can be correlated with the characteristic dimensions, d_o and a_o, of the WN-fracture models, e.g. Figure 4. The larger the values of the characteristic dimensions are, the less notch sensitive is the subject laminate, which is as expected from the analytical formulations of the WN-fracture models. The few exceptions are for the data depicted from Refs. [12] and [31] as indicated in Figure 4. The values of a_o & d_o for the laminates tested in [17] are based on approximately 20 notched strength data for each laminate. However, the data were obtained from three different specimen widths, 19.1 mm, 50.8 mm and 101.6 mm. It is possible therefore that lumping all notched strength data of the different laminate widths is the cause for this discrepancy. A more detailed discussion on the width effect is given in Section 10.3.6. The data given in [31] are for 4.2 mil borsic/aluminum which is a different system from the 5.6 mil boron/aluminum laminates tested in most other sets of data.

Similar correlation has been established for the WEK-fracture model as well, i.e. the characteristic dimensions, a_c, can be inversely correlated with the notch sensitivity. On the other hand, no correlation could be established between any of the other fracture model parameters and notch sensitivity.

A parameter commonly used to represent the notch sensitivity of materials is the critical stress intensity factor (S.I.F.) i.e. fracture toughness, K_Q. The critical S.I.F. is considered as a material parameter. Numerous investigations

determined K_Q values for a variety of composite laminates, primarily for comparison with structural metals. Emphasis has also been placed on accounting for the effect of laminate configuration, stacking sequence, specimen geometry and dimensions, notch length, etc. on K_Q. The question still remains, however, whether the critical S.I.F. actually represents the notch sensitivity of the subject material. The results shown in Figure 5 using the WEK-fracture model and the "average-stress" criterion of the WN-fracture model indicate that no correlation could be established between the critical S.I.F. and the notch sensitivity of the various boron/aluminum laminates. No correlation could be found for graphite/epoxy laminates either. Similar results were obtained using both the "point-stress" criterion of the WN-fracture model and the PS-fracture model. In other words, the actual value of the critical S.I.F. for a given composite laminate cannot serve as an indicator of the relative notch sensitivity of that laminate.

The lack of correlation between notch sensitivity (i.e. σ_N^∞/σ_o) and the critical S.I.F. is expected for composite laminates. First, there is a direct correlation between the critical S.I.F. and the laminate's unnotched strength, i.e. the higher the laminate's strength, the higher the critical S.I.F., e.g. [4,5]. Second, fracture toughness is strongly affected by the extent of damage and failure modes at the notch tip, and both fracture toughness and unnotched strength are affected by laminate configuration, constituents' properties, etc. A detailed study into the effects of type and extent of damage, lay-up, and constituents on the fracture toughness of graphite/epoxy laminates is given in [30].

9.7 Conclusions

Several of the commonly used semi-empirical fracture models proposed to predict the notched strength of composites have been critically reviewed. Emphasis has been placed on simplified, easy to operate predictive tools. Experimental results were also reviewed and compared with all fracture models. The various

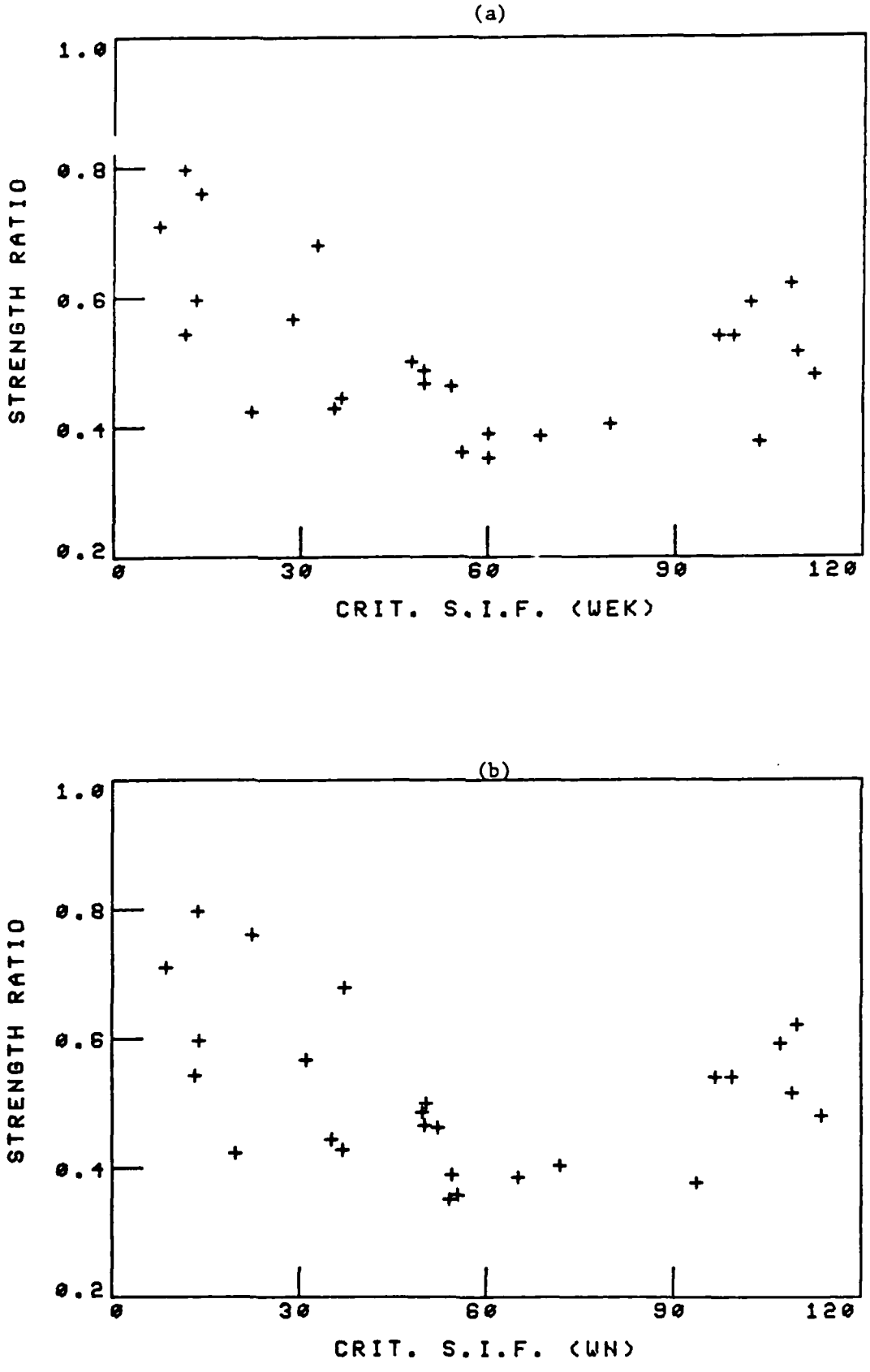

Figure 5. Correlation between notched strength ratio and critical stress intensity factor for boron/aluminum laminates containing a center crack: a. K_{IC}, WEK-fracture model; b. K_Q, "point-stress" criterion, WN-fracture model.

parameters associated with the fracture models were determined for all experimental data sets reviewed. Notch strength data for graphite/epoxy, boron/aluminum and graphite/polyimide laminates were analyzed and the effect of intrinsic and extrinsic variables on the notch sensitivity of the subject laminate were discussed. The fracture model parameters were correlated with the notch sensitivity of composite laminates and their applicability as a measure of notch sensitivity has been evaluated. Based on this extensive review, the following major conclusions could be drawn:

9.7.1 Fracture Models

1. Very good agreement between all fracture models reviewed and all experimental notched strength data can be established provided that the parameters are properly determined.

2. The fracture models are all semi-empirical, i.e. they can be applied theoretically providing that 1-2 (depending upon the fracture model) notched strength data are known a priori, including the unnotched strength and lamina elastic properties.

3. The fracture models include certain parameters which are assumed to be material constants, i.e. independent of specimen geometry.

4. These parameters strongly depend on laminate configuration and material system and on the variety of intrinsic and extrinsic variables.

5. Consequently, these parameters must be determined (experimentally) for each new material system, laminate configuration, etc. independently.

6. The actual number of tests that must be conducted in determining the fracture model parameters depends upon the level of accuracy required and the degree of inherent scatter in properties of the subject laminate.

7. In the fracture models reviewed the actual characteristics of the notch tip damage zone are by-passed by simulating the damage zone as some "effective" notch tip damage zone and assuming it to grow in a self-similar manner.

8. When the characteristic dimensions (WEK and WN fracture models) are assumed independent of notch length an excellent agreement between experiments and predictions has been established. In most cases, these characteristic dimensions are in fact independent of notch length or exhibit only a slight increase with notch length.

9. When the characteristic dimensions are assumed to be dependent on notch length (K and PWG fracture models) a better agreement between experiments and prediction has been established for those cases where the characteristic dimension increases with notch length. However, this assumption of dependency requires additional parameters and consequently additional preliminary tests to determine the relationship between the characteristic dimension and notch size.

10. The assumption that the order of singularity at the notch tip is different than $-\frac{1}{2}$ (ML-fracture model) also yields very good agreement between experiments and prediction. However, the order of singularity and the "composite fracture toughness" have to be determined experimentally.

11. The strain failure criterion (PS-fracture model) proposed a "general fracture-toughness parameter", applicable for all laminates containing the same fiber. This parameter can be applied provided that crack tip damage is localized. Additional investigation on its further applicability is warranted. However, when it is determined individually for each laminate excellent agreement with experiments has been established.

12. All fracture models reviewed provide for predictions which are, for all practical purposes, identical. Consequently, the choice of any particular model will result in comparable prediction of notched strength.

9.7.2 Experimental Results

1. Practically all laminates reviewed are highly notch sensitive. For many cases the notch strength reduces by as much as 50% for notch-length-to-width ratio of 0.2-0.3.

2. Most of the experimental studies on notched strength of composite laminates are limited to the two types of notch geometry: circular holes and straight cracks, centrally located, and subjected to uniaxial quasi-static loading.

3. The review clearly indicates that notch sensitivity of composite laminates may be affected by a variety of intrinsic (laminate configuration, stacking sequence, constituent properties, fiber volume fraction, fiber-matrix interface, fabrication procedures, etc.) and extrinsic (specimen geometry, test temperature, moisture content, loading function, rate and history, etc.) variables.

4. However, a comprehensive evaluation of the effects of these variables on the notch sensitivity of composite laminates is still lacking.

5. Also, any comparison among the notch sensitivities of different laminates obtained from different sources is of questionable value, because very few publications report fiber volume fraction, constituent (fiber) properties, fabrication conditions, environmental test conditions, etc. all of which may affect the results.

6. Very few works attempt to correlate the recorded notch sensitivity with the actual failure process and failure modes at the notch tip prior to catastrophic fracture.

7. Since the applicability of the fracture models reviewed depends on the failure processes, e.g. delamination, splitting, size of damage zone, etc. additional attention to this issue is warranted.

8. Most laminates reviewed do not exhibit a notch insensitive region, i.e. strength drops sharply with the introduction of the smallest discontinuity.

9. Among the various parameters associated with the fracture models, only the characteristic dimensions of the WEK and WN-fracture models can be related to notch sensitivity, such that the larger they are the less notch sensitive the subject laminate is. It should be noted that the WN-fracture model does not apply linear elastic fracture mechanics.

10. It seems therefore that the characteristic dimensions can serve as a relative measure of notch sensitivity of composite laminates. This relationship remains qualitative, however, until there is a more precise identification of the effects of all the variables affecting notch sensitivity.

11. Since strength does drop sharply with the introduction of a small notch in almost all laminates, the "average-stress" criterion of the WN-fracture model does fit the data better in the small notch size range.

12. None of the parameters associated with the other fracture models, including the critical stress intensity factors, could be related to the notch sensitivity.

13. Although a large body of notched strength data is available in the literature only a few definite conclusions can be made regarding the effect of the many variables affecting notch sensitivity because of the varying objectives in the different investigations. A comprehensive, methodical study into the effect of all these variables is overdue.

14. There is now a growing demand for light-weight composites in "primary" structures. Consequently, a more thorough understanding is required of the way in which pertinent material, loading and environmental prameters affect strength, toughness, fracture behavior, fatigue characteristics, impact response, etc. of composite laminates.

9.8 References

1. J. Awerbuch and M. Madhukar, "Notched Strength of Composite Laminates: Predictions and Experiments - A Review", Journal of Reinforced Plastic and Composites, Vol 4, No. 1, 1985, pp. 3-160.

2. J. Awerbuch and M. Madhukar, "Notched Strength of Composite Laminates: Predictions and Experiemtns - A Review", NASA CR , 1985, (to be published).

3. M.E. Waddoups, J.R. Eisenmann and B.E. Kaminski, "Macroscopic Fracture Mechanics of Advanced Composite Materials," J. Composite Materials, Vol. 5, 1971, pp. 446-454.

4. J.M. Whitney and R.J. Nuismer, "Stress Fracture Criteria for Laminated Composites Containing Stress Concentrations", J. Composite Materials, Vol. 8, 1974, pp. 253 -265.

5. R.J. Nuismer and J.M. Whitney, "Uniaxial Failure of Composite Laminates Containing Stress Concentrations," in Fracture Mechanics of Composites, ASTM STP 593, American Society of Testing and Materials, 1975, pp. 117-142.

6. R.F. Karlak, "Hole Effects in a Related Series of Symmetrical Laminates", in Proceedings of Failure Modes in Composites, IV., The Metallurgical Society of AIME, Chicago, 1977, pp. 105-117.

7. R.B. Pipes, R.C. Wetherhold and J.W. Gillespie, Jr., "Notched Strength of Composite Materials, J. Composite Materials., Vol 12, 1979, pp. 148-160.

8. R.B. Pipes, J.W. Gillespie, Jr., and R.C. Wetherhold, "Superposition of the Notched Strength of Composite Laminates," Polymer Engineering and Science, Vol. 19, No. 16, 1979, pp. 1151-1155.

9. R.B. Pipes, R.C. Wetherhold and J.W. Gillespie, Jr., "Macroscopic Fracture of Fibrous Composites", Materials Science and Engineering, Vol. 45, 1980, pp. 247-253.

10. K.Y. Lin, "Fracture of Filamentary Composite Materials," Ph.D. Dissertation, Department of Aeronautics and Astronautics, M.I.T., Cambridge, Mass., Jan. 1976.

11. J.W. Mar and K.Y. Lin, "Fracture Mechanics Correlation for Tensile Failure of Filamentary Composites with Holes," J. of Aircraft, Vol. 14, No. 7, July 1977, pp. 703-704.

12. C.C. Poe, Jr. and J.A. Sova, "Fracture Toughness of Boron/Aluminum Laminates with Various Proportions of 0° and ±45° Plies," NASA Technical Paper 1707, November 1980.

13. C.C. Poe, Jr., "A Unified Strain Criterion for Fracture of Fibrous Composite Laminates," Engineering Fracture Mechanics, Vol. 17, No. 2., 1983, pp. 153-171.

14. P.A. Lagace, "Static Tensile Fracture of Graphite/Epoxy," Ph.D. Dissertation, Department of Aeronautics and Astronautics, M.I.T., Cambridge, Mass., June 1980.

15. J.W. Mar and P.A. Lagace, "Tensile Fracture of Graphite/Epoxy Laminates with Holes," Proceedings of the Third International Conference on Composite Materials (ICCM-III), Paris, France, 1980, pp. 130-145.

16. J.I. Garcia, "Static Tensile Behavior of $[0]_6$, $[0/\pm5]_s$, $[0/\pm10]_s$, and $[0/\pm15]_s$ Graphite/Epoxy Laminates with Holes," Technology Laboratory for Advanced Composites, M.I.T. Department of Aeronautics and Astronautics, TELAC Report-80-7, June 1980.

17. J.I. Garcia, "Fracture of $[\pm5/0]_s$, $[\pm10/0]_s$, and $[\pm15/0]_s$, Graphite/Epoxy Coupons Under Tension," Technology Laboratory for Advanced Composites, M.I.T. Department of Aeronautics and Astronautics, TELAC Report-80-9, August 1980.

18. L.N. Hugh McManus, "Failure Modes in a Family of Graphite/Epoxy Laminates," Technology Laboratory for Advanced Composites, M.I.T. Department of Aeronautics and Astronautics, TELAC Report-81-8, May 1981.

19. J.M. Whitney and R.Y. Kim, "Effect of Stacking Sequence on the Notched Strength of Composite Laminates," Air Force Materials Laboratory Technical Report, AFML-TR-76-177, November, 1977.

20. D.L. McDanels and R.A. Signorelli, "Effect of Fiber Diameter and Matrix Alloys on Impact-Resistant Boron/Aluminum Composites," NASA TN D-9204, November 1976.

21. K.M. Prewo, "Development of Impact Resistant Metal Matrix Composites", Air Force Materials Laboratory Technical Report, AFML-TR-75-216, March 1976.

22. M.G. Bader, J.E. Bailey and I. Bell, "The Effect of Matrix Interface Strength on the Impact and Fracture Properties of Carbon-Fibre-Reinforced Epoxy Resin Composites," Journal Applied Physics, 1973, pp. 572-586.

23. R.J. Palmer, "Investigation of the Effect of Resin Materials on Impact Damage to Graphite/Epoxy Composites," NASA CR-165677, March 1981.

24. J.G. Williams and M.D. Rhodes, "The Effect of Resin on the Imapct Damage Tolerance of Graphite-Epoxy Laminates", NASA TM-83213, October 1981.

25. P.E. Hertzberg, B.W. Smith and A.G. Miller, "Effect of Matrix Resin on the Impact Fracture Characteristics of Graphite-Epoxy Laminates", NASA CR-165784, January 1982.

26. D.L. McDanels and R.A. Signrelli, "Effect of Angleplying and Matrix Enhancement on Impact-Resistant Boron/Aluminum Composites," NASA TN D-8205, October 1976.

27. J.M. Kennedy, "Fracture Behavior of Hybrid Composite Laminates," AIAA/ASME/ ASCE/AHS 24th Structures, Structural Dynamics and Materials Conference, AIAA Paper No.-83-0804-CP, Lake Tahoe, Nevada, May 2-4, 1983.

28. J. Awerbuch and H.T. Hahn, "Crack-Tip Damage and Fracture Toughness of Boron/ Aluminum Composites," Journal Composite Materials, Vol. 13, 1979, pp. 82-107.

29. M. Madhukar, "Fracture Behavior of Boron/Aluminum Laminates at Room and Elevated Temperatures," Ph.D. Dissertation, Drexel University, to be published.

30. C.C. Poe, Jr., "Fracture Toughness of Fibrous Composite Materials," NASA Technical Paper 2370, November 1984.

31. K.G. Kreider, L. Dardi and K. Prewo, "Metal Matrix Composite Technology", Air Force Materials Laboratory Technical Report, AFML-TR-71-204, December, 1971.

X. NOTCH SENSITIVITY OF CENTER-NOTCHED BORON/ALUMINUM LAMINATES

10.1 Summary

As part of characterizing the fracture behavior of boron/aluminum laminates the notched strength of the subject material has been studied. In particular, effect of laminate configuration and elevated temperatures on the notch sensitivity has been addressed. For this purpose, notched strength data for all six laminates studied were obtained for temperatures ranging from 21°C (70°F) to 315°C (600°F). These data were obtained from tests on the deformation characteristics applying the IDG technique, Section IV and V, and the acoustic emission technique, Section VII. In addition, published data were collected from the open literature from which the effects of constituents, notch shape, impact damage, laminate configuration and laminate stacking sequence on the notch sensitivity of boron/aluminum laminates were determined. All data were compared with all the fracture models discussed in Section IX and the various fracture models parameters were determined.

10.2 Introduction

Based on the data obtained in this research program and the data collected from the open literature a brief discussion on the effect of material parameters, specimens and notch geometry, temperature, etc. on notch sensitivity of boron/aluminum laminates is given below. More details can be found in [1,2]. It should be emphasized however, that the effect of the various intrinsic and extrinsic variables on notch sensitivity of any composite system are highly complex, and each variable deserves a lengthy discussion of its own. The complexity of the subject matter is due to the fact that the fabrication processes, in particular for metal-matrix composites, can significantly affect the fracture behavior and notch sensitivity of the subject material. Thus, in many cases, additional research is needed before any definite assessment can be made. This Section is only intended, therefore, to provide a general overview of the relevant parameters.

In most of the Figures shown in the following discussion only the predicted notch sensitivity curves are plotted, and the actual experimental data are excluded from most Figures for the sake of clarity. Also, since an excellent agreement between predictions and experiments has been established for all the fracture models, Section IX, the "average-stress" criterion of the WN-fracture model has been chosen for the purpose of illustration. The comparison among the various sets of experimental data yield the following observations.

10.3 Results and Discussion

10.3.1 Effect of Laminate Configuration

The experimental notched strength data indicate that laminate lay-up strongly affects the notched strength and notch sensitivity of boron/aluminum laminates containing a center crack, Figure 1. While the $[0]_8$ and $[\pm 45]_{2s}$ laminates demonstrate similar notch sensitivity, multidirectional laminates may become significantly more notch sensitive as in the cases of $[0/90]_{2s}$ and $[0/\pm 45/0]_s$ laminates, Figure 1, and $[0/\pm 22/0]_s$ (not shown here), etc. There are a few exceptions such as the quasi-isotropic laminate shown in Figure 1, for which notch sensitivity is lower than in unidirectional specimens. Generally, however, a higher notch sensitivity of multidirectional laminates compared to unidirectional specimens should be expected when the characteristics of the crack tip damage zone are taken into consideration. In unidirectional composites, a longitudinal plastic shear zone is formed in the matrix at the tip of the crack. The length of this zone increases with increasing load until fibers fracture at some weak spots along their lengths. This process repeats itself several times up to failure [3]. The plastic deformation of the matrix serves as a crack arresting medium, and additional crack extension (i.e. broken fibers) alternates with the completion of successive longitudinal plastic deformation zones, resulting in a final irregular fracture surface. In multidirectional laminates, however, no longitudinal plastic deformation zones are observed, the fracture surface is fairly coplanar, and the crack tip

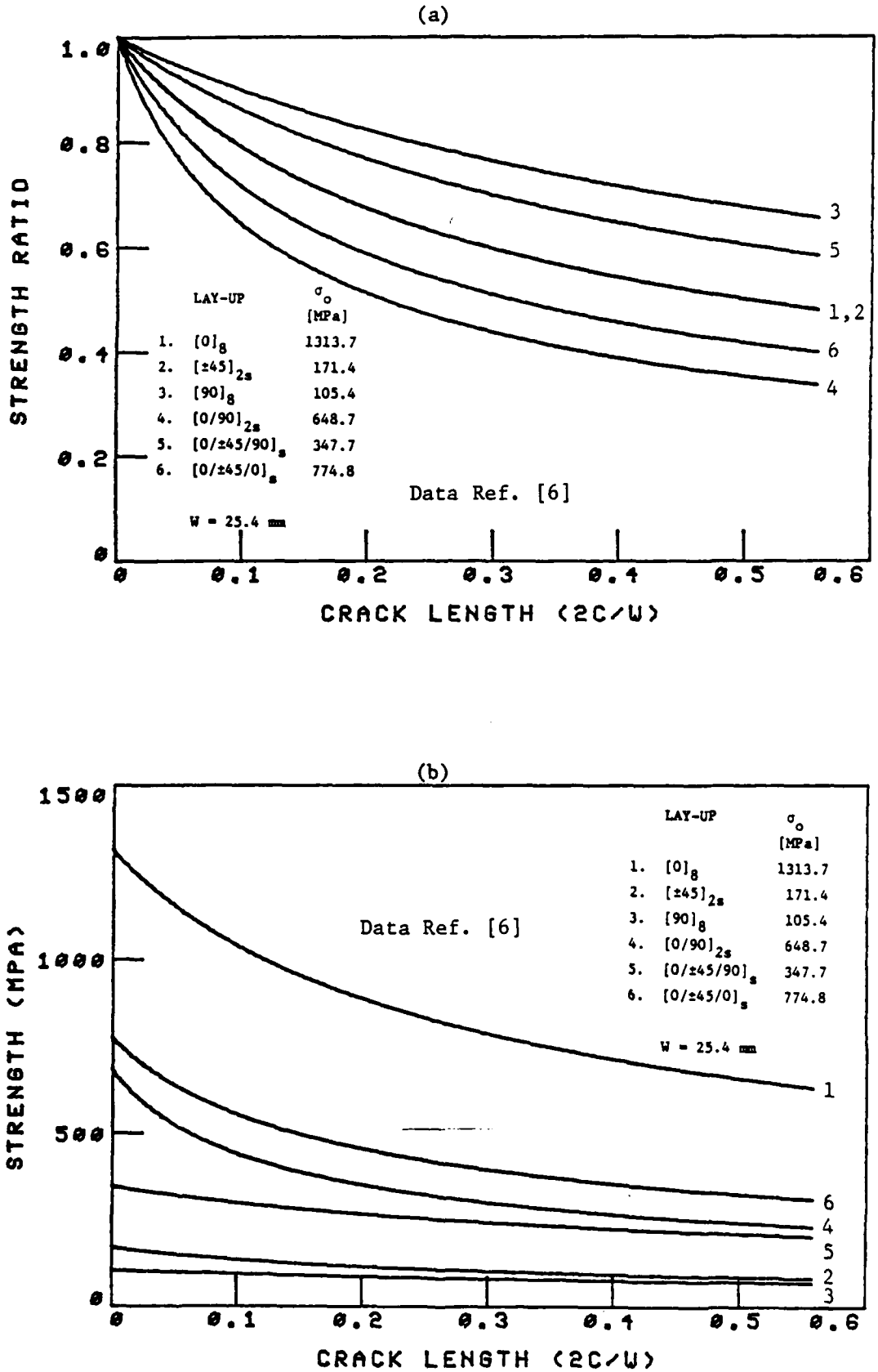

Figure 1. Notched strength versus crack length predictions (WN-fracture model, "average-stress" criterion) for several boron/aluminum laminates: a. nondimensional; b. dimensional. Laminate configuration strongly affects notch sensitivity and notched strength.

damage is fairly localized and it propagates as a nearly self-similar crack extension. The significant notch sensitivity of multidirectional boron/aluminum laminates is manifested by the unnotched strength reduction which can be as high as 20% for notch size-to-width ratios of 0.1. On the other hand, despite the significant notch sensitivity of unidirectional boron/aluminum its notched strength is still higher than the unnotched strength of either multidirectional laminate, even for notch size-to-width ratios as high as 0.4, Figure 1b.

The effect of laminate configuration on the notch sensitivity of other boron/aluminum laminates containing either a center crack or a circular hole can also be assessed from the data published in [4] and [5], respectively, Figure 2. Note that both sets of data were obtained for the same material system and laminate configurations, from the same batch of material tested at the same laboratory, i.e. NASA Langley Research Center, during the same time period. The only difference is the shape of the discontinuity. The results shown in Figure 2 indicate that laminate configuration affects the notch sensitivity of the subject material, however, the differences in notch sensitivity among the different lay-ups is not as pronounced as it is in Figure 1. Also, the interrelation between laminate configurations and notch sensitivity is different in Figure 2. The effects of fabrication procedure, constituents, notch shape, specimen width, etc., might be the cause for these differences, as discussed in this Section. In other words, no clear trend in the effect of laminate configuration on notch sensitivity can be defined at this stage.

10.3.2 Effect of Constituents

Notch sensitivity curves for four separate sets of data (including those obtained in this research program) of unidirectional boron/aluminum are shown in Figure 3. The four sets of data were obtained for a seemingly identical material system (5.6 mil - 6061F) and fiber volume fraction. However, significant differences are clearly seen in the notch sensitivity curves (and for that matter, the unnotched

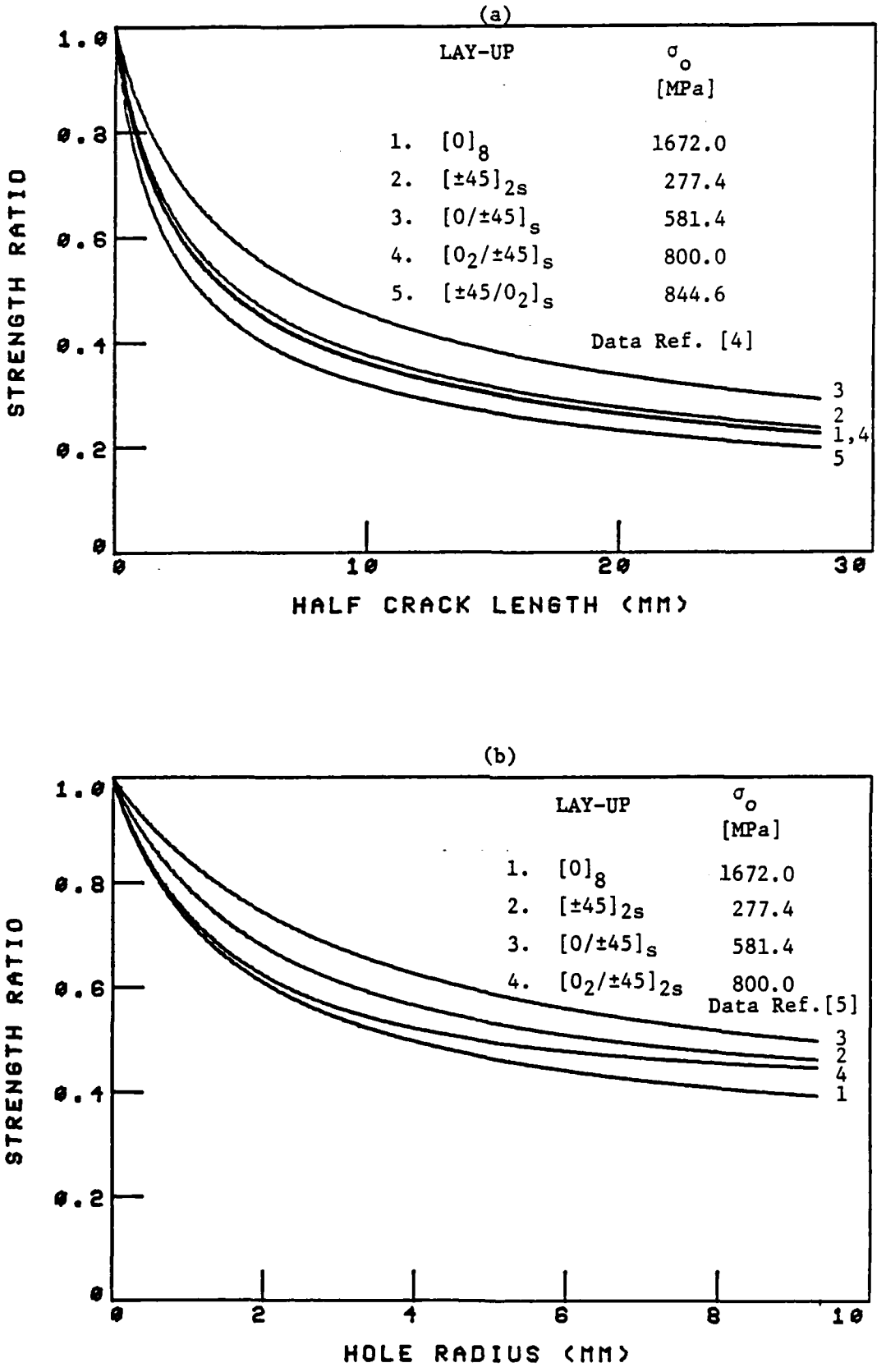

Figure 2. Notched strength versus notch length predictions (WN-fracture model, "average-stress" criterion) for several boron/aluminum laminates containing: a. a center crack; b. a circular hole. Results indicate effect of laminate configuration on notch sensitivity.

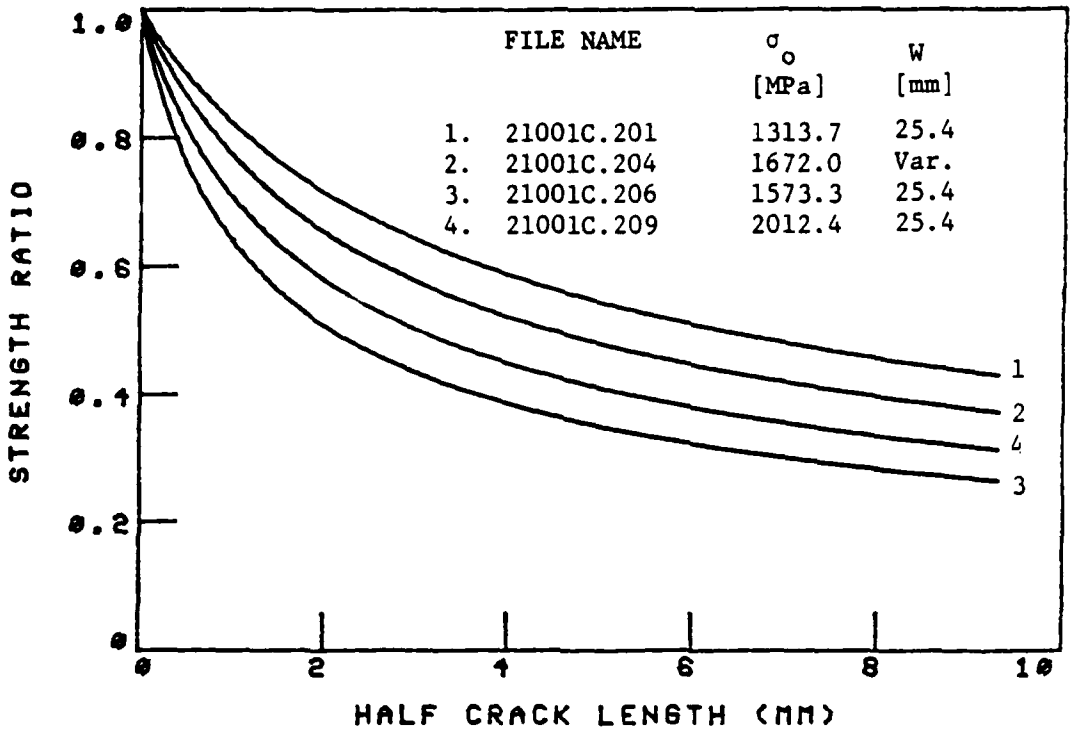

Figure 3. Notched strength versus half crack length predictions (WN-fracture model, "average-stress" criterion) for unidirectional boron/aluminum. Results indicate that constituents properties can have a significant effect on notch sensitivity.

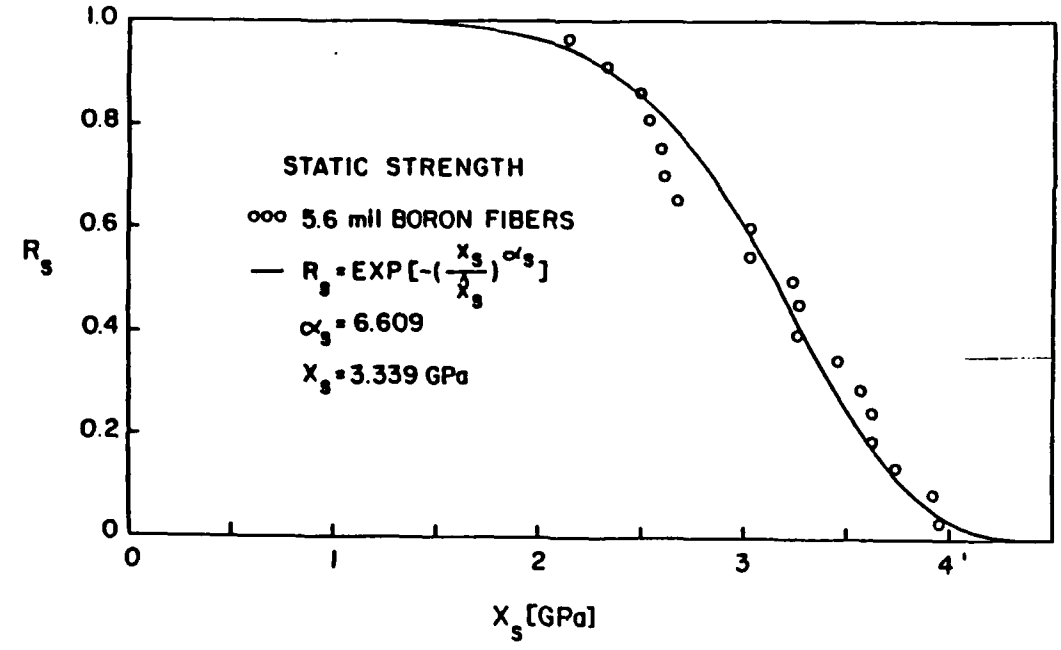

Figure 4. Static strength distribution of individual 5.6 mil diameter (140 μm) boron fibers [6], indicating significant scatter in strength.

strength as well). These differences are attributable either to different fabrication procedures or to differences in fiber strength. The former issue has been discussed in Ref. [3] showing that differences in fabrication procedure can have a significant effect on notched strength. However, the quality of fibers can also have a marked effect on the composite strength. Figure 4 shows the strength distributions of individual 5.6 mil boron fibers [6]. Clearly, significant scatter in strength has been recorded, as indicated by the relatively low Weibul shape parameter (α_s = 6.61 for 5.6 mil boron fibers obtained from 200 mm long fibers). The large scatter in strength and the relatively low characteristic strength, $\hat{X}_s$, of the 5.6 mil fibers result in similar characteristics for the unidirectional 5.6 mil boron/aluminum-6061F, i.e. α_s = 9.7, $\hat{X}_s$ = 1.4 GPa, Section VI. In summary, any meaningful comparison of strength data of boron/aluminum laminates among various investigators or among different laminate configurations, fabrication procedures, fiber volume fractions, etc. will all require precise information on the properties of the individual fibers.

Improved notch sensitivity of unidirectional boron/aluminum can be achieved through a proper choice of constituents. While most of the attention given to the mechanical behavior of boron/aluminum composites has been devoted to the 5.6 mil - 6061F system, in recent years some attention has also been given to other material systems such as 8.0 mil - 1100F, mostly for jet engine fan blade applications. For such applications, better impact resistant and less notch sensitive material systems are being sought. Charpy test results [7-9] have shown that boron/aluminum 8.0 mil - 1100F demonstrates certain advantages over the more common boron/aluminum 5.6 mil - 6061F. The choice of low shear strength matrices such as 1100 aluminum, combined with high strength fibers provide a material system capable of dissipating high levels of energy upon impact loading [8]. Limited studies have also been directed toward the use of boron/aluminum laminates [7-9], in which effect(s) of fiber diameter, type of matrix and laminate configuration on

the impact resistance of boron/aluminum laminates has been investigated. The improved notch sensitivity of boron/aluminum 8.0 mil-1100F over the 5.6 mil-6061 system is clearly seen in Figure 5. No data on multidirectional laminates of the 8.0 mil - 1100F system have been reported in the open literature. When two different aluminum alloys, e.g. 6061F and 2024F, are chosen as the matrix material, very little effect on the notch sensitivity has been recorded, Figure 6. However, heat treatment of the aluminum alloy may increase the notch sensitivity, as reported in [10] for unidirectional boron/aluminum 5.6 mil - 6061F. The annealed aluminum matrix (6061-0) is much less notch sensitive than the heat treated matrix (6061-T6), which confirms the results discussed previously regarding the use of low shear strength matrices to improve the notch sensitivity of the composite. Similar results on the effect of type of matrix and of matrix heat treatment were reported in [11-12].

10.3.3 Effect of Test Temperature

Despite the applicability of boron/aluminum composites at elevated temperatures very little data are available regarding the effect of temperature on the notch sensitivity of the subject material. Consequently, the discussion of this subject is based solely on the data obtained in this research program [6]. The results shown in Figures 7a-7b indicate that $[0]_8$ and $[0/\pm45/90]_s$ become more notch sensitive at elevated temperatures. Little if any effect of test temperature on the notch sensitivity of $[0/90]_{2s}$ and $[0/\pm45/0]_s$ (not shown here) has been recorded. The results for the $[0]_8$ are surprising, recalling from the previous discussion on the 8.0 mil - 1100F system that increased matrix ductility enhances the crack arresting mechanism that results from matrix shear deformation along the fibers. Consequently, similar behavior should be expected for the notch sensitivity at elevated temperature. Since the reverse has been recorded, Figure 5, strength degradation of the fibers should be taken into account. In summary, no definite

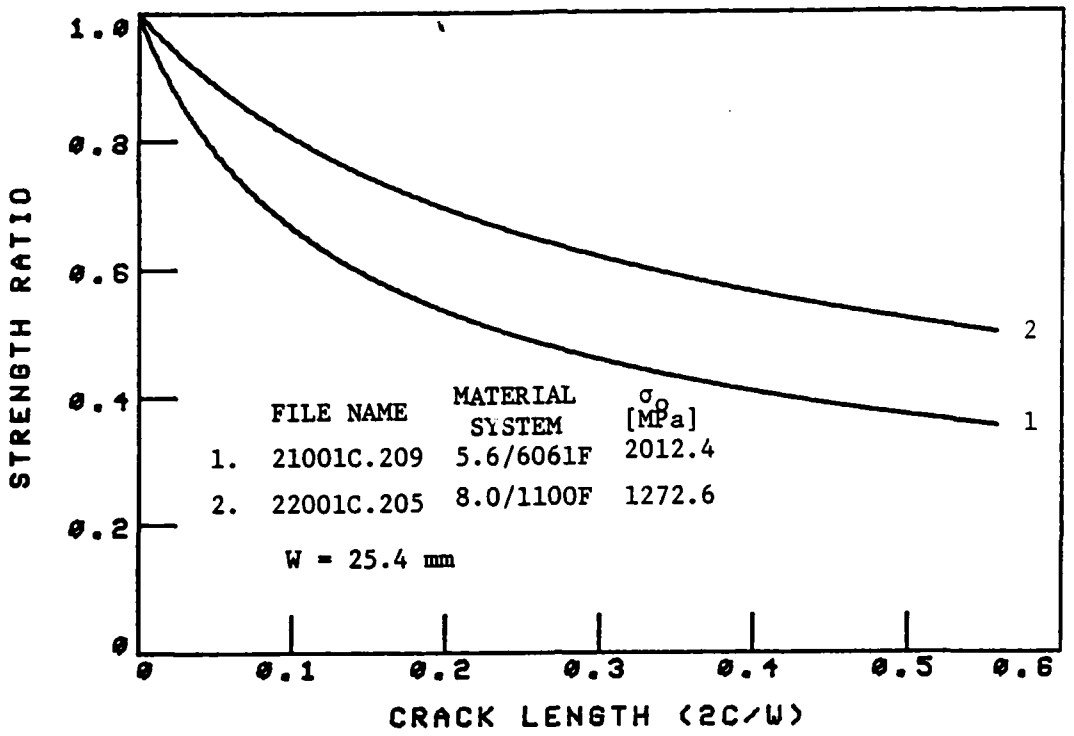

Figure 5. Notched strength versus crack length predictions (WN-fracture model, "average-stress" criterion) for unidirectional boron/aluminum with different constituents. Comparison indicates that proper selection of constituents can improve notch sensitivity.

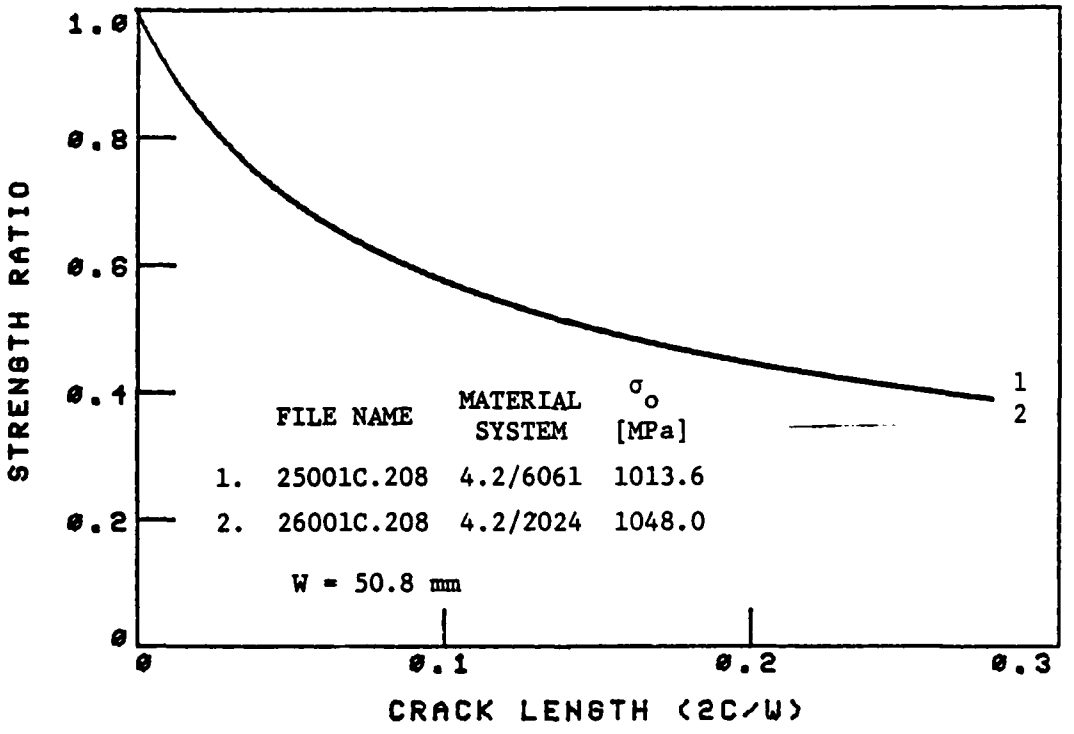

Figure 6. Notched strength versus crack length predictions (WN-fracture model, "average-stress" criterion) for unidirectional borsic/aluminum with different aluminum matrices, showing little effect of the two matrices on notch sensitivity.

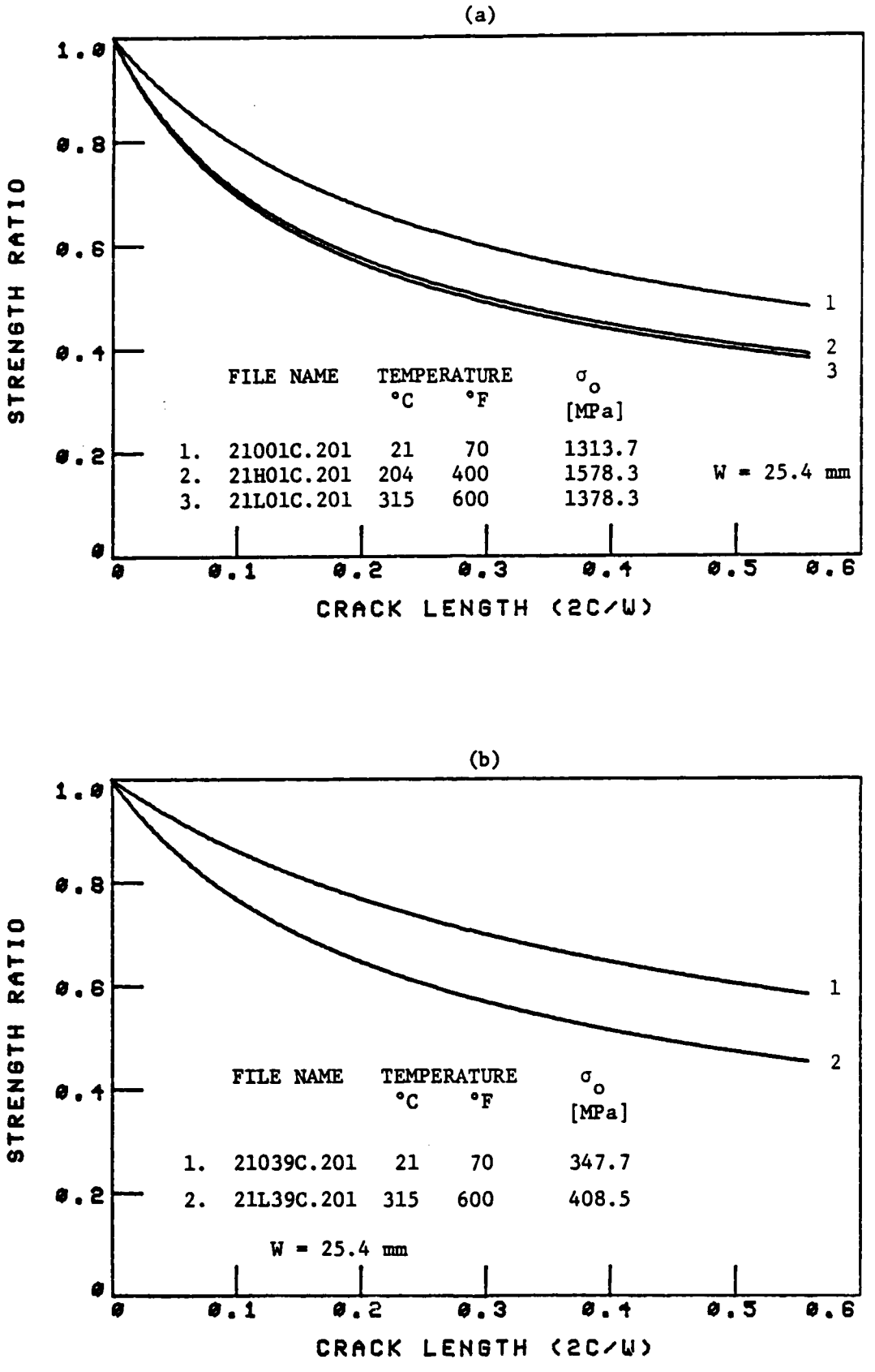

Figure 7. Effect of test temperature on notch sensitivity (WN-fracture model, "average-stress" criterion) for: a. boron/aluminum $[0]_8$; b. boron/aluminum $[0/\pm45/90]_s$ laminates.

explanation is available yet regarding the notch sensitivity of boron/aluminum at elevated temperatures and additional investigation is warranted.

10.3.4 Effect of Notch Tip Radius

The effect of notch tip radius on the notch sensitivity of composite laminates has been addressed in several studies, particularly for graphite/epoxy and boron/aluminum (unidirectional) laminates. Generally, it has been determined that notch tip radius (or shape of discontinuity) has little effect on notch sensitivity. No attempt has been made in this program to obtain independent data on the subject matter. However, based on results reported in [13] and comparing the data reported for the same material system in [4] and [5] for laminates containing a circular hole and a center crack, respectively, a similar conclusion could be reached, as shown in Figure 8. It should be noted that most fracture studies of boron/aluminum were conducted on laminates containing a straight crack rather than a circular hole. Therefore, insufficient evidence is available regarding the effect of notch shape on notch sensitivity. However, other works (e.g. [14-16] which studied the effect of notch tip radius on laminates containing a center crack also concluded that the notch tip radius has little if any effect on notched strength.

10.3.5 Effect of Impact Damage on Residual Strength

Generally, it has been determined that both resin matrix and metal-matrix composites are highly sensitive to impact damage, even when it is nonvisual damage. In the case of boron/aluminum, the lateral damage caused by hard object impact is the major cause of strength degradation. This impact damage can be measured from X-ray radiographs [18]. In order to compare the effect of impact damage on strength reduction to that of artificial damage (through-the-thickness straight cracks) the notch sensitivity curves for both impact and artifical damage are shown in Figure 9. For the case of impact damage, the crack length (2c/W) shown in the abscissa of Figure 9 represents the lateral damage measured from

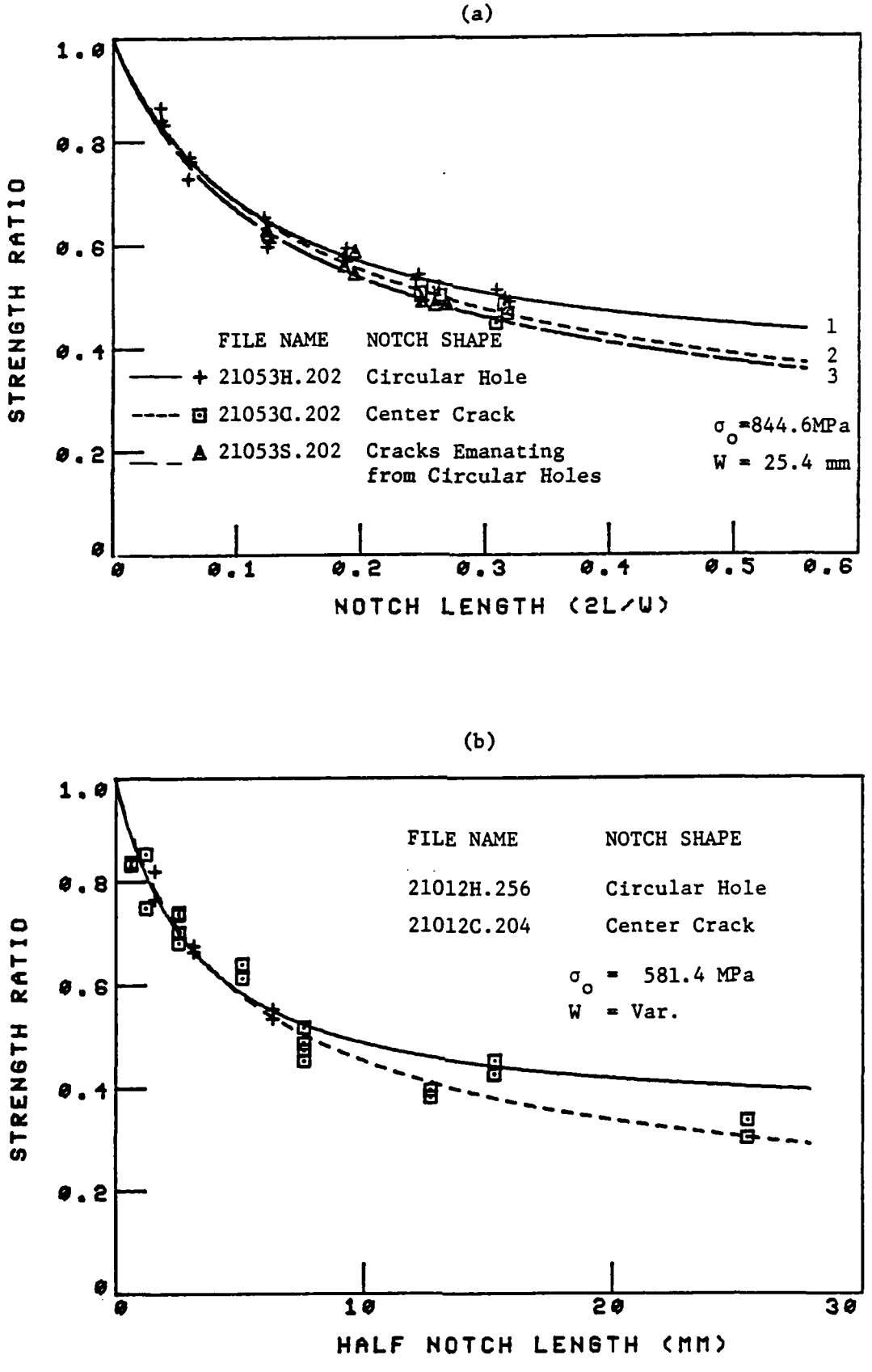

Figure 8. Effect of notch shape on notch sensitivity (WN-fracture model, "average-stress" criterion) for boron/aluminum: a. $[\pm 45/0_2]_s$; b. $[0/\pm 45]_s$ laminates.

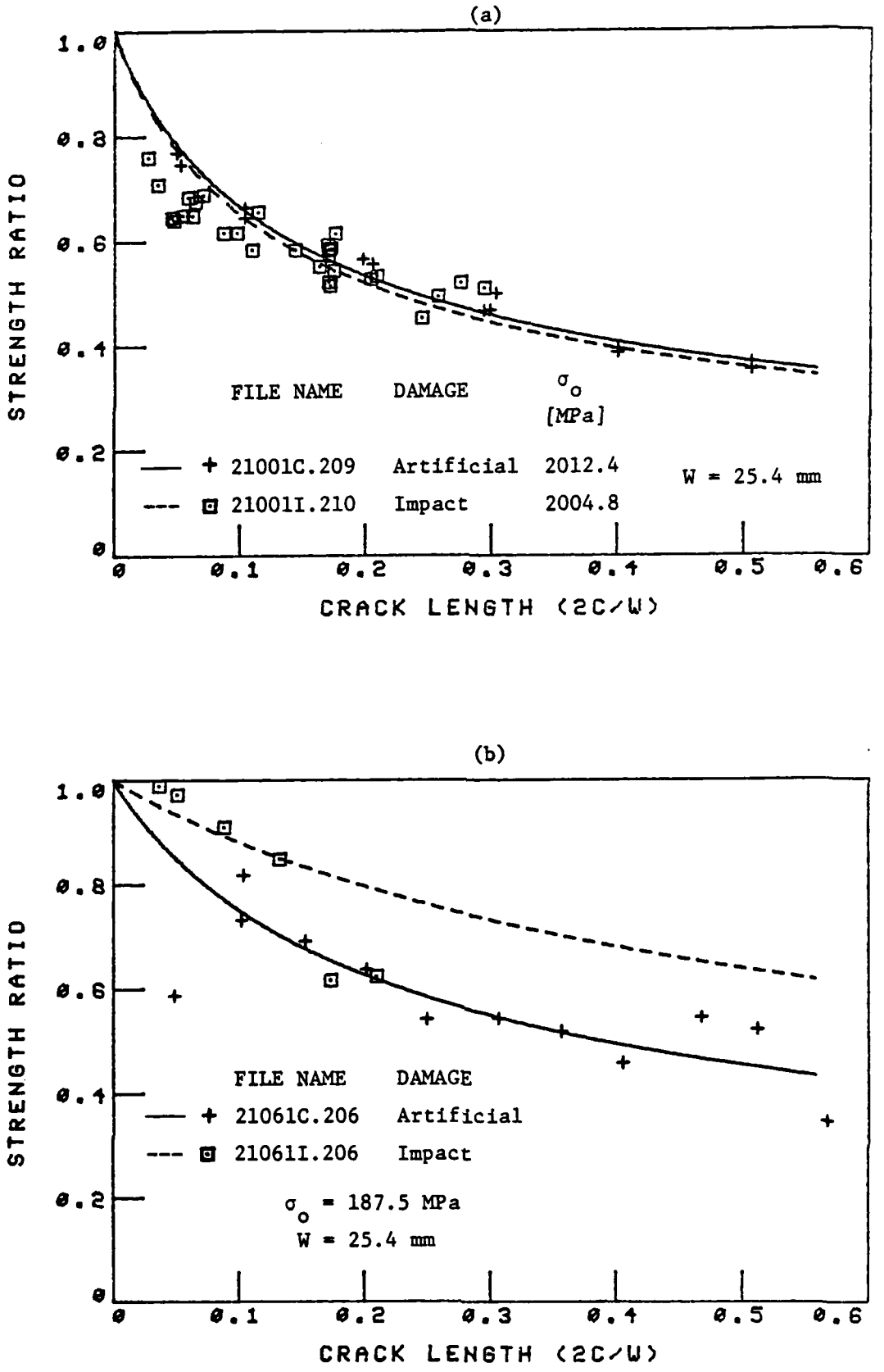

Figure 9. Residual tensile strength versus lateral damage size due to impact (measured through X-ray radiography) and artificial damage (center cracks). Predictions based on WN-fracture model ("average-stress" criterion) for boron/aluminum: a. $[0]_8$; b. $[90/\pm 68]_s$ laminates.

radiographs. For fiber dominated laminates, $[0]_8$, Figure 9a, the notch sensitivity curves are very similar. Thus, the induced lateral impact damage can be presented as through-the-thickness straight cracks for post-impact residual strength predictions. Similar correlation has been established for $[0/\pm22]_s$ laminate [19]. In the case of the matrix dominated laminate, $[90/\pm68]_s$, Figure 9b (also reported in [19]), the impact damage laminate is much less notch sensitive than the laminate which contains through-the-thickness cracks. Thus, not all the damage detected in the radiographs is critical. Since no radiographs of the impact damaged laminate are given in Ref. [19] the definition of 'impact damage' is unclear and no definite conclusions can be reached regarding the applicability of the fracture models reviewed in this work to impact damage in matrix dominated laminates.

10.3.6 Effect of Specimen Width

Several of the experimental studies reviewed include notched strength data obtained with different specimen widths. In most of these studies the data are plotted on a σ_N^∞/σ_o versus notch length (dimensional) format and the fracture models parameters are determined from the complete set of data, e.g. Figure 10. However, when the data set is divided into sub-sets of equal width specimens, the resulting notch sensitivity curves (i.e. σ_N^∞/σ_o versus 2c/W) indicate a possible width effect. The examples shown in Figure 11 indicate that the wider the specimens are, the more notch sensitive the subject laminate is. However, the values of a_o and d_o in each sub-set differ only slightly from each other (while the values obtained from the complete data set is equal approximately to their average value). Consequently, it seems that the values of the characteristic dimensions do not necessarily indicate degree of notch sensitivity unless they are being applied for data sets obtained with identical width specimens.

Similar conclusions could be drawn from the data reported by Whitney and Nuismer [20] for graphite/epoxy laminates containing a circular hole and a center crack, respectively. In [20], the data reported in dimensional format (i.e.

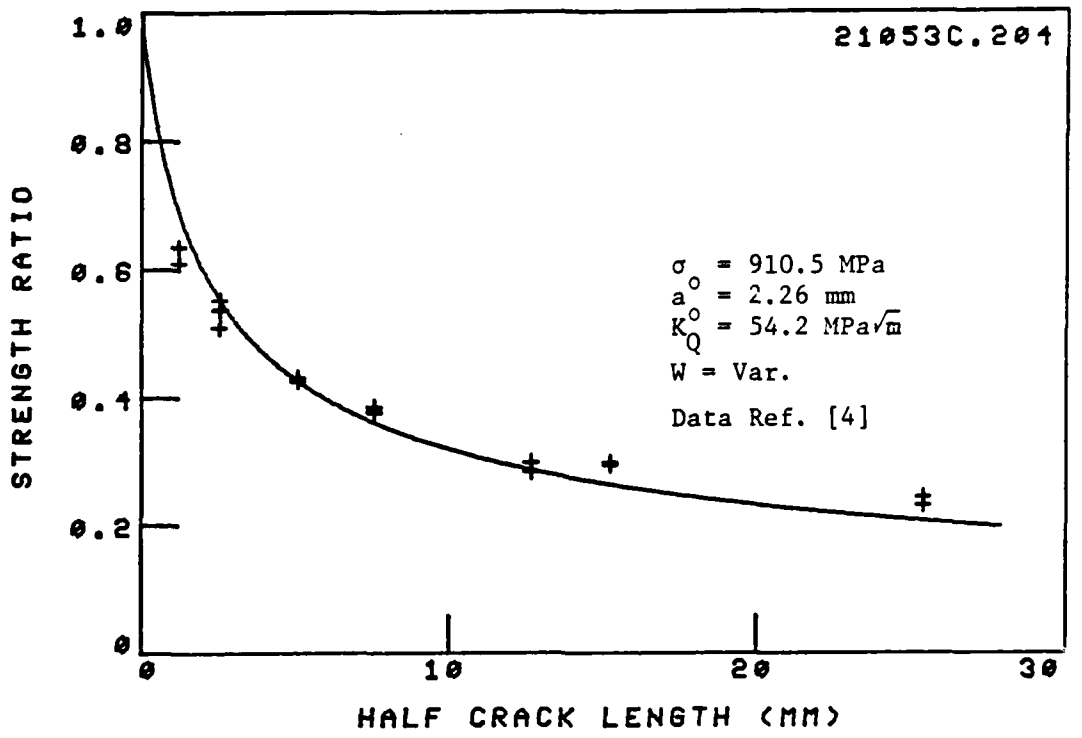

Figure 10. Comparison between experiments and prediction (WN-fracture model, "average-stress" criterion) for boron/aluminum $[\pm 45/0_2]$ laminate containing a center crack.

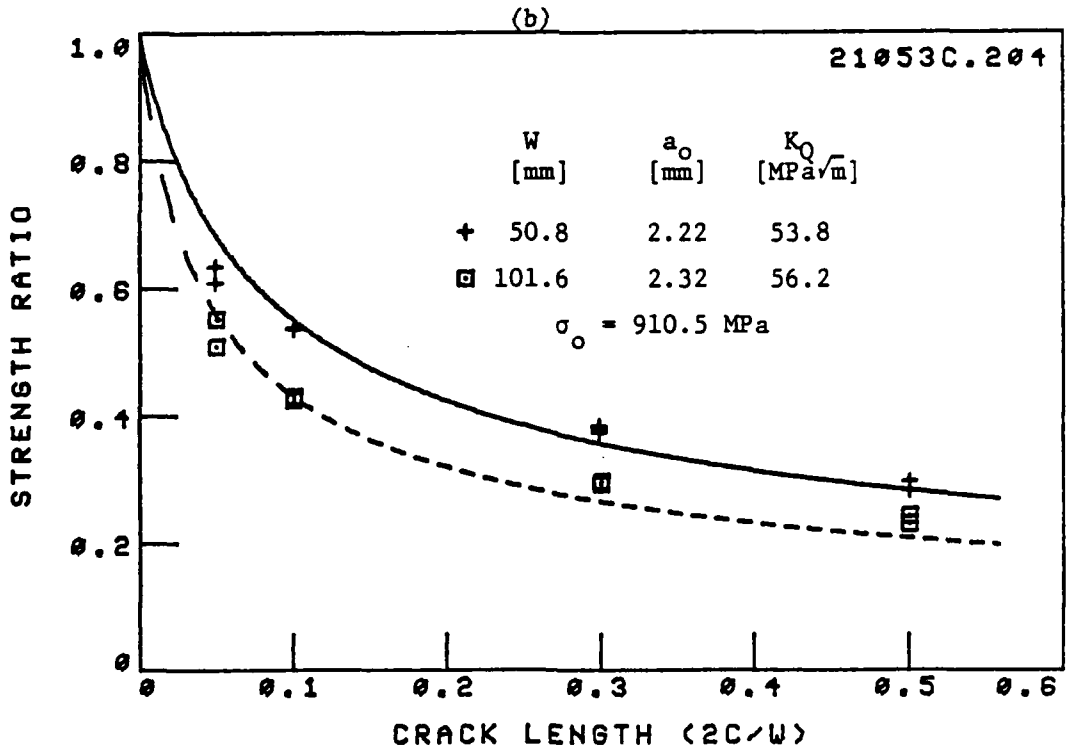

Figure 11. Effect of specimen width on notch sensitivity (WN-fracture model, "average-stress" criterion) for boron/aluminum $[\pm 45/0_2]$ laminate containing a center crack. Individual data are those shown in Figure 10.

σ_N^∞/σ_o versus 2c) did not all fit the prediction using a constant value for the characteristic dimensions, primarily for large notch sizes (obtained with the wider specimens). In fact, significantly different values of the characteristic dimensions had to be applied to fit the larger notch size data.

It seems that two contradicting conclusions regarding the effect of specimen width on the values of the characteristic dimensions can be made. While the data reported in [4] indicate little effect of specimen width on the values of the characteristic dimensions, the data reported in [20] indicate significant effect. It should be noted, however, that the data reported in [20] for the different widths are all for a single 2c/W (or 2R/W) value. Recalling that significant error can be introduced in determining a_o and d_o from a single datum (Section IX, Figure 3), it seems that no definite conclusions can be drawn from the data reported in [20]. In fact, in many of the experimental results reviewed in this study, in which different width specimens were used, the number of data reported is not sufficient to draw meaningful conclusions regarding the width effect. It should also be noted that when notched strength data are plotted in dimensional format, the effect of width on notch sensitivity is not detected. Consequently, conclusions regarding the effect of notch size on the characteristic dimensions of WN-fracture models based on data obtained with different width specimens cannot be finalized. In summary, there is an indication that specimen width may affect notch sensitivity of composite laminates and possibly also the fracture model parameters. A width effect should be expected considering the extensive notch tip damage zone size developed prior to catastrophic fracture and the dependence of the stress concentration factor (at the tip of the notch) on the notch length. Such extensive damage zone size has been reported in the literature, e.g. [21]. It seems, therefore, that this issue should be addressed in detail when the fracture behavior of composite laminates is being characterized.

10.4 Conclusions

The major conclusions which could be drawn regarding the effect of various intrinsic and extrinsic variables on the notch sensitivity of boron/aluminum laminates are given below. Additional conclusions related to this subject are given in Section 9.7.

1. Effect of Laminate Configuration: The experimental notched strength data indicate that laminate lay-up strongly affects the notched strength and notch sensitivity of boron/aluminum laminates.

2. Effect of Laminate Stacking Sequence: No sufficient data are available to draw any conclusions for boron/aluminum laminates.

3. Effect of Constituents: Significant differences in notch sensitivity (and notched strength) were obtained for a seemingly identical material system. These differences are attributable either to different fabrication procedures or to differences in fiber strength. Improved notch sensitivity of unidirectional boron/aluminum can be achieved through a proper choice of constituents. Effect of heat treatment and type of matrix, on notch sensitivity and deformation characteristics of boron/aluminum are reported in the literature.

4. Effect of Test Temperature: Very little data are available regarding the effect of temperature on the notch sensitivity of composite laminates. Results obtained in this study indicate that at elevated temperature boron/aluminum can become more notch sensitive, which might be due to strength degradation of the fibers.

5. Effect of Notch Tip Radius: It has been determined that notch tip radius (or shape of discontinuity) has little effect on notch sensitivity of boron/aluminum laminates. This characteristic has frequently been cited

in the literature, and it is attributed to the notch tip blunting during damage progression.

6. Effect of Impact Damage: Both resin matrix and metal-matrix composites are highly sensitive to impact damage, even when it is nonvisual damage. The lateral damage is the major cause of strength degradation. Results indicate that induced lateral damage can be presented as through-the-thickness straight cracks for post-impact residual strength predictions.

7. Effect of Specimen Width: Based on the review of published data it seems that specimen width affects the notch sensitivity of composite laminates. Consequently the values of the fracture model parameters may also depend on specimen width. Very little attention has been given to this issue in the notch sensitivity studies of composites and this issue in particular deserves additional study.

10.5 References

1. J. Awerbuch and M. Madhukar, "Notched Strength of Composite Laminates: Predictions and Experiments - A Review", Journal of Reinforced Plastic and Compoosites, Vol. 4, No. 1, 1985, pp. 3-160, to be published.

2. J. Awerbuch and M. Madhukar, "Notched Strength of Composite Laminates: Predictions and Experiments - A Review", NASA CR , 1985 (to be published).

3. J. Awerbuch and H.T. Hahn, "Crack-Tip Damage and Fracture Toughness of Boron/Aluminum Composites", Journal Composite Materials, Vol. 13, 1979, pp. 82-107.

4. C.C. Poe, Jr. and J.A. Sova, "Fracture Toughness of Boron/Aluminum Laminates with Various Proportions of 0° and ±45° Plies", NASA Technical Paper 1707, November 1980.

5. W.S. Johnson, C.A. Bigelow and Y.A. Bahei-El-Din, "Experimental and Analytical Investigation of the Fracture Process of Boron/Aluminum Laminates Containing Notches", NASA Technical Paper 2187, September 1983.

6 M. Madhukar, "Fracture Behavior of Boron/Aluminum Laminates at Room and Elevated Temperatures", Ph.D. Dissertation, Drexel University, to be published.

7. D.L. McDanels and R.A. Signorelli, "Effect of Fiber Diameter and Matrix Alloys on Impact-Resistant Boron/Aluminum Composites", NASA-TN D-8204.

8. K.M. Prewo, "Development of Impact Resistant Metal Matrix Composites" AFML-TR-75-216, Air Force Materials Laboratory, March, 1976.

9. D.L. McDanels and R.A. Signorelli, "Effect of Angle Plying and Matrix Enhancement on Impact-Resistant Boron/Aluminum Composites", NASA TN D-8205, October 1976.

10. J.E. Goree and W.F. Jones, "Fracture Behavior of Unidirectional Boron/Aluminum Composite Laminates", NASA CR-3753, 1983.

11. E.D. Reedy, Jr., "Notched Unidirectional Boron/Aluminum: Effect of Matrix Properties", Journal Composite Materials, Vol. 15, 1982, pp. 495-509.

12. E.D. Reedy, Jr., "Large Strain Shear Response of Unidirectional Boron/Aluminum", Proceedings of the Joint Japan Society of Mechanical Engineers/Society for Experimental Stress Analysis Conference on Experimental Mechanics, Hawaii, May 22-30, 1982.

13. J.W. Mar and K.Y. Lin, "Fracture of Boron/Aluminum Composites with Discontinuities", Journal Composite Materials, Vol. 11, 1977, pp. 405-421.

14. K.C. Kreider, L. Dardi and K. Prewo, "Metal Matrix Composite Technology", Air Force Materials Laboratory Technical Report, AFML-TR-71-204, December 1971.

15. K.C. Kreider and L. Dardi, "Fracture Toughness of Composites", Failure Modes in Composites, I.J. Toth, Ed., The Metallurgical Society of the AIME, Vol. I, New York, New York, 1972, pp. 193-220.

16. J.M. Grandemange and K.N. Street, "The Effect of Notch Root Radius and Thickness on the Static Fracture Toughness of B-Al Composites", in Proceedings of the 1975 International Conference on Composite Materials, Vol. 2, 1975, pp. 1019-1050.

17. W.F. Jones, "Uni-Directional Composite Laminate With Circular and Rectangular Cut-Outs", M.S. Thesis, Clemson University, 1981.

18. J. Awerbuch and H.T. Hahn, "Hard Object Impact Damage of Metal Matrix Composites", Journal Composite Materials, Vol. 10, 1976, pp. 231-257.

19. D.D. Dailey, "Prediction of Fracture Toughness for Specially Orthotropic Composite Laminates", M.Sc. Dissertation, School of Engineering, Air Force Institute of Technology (AFIT), December 1974.

20. R.J. Nuismer and J.M. Whitney, "Uniaxial Failure of Composite Laminates Containing Stress Concentrations", in Fracture Mechanics of Composites, ASTM STP 593, American Society of Testing and Materials, 1975, pp. 117-142.

21. C.C. Poe, Jr., "Fracture Toughness of Fibrous Composite Materials", NASA Technical Paper 2370, November 1984.

END

FILMED

1-86

DTIC